U.PORTO
FEUP FACULDADE DE ENGENHARIA
UNIVERSIDADE DO PORTO

Transport Phenomena Research Center - CEFT

Department of Chemical Engineering - DEQ

Optimisation of a passive direct methanol fuel cell for portable applications

BEATRIZ ARNOLD BRAZ

Thesis presented for the Doctor of Philosophy degree in Chemical and Biological Engineering from the Faculty of Engineering of University of Porto, Portugal

Supervisor: Professor Alexandra Maria Pinheiro da Silva Ferreira Rodrigues Pinto

Co-supervisor: Doctor Vânia Sofia Brochado de Oliveira

Porto, April 2019

STATEMENT OF ORIGINALITY

I certify that this work does not contain any material that has been used, or will be used, for the award of any other degree or diploma in my name or anyone, in any university or institution. Moreover, I certify that, to the best of my knowledge, this work does not contain any material previously published or written by another person, except where due reference has been made in the text.

(Beatriz Arnold Braz)

STATEMENT

In order to fulfil the Rules of Ethics of the Doctoral Program of Chemical and Biological Engineering (PDEQB), we hereby declare that all the contents of the thesis presented by Beatriz Arnold Braz, entitled "Optimisation of a passive direct methanol fuel cell for portable applications", are exclusively from the author. Accordingly, all the results here shown were obtained by the author of the thesis.

(Beatriz Arnold Braz)

(Alexandra Maria Pinheiro da Silva Ferreira Rodrigues Pinto)

To my grandmother Joana with all my love

“Remember to look up at the stars and not down at your feet. Try to make sense of what you see and wonder about what makes the universe exist. Be curious. And however difficult life may seem, there is always something you can do and succeed at. It matters that you don't just give up.”

Stephen Hawking

Acknowledgments

I would like to thank my supervisors, professor Alexandra and Vânia for the opportunity, conditions and support to carry out the present work, as well for the supervision and knowledge transmitted.

I would like to thank to my colleagues from laboratory E206 at the Department of Chemical Engineering.

I am very grateful especially to Joana, my friend unique in Portugal, for your friendship, support, many conversations and coffees during these years, thank you very much.

I want say thank you very much to my husband Renato for his patience, comprehension and love. His presence here was pivotal to a good development of my work. Thank you for be always by my side.

I would like to thank to my cousin-sister, Daiana, which even far, always was present for the needed moments with a friendly word.

My deepest gratitude to my grandmother, Joana, for her kindness, love, comprehension and teachings during my entire life, and for her sacrifices and her strength to bear everything. Thank you for being my special person in this life.

I am grateful by my doctoral fellowship (BEX 12997/13-7) supported by CAPES, "Coordenação de Aperfeiçoamento de Pessoal de Nível Superior" - Brazil. I also would like to thank the partial support by Project PTDC/NewPortCell-POCI-01-0145-FEDER-032116 - funded by FEDER funds through COMPETE2020 - Programa Operacional Competitividade e Internacionalização (POCI) and by national funds (PIDDAC) through FCT/MCTES. POCI (FEDER) also supported this work via CEFT.

ABSTRACT

Passive direct methanol fuel cells (pDMFCs) are promising devices to replace the conventional batteries in portable applications, since they have a compact design, instant recharging and high energy densities, use a liquid fuel, operate at room temperature and with a passive reactants supply, therefore, without any additional power consumption. However, these devices have some drawbacks that limit its competitiveness with the conventional batteries. These drawbacks include the sluggish kinetics of both anode and cathode reactions, methanol and water crossover, inefficient products removal, higher costs and lower durability. Therefore, it is mandatory to overcome these drawbacks to reach the ideal balance between these systems efficiency, cost and durability.

The main goal of this work was the optimisation of a pDMFC based on the selection of the best operating and design conditions, using the materials commercial available, in order to increase its power output and durability and decrease its costs. Consequently, the effect of methanol concentration and configurational parameters, such as diffusion layer materials and properties, current collectors design and materials, on the fuel cell behaviour was investigated, to reach higher power outputs with high methanol concentrations and lower methanol crossover rates. Towards an evaluation of the pDMFC lifetime, the best configuration found on the studies regarding the effect of the different design parameters was used to evaluate the cell degradation over the time.

The experimental studies were performed in a pDMFC with an active area of 25 cm^2 and operated at ambient conditions (ambient pressure and temperature), conditions of interest in portable applications. The cell performance was evaluated by polarisation measurements and these results were explained under the light of the electrochemical impedance spectroscopy (EIS) data and an innovative equivalent electric circuit (EEC) fitting, through the estimation of the different resistances that negatively affect the cell performance: ohmic and activation losses. The novel EEC proposed in this study allowed the identification of these different losses, including the activation resistance of the parasitic cathode reaction, methanol oxidation (a new finding) and showed a good agreement with the EIS data, revealing that the EEC reproduces with accuracy the system under study.

The best power output, 5.23 mW/cm^2, was achieve using a Nafion 117 membrane with 3 mg/cm^2 of Pt/Ru as anode catalyst and 1.3 mg/cm^2 of Pt as cathode catalyst, carbon cloth with a microporous layer (0.410 mm) as anode diffusion layer and carbon cloth (0.400 mm)

as cathode diffusion layer, a titanium current collector at the anode and a stainless steel current collector at the cathode, both with an open ratio of 34 %, and a methanol concentration of 7 M. The durability tests carried out with the best configuration showed a fuel cell lifetime of 200 hours.

Despite the power output achieved is not very attractive, comparing to those already presented in literature, it can be high enough for some specific applications and can be justified by the lower catalyst loadings used in the current work (3 mg/cm^2 Pt/Ru and 1.3 mg/cm^2 Pt), which allowed a reduction of the fuel cell costs, when compared to the common loadings used for this type of fuel cells (4 mg/cm^2 Pt/Ru and 4 mg/cm^2 Pt).

The present work shows that changes in the fuel cell structure and configuration are effective ways to improve the fuel cell performance and power output and achieve the efficiencies, lifetime and costs needed for real applications.

Keywords: Passive direct methanol fuel cell, diffusion layer, current collector, electrochemical impedance spectroscopy, resistance, methanol crossover, cost, lifetime, methanol concentration

RESUMO

As células de combustível com alimentação passiva e direta de metanol (pDMFCs) são uma tecnologia promissora para a substituição das baterias convencionais em aplicações portáteis, uma vez que são dispositivos compactos com recarga instantânea e elevada densidade energética, utilizam um combustível líquido, operam à temperatura e pressão ambiente e fornecem os reagentes recorrendo a mecanismos de transporte naturais, e por isso sem consumo adicional de energia. No entanto, estes dispositivos possuem algumas limitações que prejudicam a sua competitividade em relação às baterias convencionais. Estas residem na natureza lenta das reações eletroquímicas, no atravessamento do metanol através da membrana, remoção ineficiente dos subprodutos do ânodo e do cátodo, baixa durabilidade e elevados custos. Desta forma, torna-se imperativo superar estas limitações para alcançar um balanço ideal entre a eficiência, custo e durabilidade destes dispositivos.

O principal objetivo deste trabalho consistiu na otimização de uma pDMFC com base na seleção das melhores condições operacionais e configuracionais, utilizando materiais/componentes disponíveis comercialmente, por forma a aumentar a potência e durabilidade destes dispositivos e diminuir os seus custos. Assim, estudou-se o efeito da concentração de metanol e de parâmetros configuracionais, como os materiais e propriedades das camadas de difusão, configuração e materiais dos coletores de corrente, no desempenho da célula de combustível, para alcançar elevadas potências com altas concentrações de metanol e baixas taxas de atravessamento de metanol através da membrana. A melhor configuração encontrada nos estudos relacionados com os parâmetros configuracionais foi usada para avaliar a degradação do desempenho da célula ao longo do tempo e assim aferir a sua vida útil (durabilidade).

Os estudos experimentais foram realizados numa pDMFC com área ativa de 25 cm^2, operada à pressão e temperatura ambiente, condições de interesse para aplicações portáteis. O desempenho da célula foi avaliado através de curvas de polarização e os resultados foram explicados à luz dos dados de espectroscopia de impedância eletroquímica (EIS) e do ajuste dos mesmos com um circuito elétrico equivalente inovador (EEC), através da determinação das diferentes resistências que afetam negativamente o desempenho da célula: óhmica e de ativação. O EEC proposto neste estudo permitiu a identificação das diferentes perdas, incluindo a resistência de ativação do cátodo devido à oxidação do metanol que atravessa a membrana neste lado (resultado pela primeira vez reportado) e mostrou uma boa

concordância com os dados do EIS, revelando que o circuito reproduz bem o dispositivo em estudo.

A melhor potência, 5,23 mW/cm^2, foi obtida usando uma membrana de Nafion 117, 3 mg/cm^2 de Pt/Ru como catalisador do ânodo e 1,3 mg/cm^2 de Pt como catalisador do cátodo, tecido de carbono com uma camada microporosa (0,410 mm) como camada de difusão do ânodo e tecido de carbono (0,400 mm) como camada de difusão de cátodo, um coletor de corrente de titânio no ânodo e um coletor de corrente de aço inox no cátodo, ambos com uma área aberta de 34 % e uma concentração de metanol de 7 M. Os testes de durabilidade realizados com a melhor configuração revelaram uma durabilidade da célula de combustível de 200 horas.

Apesar de a potência obtida não ser muito atrativa, comparada com as já apresentadas na literatura, ela pode ser alta o suficiente para algumas aplicações e pode ser justificada pelas reduzidas cargas de catalisador usadas neste estudo (3 mg/cm^2 de Pt/Ru e 1,3 mg/cm^2 de Pt), o que permitiu reduzir os custos da célula de combustível, quando comparadas com as cargas usuais utilizadas para este tipo de células de combustível (4 mg/cm^2 de Pt/Ru e 4 mg/cm^2 de Pt).

O presente trabalho revelou que alterações na estrutura e configuração da célula de combustível são formas eficazes de melhorar o seu desempenho e potência e alcançar as eficiências, a durabilidade e os custos necessários para a sua aplicação e comercialização.

Palavras-chave: Células de combustível com alimentação passiva e direta de metanol, camada de difusão, coletor de corrente, espectroscopia de impedância eletroquímica, resistência, atravessamento de metanol, custo, durabilidade, concentração de metanol

List of publications

B. A. Braz, V. B. Oliveira, and A. M. F. R. Pinto, “Recent developments in passive direct methanol fuel cells” in Direct Methanol Fuel Cells Applications, Performance and Technology, Nova Science Publishers, 2017, 143–203.

B. A. Braz, C. S. Moreira, V. B. Oliveira, and A. M. F. R. Pinto, “Effect of the current collector design on the performance of a passive direct methanol fuel cell”, Electrochimica Acta, 2019, 300, 306-315. https://doi.org/10.1016/j.electacta.2019.01.131

B. A. Braz, V. B. Oliveira, and A. M. F. R. Pinto, “Experimental studies of the effect of cathode diffusion layer properties on a passive direct methanol fuel cell power output”, International Journal of Hydrogen Energy. https://doi.org/10.1016/j.ijhydene.2019.03.162

B. A. Braz, V. B. Oliveira, and A. M. F. R. Pinto, “Analysis of the anode diffusion layer properties on the performance of a passive direct methanol fuel cell using electrochemical impedance spectroscopy”. Submitted.

B. A. Braz, V. B. Oliveira, and A. M. F. R. Pinto, “Electrochemical impedance spectroscopy as a diagnostic tool for passive direct methanol fuel cells”. Submitted.

B. A. Braz, V. B. Oliveira, and A. M. F. R. Pinto, “Optimization of a passive direct methanol fuel cell with different current collectors materials”. Submitted.

B. A. Braz, C. S. Moreira, V. B. Oliveira, and A. M. F. R. Pinto, “Performance of a passive direct alcohol fuel cell fed with a mixture of alcohols”. Submitted.

List of Figures

Figure 1.1. General working principle of a fuel cell. 4

Figure 2.1. Schematic representation of a conventional passive DMFC. 12

Figure 2.2. Representation of the Nafion® chemical structure [47]. 16

Figure 2.3. Micrographs of commercially available carbon cloth (a) and carbon paper (b) [1]. 18

Figure 2.4. Schematic representation of a typical DMFC polarisation curve. 20

Figure 2.5. CO_2 bubble behaviour on the anode side. 26

Figure 2.6. Cathode flooding in a passive DMFC. 29

Figure 2.7. Some DMFC applications. 54

Figure 3.1. Representation of a typical Nyquist plot with the three major losses that negatively affect the fuel cell performance. 61

Figure 3.2. Equivalent electric circuit for a pDMFC considering the activation and mass transport losses. 63

Figure 4.1. Components of the passive DMFC. 73

Figure 4.2. In-house passive DMFC. 74

Figure 4.3. Acrylic end plates, a) anode and b) cathode. 75

Figure 4.4. Perforated current collector with different open ratios: a) 34 % (CC_1); b) 41 % (CC_2); c) 64 % (CC_3) and d) open window frame current collector (CC_4). 76

Figure 4.5. Diffusion layers used in this work: a) carbon cloth; b) carbon paper and c) carbon cloth with MPL (both sides). 77

Figure 4.6. Zahner test station. 78

Figure 5.1. Nyquist plot of a pDMFC with the DHE at the cathode side and a methanol concentration of 1 M at the anode, for different cell voltages. 86

Figure 5.2. Nyquist plot of a pDMFC with the DHE at the anode side and air at the cathode side, for different cell voltages. 86

Figure 5.3. Nyquist plot of a pDMFC fed with methanol (1 M) at the anode and air at the cathode side, for different cell voltages. 87

Figure 5.4. Equivalent electric circuit used to describe the EIS experimental data of a pDMFC with methanol and air. 88

Figure 5.5. Effect of using different carbon cloths as ADL on the cell performance for different methanol concentrations: a) 1 M, b) 2 M, c) 3 M, d) 5 M and e) 7 M. 91

Figure 5.6. Effect of using different carbon papers as ADL on cell performance for different methanol concentrations: a) 1 M, b) 2 M, c) 3 M, d) 5 M and e) 7 M. 93

Figure 5.7. Effect of using different carbon cloths as CDL on cell performance for different methanol concentrations: a) 1 M, b) 2 M and c) 3 M. 96

Figure 5.8. Effect of using different carbon papers as CDL on cell performance for different methanol concentrations: a) 1 M, b) 2 M and c) 3 M. 99

Figure 5.9. Effect of methanol concentration on the pDMFC performance with the tailored MEA. 101

Figure 5.10. Effect of methanol:ethanol ratio on the pDMFC performance for different methanol concentration of a) 2 M, b) 3 M and c) 5 M. 104

Figure 5.11. Effect of the anode CC design on the performance of a pDMFC for different methanol concentrations: a) 1 M, b) 2 M and c) 3 M; cathode CC_2. 108

Figure 5.12. Effect of the cathode CC design on the performance of a pDMFC for different methanol concentrations: a) 1 M, b) 2 M and c) 3 M; anode CC_2. 110

Figure 5.13. Effect of the CC material on the anode side on cell performance for different methanol concentrations: a) 1 M, b) 2 M and c) 3 M; cathode CC_1. 114

Figure 5.14. Effect of the CC material on the cathode side on cell performance for different methanol concentrations: a) 1 M, b) 2 M and c) 3 M; anode CC_1. 117

Figure 5.15. Polarisation curves at the beginning (0 h) and at the end (200 h) of the durability tests. 119

Figure A.1. Effect of methanol concentration on the cell performance using CC as ADL. 147

Figure A.2. Nyquist plot of a pDMFC for different methanol concentrations and 0.2 V using CC as ADL. 148

Figure A.3. Nyquist plot of a pDMFC for different methanol concentrations and 0.3 V using CC as ADL. 148

Figure A.4. Nyquist plot of a pDMFC for different methanol concentrations and 0.4 V using CC as ADL. 149

Figure A.5. Effect of methanol concentration on the cell performance using CC_T as ADL. 149

Figure A.6. Nyquist plot of a pDMFC for different methanol concentrations and 0.2 V using CC_T as ADL. 150

Figure A.7. Nyquist plot of a pDMFC for different methanol concentrations and 0.3 V using CC_T as ADL. 150

Figure A.8. Nyquist plot of a pDMFC for different methanol concentrations and 0.4 V using CC_T as ADL. 151

Figure A.9. Effect of methanol concentration on the cell performance using CC_MPL as ADL. 151

Figure A.10. Nyquist plot of a pDMFC for different methanol concentrations and 0.2 V using CC_MPL as ADL. 152

Figure A.11. Nyquist plot of a pDMFC for different methanol concentrations and 0.3 V using CC_MPL as ADL. 152

Figure A.12. Nyquist plot of a pDMFC for different methanol concentrations and 0.4 V using CC_MPL as ADL. 153

Figure A.13. Effect of methanol concentration on the cell performance using CC_MPL_E as ADL. 153

Figure A.14. Nyquist plot of a pDMFC for different methanol concentrations and 0.2 V using CC_MPL_E as ADL. 154

Figure A.15. Nyquist plot of a pDMFC for different methanol concentrations and 0.3 V using CC_MPL_E as ADL. 154

Figure A.16. Nyquist plot of a pDMFC for different methanol concentrations and 0.4 V using CC_MPL_E as ADL. 155

Figure A.17. Effect of methanol concentration on the cell performance using CP as ADL. 155

Figure A.18. Nyquist plot of a pDMFC for different methanol concentrations and 0.2 V using CP as ADL. 156

Figure A.19. Nyquist plot of a pDMFC for different methanol concentrations and 0.3 V using CP as ADL. 156

Figure A.20. Nyquist plot of a pDMFC for different methanol concentrations and 0.4 V using CP as ADL. 157

Figure A.21. Effect of methanol concentration on the cell performance using CP_T as ADL. 157

Figure A.22. Nyquist plot of a pDMFC for different methanol concentrations and 0.2 V using CP_T as ADL. 158

Figure A.23. Nyquist plot of a pDMFC for different methanol concentrations and 0.3 V using CP_T as ADL. 158

Figure A.24. Nyquist plot of a pDMFC for different methanol concentrations and 0.4 V using CP_T as ADL. 159

Figure A.25. Effect of methanol concentration on the cell performance using CP_MPL as ADL. 159

Figure A.26. Nyquist plot of a pDMFC for different methanol concentrations and 0.2 V using CP_MPL as ADL. 160

Figure A.27. Nyquist plot of a pDMFC for different methanol concentrations and 0.3 V using CP_MPL as ADL. 160

Figure A.28. Nyquist plot of a pDMFC for different methanol concentrations and 0.4 V using CP_MPL as ADL. 161

Figure A.29. Effect of methanol concentration on the cell performance using CP_MPL_T as ADL. 161

Figure A.30. Nyquist plot of a pDMFC for different methanol concentrations and 0.2 V using CP_MPL_T as ADL. 162

Figure A.31. Nyquist plot of a pDMFC for different methanol concentrations and 0.3 V using CP_MPL_T as ADL. 162

Figure A.32. Nyquist plot of a pDMFC for different methanol concentrations and 0.4 V using CP_MPL_T as ADL. 163

Figure A.33. Effect of methanol concentration on the cell performance using CC_T as CDL. 163

Figure A.34. Nyquist plot of a pDMFC for different methanol concentrations and 0.2 V using CC_T as CDL. 164

Figure A.35. Nyquist plot of a pDMFC for different methanol concentrations and 0.3 V using CC_T as CDL. 164

Figure A.36. Nyquist plot of a pDMFC for different methanol concentrations and 0.4 V using CC_T as CDL. 165

Figure A.37. Effect of methanol concentration on the cell performance using CC_MPL as CDL. 165

Figure A.38. Nyquist plot of a pDMFC for different methanol concentrations and 0.2 V using CC_MPL as CDL. 166

Figure A.39. Nyquist plot of a pDMFC for different methanol concentrations and 0.3 V using CC_MPL as CDL. 166

Figure A.40. Nyquist plot of a pDMFC for different methanol concentrations and 0.4 V using CC_MPL as CDL. 167

Figure A.41. Effect of methanol concentration on the cell performance using CC_MPL_E as CDL. 167

Figure A.42. Nyquist plot of a pDMFC for different methanol concentrations and 0.2 V using CC_MPL_E as CDL. 168

Figure A.43. Nyquist plot of a pDMFC for different methanol concentrations and 0.3 V using CC_MPL_E as CDL. 168

Figure A.44. Nyquist plot of a pDMFC for different methanol concentrations and 0.4 V using CC_MPL_E as CDL. 169

Figure A.45. Effect of methanol concentration on the cell performance using CP as CDL. 169

Figure A.46. Nyquist plot of a pDMFC for different methanol concentrations and 0.2 V using CP as CDL. 170

Figure A.47. Nyquist plot of a pDMFC for different methanol concentrations and 0.3 V using CP as CDL. 170

Figure A.48. Nyquist plot of a pDMFC for different methanol concentrations and 0.4 V using CP as CDL. 171

Figure A.49. Effect of methanol concentration on the cell performance using CP_T as CDL. 171

Figure A.50. Nyquist plot of a pDMFC for different methanol concentrations and 0.2 V using CP_T as CDL. 172

Figure A.51. Nyquist plot of a pDMFC for different methanol concentrations and 0.3 V using CP_T as CDL. 172

Figure A.52. Nyquist plot of a pDMFC for different methanol concentrations and 0.4 V using CP_T as CDL. 173

Figure A.53. Effect of methanol concentration on the cell performance using CP_MPL as CDL. 173

Figure A.54. Nyquist plot of a pDMFC for different methanol concentrations and 0.2 V using CP_MPL as CDL. 174

Figure A.55. Nyquist plot of a pDMFC for different methanol concentrations and 0.3 V using CP_MPL as CDL. 174

Figure A.56. Nyquist plot of a pDMFC for different methanol concentrations and 0.4 V using CP_MPL as CDL. 175

Figure A.57. Effect of methanol concentration on the cell performance using CP_MPL_T as CDL. 175

Figure A.58. Nyquist plot of a pDMFC for different methanol concentrations and 0.2 V using CP_MPL_T as CDL. 176

Figure A.59. Nyquist plot of a pDMFC for different methanol concentrations and 0.3 V using CP_MPL_T as CDL. 176

Figure A.60. Nyquist plot of a pDMFC for different methanol concentrations and 0.4 V using CP_MPL_T as CDL. 177

Figure A.61. Effect of methanol concentration on the cell performance using CC_1 as anode CC. 177

Figure A.62. Nyquist plot of a pDMFC for different methanol concentrations and 0.2 V using CC_1 as anode CC. 178

Figure A.63. Nyquist plot of a pDMFC for different methanol concentrations and 0.3 V using CC_1 as anode CC. 178

Figure A.64. Nyquist plot of a pDMFC for different methanol concentrations and 0.4 V using CC_1 as anode CC. 179

Figure A.65. Effect of methanol concentration on the cell performance using CC_3 as anode CC. 179

Figure A.66. Nyquist plot of a pDMFC for different methanol concentrations and 0.2 V using CC_3 as anode CC. 180

Figure A.67. Nyquist plot of a pDMFC for different methanol concentrations and 0.3 V using CC_3 as anode CC. 180

Figure A.68. Nyquist plot of a pDMFC for different methanol concentrations and 0.4 V using CC_3 as anode CC. 181

Figure A.69. Effect of methanol concentration on the cell performance using CC_4 as anode CC. 181

Figure A.70. Nyquist plot of a pDMFC for different methanol concentrations and 0.2 V using CC_4 as anode CC. 182

Figure A.71. Nyquist plot of a pDMFC for different methanol concentrations and 0.3 V using CC_4 as anode CC. 182

Figure A.72. Nyquist plot of a pDMFC for different methanol concentrations and 0.4 V using CC_4 as anode CC. 183

Figure A.73. Effect of methanol concentration on the cell performance using CC_1 as cathode CC. 183

Figure A.74. Nyquist plot of a pDMFC for different methanol concentrations and 0.2 V using CC_1 as cathode CC. 184

Figure A.75. Nyquist plot of a pDMFC for different methanol concentrations and 0.3 V using CC_1 as cathode CC. 184

Figure A.76. Nyquist plot of a pDMFC for different methanol concentrations and 0.4 V using CC_1 as cathode CC. 185

Figure A.77. Effect of methanol concentration on the cell performance using CC_3 as cathode CC. 185

Figure A.78. Nyquist plot of a pDMFC for different methanol concentrations and 0.2 V using CC_3 as cathode CC. 186

Figure A.79. Nyquist plot of a pDMFC for different methanol concentrations and 0.3 V using CC_3 as cathode CC. 186

Figure A.80. Nyquist plot of a pDMFC for different methanol concentrations and 0.4 V using CC_3 as cathode CC. 187

Figure A.81. Effect of methanol concentration on the cell performance using CC_4 as cathode CC. 187

Figure A.82. Nyquist plot of a pDMFC for different methanol concentrations and 0.2 V using CC_4 as cathode CC. 188

Figure A.83. Nyquist plot of a pDMFC for different methanol concentrations and 0.3 V using CC_4 as cathode CC. 188

Figure A.84. Nyquist plot of a pDMFC for different methanol concentrations and 0.4 V using CC_4 as cathode CC. 189

Figure A.85. Effect of methanol concentration on the cell performance using CC_1 as anode and cathode CC. 189

Figure A.86. Nyquist plot of a pDMFC for different methanol concentrations and 0.2 V using CC_1 as anode and cathode CC. 190

Figure A.87. Nyquist plot of a pDMFC for different methanol concentrations and 0.3 V using CC_1 as anode and cathode CC. 190

Figure A.88. Nyquist plot of a pDMFC for different methanol concentrations and 0.4 V using CC_1 as anode and cathode CC. 191

Figure A.89. Effect of methanol concentration on the cell performance using SS+Au as anode CC with an open ratio of 41 % (CC_2). 191

Figure A.90. Nyquist plot of a pDMFC for different methanol concentrations and 0.2 V using SS+Au as anode CC with an open ratio of 41 % (CC_2). 192

Figure A.91. Nyquist plot of a pDMFC for different methanol concentrations and 0.3 V using SS+Au as anode CC with an open ratio of 41 % (CC_2). 192

Figure A.92. Nyquist plot of a pDMFC for different methanol concentrations and 0.4 V using SS+Au as anode CC with an open ratio of 41 % (CC_2). 193

Figure A.93. Effect of methanol concentration on the cell performance using SS+Au as anode CC with an open ratio of 34 % (CC_1). 193

Figure A.94. Nyquist plot of a pDMFC for different methanol concentrations and 0.2 V using SS+Au as anode CC with an open ratio of 34 % (CC_1). 194

Figure A.95. Nyquist plot of a pDMFC for different methanol concentrations and 0.3 V using SS+Au as anode CC with an open ratio of 34 % (CC_1). 194

Figure A.96. Nyquist plot of a pDMFC for different methanol concentrations and 0.4 V using SS+Au as anode CC with an open ratio of 34 % (CC_1). 195

Figure A.97. Effect of methanol concentration on cell the performance using Ti as anode CC with an open ratio of 41 % (CC_2). 195

Figure A.98. Nyquist plot of a pDMFC for different methanol concentrations and 0.2 V using Ti as anode CC with an open ratio of 41 % (CC_2). 196

Figure A.99. Nyquist plot of a pDMFC for different methanol concentrations and 0.3 V using Ti as anode CC with an open ratio of 41 % (CC_2). 196

Figure A.100. Nyquist plot of a pDMFC for different methanol concentrations and 0.4 V using Ti as anode CC with an open ratio of 41 % (CC_2). 197

Figure A.101. Effect of methanol concentration on cell performance using Ti as anode CC with an open ratio of 34 % (CC_1)..... 197

Figure A.102. Nyquist plot of a pDMFC for different methanol concentrations and 0.2 V using Ti as anode CC with an open ratio of 34 % (CC_1). 198

Figure A.103. Nyquist plot of a pDMFC for different methanol concentrations and 0.3 V using Ti as anode CC with an open ratio of 34 % (CC_1). 198

Figure A.104. Nyquist plot of a pDMFC for different methanol concentrations and 0.4 V using Ti as anode CC with an open ratio of 34 % (CC_1). 199

Figure A.105. Effect of methanol concentration on the cell performance using SS+Au as cathode CC with an open ratio of 34 % (CC_1). 199

Figure A.106. Nyquist plot of a pDMFC for different methanol concentrations and 0.2 V using SS+Au as cathode CC with an open ratio of 34 % (CC_1). 200

Figure A.107. Nyquist plot of a pDMFC for different methanol concentrations and 0.3 V using SS+Au as cathode CC with an open ratio of 34 % (CC_1). 200

Figure A.108. Nyquist plot of a pDMFC for different methanol concentrations and 0.4 V using SS+Au as cathode CC with an open ratio of 34 % (CC_1). 201

Figure A.109. Effect of methanol concentration on the cell performance using Ti as cathode CC with an open ratio of 34 % (CC_1). 201

Figure A.110. Nyquist plot of a pDMFC for different methanol concentrations and 0.2 V using Ti as cathode CC with an open ratio of 34 % (CC_1). 202

Figure A.111. Nyquist plot of a pDMFC for different methanol concentrations and 0.3 V using Ti as cathode CC with an open ratio of 34 % (CC_1). 202

Figure A.112. Nyquist plot of a pDMFC for different methanol concentrations and 0.4 V using Ti as cathode CC with an open ratio of 34 % (CC_1). 203

Figure A.113. Nyquist plot of a pDMFC for different methanol:ethanol ratios, a fuel concentration of 2 M and 0.2 V. 204

Figure A.114. Nyquist plot of a pDMFC for different methanol:ethanol ratios, a fuel concentration of 2 M and 0.3 V. 204

Figure A.115. Nyquist plot of a pDMFC for different methanol:ethanol ratios, a fuel concentration of 2 M and 0.4 V. 205

Figure A.116. Nyquist plot of a pDMFC for different methanol:ethanol ratios, a fuel concentration of 3 M and 0.2 V. 205

Figure A.117. Nyquist plot of a pDMFC for different methanol:ethanol ratios, a fuel concentration of 3 M and 0.3 V. 206

Figure A.118. Nyquist plot of a pDMFC for different methanol:ethanol ratios, a fuel concentration of 3 M and 0.4 V. 206

Figure A.119. Nyquist plot of a pDMFC for different methanol:ethanol ratios, a fuel concentration of 5 M and 0.2 V. 207

Figure A.120. Nyquist plot of a pDMFC for different methanol:ethanol ratios, a fuel concentration of 5 M and 0.3 V. 207

Figure A.121. Nyquist plot of a pDMFC for different methanol:ethanol ratios, a fuel concentration of 5 M and 0.4 V. 208

Figure A.122. Nyquist plot of a pDMFC at the beginning (0 h) and at the end (200 h) of the durability tests for 0.2 V. 209

Figure A.123. Nyquist plot of a pDMFC at the beginning (0 h) and at the end (200 h) of the durability tests for 0.3 V. 209

Figure A.124. Nyquist plot of a pDMFC at the beginning (0 h) and at the end (200 h) of the durability tests for 0.4 V. 210

List of Tables

Table 1.1. Fuel cell types. 5

Table 1.2. Electrochemical reactions that take place in DMFCs and DEFCs. 6

Table 2.1. Single cell performance studies based on the parameters investigated, and the maximum power output achieved. 39

Table 2.2. Cost of the main components used in a passive DMFC and available in the market. 52

Table 4.1. Design characteristics of the different current collectors tested. 76

Table 4.2. Properties of the materials used as diffusion layers. 78

Table 5.1. Values of the different resistances obtained by fitting the Nyquist plots of the pDMFC (Figure 5.3) with the EEC proposed in this work (Figure 5.4) for different fuel cell voltages. 88

Table 5.2. Values for the different resistances of the EEC for different carbon cloths as ADL and its maximum power density. 92

Table 5.3. Values for the different resistances of the EEC for different carbon papers as ADL and its maximum power density. 94

Table 5.4. Values of the different resistances of the EEC for different carbon cloths tested as cathode DL and its maximum power density. 97

Table 5.5. Values of the different resistances of the EEC for different carbon papers tested as cathode DL and its maximum power density. 100

Table 5.6. Values for the different resistances of the EEC for different methanol concentrations its maximum power density. 102

Table 5.7. Methanol and ethanol ratios used for the different fuel concentrations: 2 M, 3 M and 5 M 103

Table 5.8. Values for the different resistances of the EEC for the pDMFC tested with different methanol:ethanol ratio and its maximum power densities 105

Table 5.9. Values of the different resistances in the EEC for different CC designs tested on the anode side and its maximum power density; cathode CC_2. 109

Table 5.10. Values of the different resistances in the EEC for different CC designs tested on the cathode side and its maximum power density; anode CC_2. 111

Table 5.11. Values of electrical conductivity and costs for different materials used as CCs. 113

Table 5.12. Values for the different resistances of the EEC for different materials tested as CCs on both anode and cathode sides and its maximum power density. 115

Table 5.13. Values for the different resistances of the EEC at the beginning (0 h) and at the end (200 h) of the two durability tests and its maximum power density 120

Table 5.14. Price of the different materials tested as anode and cathode DL (values obtained from QuinTech and Fuel Cells Etc) and total DL cost (25 cm^2). 121

Table 5.15. Cost of a 3-layer MEA for pDMFC systems. 121

Nomenclature

a	specific surface area of the anode (cm^{-1}) (Equations (2.17))
C	capacitor
$C_{CH_3OH}^{AC}$	methanol concentration at the anode catalyst layer (mol/cm^3)
$C_{O_2}^{CC}$	oxygen concentration at the cathode catalyst layer (mol/cm^3)
$C_{O_{2,ref}}^{CC}$	oxygen reference concentration (mol/cm^3)
CPE	constant phase element
e^-	electron
E_{cell}	thermodynamic equilibrium potential (V)
F	Faraday constant (C/mol)
I	current (A)
I_{cell}	cell current density (A/cm^2)
I_{CH3OH}	leakage current density due to methanol crossover (A/cm^2)
$I_{0,ref}^{CH_3OH}$	exchange current density of methanol (A/cm^2)
$I_{0,ref}^{O_2}$	exchange current density of oxygen (A/cm^2)
k	constant in the rate expression (Equation (2.17))
L	inductor
n	number of electrons
R	ideal law gas constant (J/(molK)) (Equations (2.17) and (3.6))
R	resistor
R_{act}	resistance due to activation losses (Ω)
R_A	activation resistance due to the anode reaction (Ω)
R_C	activation resistance due to the oxygen reduction reaction (Ω)
$R_{Crossover}$	activation resistance due to the methanol oxidation at the cathode (Ω)
R_{mt}	resistance due to mass transport losses (Ω)
R_{Ohm}	resistance due to ohmic losses (Ω)
R_Ω	ohmic resistance (Ω)
T	temperature (K)
T_{AC}	temperature at the anode catalyst layer (K)
T_{CC}	temperature at the cathode catalyst layer (K)

V	Voltage (V)
W	Warburg element
W_{actual}	actual electric work (W)
$W_{maximum}$	maximum work (W)

Greek symbols

ΔE	variation of thermodynamic equilibrium potential (V)
ΔG	variation of Gibbs free energy (kJ/kg)
ΔH	variation of enthalpy of reaction (kJ/kg)
ΔS	variation of entropy of reaction (kJ/K)
α	net water transfer coefficient
α_A	anodic transfer coefficient
α_C	cathodic transfer coefficient
η	overpotential (V) or total energy efficiency
η_A	anodic overpotential (V)
η_C	cathodic overpotential (V)
η_{fuel}	fuel efficiency
η_{rev}	thermodynamic efficiency
$\eta_{voltaic}$	voltaic efficiency
λ	constant in the rate expression
σ_i	Warburg coefficient for species *i*
ω	radial frequency (Hz)

List of Abbreviations

1D	One Dimension
2D	Two Dimensions
3D	Three Dimensions

AC	Anode Catalyst layer (Figure 2.1)
AC	Alternating Current
AD	Anode Diffusion layer (Figure 2.1)
ADL	Anode Diffusion Layer
ADT	Accelerated Degradation Test
AFC	Alkaline Fuel Cell
BL	Backing Layer
CC	Current Collector
CC	Carbon cloth (thickness of 0.400 mm)
CC	Cathode Catalyst layer (Figure 2.1)
CC_1	Current collector with an open ratio of 34 %
CC_2	Current collector with an open ratio of 41 %
CC_3	Current collector with an open ratio of 64 %
CC_4	Current collector with an open window frame
CC_MPL	Carbon cloth with MPL (0.410 mm)
CC_MPL_E	ELAT Carbon cloth with MPL (0.454 mm)
CC_T	Carbon cloth a higher thickness (0.425 mm)
CD	Cathode Diffusion layer (Figure 2.1)
CDL	Cathode Diffusion Layer
CE	Counter Electrode
CFD	Computational Fluid Dynamics
CNFs	Carbon Nanofibers
CNT	Carbon nanotube
CP	Carbon paper (0.110 mm)
CP_MPL	Carbon paper with MPL (0.240 mm)
CP_MPL_T	Carbon paper with MPL and a higher thickness (0.340 mm)
CP_T	Carbon paper with a higher thickness (0.190 mm)
CPSR	Capillary Pressure and Saturation Relation
CV	Cyclic Voltammetry
DAFC	Direct Alcohol Fuel Cell
DEFC	Direct Ethanol Fuel Cell
DHE	Dynamic Hydrogen Electrode
DL	Diffusion Layer

DMFC	Direct Methanol Fuel Cell
DOE	U.S. Department of Energy
EEC	Equivalent Electric Circuit
EIS	Electrochemical Impedance Spectroscopy
EMCCs	Expanded Metal Mesh Current Collectors
FC	Fuel Cell
FRA	Frequency Response analyser
FSPES-x	Cardo poly(arylene ether sulfone/nitrile)
G-CNTs	Graphene – Carbon Nanotubes
GE	General Electric
GO	Graphene Oxide
HC	High Concentration
IAS	Integrated Anode Structure
MC	Mesoporous carbon
MCFC	Molten Carbonate Fuel Cell
MEA	Membrane Electrode Assembly
MFC	Microbial Fuel Cell
MPL	Microporous Layer
MWCNTs	Multi-walled Carbon Nanotubes
NASA	National Aeronautics and Space Administration
NNCL	Nanofiber network catalyst layer
OCV	Open Circuit Voltage
ORR	Oxygen Reduction Reaction
PAFC	Phosphoric Acid Fuel Cell
PDDA	Poly(diallyldimethylammonium chloride)
pDMFC	Passive Direct Methanol Fuel Cell
PEM	Polymer Electrolyte Membrane
PEMFC	Polymer Electrolyte Membrane Fuel Cell
PEO	Plasma Electrolytic Oxidation
PMFSF	Porous Metal-Fibre Sintered Felt
PPNNs	Polypyrrole nanowire networks
PTFE	Polytetrafluorethylene
RE	Reference Electrode

rGO	Reduced Graphene oxide
RS	Raman Spectroscopy
SAC	Sulfonated Activation Carbon
SEM	Scanning Electron Microscopy
SGO	Sulfonated Graphene Oxide
SOFC	Solid Oxide Fuel Cell
SPE-x	Sulfonated cardo poly(arylene ether sulfone)
SPP-co-PAEK	Sulfonated poly(p-phenylene-co-aryl ether ketone
SRSR	Star-run-stop-run
SS	Stainless steel
SS+Au	Gold plated stainless steel
SSFF	Stainless-steel Fibre Felt
TEM	Transmission Electron Microscopy
U.S.	United States
WAMD	Water/Air Management Device
WCFF	Woven Carbon-Fibre Fabric
WE	Working Electrode
XPS	X-ray Photoelectron Spectroscopy

TABLE OF CONTENTS

CHAPTER 1 ..... **1**
1. INTRODUCTION TO FUEL CELLS TECHNOLOGY **1**
1.1. Why fuel cells? 1
1.2. Historical perspective of fuel cells 1
1.3. Fuel cells working principle 3
1.4. Fuel cell types and target applications 4
1.5. Advantages and Disadvantages 6
1.6. Objectives 7
1.7. Thesis structure 7
CHAPTER 2 ..... **9**
2. PASSIVE DIRECT METHANOL FUEL CELLS **9**
2.1. Introduction 9
2.2. Operating principle and challenges 11
2.3. Fundamentals 15
2.3.1. Components 15
2.3.1.1. Polymer electrolyte membrane 15
2.3.1.2. Catalyst layers 16
2.3.1.3. Diffusion layers 17
2.3.1.4. Current collectors 18
2.3.1.5. End plates 19
2.3.2. Performance evaluation 19
2.3.2. Anode and cathode kinetics 22
2.4. Two-phase flow phenomena 25
2.4.1. Carbon dioxide in the anode 26
2.4.2. Liquid water in the cathode 28
2.5. Mass transport 32
2.5.1. Methanol crossover 32
2.5.2. Water management 35
2.6. Single cell performance 38
2.7. Mathematical modelling 46
2.8. Lifetime/Durability 48
2.9. Economic evaluation 50

2.10. Applications 52
2.11. Summary 55
CHAPTER 3 57
3. ELECTROCHEMICAL IMPEDANCE SPECTROSCOPY 57
3.1. Introduction 57
3.2. Electrochemical Impedance Spectroscopy 58
3.2.1. EIS measurements 59
3.2.2. Impedance Spectrum: Nyquist Plot 60
3.2.3. Equivalent electric circuit (EEC) 62
3.3. EIS in passive DMFCs 63
3.3.1. Diffusion layers 63
3.3.2. Catalyst layers 64
3.3.3. Membrane 66
3.3.4. Current collector 66
3.3.5. Water crossover 67
3.3.6. Manufacturing method 68
3.3.7. Lifetime/durability 68
3.4. Summary 71
CHAPTER 4 73
4. EXPERIMENTAL SETUP FOR A PASSIVE DMFC 73
4.1. Fuel cell design 73
4.1.1. End plates and insulating plates 74
4.1.2. Current collectors 75
4.1.3. Membrane electrode assembly (MEA) 77
4.1.4. Diffusion layers 77
4.2. Test station 78
4.3. Experimental procedure 79
4.3.1. Polarisation measurements 79
4.3.2. EIS measurements and EEC fitting 80
4.3.3. Durability test 80
CHAPTER 5 83
5. EXPERIMENTAL RESULTS AND DISCUSSION 83
5.1. Electrochemical impedance spectroscopy 84
5.2. Effect of anode diffusion layer properties 89
5.2.1. Effect of carbon cloth as anode DL 90

5.2.2. Effect of carbon paper as anode DL 92
5.3. Effect of cathode diffusion layer properties 95
5.3.1. Effect of carbon cloth as cathode DL 95
5.3.2. Effect of carbon paper as cathode DL 98
5.4. Effect of methanol concentration 100
5.5. Effect of methanol:ethanol ratio 102
5.6. Effect of current collector design 106
5.6.1. Effect of anode current collector design 106
5.6.2. Effect of cathode current collector design 109
5.7. Effect of current collector material 112
5.8. Durability 118
5.9. Economic evaluation 120
5.10. Summary 122
CHAPTER 6 125
6. CONCLUSIONS AND FUTURE WORK 125
6.1. Conclusions 125
6.2. Future work 127
REFERENCES 129
APPENDIX A: POLARISATION AND EIS DATA 147
A.1. Effect of anode diffusion layer properties 147
A.2. Effect of cathode diffusion layers properties 163
A.3. Effect of anode current collector design 177
A.4. Effect of cathode current collector design 183
A.5. Optimised current collectors design 189
A.6. Effect of anode current collector material 191
A.7. Effect of cathode current collector material 199
A.8. Effect of methanol:ethanol ratio 203
A.9. Durability 208

CHAPTER 1

1. INTRODUCTION TO FUEL CELLS TECHNOLOGY

1.1. Why fuel cells?

Nowadays, each time more, people depend on energy sources to carry out its basic needs, which is a problem because still the main source of energy is from fossil fuels, such as coal, oil and natural gas. However, fossil fuels are limited and finite, so they will be depleted someday. Besides that, fossil fuels are harmful for the environment, causing several pollution problems in the air, water and soil. Fuel cells emerge as an efficient and more environmentally friendly solution than fossil fuels and a complement to renewable energy.
In this situation, fuel cells excel among different technological routes generating electrical energy, because they are electrochemical devices that convert a fuel directly into electrical energy without combustion and involving any moving parts. As long as the fuel is supplied, the fuel cell will continue to generate its main product, electricity. A fuel cell operates quietly and efficiently, and when hydrogen is used as fuel and oxygen as oxidant, it generates only power and water. The typical reactants for fuel cells are hydrogen and oxygen. However, hydrogen may be present either mixed with other gases (such as CO_2, N_2, and CO) or in hydrocarbons such as natural gas and CH_4, or even in liquid hydrocarbons such as methanol (CH_3OH) and ethanol (CH_2CH_3OH). Ambient air contains enough oxygen to be used in fuel cells [1]. When a fuel cell runs with hydrocarbons, besides generating electricity and water it also produces a small amount of CO_2. However, as the use of these devices has potential to substitute a part of the non-green electricity from the grid, the balance is positive regarding CO_2 emissions.

1.2. Historical perspective of fuel cells

The first fuel cell was demonstrated by Sir William Grove in 1839, but only in 1842 this fuel cell, called at the time a gaseous voltaic battery, produce electrical energy by combining, hydrogen and oxygen. The system developed by Grove was made up of platinum electrodes inside glass tubes that were inverted and immersed in diluted sulphuric acid where one tube

contained hydrogen and the other oxygen. When these tubes were immersed in the solution, an electric current began to flow between the two electrodes and water was formed. However, the current produced was very small, so Grove linked several of these devices in series to increase the voltage.

In 1889, Ludwig Mond and Charles Langer adopted the expression “fuel cell” and attempted to build the first practical device using air and industrial coal gas, but this was unsuccessful. Friedrich Wilhelm Ostwald, founder of the field of physical chemistry, provided much of the theoretical understanding on how fuel cells operate, relating their physical properties and chemical reactions. This exploration was the groundwork for later fuel cell researchers.

Francis Thomas Bacon, in 1932, started working on a practical fuel cell. He improved the device developed by Mond and Langer, replacing the platinum electrodes by nickel electrodes, which are less expensive. He also used a less corrosive alkali electrolyte (potassium hydroxide) instead of sulphuric acid. This device was the first alkaline fuel cell, which he named the "Bacon Cell". However, it was only in 1959 that Bacon demonstrated a device capable of producing 5 kW of power, enough to power a welding machine. The first practical alkaline fuel cell applications were in the U.S. by National Aeronautics and Space Administration (NASA) during the Apollo project, as one of the sources of energy and water for space travel. These fuel cells were built by Pratt & Whitney, aircraft engine manufacturers who obtained the license for Bacon’s patents and improved the original design, reducing their weight and making them longer-lasting. Alkaline fuel cells have been used ever since in most manned U.S. space missions until today, including those of the Space Shuttle.

In 1955, two scientists who worked at General Electric (GE), modified the original fuel cell design. Willard Thomas Grubb used a sulphonated polystyrene ion-exchange membrane as the electrolyte and three years later, Leonard Niedrach developed a way of depositing platinum onto this membrane, which resulted in the "Grubb-Niedrach fuel cell". Then GE and NASA worked together on the development of this technology and the first cells with polymer electrolyte membrane were used in the Gemini space project. The first fuel cell-powered buses were shown in 1993 by Ballard Power Systems, while in the same year Energy Partners demonstrated the first passenger car running on a polymer electrolyte membrane (PEM) fuel cell.

In 2005, the Kyoto Protocol came into force with the intention of contain the emissions of gases responsible for the greenhouse effect. With this agreement, the interest in fuel cells

increased greatly, mainly in the transport sector. Therefore, major manufacturers in the automotive industry developed and have several car prototypes in circulation with different types of fuel cells, but none of them has reached the market in a widespread way.

Since 2014, Hyundai, Toyota and Honda have been marketing vehicles powered by polymer electrolyte membrane fuel cells fed by hydrogen, like Hyundai ix35 Fuel Cell, Toyota Mirai and Honda Clarity, respectively. In these vehicles, the hydrogen is stored in high-pressure tanks and its supply takes a few minutes. This fuel cell system is more efficient than an internal combustion engine and does not emit greenhouse-gases, like CO_2 or any other pollutant. The product coming out from these fuel cells is only water.

1.3. Fuel cells working principle

As already mentioned, fuel cells are devices that convert chemical energy from a fuel by electrochemical reactions directly into electrical energy. The electrons generated by an electrochemical reaction pass through an external circuit, resulting in an electrical energy transfer.

The general working principle of a fuel cell consists of an electrolyte that is in contact with two electrodes, an anode where the oxidation reaction occurs liberating electrons and a cathode where the reduction reaction, eager for electrons, takes place (Figure 1.1). Both the anode and the cathode are porous and include the catalyst layers. The fuel is supplied in the anode and the oxidant (usually oxygen) feeds the cathode. This supply must be continuous in order to produce electricity. At high current densities, the demand for reactants is very high, which can make this process more complex.

The electric current generated by the fuel cell is directly related with the reaction rates of the electrochemical reactions that take place at the anode and cathode sides. Thus, catalysts are used to increase the velocity and efficiency of these reactions.

A thin electrolyte layer separates the fuel and the oxidant, ensuring that the two half reactions occur isolated from each other, and makes possible the transport of protons from the anode to the cathode. The fuel cell reactions will also generate products and heat. These products must be removed from the fuel cell, otherwise, they will accumulate and prevent the reactants further reaction.

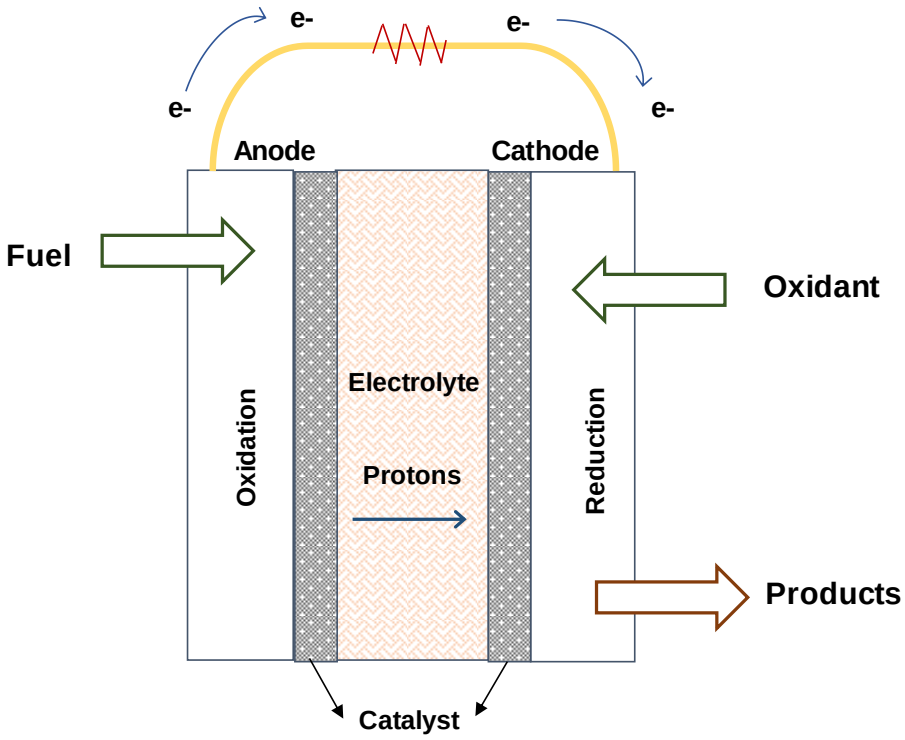

Figure 1.1. General working principle of a fuel cell.

1.4. Fuel cell types and target applications

Fuel cells are classified according to the electrolyte and fuel used, thereby, they will operate at different operating temperatures and with different materials. Therefore, each fuel cell type will have a different electrical efficiency, characteristics and main applications (Table 1.1).

As can be seen in Table 1.1, DAFCs are similar to the PEMFC since both use a polymer membrane as electrolyte and H^+ as the charge carrier. DAFCs are one of the most promising fuel cells types, for portable applications, due to their high energy density, simple structure and instant recharging. The use of liquid fuels usually produces a higher volumetric energy density and suppress the complex problem of the PEMFC regarding the hydrogen gas production, storage and distribution [2]. As another advantage, it can be stated that the DAFCs can be operated at ambient temperature, which significantly reduces the thermal management challenges for small systems. In this way, the DAFCs become a technology attractive for powering portable electronic devices. However, DAFCs have slow anode kinetics that result in higher anodic overpotentials, since the alcohol oxidation reaction

occurs by multi steps, which can lead to the formation of undesirable intermediates, as carbon monoxide (CO), that poisons the cell [3]. Other disadvantage is the fuel crossover through the membrane (electrolyte) from the anode to the cathode, which decreases the fuel utilisation, degrades the cathode performance and, consequently the overall cell performance.

Table 1.1. Fuel cell types.

Fuel cell type	***Electrolyte***	***Charge carrier***	***Operating Temperature***	***Fuel***	***Electrical Efficiency***	***Target applications***
Polymer Electrolyte Membrane Fuel Cell (PEMFC)	Polymer membrane	H^+	20 – 100 °C	Hydrogen	40 – 50 %	Transportation, small-scale stationary power generation, backup power.
Direct Alcohol Fuel Cell (DAFC)	Polymer membrane	H^+	20 – 80 °C	Alcohol, such as methanol, ethanol, propanol, glycerol.	40 – 50 %	Portable applications, backup power.
Alkaline Fuel Cell (AFC)	Liquid potassium hydroxide	OH^-	60 – 220 °C	Hydrogen	50 %	Stationary power generation.
Phosphoric Acid Fuel Cell (PAFC)	Liquid phosphoric acid	H^+	≈ 220 °C	Hydrogen	40 %	Stationary power generation.
Molten Carbonate Fuel Cell (MCFC)	Molten carbonate	CO_3^{2-}	≈ 650 °C	Hydrogen and methane	45 – 55 %	Stationary power generation.
Solid Oxide Fuel Cell (SOFC)	Ceramic	O^{2-}	600 – 1000 °C	Hydrogen, methane and carbon monoxide	50 – 60 %	Stationary power generation, auxiliary power unit.
Microbial Fuel Cell (MFC)	Polymer membrane	H^+	20 – 50 °C	Organic matter	15 - 65 % (Columbic efficiency)	Electricity production and wastewater treatment.

Alcohols, such as methanol and ethanol, are the most used fuels for DAFCs, leading to two specific types of fuel cells, the Direct Methanol Fuel Cells (DMFCs) and the Direct Ethanol Fuel Cells (DEFCs). Propanol, glycerol and ethylene glycol are also used, but in a less extent. Table 1.2 displays the electrochemical reactions that occur on both DMFCs and DEFCs and as can be seen, the alcohol oxidation occurs at the anode side, releasing protons and electrons and producing also a small amount of carbon dioxide. The protons pass through the electrolyte to the cathode while the electrons flow through an external circuit producing

electric power. At the cathode, the oxygen (usually from air) reacts with the electrons and protons, producing water.

Table 1.2. Electrochemical reactions that take place in DMFCs and DEFCs.

Reactions	***Fuels***	
	Methanol	*Ethanol*
Anode	$CH_3OH + H_2O \rightarrow CO_2 + 6H^+ + 6e^-$	$C_2H_5OH + 3H_2O \rightarrow 2CO_2 + 12H^+ + 12e^-$
Cathode	$O_2 + 4H^+ + 4e^- \rightarrow 2H_2O$	$3O_2 + 12H^+ + 12e^- \rightarrow 6H_2O$
Overall	$CH_3OH + \frac{3}{2}O_2 \rightarrow CO_2 + 2H_2O$	$C_2H_5OH + 3O_2 \rightarrow 2CO_2 + 3H_2O$

1.5. Advantages and Disadvantages

Fuel cells, which produce electricity directly from chemical energy, are often more efficient than combustion engines and have some advantages over batteries. Therefore, this technology has several applications, as mentioned before, according to their attractive properties. The fuel cell emissions when hydrogen is used as fuel is zero, since only water is produced. If the system is supplied with methanol, e.g., some emissions are generated, like carbon dioxide, although these emissions are lower than those of the conventional technologies. Since fuel cells do not have any moving parts, they are mechanically ideal. Without moving parts, fuel cells are silent, highly reliable and expected to exhibit a longer life. Fuel cells can be scaled at different sizes, adaptable to power from small electronic devices to power plants. Fuel cell systems do not require a time-consuming recharge like batteries.

Despite presenting interesting advantages, fuel cells also present some disadvantages. Cost is a dominant drawback for the implementation of these devices. The platinum catalyst used in fuel cells, needed to promote the power generation reaction, is an expensive material, leading to prohibitive costs for its real applications and commercialisation. Another disadvantage concerns the hydrogen gas, since is not widely available and its production processes are expensive and usually demand the use of fossil fuels. Besides that, hydrogen has a low volumetric energy density and is difficult to store. Its power density, that represents how much power a fuel cell can produce per active area, is another significant limitation, since is lower than the desirable. Therefore, before fuel cells commercialisation, further

improvements are required and different technological solutions should be developed, to overcome these disadvantages and promote its spreading use.

1.6. Objectives

Passive DMFCs have been enthusiastically investigated as portable power sources due to their high power density, rapid recharging and compact size. Therefore, the motivation for this work was the optimisation of a passive DMFC, using commercial components, aiming its optimisation and effective applications of this type of fuel cells in portable electronic devices.

The main goal of this work was to achieve the optimal performance of an in-house passive DMFC based on the selection of the best operation conditions and structural parameters, in order to obtain the information needed to build a prototype of a mobile phone charger working with this technology.

This work starts with the evaluation of the effect of methanol concentration and configuration components of the passive DMFC, such as diffusion layers materials and properties, and current collectors with different designs and materials on the fuel cell behaviour and power output. MEAs proposed in this work use materials commercially available, aiming to achieve the highest power density, with high methanol concentrations and low methanol and water crossover rates.

The passive DMFC behaviour, for the different conditions tested, was analysed through polarisation measurements and, for the first time on group, through electrochemical impedance spectroscopy (EIS) measurements. Therefore, besides the development of the methodology needed to perform these measurements and its implementation, this work intended also to develop an equivalent electric circuit used to fit the EIS data, and access the meaningful properties of the system under study.

1.7. Thesis structure

The research activities conducted in the present work were carried out at CEFT (Centro de Estudos de Fenómenos de Transporte) in the Chemical Engineering Department of Faculty of Engineering in University of Porto (FEUP).

This thesis is organized in six principal chapters. Chapter 1 considers a general introduction regarding the fuel cells technology with a description of their working principle and also presenting different fuel cell types and its main applications, and a general view on the main advantages and disadvantages of fuel cells.

Chapter 2 is dedicated to the passive DMFCs' state-of-the-art including its operating principle, fundamentals, such as components, performance evaluation and anode and cathode kinetics, the main critical challenges of this technology (two-phase flow phenomena, methanol crossover, water management, durability and costs), single cell design and performance and mathematical modelling.

In Chapter 3, a review of EIS technique is presented, describing the measurements methodology, the data interpretation by fitting with an equivalent electric circuit and some applications of this technique with special focus in passive DMFCs.

Chapter 4 is devoted to the experimental setup and experimental procedure description.

Chapter 5 presents the experimental results obtained towards the optimisation of a passive DMFC, as well as its performance evaluation by polarisation curves and EIS measurements.

Finally, the main conclusions of the present work and suggestions for future work are outlined in Chapter 6.

CHAPTER 2

2. PASSIVE DIRECT METHANOL FUEL CELLS

Direct methanol fuel cells (DMFCs) are in the Energy Agenda due to their market potential to replace the conventional batteries in portable applications, either for recreational, professional, military and medical purposes, since they enable the direct conversion of the chemical energy stored in a fuel, methanol, to electrical energy with water and carbon dioxide as final products. Additionally, DMFCs offer higher energy densities than batteries, longer runtime, instant recharging, use a liquid fuel, operate at room temperature and can rely on a passive flow of reactants, making possible to operate the cell without any additional power consumption. Therefore, in the last years, the passive DMFCs systems, where the fuel and the oxidant are feed in a passive mode, have been studied and some progress towards its commercialization has already been achieved. However, the current systems still have higher costs, lower durability and power outputs, due to the slow electrochemical reactions, water and methanol crossover and an inefficient products removal from the anode (gaseous carbon dioxide) and cathode sides (liquid water), which may hinder the fuel and the oxidant supply to the reaction zone.

This chapter discusses the key work developed in order to improve the passive DMFC performance based on the challenges of this technology. The main goal is to provide a review on the most recent developments in passive DMFCs, on the recent work concerning the optimisation of the operating and design conditions and on empirical and fundamental modelling. This chapter starts by a brief introduction recalling the passive DMFCs technology followed by a description of the fundamentals of these systems. Then an intensive review on the recent experimental and modelling works performed with these cells is presented. Towards the introduction of passive DMFCs in the market, studies regarding its lifetime and durability, as well as a cost benefit analysis where this technology is compared with the traditional ones is also presented.

The contents of this Chapter were published in Braz, B.A., Oliveira, V.B and Pinto, A.M.F.R., "Recent developments in passive direct methanol fuel cells" in Direct Methanol Fuel Cells: Applications, Performance and Technology, Nova Science Publishers, 2017, 143-203.

2.1. Introduction

In the last years, the interest in the different types of fuel cells (FCs) has increased drastically, since they were identified as a promising power source for transportation, stationary and portable electronic devices [4, 5]. This was due to their ability to convert the chemical energy of a fuel directly into electrical energy, to the fact that have zero or low emissions and the absence of moving parts. Moreover, regarding the portable applications the traditional batteries are becoming inadequate to the energy demand of the new devices due to an increase of its functionalities. Nowadays the mobile phones incorporate graphics and games, internet service, instant messaging and are even helpful to find a restaurant or a museum. The consumers demand encouraged researchers to find alternative portable power sources to overcome limitations of the conventional batteries. The target technology was the direct methanol fuel cells (DMFCs) since they offer high energy densities than batteries, longer runtime, instant recharging, use a liquid fuel, allow the operation of the cell under ambient conditions (room temperature and pressure) and with the advance of micromachining technologies, fuel cell miniaturization promises higher efficiency, performance and lower costs [6, 7].

There are two types of fuel and oxidant supply in a DMFC: active and passive. Active systems use extra components to feed and manage the fuel and the oxidant, such as pump and blowers, allowing the operation of the fuel cell under favourable conditions regarding the fuel cell temperature, pressure, reactants concentration and flow rate. However, these systems need an input of energy, have lower system energy densities, are more complex and have higher sizes and costs, being for that reasons unsuitable for portable applications. Passive systems use natural transport mechanisms – diffusion, convection and evaporation – to achieve all the processes without any additional power consumption. Therefore, compared to active systems, passive ones enable a more compact and simpler design, since in this case the space assigned for pumps, fans and tubing is used for the fuel reservoir, thus increasing the whole system energy capacity. In addition, these systems do not have any additional power consumption, have a fast refuelling and the fuel can last several months. Consequently, they become more suitable for portable power sources and major efforts are being made towards the development of optimised passive DMFC systems. However, besides the common challenges of the two feed systems (higher costs, lower durability and power outputs due to the slow electrochemical reactions, water and methanol crossover and

an inefficient product removal from the anode and cathode sides) the passive systems also suffer from the difficulty in getting a continuous and homogeneous supply of reactants.
In the last years, many advances have been achieved in the DMFC technology and different review articles, with diverse targets, are available in literature. These include the following: anode and cathode catalysts [6, 8–14], MEA preparation, procedure and materials [12–18], cell design and performance [13, 14, 18–25] , current collectors [13, 14, 26], operating conditions [13, 18–21, 24], costs [6–8, 10, 13 14, 27], DMFC challenges (methanol crossover, water and heat management) [6, 13, 18, 20–22, 24, 27, 28] durability and stability [8, 13, 14, 27] , applications [6, 16, 21, 28], modelling [25, 29, 30] and stacks and prototypes [21].
Based on the review articles already published and due to a lack of a recent work regarding the experimental and modelling studies and the challenges of the passive DMFCs, the main goal of this chapter is to provide a recent review concerning these issues. This chapter aims to be a useful and powerful tool for researchers who already work with this technology and those that want to start working in the field in order to promote optimisation and massive commercialization of passive DMFCs.

2.2. Operating principle and challenges

A DMFC is an electrochemical device that transforms the chemical energy into electric energy based on the methanol oxidation and oxygen reduction reactions and using a polymer electrolyte membrane (PEM) as the electrolyte. This polymer is permeable to protons who are the ionic charge carrier. A typical passive DMFC comprises an end plate with a fuel reservoir, a current collector, a diffusion layer (AD) and a catalyst layer (AC) at the anode side, a proton exchange membrane (PEM) and a catalyst layer (CC), a diffusion layer (CD), a current collector and an end plate opened to the surroundings at the cathode side (Figure 2.1). The most important component of this system is the membrane electrode assembly (MEA), formed by sandwiching the PEM between an anode and a cathode electrode (catalyst layer and diffusion layer). Upon hydration, the PEM shows good proton conductivity. On both sides of the PEM, there are the catalyst layers where the reactions take place, outside of these layers, diffusion layers are put to optimise the distribution of the fuel and oxidant towards the catalyst layers and the products removal towards the anode and

cathode outlets. Outside of the MEA, there are the current collectors to provide the current collection and the structure is closed with end plates.

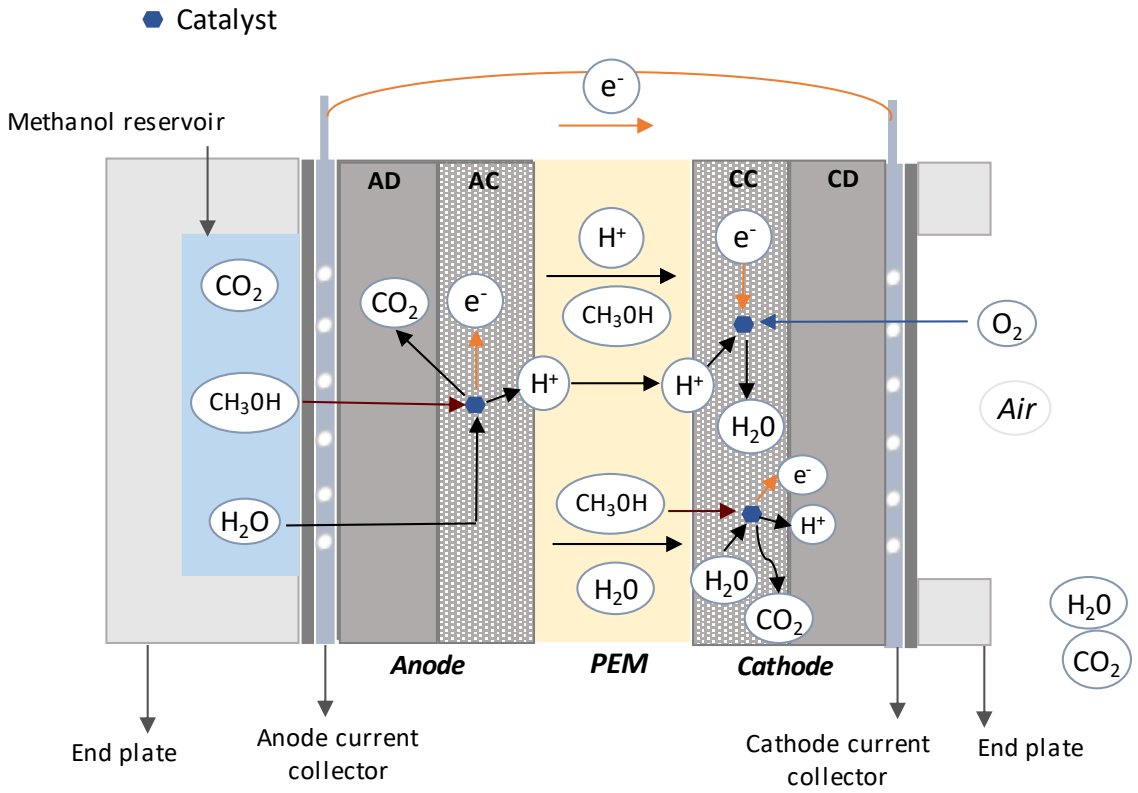

Figure 2.1. Schematic representation of a conventional passive DMFC.

As can be seen in Figure 2.1, methanol or an aqueous methanol solution is introduced on the anode reservoir. The reactant diffuses through the anode diffusion layer towards the anode catalyst layer where it is oxidized producing carbon dioxide, protons and electrons.
The oxidation reaction that occurs at the anode catalyst layer is given by:

$$CH_3OH + H_2O \rightarrow CO_2 + 6H^+ + 6_{e-} \quad (2.1)$$

The carbon dioxide generated emerges as bubbles and diffuses through the anode diffusion layer towards the anode end plate, since the membrane is almost impermeable to gases. The protons are transported through the membrane and the electrons through the external circuit, both, to the cathode side. Simultaneously, air is fed to the cathode side by natural convection and the oxygen is transported by diffusion through the cathode diffusion layer towards the

cathode catalyst layer, where it reacts with electrons and protons to form water. This reduction reaction is given by:

$$O_2 + 4H^+ + 4_{e-} \rightarrow 2H_2O \quad (2.2)$$

The water produced moves counter-currently towards the cathode outlet via the cathode diffusion layer and under some operating conditions, by back diffusion towards the anode. The overall reaction occurring in a DMFC is:

$$CH_3OH + \frac{3}{2} O_2 \rightarrow CO_2 + 2H_2O \quad (2.3)$$

It is commonly accepted by the scientific community that to achieve the desirable levels of energy density, costs and lifetime, the passive DMFC systems must overcome the following key challenges:

1) Low rate of methanol and oxygen kinetics;
2) Methanol and water crossover;
3) Two-phase flow patterns;
4) Higher costs;
5) Lower Durability/Lifetime.

One of the major disadvantages of using methanol as fuel is the slow anode kinetics arising from a multi-step fuel oxidation process, which result in higher anodic overpotentials. To overcome this difficulty, it would be desirable to use higher methanol concentrations, however these conditions generate higher rates of fuel crossover through the membrane towards the cathode side. This leads to a decrease of the cell performance due to a lower potential at the anode side, the formation of a mixed potential on the cathode side and a loss of the available fuel. Traditionally, a DMFC operates with diluted methanol solutions to avoid this drawback. However, more concentrated solutions are needed to achieve the energy densities requirements for portable applications. Additionally, low methanol concentrations lead to a higher water content on the anode reservoir and consequently at the anode side. This water tends to cross the membrane towards the cathode side causing a water loss from

the anode and thus, make-up of water is needed. In addition, a high rate of water crossover increases the possibility of cathode flooding, decreasing the fuel cell performance. To solve these two problems, a deep knowledge of the influence of the different design and operating parameters on water and fuel transport is mandatory for the design of ground-breaking passive DMFC systems [6, 13, 18, 20–22, 24, 27, 28].

As already referred, an important issue in DMFC technology is the two-phase flow pattern that occur both on the anode and cathode side due to the formation of gaseous CO_2 and liquid water, respectively. An efficient product removal is crucial to obtain higher performances, since bubbles and drops tend to remain attached to the catalyst limiting the continuous supply of reactants. Therefore, understanding the two-phase flow is crucial to develop an air breathing operation. Hence, both numerical and visualisation studies are needed to clearly understand the dynamic effects of the two-phase flow on the fuel cell performance optimisation [31–46].

The DMFC efficiency is limited by the reactions occurring at both electrodes (anode and cathode), since the slow kinetics of these reactions lead to significant potential losses. Moreover, even using the current state-of-the-art catalysis for each reaction (Pt/Ru at the anode and Pt at the cathode) until now, it is only possible to reach reaction efficiencies of about 25-35 % [6, 8–14]. Additionally, to achieve these efficiencies the catalyst loadings recommended are approximately 4 mg/cm^2 at the anode and 4 mg/cm^2 at the cathode. However, both Pt and Ru are expensive and represent a major fraction on the total system cost [6, 8, 10, 13, 14, 27]. While new low cost catalysts are not commercially available, the solution is to reduce the loadings of the available ones by improving its activity with higher surface areas, by controlling the particles size distribution, morphology and crystallinity [6, 8–14].

Degradation is another important challenge to overcome on the DMFC technology. Studies have shown a power density loss with the operation time of 30 %. This was primarily due to the delamination of the catalyst layer and agglomeration of the catalyst particles, which lead to a loss of the electrochemical active surface area of the catalysts and membrane degradation [8, 13, 14, 27]. Although the loss of efficiency is unavoidable, the degradation rate can be minimized through an understanding of the degradation and failure mechanisms.

2.3. Fundamentals

The present section deals with the fundamentals of a DMFC, describing with some detail its mains components and properties, its performance evaluation and anode and cathode kinetics.

2.3.1. Components

As referred, the main part of a DMFC is the MEA, which is composed by a diffusion layer (AD) and a catalyst layer (AC) at the anode side, a polymer electrolyte membrane (PEM) and a catalyst layer (CC) and a diffusion layer (CD) at the cathode side (Figure 2.1). The MEA is sandwiched between the current collectors, that provide the pathways for the flow of reactants and products, give mechanical support to the MEA and collect the electrons. Finally, end plates are used for bracing the cell and perform the cell assembly.

2.3.1.1. Polymer electrolyte membrane

The membrane plays an essential role in a DMFC, since it is responsible for the protons transport from the anode to the cathode side. Therefore, the PEM must have a high proton conductivity, which is favoured by its hydration, must be a barrier to the mixing of fuel and reactant gases and chemically and mechanically stable in the fuel cell environment. The membranes for DMFCs are made of organic polymers, which ions are added, i.e., are ionomers obtained through of copolimerisation of monomeric units of perfluorosulfonate and tetrafluorethylene resulting in a perfluorocarbon-sulfonic acid ionomer, with a sulfonic ion (SO_3^-) and a H^+ ion at the end of the chain. The most-known membrane used in fuel cells is Nafion®, developed by Dupont. Figure 2.2. shows the chemical structure of a Nafion membrane.

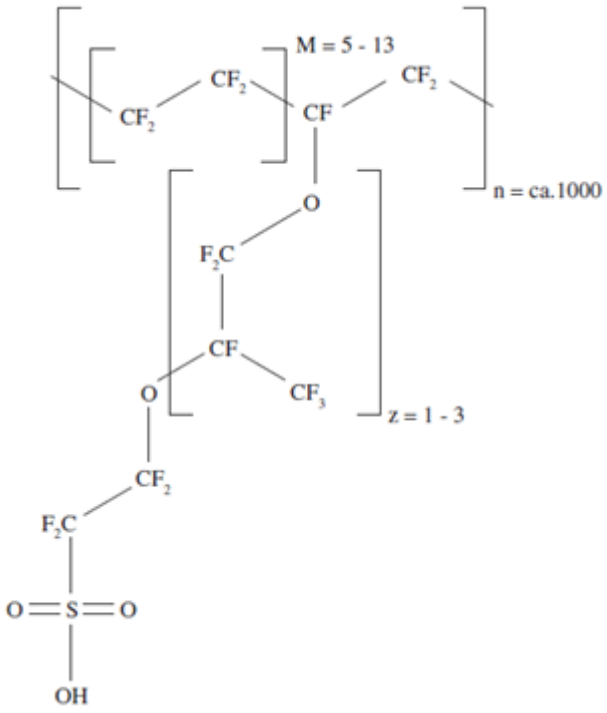

Figure 2.2. Representation of the Nafion® chemical structure [47].

Nafion® is a polymer that present hydrophilic and hydrophobic domains. The backbone structure, which corresponds to polytetrafluoroethylene (PTFE), is the hydrophobic region and at the end of the side chains, which correspond to the sulphonic acid (SO_3H) groups, is the hydrophilic region that is responsible for the hydration and protonic mobility of the membrane. Due to sulphonated side chains, the Nafion has the capacity to absorb large amounts of water (in some cases up to 50 % by weight). With hydration, the sulphonic acid group is dissociated and releases H^+; these ions move within the membrane, making these materials proton-conductive. Nafion membranes are available in different sizes and thicknesses, and are characterized by a letter, N, and a number, whose last digit or two represent the membrane's thickness, in mills, for example, N117 has 7 mills (0.178 mm).

2.3.1.2. Catalyst layers

The thin catalyst layers at the anode and cathode side are placed between the PEM and the diffusion layers. The electrochemical reactions, in which gaseous and liquid reactants, electrons and protons participate, take place in a portion of the catalyst surface where all these species have access. Electrons move through electrically conductive solids, including the catalyst itself, the protons move through the ionomer and the reactants and products move

through the voids. Thus, these layers must be porous to allow the reactants to move towards the reaction sites and simultaneously, remove the products formed in the electrochemical reactions, allowing the access of the reactants.

The most common catalysts used in DMFCs are platinum/ruthenium (Pt/Ru) at the anode side and Pt at the cathode side. The platinum catalyst is a very small particles compound impregnated on the surface of somewhat larger particles, usually, finely divided carbon powders. Therefore, Pt is dispersed in a very high proportion of the surface area where will be in contact with the reactants.

2.3.1.3. Diffusion layers

Diffusion layers (DLs) do not participate directly in the electrochemical reactions, but they play important roles in a passive DMFC. The DLs allow the reactants access to the catalyst active area and products removal, provide mechanical support to the MEA, provide the electrical connection between the catalyst layer and the current collector and allow the heat removal from the fuel cell [48]. Therefore, these layers should be porous to allow the flow of both reactants and products, electrically and thermally conductive, sufficiently rigid to support the MEA, but must have some flexibility to maintain good electrical contacts. As already mentioned, the diffusion layers are placed between the catalyst layers and the current collectors and the materials that better match their specific requirements are carbon-based materials, such as carbon paper and carbon cloths.

The DLs can have a single layer structure typically, made of carbon-based materials or a dual layer structure, where one layer is the backing layer (BL), similar to the one of the single layer structure, which serves as a substrate for the second layer. The second layer is a thin microporous layer (MPL), which contains carbon powder and hydrophobic or hydrophilic characteristics. Each layer acts as a diffusion layer for gas and liquid transport in DMFCs.

As carbon is a hydrophilic material, the carbon-based materials are usually treated with polytetrafluoroethylene (PTFE), to a proper water transport within the cell. This will change the DL wetting characteristics and effectively prevent water accumulation inside the cell and improve the anode and cathode mass transfer. However, caution must be taken when performing this treatment, since the use of a hydrophobic material may decrease the DL pore size and consequently decrease the mass transfer coefficient due to an increase of the flow resistance.

The structural parameters of the diffusion layers that have an impact on the fuel cell performance are: i) its thickness, affecting the transport resistances, ii) its porosity, influencing the species transport and iii) its surface properties, the wettability and roughness, which control the droplet/bubble attachment or coverage of the DL surface. Therefore, layers with different thicknesses, porosities, permeability, surface wettability and liquid retention, will result in different two-phase flow patterns and transport characteristics. Regarding the two materials commonly used as DLs in passive DMFCs, carbon cloth is more porous and less tortuous than carbon paper, whilst carbon paper has an excellent electronic conductivity [2]. These features of the carbon cloth and carbon paper can be seen in Figure 2.3.

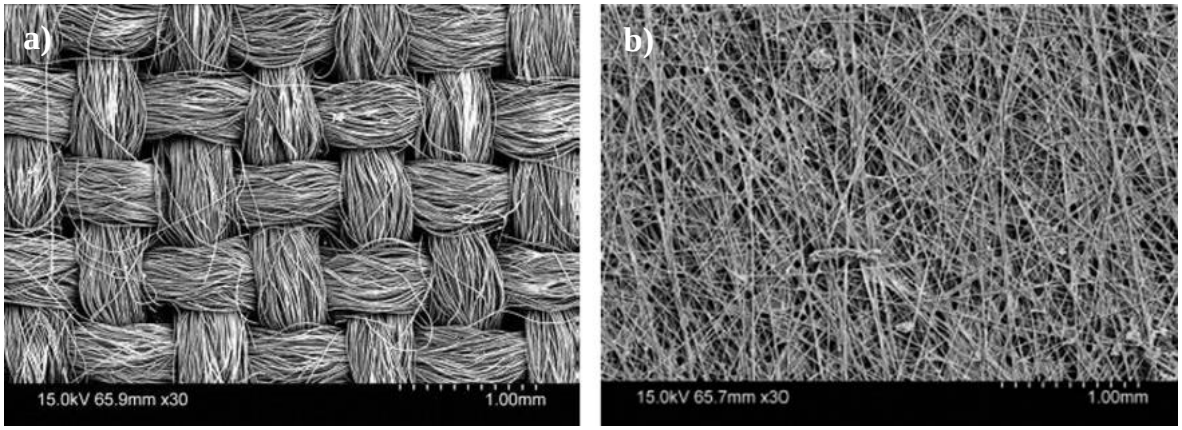

Figure 2.3. Micrographs of commercially available carbon cloth (a) and carbon paper (b) [1].

2.3.1.4. Current collectors

Current collectors (CCs) are key components in a passive DMFC, providing fuel and oxidant supply to the DLs, electron collection at the anode side, and its conduction though the external circuit to the cathode side, give structural support to the membrane and allow the products to be removed from the cell. Moreover, they are responsible for about 80 % of the cell's total weight. Therefore, to fulfil the passive DMFC requirements, like compact structure, low cost, high durability and power, CCs must have high electrical conductivity, corrosion resistance and mechanical strength, low weight and cost, and simple design (easy to machine) [23, 26, 49, 50] . The most common material used for CCs is the stainless steel (SS) [34, 51–59], but other materials like aluminium [44], titanium [60] and printed circuit board [33, 61, 62] can also be used. However, most on them, after long-term operation, may suffer from corrosion, which increases the contact resistance and leads to the presence and

accumulation of corrosion products on the different fuel cell layers, poisoning them. Therefore, to avoid this, these plates are usually coated with precious metal such as platinum, gold and titanium, which increase the cost of the fuel cell [23, 26].

2.3.1.5. End plates

End plates are used for bracing the cell and applying the desired tension on the different cell components. Therefore, they must be compact, strong and not electrically conductive. Materials like glass, fibre, acrylic and metals have been used as the anode and cathode end plat. However, when a metallic material is used, in order to avoid electrical conductivity, isolate gaskets are placed between the CCs and the end plates. These gaskets also prevent the leakage of the reactants, methanol and air. Nevertheless, it is important to select the appropriate gasket to maintain a minimum contact resistance between the end plates and the CCs [14].

2.3.2. Performance evaluation

The performance of a fuel cell is normally evaluated by polarisation curves – also called I-V curves – which relate the cell's voltage with the operating current or current density. An ideal fuel cell would supply any amount of current while maintaining a constant voltage, determined by thermodynamics. However, in real conditions, the voltage output, called open voltage circuit (OCV), is significantly lower than the ideal one (1.21 V). This decrease is mainly due to species crossover from one side of the cell to the other – in DMFCs some methanol feed to the anode crosses the membrane towards the cathode. Besides this discrepancy, the voltage drops even further with the extraction of the electric current due to irreversible losses, which can be divided into three loss mechanisms: activation, ohmic and mass transfer [3]. Figure 2.4 shows an example of a typical DMFC polarisation curve.

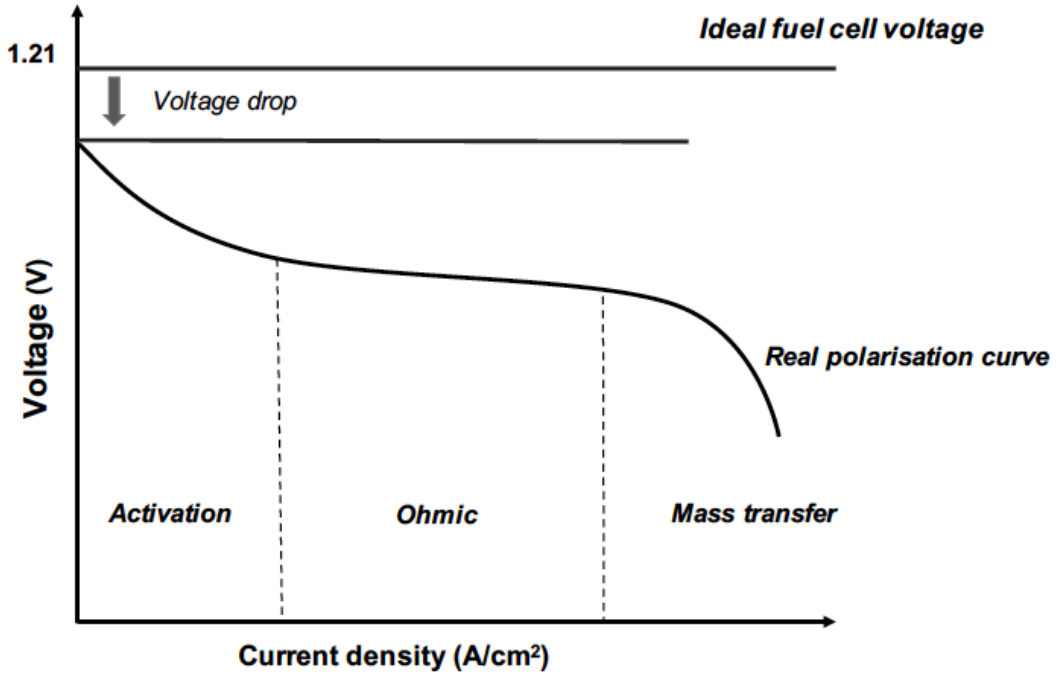

Figure 2.4. Schematic representation of a typical DMFC polarisation curve.

Activation losses are due to sluggish electrochemical reactions since they need more energy to catalyse than in the ideal case. This activation barrier is the major factor that contributes to an efficiency loss when the cell is operating at high voltages and low current densities. Ohmic losses, due to proton transport resistance and electrical contact resistance, are responsible for the linear voltage decrease at intermediate current densities. The major loss at very high current densities, is the concentration loss or mass transfer loss associated with the mass transport limitations [2]. These limitations occur when the concentration of reactants reaching the cell's active area is not enough and the fuel cell cannot produce more energy.

The maximum chemical potential that an ideal fuel cell could achieve can be estimated based on the thermodynamic laws, by the quantification of the chemical energy that is converted into electrical energy [2, 63]. So, the thermodynamic equilibrium potential (ΔE) of a DMFC can be calculated as:

$$\Delta E = -\frac{\Delta G}{nF} = -\frac{\Delta H - T\Delta S}{nF} \quad (2.4)$$

where ΔG, ΔH and ΔS are, respectively, -704 kJ/kg, -727 kJ/kg and -77 kJ/K, at 25ºC and 1 atm; n represents the number of the electrons involved in the electrochemical reaction (n = 6), and F is the Faraday constant. For a liquid feed DMFC the thermodynamic equilibrium potential is 1.21 V.

The thermodynamic efficiency of a fuel cell (η_{rev}) can be defined as the ratio between the maximum possible electrical work and the total chemical energy (Equation 2.5).

$$\eta_{rev} = \frac{\Delta G}{\Delta H} = -\frac{nF\Delta E}{\Delta H} \tag{2.5}$$

The theoretical thermodynamic efficiency of DMFC reaches 97 % at 25ºC. However, the practical energy efficiency is much lower due the voltage losses mentioned above: fuel crossover, activation, ohmic and concentration losses.

The fuel cell voltaic efficiency ($\eta_{voltaic}$) is defined as the ratio of the actual electric work and the maximum possible work, as:

$$\eta_{voltaic} = \frac{W_{actual}}{W_{maximum}} = \frac{-nFE_{cell}}{\Delta G} = \frac{-nFE_{cell}}{-nF\Delta E} = \frac{E_{cell}}{\Delta E} \tag{2.6}$$

where E_{cell} is the cell voltage at a current, *I*. As substantial overpotential losses exist in both sides of a DMFC, its voltaic efficiency is rather low. As DMFCs suffer from a loss of fuel to the cathode side, it is also possible to estimate the fuel efficiency (η_{fuel}) due to methanol crossover, as shown in Equation 2.7. I_{CH3OH} is an equivalent current density caused by methanol crossover under the operating current density, I_{cell}.

$$\eta_{fuel} = \frac{I_{cell}}{I_{cell} + I_{CH3OH}} \tag{2.7}$$

Therefore, the total energy efficiency of a DMFC is given by:

$$\eta = \eta_{rev} \times \eta_{voltaic} \times \eta_{fuel} \tag{2.8}$$

In order to achieve a higher energy efficiency in a DMFC, it is mandatory to control and reduce the methanol crossover rate towards the cathode side.

2.3.2. Anode and cathode kinetics

Electrochemical kinetics is a critical point for solving the technical challenges of a DMFC, since the methanol oxidation is more complex and slower than the hydrogen oxidation, as it involves the transfer of six electrons to the electrode for a complete oxidation to carbon dioxide (Equation 2.1). Methanol and other fuels with low exchange current densities often need a metal catalyst like Pt to obtain a reasonable and stable reaction rate.

The product resulting from complete oxidation of the alcohol fuels is an adsorbed CO_2 species, and in neutral or acidic solutions the bubbles can block portions of the catalyst surface, reducing the available catalyst active sites and hindering further fuel oxidation. Side reactions or an incomplete oxidation can also occur, and these obviously impair efficiency. One of the main limitations of an alcohol fuel cell, such as methanol, is the poisoning of the electrode by an intermediary reaction.

The existence of multiple pathways for the methanol oxidation reaction leads to the difficulty in getting a complete understanding of the mechanism by which this oxidation occurs. Despite this, the mechanisms for the methanol oxidation on Pt-based catalyst were reviewed by Parsons and VanderNoot [64] and can be divided in two major steps: i) adsorption of methanol on energetically favoured sites followed by several steps of dehydrogenation/deprotonation and ii) addition of oxygen, which allows the adsorbed carbon containing intermediaries to generate carbon dioxide. A scheme of this mechanism is:

$$CH_3OH + Pt \rightarrow PtCH_2OH + H^+ + 1e^- \quad (2.9)$$

$$PtCH_2OH + Pt \rightarrow Pt_2CHOH + H^+ + 1e^- \quad (2.10)$$

$$Pt_2CHOH + Pt \rightarrow Pt_3 - COH + H^+ + 1e^- \quad (2.11)$$

The carbon monoxide is then produced by the rearrangement of methanol oxidation intermediates. The water is discharged at high anodic overpotentials on Pt, and OH species are formed. In the final step occurs the production of carbon dioxide.

$$Pt_3COH \rightarrow Pt - CO + 2Pt + H^+ + 1e^- \quad (2.12)$$

$$Pt + H_2O \rightarrow Pt - OH + H^+ + 1e^- \quad (2.13)$$

$$PtOH + PtCO \rightarrow 2Pt + CO_2 + H^+ + 1e^- \quad (2.14)$$

An active catalyst for methanol oxidation should allow water discharges at low potentials, and unstable CO chemisorption. It should also catalyse the oxidation of carbon monoxide by providing oxygen. However, pure Pt is not sufficiently active to achieve these roles. Therefore, there has been an intensive search for a secondary active material to combine with Pt and improve its electrocatalytic behaviour, either by minimizing the poisoning of the catalyst or by increasing the oxidation reaction rate. Some examples of these materials are metals, such as Ruthenium (Ru), Sn (tin), Os (osmium), W (tungsten), Ir (iridium) and Mo (molybdenum), that weaken the chemical bond between Pt and the intermediary surface and the second elements that increase OH adsorption on the catalyst surface at lower overpotentials, decreasing the adsorption strength of the poisoning species. Nevertheless, Pt/Ru is the most researched and commonly used anode catalyst in DMFCs. The key factor for promotion of these species is the supply of oxygen in an active way which facilitates the oxidation of intermediaries on the secondary metal at potentials lower than for Pt [2, 65, 66].

The Pt sites in Pt/Ru alloys are involved in both the methanol dehydrogenation step and in the strong chemisorption of methanol residues. At low electrode potentials, water discharge occurs on Ru sites with the formation of Ru-OH groups at the catalyst surface, and at the end of the reaction, carbon dioxide is produced. The OH species play a double role, since they facilitate the adsorbed CO oxidation and also inhibit methanol adsorption [2, 65, 66].

$$Ru + H_2O \rightarrow Ru - OH + H^+ + 1e^- \quad (2.15)$$

$$RuOH + PtCO \rightarrow Ru + Pt + CO_2 + H^+ + 1e^- \quad (2.16)$$

The kinetic expression to described the methanol oxidation reaction (MOR), in Pt/Ru, was proposed by Meyers and Newman [67]:

$$I_{cell} = \int a I_{0,ref}^{CH_3OH} \frac{k C_{CH_3OH}^{AC}}{C_{CH_3OH}^{AC} + \lambda \exp\left(\frac{\alpha_A \eta_A F}{R T_{AC}}\right)} \exp\left(\frac{\alpha_A \eta_A F}{R T_{AC}}\right) dx \quad (2.17)$$

where I_{cell} is the cell current density, $I_{0,ref}^{CH_3OH}$ is the exchange current density of methanol, *a*, *k* and λ are constants in the rate expression, $C_{CH_3OH}^{AC}$ is the methanol concentration at the anode catalyst layer, α_A is the anodic transfer coefficient, η_A is the anode overpotential, T_{AC} is the temperature on the anode catalyst layer and *R* is the ideal law gas constant. As the MOR is the limiting step under most operating conditions, many studies have been performed with the aim of obtaining an electrocatalyst with a high efficiency and stability for this reaction [68–83]

The oxygen electrochemical reaction also plays a significant role in the DMFC performance, although as the anodic reaction is much slower than the cathodic one, this is not the main reaction responsible for the lower efficiencies of these fuel cells. The oxygen reduction to water usually takes place on Pt catalysts. These catalysts are extensively used in low temperature fuel cells, as DMFCs, due to their efficiency and stability. However, there is still the interest in the development of more active and selective electrocatalysts and especially with reduced cost for the cathode reaction. Some works regarding the cathode catalysts has been done in order to improve the oxygen reduction reaction (ORR) kinetics and at the same time increase the methanol tolerance due to methanol crossover towards the cathode side. Lately the researches have been focused on the development of binary and/or ternary catalysts using Pt or with Pd-based materials to reduce the catalyst costs, where metals like Co, Fe and Ni are employed as alloy, or using carbon nanoparticles as a secondary support to reduce the catalyst loadings [84–89].

At the cathode side, a second reaction, methanol oxidation, also takes place at the catalyst sites. When two reactions – methanol oxidation and oxygen reduction – compete for the same sites, this produces a mixed potential, which reduces the cell potential and

performance. Thus, a decrease on the methanol crossover is desirable to improve the cathode performance and consequently the fuel cell performance. Several studies are being done in order to decrease the methanol permeability, e.g. membranes with different materials or composition, optimisation of the methanol feed concentration, different diffusion layer materials, etc. The next sections will deal with this subject with more detail.

The ORR on the DMFC cathode is described using Tafel equation, taking into account the mixed potential due to methanol crossover:

$$I_{cell} + I_{CH_3OH} = I_{0,ref}^{O_2} \frac{C_{O_2}^{CC}}{C_{O_{2,ref}}^{CC}} \exp\left(\frac{\alpha_C \eta_C F}{R T_{CC}}\right) \quad (2.18)$$

where I_{CH_3OH} is the leakage current density due to the oxidation of methanol that crosses the membrane, I_{cell} is the cell current density, $I_{0,ref}^{O_2}$ is the exchange current density of oxygen, $C_{O_2}^{CC}$ is the oxygen concentration on the cathode catalyst layer, $C_{O_{2,ref}}^{CC}$ is the reference concentration of oxygen, α_C is the cathodic transfer coefficient, η_C is the cathode overpotential and T_{CC} is the temperature on the cathode catalyst layer.

2.4. Two-phase flow phenomena

Two-phase flow phenomena are one of the great challenges in DMFCs since they involve gaseous carbon dioxide flow in the anode and liquid water flow in the cathode, both products of the electrochemical reactions. These by-products must be removed quickly and efficiently from the fuel cell to allow proper supply of the reactants (fuel and oxygen) to the catalyst layers, ensuring higher electrochemical reaction rates. The water and the CO_2 can adhere to the surface of the diffusion layers and catalyst layers, blocking the pores and preventing fuel and oxidant from spreading uniformly into the anode and cathode porous media. This will lead to a severe loss of fuel cell performance. Hence, studies on the two-phase flow serve as guides for the improvement of the performance of a DMFC [31–46]. Flow visualization is an effective way of quantitatively and qualitatively investigating the dynamic behaviour of carbon dioxide gas bubbles in the anode channels and liquid water bubbles in the cathode of an operating DMFC. Although the number of papers published on passive DMFCs has

grown, little research has been reported on visualization experiments due to the difficulties of performing such studies.

2.4.1. Carbon dioxide in the anode

As mentioned before, at the anode side of a DMFC, gaseous carbon dioxide is produced by the methanol oxidation reaction. If carbon dioxide cannot be efficiently removed from the anode diffusion layer (AD), (Figure 2.1), it remains covering this surface and consequently decreases the effective mass transfer area, as can be seen in Figure 2.5. Therefore, gas management on the anode side is an important and critical issue in the DMFC design. In recent years, different research groups have carried out studies regarding this issue, but few are related to passive systems [31–38]. However, CO_2 removal is very important in passive systems, which do not have external auxiliary equipment to control the flow of the different species.

In order to understand the two-phase patterns at the anode side, both experimental studies, through direct visualization of the bubbles' behaviour [31–36], and modelling studies [37, 38] have been performed.

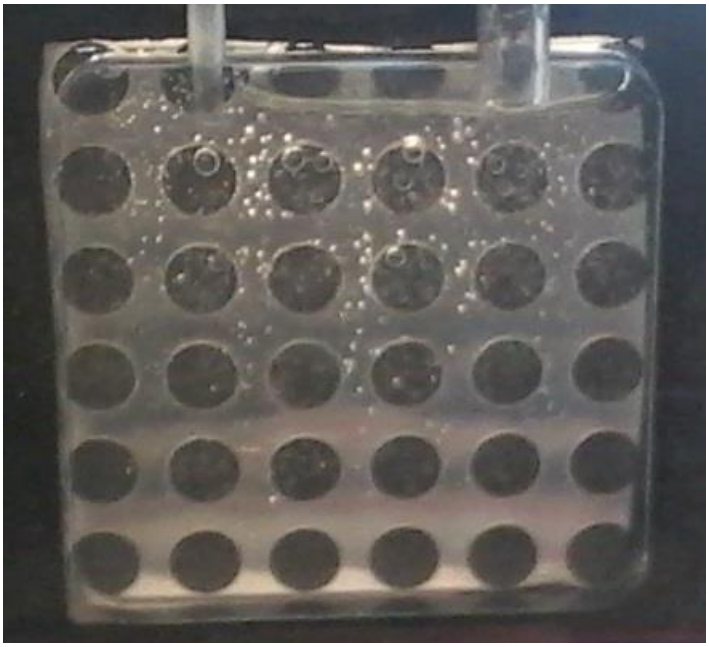

Figure 2.5. CO_2 bubble behaviour on the anode side.

Chen et al. [31] investigated the CO_2 microbubbles removal behaviour on carbon nanotube (CNT)-supported Pt catalysts, through an in-situ visualization technique. According to the experimental data, the CO_2 microbubble removal behaviour is directly related to the high current, and the nanostructure characteristics of the electrode contributed to an enhancement of the mass transfer rate. Yuan et al. [32] presented the effect of the anode and cathode structural properties on CO_2 removal rate, as well as the effect of the cell orientation on the performance of a passive DMFC. The results indicated that the cell performance can be enhanced using carbon cloth as anode DL and carbon paper as cathode DL. The authors recommended the use of the current collectors with a circular-hole-array pattern and with a small open ratio at the anode and the parallel-fence pattern with a high open ratio at the cathode, since these layouts yield the highest performances for a wide range of methanol concentrations.

Gholami et al. [33] studied the effects of current collector design and methanol concentration on the performance of a passive DMFC and on the CO_2 removal rate. Tests were performed with two different designs and arrangements for current collectors. In the first one, non-uniform parallel channels were machined on the CCs and used on the anode side. A perforated design was used on the cathode CC. In the second design, uniform parallel channels were machined on both anode and cathode CCs. The results showed a higher performance for the first arrangement using a methanol concentration of 4 M (20 mW/cm^2) and this was explained by a higher removal rate of carbon dioxide produced by the positive slope of the channels and by a higher methanol mass transfer rate, due to a higher open ratio. Yuan et al. [34] studied the optimisation of the anode design by developing a composed diffusion medium with different porosities, which included three carbon-based layers: a woven carbon-fibre fabric (WCFF), a carbon paper and a carbon-powder micro-porous layer. The intention of using the WCFF was to control the mass transfer of reactants and products at the anode, to reduce the methanol crossover and to facilitate the removal of the products. It was found that when using the WCFF the fuel cell achieved the highest performance at a methanol concentration of 12 M due to a more uniform distribution of the reactant and a rapid removal of the gas bubbles. Falcão et al. [35] investigated the effect of using stainless steel meshes, as an effective way of controlling the two-phase flow phenomena, on the performance of the passive micro-DMFC. Higher performances were obtained with the cells employing a metallic mesh due to an increase of the current collection, a decrease of the methanol crossover rate and a better distribution of the CO_2 bubbles. Meshes with larger

open ratios produced better results; however, they lead to higher compression rates and leakage problems. The best power output obtained was 29.3 mW/cm^2 using stainless steel meshes at both the anode and the cathode sides.

Chen et al. [36] investigated the CO_2 behaviour and its effects on the performance of a passive DMFC with a composite anode structure, through visualization studies. Different flow field designs, a parallel-fence structure and a new composite structure with a sintered porous metal fibre felt were tested in the anode side. The results indicated that the cell with the composite structure presented the best performance, since enhance the convection due to CO_2 self-promoting behaviour and the gas storage in the channel controlling the methanol concentration. The presence of CO_2 is helpfulness to control the methanol crossover rate allowing that the cell operates with higher methanol concentrations.

As indicated above, a better understanding of the basic transport phenomena of carbon dioxide bubbles at the anode side can be achieved combining both visualization studies and numerical simulations. Considering this, Zheng et al. [37] developed and used a two-dimensional model to investigate the multiphase flows and the interactions between the different layers on the anode side of a DMFC, focusing on the flow of a single CO_2 gas bubble. The simulation results show that as the power output increases, the porosity and the DL contact angle play a significant role on the size of the CO_2 bubbles, allowing bubbles to grow to their maximum size. The thickness of the DL has an effect on CO_2 bubble size at lower power outputs and the thickness can be estimated by the maximum size of the bubbles. The model suggests that, to achieve optimal performance, the DL in passive DMFCs should be thick enough to allow bubbles to grow to their maximum size. Liu et al. [38] proposed a new approach to promote CO_2 removal from the anode catalyst layer of a passive DMFC by introducing Lorentz force, via the integration of magnetic field on the system. This forced convection around the CO_2 bubbles was studied through mathematical simulations. The results indicate that the magnetic field improved the maximum power density on 12.5%, due to an increase of the CO_2 removal rate.

2.4.2. Liquid water in the cathode

Another important aspect of the DMFCs is the possibility of water flooding at the cathode pores and structure, due to water transport through the membrane and water production by cathode reaction. The formation of water within the cathode catalyst layer and its transport

through the cathode diffusion layer represent a mass transport resistance and disturb the diffusion of oxygen towards the reaction zone, which can reduce the limiting current density of the cell. An appropriate water level at the cathode side is necessary to hydrate the polymer membrane, increasing proton conductivity. However, a large amount of water in the cathode side leads to flooding at the pores decreasing the cathode performance [39] (Figure 2.6). An optimised water management is necessary in passive DMFC systems to overcome this difficulty, thus inspiring new design concepts. In order to accurately predict the operation and design conditions that avoid flooding, visualization and modelling studies regarding the cathode side are essential to yield physics fundamental behind the flooding occurrence [39–46].

Figure 2.6. Cathode flooding in a passive DMFC.

Zhou et al. [39] developed an air-breathing micro DMFC with a water collecting and recycling structure to control the water distribution inside the cell. To that end, capillary channels with a hydrophilic surface were placed along the ribs of the air-breathing cathode window, to collect excess water and release it into the exhaust pipe. The results showed that the power and the current density of the cell with this system were 9.7 mW/cm^2 and 95 mA/cm^2, respectively. These values were higher than those obtained with the conventional layout, 9 mW/cm^2 and of 75 mA/cm^2. Xu and Faghri [40] investigated the water transport characteristics in a passive DMFC, considering a porous diffusion medium with both hydrophilic and hydrophobic pores. This study was based on a mathematical

model that uses as input a mixed-wet capillary pressure and a saturation relation (CPSR), determined experimentally. The liquid water transport predicted by the mixed-wet CPSR was compared with the uniform-wet Leverett CPSR. It was found that, the use of Leverett CPSR underestimated the liquid saturation in the DL, and therefore overestimated the cell performance. Additionally, it was found that using the mixed-wet CPSR, the liquid saturation in the DL is nearly independent of the operating current and mainly depends on the wettability of the porous structure, such as the fraction of the hydrophilic pores.

Li et al. [41] worked with a semi-passive high-concentration (HC)-DMFC, where the water management is much more critical due to a small amount of water in the fuel reservoir. They used a PTFE layer as a methanol barrier layer between the fuel reservoir and the current collector to improve the water management and analyse the effect of different parameters on the overall HC-DMFC performance. The results showed that a methanol barrier layer could significantly decrease both methanol and water crossover and increase fuel efficiency. The membrane resistance was the predominant factor affecting the HC-DMFC performance, especially for high current densities. Since in this case, the water backflow towards the anode is very important to hydrate the membrane, they found that this can be enhanced, increasing cathode's relative humidity and pressure. The water flooding at the cathode of a HC-DMFC with a porous PTFE plate was not relevant, and a lower oxygen flow rate is desirable to decrease the water losses and to achieve better performances.

Chen et al. [42] designed and fabricated a novel cathode catalyst layer with PTFE and Nafion impregnations and with a discontinuous hydrophobicity gradient, since this distribution can be beneficial to oxygen diffusion inside this layer and to water removal. The authors concluded that the hydrophobic gradient could accelerate oxygen transport in the catalyst layer and enhance water back diffusion, improving DMFC performance and stability.

Yousefi et al. [43] designed and studied the effect of the cell orientation and environmental conditions on a passive DMFC and found that the best performance was achieved under vertical orientation since with horizontal orientation, with the anode facing downward, occurred cathode flooding and CO_2 accumulation on the anode side. According to the results, a higher environmental temperature leads to an improvement of the electrochemical kinetics, a decrease of the cell internal resistance and a decrease in cathode flooding, resulting in better performances. However, an increase in the air relative humidity leads to reduced performance. Wang et al. [44] used plasma electrolytic oxidation (PEO) to prepare a super-hydrophilic coating on the surface of an aluminium based cathode CC in order to solve the

water flooding problems in a passive micro DMFC. The results showed that the liquid water spreads quickly as a plane on the surface of the porous PEO, proving that this treatment can prevent the cathode flooding. Therefore, the fabricated PEO cell showed better power outputs than the normal cell and a significantly higher stability.

Zhang et al. [45] developed a novel water management system for a metal-based passive micro DMFC that includes a hydrophilic coating, achieve with the PEO technique. This technique was applied in some channels of the cathode end plate, a stainless steel felt as cathode CC and an aluminium-based cathode end plate with a perforated flow field (holes). Due to the highly hydrophilic nature of the PEO, the results showed that the channels efficiently collect/remove the liquid water produced in the cathode reaction, suppressing water accumulation along the air-breathing holes, preventing water flooding and improving cell performance and stability. It was also found that the cathode end plate design allows the liquid water to be removed from the cell and recycled.

Bahrami and Faghri [46] investigated the fuel delivery and its relation with the water and methanol crossover using a two-dimensional, steady-state, non-isothermal, non-equilibrium and multi-fluid model for a passive DMFC. Is this work, the authors used a porous layer, called the fuel delivery layer, between the anode DL and the anode reservoir, in order to use a high methanol concentration. A hydrophobic MPL was used at the cathode to decrease methanol and water transport through the membrane. The results showed that an increase of the fuel delivery layer thickness was not effective to control the methanol transport through the membrane without simultaneously controlling the water crossover rate. On the contrary, the use of a cathode MPL leads to a reduction of water and methanol crossover and significantly reduces the liquid saturation at the cathode DL, reducing water flooding.

In spite of these studies, much remains to be understood regarding fundamental processes of two-phase flow phenomena that affect the anode and cathode sides of a passive DMFC and its relation with the different materials used in the cell layers. As can be seen, the introduction of metallic meshes between the MEA and the current collectors, using CCs with different designs and different orientations for the fuel cell is an effective way to control the carbon dioxide flow and release at the anode. Regarding the water on the cathode side, the use of additional layers and the common ones with hydrophobic/hydrophilic treatments is an effective way to reduce cathode flooding through a more efficient water removal from the cathode outlet and a higher water backflow rate towards the anode side.

2.5. Mass transport

A deep understanding of mass transport phenomena is essential to improve fuel cell performance and stability. Many authors propose different solutions to eliminate or reduce fuel loss across the membrane, as well as to solve the water management issues through different approaches: experimental studies and modelling/simulation [57, 90–113]. Xiao et al. [90] developed a two-dimensional, non-isothermal, transient and multi-phase model to study heat and mass transport in a passive and semi-passive liquid-feed DMFC. The results showed that, as expected, an improved mass transport system leads to improved fuel cell performance. However, to achieve even higher performances, an improved heat transport system is also needed. Xu et al. [91] investigated the characteristics of the methanol and water crossover in a passive DMFC and the results demonstrated that cell performance and methanol and water crossover through the membrane strongly depended on heat and water managements issues. The water crossover increased almost linearly with the current density but was almost the same for the different methanol concentrations tested. In addition, the results showed that although the water in the cathode leads to cathode flooding and increases the oxygen mass transport resistance, it also allowed a reduction of both water and methanol crossover rates, thus increasing the fuel efficiency. The authors found that a reduction of the water crossover rate was always followed by a reduction of the methanol crossover rate.

2.5.1. Methanol crossover

As mentioned above, methanol crossover occurs in DMFCs by the permeation of the methanol through the membrane from the anode to the cathode side. The Nafion membranes are unable to prevent the methanol from permeating its polymer structure, because of the small size of its molecules. Diffusion and electro-osmotic drag are the prime driving forces for its transport through the membrane. The methanol that reaches the cathode side reacts in the Pt catalyst sites on the cathode, leading to a mixed potential, which causes a decrease in cell voltage. Methanol reaching the cathode also leads to a decrease in fuel efficiency due to a fuel loss on the cathode side, lowering the energy density of the system. In order to improve the performance of a DMFC, it is necessary to eliminate or reduce the loss of fuel across the membrane. Therefore, the major challenge is to find an optimised DMFC design that allows the cell to work with high methanol concentrations or even pure methanol without generating

higher rates of methanol crossover. In this section, special attention is given in showing the most recent studies performed on this issue and some possible solutions to solve this problem.

Feng et al. [92] studied a passive DMFC with an active area of 9 cm^2 fed with pure methanol using a pervaporation membrane to control the methanol transport. The results demonstrated that the proposed configuration can successfully operate with pure methanol making it possible to obtain a maximum power density of 21 mW/cm^2. The results showed that at a current of 100 mA, the energy density of the cell supplied with pure methanol increased about 6 times more than that of a fuel cell fed with a diluted methanol solution. Park et al. [93] designed a MEA with multi-layer electrodes, which includes a fuel control layer to decrease the fuel crossover, a hydrophobic layer to reduce water crossover and a hydrophilic layer to improve the water backflow towards the anode, which was used on the anode side of a passive DMFC operated with high methanol concentrations. The results showed that the MEA proposed improved the cell performance by decreasing both methanol and water crossover rates. Zhang et al. [94] studied a passive DMFC fed with neat methanol and using a methanol and water-resisting pervaporation film and a buffer cavity incorporated in the anode structure to control the methanol transport rate on the anode and for retention of water recovered from the cathode to the anode. The results indicated that this novel anode structure facilitated the anodic reaction and allowed a high proton-conduction of the Nafion membrane. The passive DMFC tested reached a maximal power density of 29.0 mW/cm^2 and the performance remained constant over 400 h of continuous operation. Yuan et al. [57, 95] designed and studied the performance of passive DMFC using a porous metal-fibre sintered felt (PMFSF) on the anode side of the cell as a mass-transfer-controlling medium, to mitigate the negative effects of the methanol crossover. The experimental results revealed a significant improvement in cell performance, using a PMFSP with a thickness of 2 mm, especially at higher methanol concentrations. The same authors prepared and added graphene-carbon nanotubes (G-CNTs) into the anodic MPL to form a crack-free anode DL for a passive DMFC. The intention was to decrease the methanol crossover rate and improve the electron contact between the diffusion and the catalyst layer [96]. In this work, a maximum power density of 41.6 mW/cm^2 was achieved at an operating temperature of 25ºC. The use of the electrode with G-CNTs as MPL indicated an improvement on the anode catalyst utilization by an increase of 36.1 % in the electrochemical active surface area estimated through carbon monoxide stripping measurements. In addition, there was a

decrease in the charge transfer and contact resistance as well as a decrease in the methanol crossover rate.

Huang et al. [97] developed a new porous anode electrode by adding magnesium oxide (MgO) nanoparticles as pore-former into the catalyst layer and MPL. The novel MEA showed improved performances and striking reduction in the use of noble metals as catalysts, due to an increased electrochemical surface area and a decreased charge-transfer resistance. Abdelkareem et al. [98] investigated the effect of carbon nanofibers (CNFs) as 1D nanostructure on the cathode MPL of a passive DMFC. The polarisation curves and the in-situ cyclic voltammetry measurements indicated that the CNFs content has a significant influence on both mass transport and electrochemical surface area. The highest catalyst utilization was observed with a CNFs content of 40 wt.%, however the maximum power density (36 mW/cm^2) was achieved at a CNFs content of 20 wt.% due to a lower mass transfer resistance under these conditions. Wu et al. [99] studied the effect of using polypyrrole nanowire networks (PPNNs) as anodic MPLs on the carbon paper surface on fuel cell performance. The results demonstrated that the use of PPNNs can effectively increase the surface area of the carbon fibre, improving catalyst utilisation and promoting the mass transport of methanol, and consequently decreasing methanol crossover. Zhang et al. [100] developed a novel anode mass transfer barrier layer using reduced graphene oxide (rGO) deposited on a stainless-steel fibre felt (SSFF). The SSFF-rGO layer was used as both anode current collector and methanol mass transfer barrier. The results showed that the SSFF-rGO layer can increase methanol mass transport resistance, decreasing the methanol crossover rate but allowing an appropriated methanol concentration in the reaction zone, thus leading to better performances. Oliveira et al. [101] investigated the effect of the anode diffusion layer properties on the performance of a passive DMFC, aiming to achieve optimised performances by working the cell at high methanol concentrations. The results showed that using carbon paper with lower thicknesses and with a MPL lead to higher fuel cell performances due to a decrease of the anode overpotential and a higher methanol oxidation rate on the catalyst layer. However, the best power density, 24.3 mW/cm^2, was achieved using carbon cloth with higher thicknesses as an anode DL layer and a methanol concentration of 3 M, mainly due to the lower methanol crossover rates generated. Yan et al. [102] studied the effect of the anode backing layer on the performance and methanol crossover rate of a passive DMFC operated with a highly-concentrated fuel. The results showed that a reduction on the BL porosity lead to a higher mass transport resistance and

therefore a lower methanol crossover rate towards the cathode side. The proposed BL enabled the cell operation with a high fuel concentration, up to 10 M, without an increase of the methanol crossover rate.

2.5.2. Water management

In order to compete with the conventional batteries, the most important requirement for a passive DMFC is to have higher energy densities. Recent studies [103–113] indicate that the water management is a critical challenge for DMFCs achieve the desirable energy levels. The amount and distribution of water within the fuel cell strongly affects its efficiency and reliability. As described in the previous sections, methanol crossover is an important challenge to overcome in DMFCs and one possible solution would be to use lower methanol concentrations. However, this also leads to the presence of higher amounts of water at the anode side and consequently a large amount of water needs to be removed from the system, thereby reducing the energy content of the fuel mixture. The presence of a large amount of water in the fuel cell system floods the cathode and reduces its performance. Therefore, an important engineering issue is to remove water from the cathode to avoid severe flooding and subsequently supply water to the anode to make up for water loss due to water crossover through the membrane. Low water flux through the membrane is desirable for DMFCs, as the anode does not require an excessive amount of water replenishment and the cathode is less susceptible to severe flooding. Formally, the water flux through the membrane caused by diffusion and electroosmotic can be quantified in terms of a net water transfer coefficient (α-alfa value) [110]. The ideal value for this coefficient is a negative one, meaning that no water is necessary from the anode fuel solution and the water needed to oxidize methanol comes from the water produced at the cathode side.

Shaffer and Wang [103] developed and used a 1D, two-phase model that accounts for the capillary-induced liquid flow in porous media to show how a hydrophobic anode MPL controls the water crossover rate. The results indicated that a lower water crossover rate could lead to a lower methanol crossover rate due to a dilution effect of the methanol in the anode catalyst layer. Finally, through a parametric study it was possible to show that a thicker anode MPL with higher hydrophobicity and lower permeability can be an effective solution to control the water crossover. Cao et al. [104] proposed a novel MEA design with a double MPL at the cathode side, employing a Ketjen Black carbon as an inner-MPL and Vulcan

XC-72R carbon as an outer-MPL. The experimental results showed that this structure provided higher oxygen transfer rates and a reduction of the water crossover rate, leading to higher cell performance and stability. Shaffer and Wang [105] used the low-α MEA concept, with lower or negative water crossover using a hydrophobic anode and cathode MPL, and an anode transport barrier between the BL and the hydrophobic MPL. To show the effectiveness of this novel design the authors used a 1D, two-phase DMFC model. According to the results, a thicker, more hydrophilic and permeable anode transport barrier and a thicker, more hydrophobic and less permeable anode MPL lead to lower methanol and water crossover rates. Wu et al. [106] analysed the water retention in the membrane of a DMFC operating with pure methanol through the use of a thin layer (retention layer) consisting of nanosized SiO_2 particles and Nafion ionomer coated onto each side of the membrane. The hygroscopic nature of SiO_2 makes it possible to maintain a higher water concentration level at the cathode side, enhancing the water transport towards the anode, while the anode retention layer can retain the recovered water from the cathode side and ensure an appropriate water concentration at the anode catalyst layer, improving the anode reaction kinetic and the overall cell performance. Peng et al. [107] proposed and demonstrated cathodic water/air management device (WAMD) for a passive micro-DMFC. The apparatus consists of micro-channels and air-breathing windows, with hydrophobicity treatment on the rib structures as a way of rapidly removing water and maintaining a high gas pathway for air convection. The WAMD resulted in a water removal rate of 5.1 µl/(s cm^2), which is about 20 times faster than the water generation rate in a DMFC operated at 400 mA/cm^2. The water vapour was also collected and the water was recirculated through the micro-channels, which act as a passive water recycling system. Wu et al. [108] showed the effect of the cathode diffusion layer design, namely the PTFE content in the BL and MPL and the carbon load in the MPL, on the water and oxygen flux and on the performance of a passive DMFC operating with neat methanol. The results indicated that the cell performance increased with the PTFE content both in the cathode BL and MPL due to a reduction of the water crossover. Zhang et al. [109] studied the performance of a passive air-breathing DMFC fed with pure methanol with a homemade wet-proofing carbon papers used as BL on the cathode side. Different amounts of hydrophilic ionomer (5 wt. % Nafion solution) and hydrophobic additive (PTFE) were added to achieve a hydrophobic gradient for dynamic water backflow. The results demonstrated that the energy density of the DMFC fed with pure methanol using a BL with 40 wt. % PTFE on the cathode was increased by six

times when compared to a conventional DMFC fed with a methanol concentration of 2 M. The results confirmed that highly hydrophobic cathode DL exhibited excellent water management and was crucial for water backflow during a long-term operation of a passive DMFC. Oliveira et al. [110] studied the water transport through the membrane towards the cathode using a mathematical model. The authors analysed the effect of methanol concentration, membrane thicknesses, diffusion layer materials and thicknesses and catalyst load on the water crossover rate and consequently on the passive DMFC's performance. The results showed that the methanol concentration clearly affects the water transport rate through the membrane, since lower methanol concentrations resulted in higher water concentration gradients between the anode and cathode side and, consequently, higher water crossover rates. Concerning the different materials for the diffusion layers tested, better performances were achieved using carbon cloth, mainly due to its greater thickness, which lead to lower methanol and water crossover rates. Lower water crossover rates were also achieved with higher catalyst loads on the anode side, since higher loads lead to thicker catalyst layers and higher mass transport resistances. Regarding the membrane's thickness, it was found that thinner membranes exhibit lower water crossover rates. Deng et al. [111] proposed the use of CNT paper as cathode DL for a passive μ-DMFC, to control the water management issues. The passive μ-DMFC using the CNT paper showed higher performances than those with carbon paper and allowed the cell's operation with higher methanol concentrations due to a higher water back diffusion and lower methanol crossover rates. Yan et al. [112] investigated a new MPL with a hydrophilic-hydrophobic dual layer to trap and retain the water, and simultaneously create a capillary pressure to prevent a lack of water in the anode side of a passive DMFC operating with neat methanol. The results showed a higher water concentration on the anode side, which improved the anode reaction kinetics and the overall cell performance. Xue et al. [113] proposed and developed a novel cathode structure for a passive μ-DMFC to control the water management issues and allow the operation of the cell with high methanol concentrations. The cathode electrode was made of a reduced graphene oxide deposited in a stainless steel fibre felt to enhance the water back diffusion, avoiding the cathode flooding, and decreasing the methanol crossover. The proposed passive μ-DMFC exhibited a higher performance than a traditional one, achieving a maximum power density of 23.8 mW/cm^2 with a methanol concentration of 3 M and operated at room temperature.

Based on the work done regarding the methanol and water crossover phenomena, it can be concluded that the methanol and water crossover are unavoidable. Additionally, both phenomena are interconnected and the reduction of one can lead to the reduction of the other. Based on the methanol crossover state-of-the-art it can be realised that its rate can be mitigated/minimised through the improvement of the activity of the methanol electroxidation catalysts, the use of different catalyst loads, different materials for the anode diffusion layer and with different thicknesses and methanol mass transport barriers/layers. Regarding the water management issue, a low or even negative net water transport coefficient is mandatory to achieve higher power outputs. This can be accomplished using different layers or mass control layers from different materials, with different properties and/or treatments (hydrophobic or hydrophilic) and thicknesses, both at the anode and the cathode sides.

2.6. Single cell performance

A passive DMFC is a multiphase system involving simultaneous mass, charge and energy transfer. All these processes are intimately coupled, resulting in a need to research optimal cell design (current collectors design, membrane, diffusion and catalyst layer properties, fuel cell layout) and operating conditions (cell temperature, methanol concentration). A good understanding of these complex phenomena is thus essential to optimise the cell performance, and this can be achieved through a combination of mathematical modelling and a detailed experimental approach. In fact, some experimental work has been done in order to achieve optimal performances [48, 52, 54, 56, 58–60, 84–89, 114–166]. To improve the power outputs of a passive DMFCs, there is increasing interest in reducing mass transport, kinetic and ohmic limitations.

To achieve these goals, some work has been done in order to evaluate the effect of the methanol concentration (Met C) on the cell performance, and to improve the design of current collectors (CC), the catalyst loading (Cat L), and the characteristics of the diffusion layer (DL) and membrane (Mem) in terms of materials and thicknesses (Table 2.1).

Table 2.1. Single cell performance studies based on the parameters investigated, and the maximum power output achieved.

Ref.	Details	Parameters investigated					Max. Power (mW/cm^2)
		Met C	DL	CC	Cat L	Mem	
[48]	Analysed the effect of diffusion layer compression on the performance of a passive DMFC.	X			X		5.78
[52]	Studied structural aspects on the cell performance.		X	X		X	10.7
[54]	Investigated different structural factors on the cell performance by means of orthogonal array analysis.	X	X	X		X	10.7
[56]	Developed a passive DMFC with 100 cm^2.	X		X			5.2
[58]	Investigated the effects of a porous metal fibre used as a methanol barrier on the anode side.	X		X			–
[59]	Investigated the performance of a passive DMFC with different structural configurations.	X		X			–
[60]	Developed an integrated anode structure based on a microporous titanium plate (Ti-IAS) as current collector and with a pervaporation film.	X		X		X	40
[84]	Studied the catalytic activity of Pd and of Pd_xCo alloy nanoparticles for the oxygen reduction reaction.				X	X	–
[85]	Synthesised Pd-based alloy electrocatalysts and evaluate it as cathode catalyst in a passive DMFC.				X	X	2.53
[86]	Investigated the effect of double-layered cathodes with a reduction up to 50% on the catalyst load, on cell performance.				X		39.4
[87]	Developed a methanol-tolerant catalyst, with PtM/C and PtMRu/C combinations (M = Co or Fe) to study the enhancement for the oxygen reduction reaction.				X		–
[88]	Synthesised binary carbon supported Pd_3CO nanocatalyst for oxygen reduction reaction.				X		3.81
[89]	Prepared Pd-Ni/C electro-catalyst with different atomic ratios to improve the oxygen reduction reaction.				X		–
[114]	Developed a microfluidic-structure anode flow field.	X					23.5
[115]	Designed a new structure with two methanol reservoirs separated by a porous medium layer.	X					16.4
[116]	Analysed operational characteristics, with a focus on the fuel concentration, of a small-scale passive DMFC.	X	X			X	5.97

[117]	Developed two stacks, one with dilute methanol solutions and the other with pure methanol.	X					30.1
[118]	Investigated the use of a porous metal fibre as an anodic methanol barrier.	X					–
[119]	Developed a passive and self-adaptive DMFC using a polypropylene based pervaporation film to supply the methanol in vapour form.	X					42
[120]	Developed a micro-porous anode current collector.	X		X			41.4
[121]	Investigated the effect of the key system parameters that influence the performance of passive DMFC operated with concentrated fuel.	X	X				24
[122]	The effect of cell orientation on cell performance employing a porous carbon plate.	X					35
[123]	Studied some operating parameters on the performance of a passive DMFC.	X					–
[124]	Improved a tubular-shaped passive DMFC to achieve stable operation with high concentrations of fuel.	X				X	16.5
[125]	Proposed a dual-chamber anode structure, with different methanol concentration, for a passive µ-DMFC.	X					–
[126]	Investigated the optimised design of a metallic passive µ-DMFC for portable applications.	X	X				19.2
[127]	Developed a bi-layer composite membrane of sulfonated graphene oxide (SGO)/Nafion and sulfonated activated carbon (SAC)/Nafion.	X				X	29.1
[128]	Evaluated the performance of Nafion recast with addition of palladium-silica nanofibres (Pd-SiO_2).	X				X	10.4
[129]	Investigated a methanol-blocking membrane prepared by assembly of poly(diallyldimethylammonium chloride) - PDDA and graphene oxide (GO) nanosheets onto the surface of Nafion® membrane.	X				X	20.6
[130]	Prepared and characterised a series of sulfonated poly(p-phenylene-co-aryl ether ketone)s (SPP-co-PAEK) membranes.					X	24.5
[131]	Developed proton-conducting membranes based on a series of side-chain-type sulfonated poly(ether ketone/ether benzimidazole)s via benzimidazolization and acylation.					X	39.3
[132]	Synthesised and evaluated a series of sulfonated cardo poly(arylene ether sulfone)s (SPES-x) membranes based on a novel bisphenol monomer containing electron rich tetraphenylmethane groups.					X	29.4

[133]	Developed a novel membrane based on a new series of cardo poly(arylene ether sulfone/nitrite)s FSPES-x with pefluoroalkyl sulfonic acid groups.					X	25.9
[134]	Analysed the effect of the Nafion®115 membrane on the cell performance considering its roughness factor.				X	X	27.2
[135]	Investigated the effect of the decrease of Nafion ionomer size in the anode catalyst layer on the cell performance.				X		32.9
[136]	Prepared and characterised a series of Nafion composite with microporous organic polymer networks.					X	21.5
[137]	Polymerised a PEM to high the proton conductivity by plasma technique for a semi-passive μ-DMFC.					X	20.1
[138]	Synthesised and investigated a tetra-sulfonated poly(*p*-phenylene-*co*-aryl ether ketone) membranes with microblock moieties.					X	31.9
[139]	Designed a Nafion sandwich, with a monolayer graphene between two membranes, to improve the permeability of protons.					X	25.2
[140]	Developed, with the aid of electrospinning, nanofibre 3D network structure to use as anode catalyst layer.				X		43
[141]	Designed a membrane with synthesised electrocatalysts.	X	X		X		11.9
[142]	Prepared the nano-network structure by zinc oxide nanorods within anode catalyst layer and MPL to reduce the noble metal catalyst load.				X		40.2
[143]	Investigated methanol oxidation on Pt-Sn electrocatalyst supported on carbon-polyaniline composite.				X		4
[144]	Prepared the ordered Pt nanorod array onto MPL by electrodeposition to use as the catalytic cathode.		X		X		17.3
[145]	Ordered nanostructured cathodes based on vertically aligned Pt nanotubes for ultra-low Pt load passive DMFC.				X		15.1
[146]	Analysed three anode electrodes made with different carbon materials.	X	X				23
[147]	Investigated the degradation mechanisms in a membrane, with CNF as anode porous layer, under different modes of operation.		X				22.9
[148]	Developed a cathode diffusion layer with mesoporous carbon.		X				31.4
[149]	Studied the effect of different types of carbon materials (graphene nano-sheets) as anode diffusion layers.		X				13.7

[150]	Analysed the feasibility of using a stainless steel wire mesh as current collector in a passive DMFC.			X			2.26
[151]	Analysed the effect of design of expanded metal mesh current collector and supporting plates in the performance of passive DMFC.			X			3.04
[152]	Investigated the structural effects of stainless steel expanded mesh as flow field/current collector in a passive DMFC.	X		X			–
[153]	Investigated the effect of anode and cathode flow field geometry on passive DMFC.	X		X			–
[154]	Analysed the clamping effects on passive DMFC using electrochemical impedance spectroscopy.	X					–
[155]	Studied the effect of size and shape of active area on the performance of passive DMFC.	X					3.5
[156]	Proposed a new structure for lower power applications, with a metal mesh directly welded onto the membrane.				X	X	1.62
[157]	Developed a tubular-shaped passive DMFC with a higher instantaneous volumetric power energy density.	X				X	24.5
[158]	Designed a flexible tubular μDMFC to power the practical wearable devices.		X	X			15.3/stack
[159]	Developed a stack (8 unit cells) with a porous carbon plate.	X					30/stack
[160]	Developed six dual cells connected in series for portable electronic devices.	X	X			X	25/stack
[161]	Evaluated practical operating performances with a small passive DMFC stack.	X					26/stack
[162]	Investigated different membranes to be used in stacks.	X	X		X		20/stack
[163]	Designed and fabricated a “4-cell” modular passive DMFC stack and tested in electronic devices.	X					27/stack
[164]	Investigated the effects of a lightweight current collector based on printed-circuit-board technology on a single and 8-cell mono polar passive DMFC.			X			18.3/stack
[165]	Developed a simple and functional DMFC stacks designs with the aim of reducing costs.	X					30/stack
[166]	Designed and tested a 6-cell stack passive DMFC for long-term operation, more than 3000 h.	X					21.5/stack

The effect of methanol concentration on the performance of a passive DMFC generally reflects two different phenomena: an increase on methanol concentration leads to an increase

of the coverage of the electrocatalyst sites by methanolic species, but also increases the concentration gradient between the anode and cathode side, with a consequent increase of the methanol crossover rate through the membrane. At the cathode side, the crossed methanol reacts with the oxygen to form a mixed potential, resulting in lower cell performance. This requires a balance among the positive effects on the methanol oxidation kinetics and the negative ones on methanol crossover in order to enhance the cell performance. Another point that should be accounted for, is the fact that the polarisation behaviour in the mass transfer region is directly related to the methanol concentration, so an increase in the limiting current density is achieved with an increase in methanol concentration. In addition, it should be pointed out that in passive feed systems the fuel pump is eliminated and therefore the fuel is supplied to the anode from a fuel reservoir by natural forces such as natural convection and diffusion. This simple design generates lower system performances due to the difficulty of getting a continuous and homogeneous supply of the fuel to the anode, so a more concentrated fuel solution is desirable. Among the different experimental studies reported in the literature, most of them highlight the need to work with more concentrated methanol solutions to achieve the desirable levels of power outputs and use different structural parameters to act as a methanol barrier layer in order to reduce a crossover rate [56, 58, 60, 114–126].

The PEM is an important component of a fuel cell and must exhibit a high proton conductivity, must be chemical and mechanical stability in the fuel cell environment and that it should be a barrier to the contact and mixing of fuel and oxidant. The most commonly used membranes for DMFCs are Nafion® membranes. However, since these membranes are subject to high rates of fuel crossover different approaches are being adopted towards the development of membranes from alternative materials that meet the necessary requirements: high proton conductivity, low methanol permeability, high chemical and mechanical stability and low cost [127–139].

Regarding the catalyst layers, their microstructure is very important for the electrochemical reactions and for the diffusion of the involved species. Therefore, these must be porous to allow access of the reactants into the active sites and to remove the products formed in the electrochemical reactions. Moreover, DMFC efficiency is limited by the reactions occurring at both electrodes (anode and cathode), since the slow kinetics of these reactions lead to significant potential losses. Even using the current state-of-the-art catalysts for each reaction (Pt/Ru at the anode and Pt at the cathode), until now it has only been possible to reach

reaction efficiencies of about 25-35 %. Additionally, to achieve these efficiencies the catalyst loads recommended are approximately 4 mg/cm^2 at the anode and 2 mg/cm^2 at the cathode side. However, the use of Pt and Ru is expensive and represents a significant part of the total system costs. Therefore, to decrease the cost of the catalyst, some studies have been carried out in order to evaluate the influence of the catalyst load on cell performance, as well as other studies on the development of new catalysts using low cost materials [84–89, 140–145] .

Two essential properties of the electrode, electronic conductivity and electrode thickness, can be affected by changes in the catalyst loads. At low current densities, the activation overvoltage is a major portion of the total overvoltage at the anode, so an increase in the Pt/Ru loads reduces the activation overvoltage at the anode, enhancing cell performance. With the increase of the load, the thickness of the catalyst layer increases and therefore the mass transfer resistance through this layer becomes greater. In addition, cell performance increases with the metal load because a thicker anode catalyst layer creates a higher resistance to methanol transport, thereby controlling the rate of methanol that reaches the membrane and reducing the methanol crossover. However, at high current densities, a higher catalyst load leads to a decrease in cell performance due to a higher concentration overpotential loss caused by the higher mass transfer resistance rate of methanol through this layer. At the cathode side, a reduction in the catalyst load leads to a decrease in cell performance due to a reduction of the active surface area, an increase in resistivity, and consequently a decrease in electronic conductivity. An increase of catalyst load leads to a thicker layer, which will result in higher mass transport resistance. However, this may be advantageous at the cathode, since the mixed potential formation may be partially avoided. In a thicker electrode, not all the catalyst particles are reached by the permeated methanol flux, so more active sites are free for oxygen reduction reaction.

A possible solution to work with lower catalyst loads and ensure the electronic conductivity of the electrode is to use carbon supported materials. However, the use of carbon supported catalyst with a much lower bulk density is associated with a higher thickness of the active layer which is an important parameter for the cell performance. A thicker electrode on the anode side may conduct to a higher mass transport resistance of methanol, leading to a decrease of the fuel cell performance. On the other hand, as explained above, this higher resistance may be beneficial on the cathode side. Therefore, the use of carbon supported catalysts and their optimisation in the electrode structure has the potential to significantly

reduce the metal load, contributing to a reduction of the overall costs of passive DMFC systems.

Besides providing a good distribution of reactants and products, the diffusion layers must electrically connect the catalyst layer to the current collector, allowing that heat is removed and providing mechanical support to the membrane, to prevent it from sagging into the current collector channels/holes. The operation of a DMFC requires that methanol has good access to the anode catalyst layer, while the carbon dioxide moves freely away from the catalyst sites on the catalyst surface. However, to avoid a two-phase flow pattern with gas bubbles moving against a liquid flow, the ideal situation would be to isolate these flows so that there are discrete paths for gas and liquid. The simplest way to approach this ideal situation is to make the diffusion layer surface hydrophobic by treating it with PTFE. The cathode of the DMFC may be similarly affected by possible flooding problems, but in comparison to the anode this is a less critical issue. Some work has been done in order to explore the effect of the PTFE content as an effective way to mitigate the two-phase flow problems and obtain optimised performances [48, 54, 146–149].

In addition, in passive DMFCs, the current collectors are responsible for collecting electrons and supplying fuel and oxidant to the reaction zone. Therefore, the CCs must have high electrical conductivity, low thermal conductivity, high corrosion resistance and low cost. CCs may be in the form of channels or a specific pattern, covering the entire area or may have a porous structure with different open ratios and sizes. Several studies were performed in order to investigate the effect of the CCs material and design on the fuel cell performance [52, 54, 59, 150–153].

Besides the optimisation of the different fuel cell components, it is also possible to enhance the performance of a passive DMFC through clamping effects [154], the shape and size of the active area [155], and different cell layouts [156, 157]. It is also possible to increase the power output for specific applications (volume and weight) by connecting single cells to obtain a stack configuration [158–166]. A fuel cell stack should have a uniform distribution of reactants in each cell, proper heat management, lower ohmic losses and no leakage of reactants. To achieve these requirements some work has been done towards the development of high performance and efficient passive DMFC stacks [158–166].

The power output of passive DMFCs has been considerably increased in the last years, but it must be further increased in order to achieve the levels needed for portable applications. Another important issue is the DMFC's cost, since in order to reduce costs, while new low-

cost catalysts are not commercially available, the solution is to reduce the catalyst loadings of the available ones by developing more active catalysts, with higher surface areas, controlling the particles size distribution, morphology and crystallinity. The development of a MEA, with a low methanol and water crossover rates and cost, by changing the catalyst layer loadings, DL properties and membrane thickness, will be the key issue to develop a reasonable DMFC system.

2.7. Mathematical modelling

Mathematical models have been used as the fundamental tool for design and optimisation of the fuel cells systems, since they help to better understand the different phenomena occurring within the cell. The development of a DMFC involves multidisciplinary knowledge of electrochemistry, material science and engineering. Besides, the performance of these devices is affected by different phenomena and parameters. Investigation of the effect of each one independently and/or possible combinations of them using experimental work is costly and time-consuming, so the development of mathematical models is a crucial tool to define the most suitable set of parameters to be used in the design and optimisation of DMFC systems with limited time and money.

Different modelling approaches are available in literature, and these include the basic models (analytical and semi-empirical models) and the phenomenological ones (mechanistic models) [115, 167–201].

The basic models – usually one-dimensional (1D) – are satisfactory tools for understanding the elementary effect of the different operating conditions and design parameters on cell performance. These models can also help to evaluate issues such as water and methanol crossover and can be useful for rapid calculations. However, they overlook some of the most important features, such as transient performance and spatial non-uniformities. The semi-empirical models combine theoretical differential and algebraic equations with empirically determined correlations. The great advantage of these models is their simple structure and the small computational effort to perform calculations. However, the parameters estimated from the experimental data are normally specific to a certain type of cell and valid for a limited range of operating conditions. These models are very useful to perform quick predictions for existing designs but fail to predict innovative ones. Mechanistic models are transport models using differential and algebraic equations whose derivation is based on the

electrochemistry and physics governing the phenomena taking place in the cell. These equations are numerically solved by different computational methods involving extensive calculations, but accurately predict all the phenomena occurring in the cell. Moreover, since the transport phenomena in a DMFC is inherently three-dimensional due to the two-phase flow pattern both at the anode and cathode, a deep understanding of the cell's operation is needed, and computational fluid dynamics (CFD-based) models can provide very important information regarding the two-phase flow effects on the cell performance [180, 189, 192, 197–199]. These models enable a user-defined multidimensional cell geometry and a sophisticated treatment of the transport phenomena based on the mass, momentum, energy and charge conservation equations, thus providing great insights towards the understanding and optimisation of the cell design. However, the high computational time demands significantly limit their practical use. Therefore, these models are only suitable when focusing on the design of passive DMFCs, where real-time system-level simulations (including DMFC stacks) are considered unworkable.

The majority of the fuel cell models aims to describe the interactions occurring among the several physical and electrochemical phenomena within the different layers of the cell [168–172, 175, 178, 179, 182, 186, 190–193, 195]. However, some of them allow a detailed study of the effect of a specific parameter on cell performance, such as methanol concentration, cell design or DL properties [115, 173, 183, 184, 187–189, 191–193, 200, 201] and/or phenomena, like methanol and water crossover [174, 180, 181, 185, 194–196]. Since thermal management is a key issue in portable DMFC systems, it is important to develop models accounting for this effect, but until now few passive DMFC models account for this effect [167, 171, 175, 187].

In spite of the modelling work on passive DMFCs developed in the past years, a number of unsolved issues demand for intensive research. One of the most important areas to investigate is the numerical modelling of two-phase flows (both in the anode and cathode sides) and parallel experimental studies on visualization of these phenomena. In order to go ahead with passive DMFC modelling, it is desirable to use the advantages of each modelling approach (simpler and more complex models), coupling 1D analytical models, which describe heat, mass and electrochemical phenomena occurring in the MEA with more complex models, which describe the two-phase flow patterns in the other layers. The final goal of this innovative approach is to obtain simpler 1D+2D/3D models able to correctly

describe the cell performance, as well as the two-phase flow patterns and their effects on the cell performance and methanol and water crossover rates, with reduced simulation times.

2.8. Lifetime/Durability

The lifetime of a passive DMFC can be described as the ability to maintain a constant power output over time. Studies on this issue have shown a power density loss of 30 % with the operation time. This was primarily due to permanent losses, such as delamination of the catalyst layer, effects on the membrane, and agglomeration of the catalyst particles, which lead to a loss of the electrochemical active surface area of the catalysts [13, 27, 61, 147, 202–211]. However, in order for passive DMFCs to become an accepted alternative power source for portable applications, the target requirements from the DOE (U.S. Department of Energy) are 5000 hours with an efficiency loss of up to 20 %. Therefore, cell degradation is another important challenge to overcome on the passive DMFC technology. Despite the fact that the loss of efficiency during the fuel cell's lifetime is unavoidable, it can be minimized through an understanding of the degradation and failure mechanisms.

The durability of a fuel cell can be analysed by monitoring the current under the desired operating conditions and recording the changes in cell voltage over the time. In this test, a polarisation curve is recorded at the beginning and at the end of the lifetime test and both results give the degradation rate, which is estimated using the voltage drop measured. However, this procedure implies the operation of the cell for hundreds or thousands of hours and since each component and operating condition requires a lifetime test, this will lead to long test periods and high costs. Therefore, to reduce the experimental time, different strategies to accelerate the fuel cell and its components degradation have been set. The fuel cell and/or fuel cell components degradation can be accelerated by strongly increasing the stress levels, or by increasing the frequency of the stress applied. The stress factors that can be used to accelerate the degradation mechanisms in fuel cells are the operating temperature, voltage and current density. Hence, the accelerated stress tests (ASTs) are often conducted under very stressful conditions, such as OCV, high temperature or high current densities.

Despite the usefulness of the durability tests, they do not allow us to identify the type of degradation and failure mechanisms that lead to those losses, since they are different: for example, decomposition of catalyst particles, poisoning of catalysts by by-products or impurities, corrosion of the carbon support, membrane thinning, corrosion of the current

collectors, variation of hydrophobic/hydrophilic properties in the catalyst and diffusion layer, among others.

The fuel cell degradation can be permanent/irreversible or temporary/reversible; in this last case, performance losses during the cell's operation can be recovered. Some examples of temporary degradation are cathode flooding and carbon dioxide accumulation at the anode side, with hinder oxygen and methanol transport, respectively [13, 27, 147]. To avoid cathode flooding, the cathode diffusion layers are usually PTFE treated to create a hydrophobic surface. However, the degradation of the diffusion layer characterized by loss of hydrophobic property leads to a water accumulation on the cathode side, obstruction of oxygen diffusion to catalyst sites [202, 205, 206, 209]. These issues affect the performance and lifetime of DMFCs.

The permanent degradation has a chemical, thermal or mechanical nature and occur, due to the presence of foreign ions and contaminants, due to an increase of the cell temperature during cell operation and due to the compression during the cell assembly or MEA fabrication, respectively. The chemical degradation can cause changes on the chemical composition of the different fuel cell layers and membrane thickness, the thermal one lead to a decrease of the ionic conductivity and mechanical strength of the membrane and the mechanical degradation occur due to perforations, cracks and pinholes in the membrane [13, 27, 61, 147, 202, 204, 205–209].

The most relevant factors responsible for a permanent degradation are the catalyst degradation (degradation of ruthenium and platinum particles, delamination), membrane degradation (degradation of the sulphonic acid groups, delamination), catalyst support and diffusion layer degradation (changes in hydrophobic and hydrophilic properties and pore size) and current collector degradation (corrosion). As mentioned above, Pt/Ru is used as anode catalyst in DMFCs to ensure an effective methanol oxidation and to avoid the catalyst poisoning. However, due to the limited stability of the ruthenium in the Pt/Ru alloy, at high current densities Ru can cross the membrane towards the cathode via electro-osmotic water flux, reducing the CO poisoning tolerance of the anode catalyst, due to the adsorption of the oxidation intermediate products, such as formaldehyde and formic acid, which hinder the oxidation reaction of fresh methanol, decreasing the anode electrochemical reaction rate.

This also leads to a deposition of Ru at the cathode, lowering the efficiency of the oxygen reduction reaction and increasing the ohmic resistance of the ionomer and the oxidation of the catalyst [13, 147, 204, 205, 208–211]. The phenomenon of Ru dissolution and crossover

has been extensively studied in normal fuel cell tests under different operating conditions and in accelerated degradation test (ADT) with potential cycling [202]. During long-term operation, a degradation of the catalyst may also, occur due to sintering and decomposition, agglomeration, growth and dissolution of its particles, leading to a reduction of the catalyst active surface area [147, 202, 205].

Another problem that damage the DMFC's durability is a failure on the cell water management, which will lead to corrosion problems on the current collectors and cell flooding, decreasing the cell's lifetime. Current collectors used in passive DMFCs are generally made from stainless steel, which suffers from corrosion after a long-term operation, increasing the contact resistance between the current collector and the MEA and leading to the presence and accumulation of the corrosion products on membrane, catalyst and diffusion layers, poisoning them [13, 27, 61]. The presence of these compounds on the membrane lead to a decrease of the membrane conductivity and hinders the transport of protons to the cathode side [61].

Therefore, it is mandatory to understand the different degradation mechanisms by investigating the state of the different fuel cell components before and after the lifetime test. It is necessary to use complementary electrochemical measurements, such as electrochemical impedance spectroscopy (EIS) [204, 207–211] and cyclic voltammetry (CV), besides physical and chemical techniques, such as X-ray photoelectron spectroscopy (XPS), scanning electron microscopy (SEM), transmission electron microscopy (TEM) and Raman spectroscopy (RS), to identify the different specific phenomena that lead to overall efficiency loss [204].

2.9. Economic evaluation

As mentioned before, passive DMFCs are ideal candidates for replacing the conventional batteries in portable applications. However, one of the main barriers to their wide commercialization is its high cost. Passive DMFCs cost more than Li-ion batteries due to the need of relatively high catalyst loads of expensive catalytic materials such as noble metals like Pt and Ru, the expensive Nafion membranes and the costly metal coating (such as Au) on the current collector. As reported by a Korean company in 2007, the production cost of a 20 W DMFC for powering a laptop was estimated to be 297 €, which is ten times higher than the cost of manufacturing a Li-ion battery with the same power output [212].

Moreover, the DOE target cost of portable DMFC systems is between 4.5 €/W and 6.2 €/W for systems of 100-250 W and 10-50 W in size, respectively.

In 2009, Rashidi et al. [7] studied the feasibility of using a passive DMFC to power portable devices for an operational period of 4 years by comparing these results with the ones obtained with a Li-ion battery. The results showed that during the first year of operation the conventional battery had a lower cost than the passive DMFC. However, after 4 years of operation, the cost of the passive DMFC system was lower because during the operation time it was necessary to replace the battery more than once, which drastically increased its overall cost. In addition, CO_2 emissions during the operation of the DMFC were lower than the battery system leading to a lower carbon offset cost, which proved that DMFCs are a more environmentally friendly technology. Also, in 2009, Hashim et al. [213] developed a passive micro-DMFC stack carried out a cost analysis, where it was concluded that the cost of using a micro-DMFC stack is equivalent to the costs of Li-ion batteries.

In the recent years significant progress has been made to decrease the cost of passive DMFC systems by developing new catalyst made from low-cost materials, non-Pt catalyst, reducing the catalyst loads, using new low-cost membranes and current collectors with materials that have lower costs and higher corrosion resistance.

In 2017, Munjewar et al. [14] presented a review paper concerning the development of materials for passive DMFC systems, among which were the development of electrolyte membranes, different catalysts and current collectors, based on the economic viability of the passive DMFCs. It was shown that non-fluorinated membranes involved lower costs and methanol and Ru crossover rates, than the fluorinated (Nafion®) ones, but they were not competitive in terms of fuel cell performance. The development of novel low-cost anode electro-catalyst with better kinetics and an optimised coating of the current collect in order to ensure and optimal balance between the corrosion resistance and its cost were identified as key factors in favour of the commercialization of passive DMFCs. In other work, Munjewar et al. [13] reinforce that the ways to reduce the costs of a passive DMFC are reducing the catalyst loadings, developing non-Pt catalyst and looking for alternative and less costly membrane materials.

Table 2.2 shows some components usually used on the development of a passive DMFC and its costs. These materials are available in the market, and can be acquired, for example, to QuinTech (a Germany company) and Fuel Cell Store (a U.S. company), and some of them will be used in the course of the current work.

Table 2.2. Cost of the main components used in a passive DMFC and available in the market.

Component	Characteristic	Cost (€)	Cost (€/cm^2)
Nafion 117	10 x 10 cm	32.50	0.325
Pt-Ru	20% Pt Ru on Vulcan Carbon – 1g	89.00	-
Pt	20% Pt On Vulcan Carbon – 1 g	79.00	-
Carbon cloth (CC)	Thickness 0.400 mm; 30 x 30 cm	95.00	0.106
Carbon cloth (CC_T)	Thickness 0.425 mm, 30 x 30 cm	108.00	0.120
Carbon cloth with MPL (CC_MPL)	Thickness 0.410 mm; 20 x 20 cm	45.00	0.113
Carbon cloth with MPL (CC_MPL_E)	Thickness 0.454 mm; 10 x 10 cm	35.00	0.350
Carbon paper (CP)	Thickness 0.110 mm; 19 x 19 cm	130.00	0.360
Carbon paper (CP_T)	Thickness 0.190 mm; 19 x 19 cm	101.00	0.280
Carbon paper with MPL (CP_MPL)	Thickness 0.240 mm; 20 x 20 cm	45.00	0.113
Carbon paper with MPL (CP_MPL_T)	Thickness 0.340 mm; 20 x 20 cm	45.00	0.113
End plates	Acrylic; 10 x 10 cm	98.00	-
Current collector	Stainless steel	0.50	-
Current collector	Titanium	4.70	-
Coating	Au, 10 x 10 cm	73.00	0.730
3-layer MEA	Anode 3.0 mg/cm^2 Pt/Ru, Cathode 1.2 – 1.4 mg/cm^2 Pt, Nafion 117	132.00	-

2.10. Applications

DMFCs are promising candidates for portable applications because of their high energy density, light weight, compactness and simplicity, as well as providing longer power-on times with rapid refills. Compared to conventional power technologies, passive DMFCs also have other advantages, such as increased efficiency, greater scaling flexibility and reduced emissions. DMFCs theoretically have five to ten times higher specific energy density than rechargeable batteries, and can operate for a longer time, i.e., more conversation time when using mobile phones, more time when using laptop computers and more power available on these devices to support the consumer demand [6]. Another advantage of DMFCs is their potential for instant refuelling, since a rechargeable battery requires hours to charge, while a DMFC can be charged in minutes by a simpler replacement of the fuel. Micro passive

DMFCs are expected to enable consumers to use a mobile phone for up to a month without recharging.

Passive DMFCs can be used, mainly as substitutes of conventional batteries like those in mobile phones, laptops, tablets, portable music players or portable power tools, as well as low-power remote devices such as hearing aids, smoke detectors, burglar alarms, hotel locks and meter readers. Some companies developing these systems for portable power sources are Casio, Direct Methanol Fuel Cell Corporation, Hitachi, MTI Micro Fuel Cells, Motorola, Panasonic, Samsung Advanced Institute of Technology, Sanyo, Smart Fuel Cells and Toshiba [2].

DMFCs can also be used in stationary applications, such as auxiliary power units supplying energy to residences and industries. They can be connected to the electric grid to provide supplementary power and/or as backup power or installed as a grid-independent generator or decentralized power supply, for on-site services in areas where there is no power lines. In transportation, these fuel cells are incorporated into buses, trains, scooters and golf carts. Ships, yachts and fishing boats can also be powered using on-board DMFCs. Some examples of DMFC applications are shown in Figure 2.7.

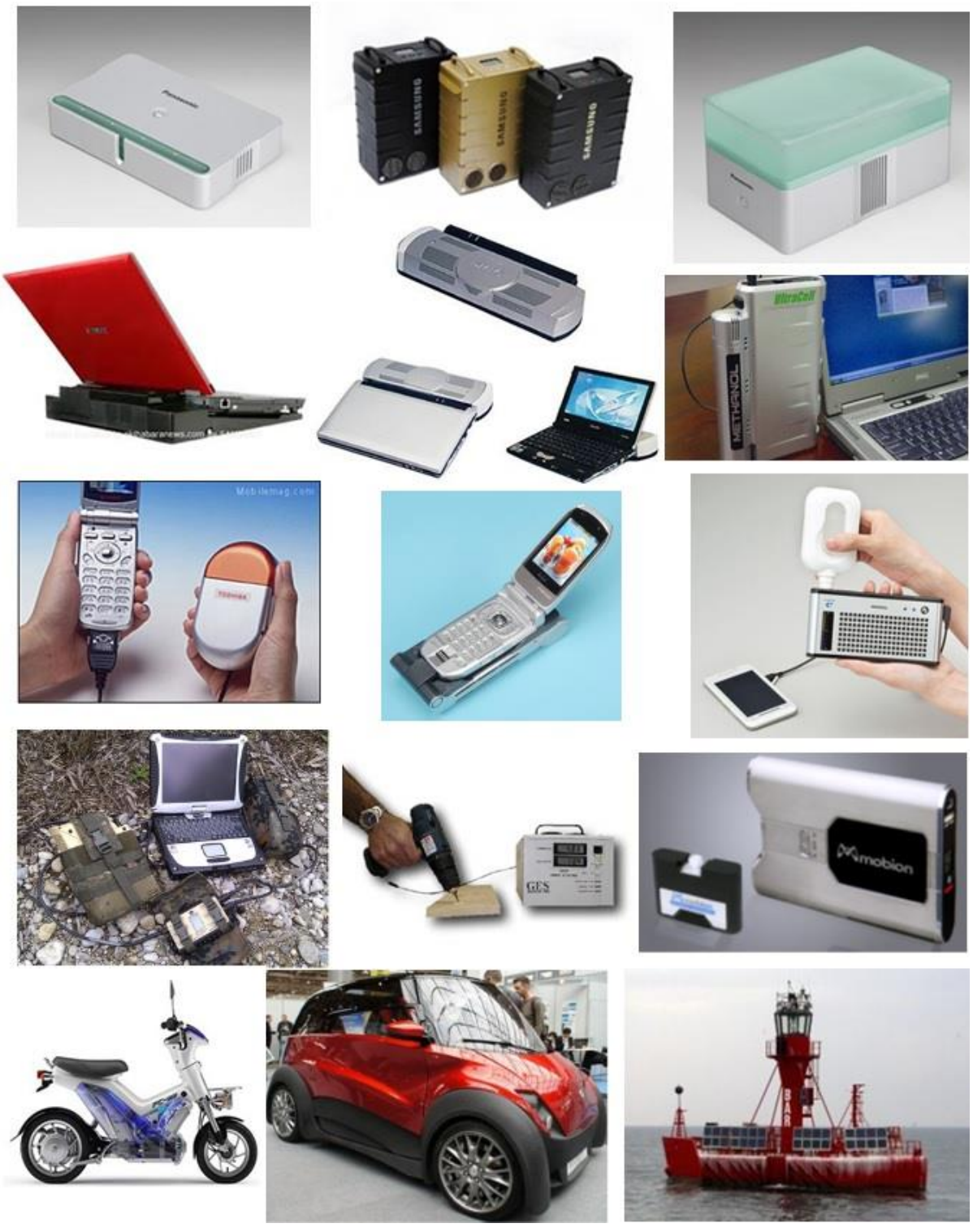

Figure 2.7. Some DMFC applications.

2.11. Summary

The fundamentals and challenges of passive DMFCs have been summarized and the recent modelling and experimental studies have been reviewed. An economic outlook of this technology was also presented. As was mentioned, for the practical applications of this technology cost effectiveness is essential. Additionally, the passive fuel cell systems must be made small and compact for portable applications, and each application has different power requirements.

In the last years, some efforts have been made on the development of passive DMFC systems with enhanced performances at an attractive cost. Some studies have been focused on the analysis and improvement of single parts of these systems and different materials, designs and operating conditions have been suggested. Although the results of these studies are useful, it is important to refer that materials and conditions optimised for one type of fuel cell may not always be recommended for another one. Therefore, when developing a passive DMFC, the materials and conditions must be carefully chosen in order to achieve optimal performances.

A great challenge on the progress of this type of fuel cell, for its use in real applications, is the development of cost-effective materials. To achieve that, different materials must be explored as current collectors, membrane, and diffusion and catalysts layers. Furthermore, it is mandatory to reduce the actual catalyst loadings through the development of more active catalysts, with higher surface areas, by controlling its particle size distribution, morphology and crystallinity. Despite the work already performed, additional studies on cost-efficient electrode materials with optimised configurations are needed.

A key issue in DMFCs is the methanol crossover, since methanol diffuses through the membrane generating heat but no power. This can be limited if the cell operates with low methanol concentrations, but this significantly reduces the system energy density since large amounts of water are present in the system. In addition, this creates a higher water concentration gradient between the anode and cathode side, so more water crosses the membrane. The existence of large amounts of water at the cathode, due to crossover and water production at the cathode reaction, may lead to cathode flooding, with a consequent decrease of the cell performance. The solution is to operate the cell under high methanol concentrations and use different membranes, diffusion and catalyst layers materials with different thicknesses.

Mathematical models appear as a useful tool to understand and predict the main transport phenomena and electrochemical processes, helping in fuel cells optimisation in terms of design and power output. In spite of the modelling work on passive DMFCs developed in the last years, a number of unsolved issues still demand for intensive research, such as the two-phase flow phenomena at both anode and cathode sides. Such models will be helpful for the development of new cell designs and operation regimes for passive DMFC systems. For commercialization of these devices, significant effort has to be put on the development of optimised systems with an optimum balance between its cost, efficiency, reliability and durability.

CHAPTER 3

3. ELECTROCHEMICAL IMPEDANCE SPECTROSCOPY

Passive direct methanol fuel cells (pDMFCs) are a promising power source for portable electronic devices since they achieve higher power densities than the traditional batteries, and use a liquid fuel, methanol, which is easy to handle, storage and distribute. However, some key challenges, such as fuel and water crossover through the membrane and the system durability/lifetime and costs, need to be overcome in order to introduce these systems in the market. The electrochemical impedance spectroscopy (EIS) is used in fuel cell systems as a powerful tool to diagnose the cell behaviour and acquire useful information regarding the different losses that negatively affect the cell performance, towards its optimisation. This section presents a review of the work developed with pDMFCs using the EIS technique as a diagnostic tool. This section also includes the EIS fundamentals and the equivalent electric circuit concept.

The contents of this Chapter conducted to the preparation and submission of the manuscript: B. A. Braz, V. B. Oliveira, and A. M. F. R. Pinto, "Electrochemical impedance spectroscopy as a diagnostic tool for passive direct methanol fuel cells".

3.1. Introduction

The energy demand of portable electronic devices is increasing day by day mainly due to an increase of their functionalities, which decrease their autonomy and require their constant recharge. However, this energy can no longer rely only on fossil fuels because, as it is well known, these fuels lead to serious environmental problems and are limited. Therefore, the search and use of alternative technologies to produce energy, such as fuel cells is mandatory. Passive DMFCs were targeted as a promising technology mainly for portable electronic devices, since they convert directly the chemical energy of a fuel, methanol, into electricity, without any additional power consumption. Additionally, methanol is a liquid fuel at room temperature, is easy to handle, store and distribute, has the highest energy to carbon ratio of any other alcohol and can be environmentally friendly if generated from biomass. Furthermore, passive systems are simpler and compact, operate at ambient conditions and

without any power consumption, being for these reasons more suitable for powering portable power sources [13, 27, 214]. However, pDMFCs have some key challenges that need to be overcome before their implementation in the market, such as slow kinetics, methanol and water crossover, short lifetime and high costs.

The performance of a pDMFC is commonly evaluated through its polarisation or power density curve. This procedure allows accessing the key losses affecting the cell performance, such as activation, ohmic, concentration and crossover losses. However, it is a hard task to quantify and relate them to the different processes and parameters that characterize this type of fuel cell. Additionally, each type of loss depends on both the fuel cell operating conditions and configuration (materials, design, construction and manufacturing), being the experimental examination of the impact of each operating condition and configuration parameter on the cell performance time consuming and costly. Therefore, different diagnostic tools, such as EIS, have been used in fuel cell systems characterization and are helping to identify the synergies between the fuel cell behaviour and the structure/properties of each component.

EIS is a non-intrusive and well establish diagnostic technique that has been widely used in electrochemical systems due to its precision and flexibility, allowing to cover a wide range of phenomena and characteristics of fuel cell systems [211, 215–217].

This section presents a review on the studies conducted in pDMFCs using EIS as a diagnostic tool, after introducing the EIS methods and other different aspects, such as, the equivalent electric circuit concept. The text also includes the uncertainty associated and possible errors performed on the explanation of the EIS data of pDMFCs and new interpretation lines.

3.2. Electrochemical Impedance Spectroscopy

The EIS technique is used to measure the frequency dependence of the impedance, which can be defined as the ratio between the time-dependent voltage and the time-dependent current. This measurement is carried out by applying a sinusoidal perturbation to the system and measuring the response in a wide range of frequencies. This can be performed using a frequency response analyser (FRA) and a load bank, since the FRA produces the perturbation that is applied to fuel cell by the load bank and captures the corresponding system response. Then, this response is presented in an impedance spectrum, represented by a Nyquist or Bode plot [211, 215–217]. The Nyquist plot is the most commonly one and

where the imaginary part of the impedance is plotted against the real one. In a Bode plot the amplitude or phase of the impedance are plotted as a function of the frequency.

3.2.1. EIS measurements

EIS measurements can be performed either in galvanostatic or potentiostatic modes, applying a perturbation, respectively, on the current or on the voltage. It has been reported that there are no significant differences between the galvanostatic and potentiostatic results [211, 215–217]. Contrarily, the amplitude of the perturbation induced to the system as a significant impact on the system response, since when performing an EIS measurement it is mandatory to ensure a linearity of the system response. The impedance is calculated by measuring the changes in the potential/current over the changes in the current/potential and this estimation can only be accepted if the potential/current changes linearly with the current/voltage. However, as this do not happen in fuel cells systems, the amplitude selected to perform the tests needs to be small enough to ensure linearity, but it also has to be high enough to be captured within the measuring range and consequently not confused with noise. Impedance measurements in pDMFCs generally use amplitudes between 5 to 15 mV, in potentiostatic mode, and a frequency range from 1 mHz to 100 kHz with 10 points/decade [48, 88, 96, 127, 128, 133, 137, 139, 144, 149, 211, 215].

The EIS measurements can be conducted *in-situ*, to analyse a single fuel cell as a whole or a fuel cell stack, or *ex-situ,* to study individually the different fuel cell components, such as membranes, catalysts, diffusion layers and current collectors. Although these measurements are carried out outside the fuel cell environment, the conditions used to perform the *ex-situ* measurements are as close as possible to the ones of a working fuel cell. These measurements are carried out using a classic three-electrode configuration, which includes a working electrode (WE), a reference electrode (RE), and a counter electrode (CE), using sulphuric acid [55, 146, 218–222] or an Ag/AgCl electrode as counter and reference electrode [85, 223, 224].

In-situ measurements in a passive DMFC are normally performed in a two-electrode configuration, the usual fuel cell configuration, with hydrogen fed to the anode or to the cathode, which acts as the counter and reference electrode, and methanol to the anode or oxygen to the cathode, respectively, being this side the working electrode [225, 226]. This is possible since it is commonly accepted that the losses associated with the DHE (dynamic

hydrogen electrode) are irrelevant and consequently all the measurements are attributed to the other electrode. Accordingly, if in a pDMFC the DHE is used at the cathode, it is possible to study the anode behaviour and obtain the anode spectrum. Afterwards, performing the impedance measurement with the cell working with methanol at the anode and air/oxygen at the cathode, it is possible to obtain the overall pDMFC spectrum. Then the cathode spectrum is obtained by the difference between the overall and the anode spectrums [96, 97, 99, 134, 135, 140, 211, 215, 227]. The *in-situ* measurements can also be performed with an independent reference electrode, such as Ag/AgCl, allowing to realize the measurements in a real pDMFC environment, with methanol and oxygen, respectively at the anode and cathode sides [84, 88]. Nevertheless, adding an additional electrode requires an adaptation of the fuel cell system and the hardware used to execute the measurements, which is still a challenge for systems that work with solid electrolytes [215, 225].

3.2.2. Impedance Spectrum: Nyquist Plot

As already mentioned, the most common way to represent an impedance spectrum is through a Nyquist plot, where the imaginary part of the impedance is plotted against the real one [211, 215–217]. This plot can present one, two or three semicircles in different frequency ranges, which represent the major losses that affect the fuel cell systems, as depicted in Figure 3.1. The Nyquist plot depends on the conditions used to perform the impedance measurements, and in some situations, the arcs that represent the different losses that negatively affect the system under study can be observed without a distinct separation and in different patterns. In this case, the study of a specific system parameter/condition becomes more complex and a deeper investigation is required [216, 225].

Considering the ideal behaviour, at the high-frequency region, the imaginary impedance axis intercepts the real impedance one at a value called the high-frequency resistance (HFR) of the system representing the ohmic losses, ohmic resistance (R_Ω), including contact, ionic and electronic resistances [215, 216] (as shown in Figure 3.1).

At the medium-frequency region, the Nyquist plot shows an arc due to the activation losses and/or charge-transfer resistances, which decreases with a decrease of the voltage. These losses are due to the methanol oxidation reaction at the anode side and oxygen reduction reaction at the cathode side. Considering the EIS measurements carried out in a pDMFC fed with methanol and oxygen/air, the charge-transfer resistance occurs at both sides

simultaneously. Therefore, this may lead to an overlap of the two arcs, making impossible to distinguish the activation losses of each reaction. This region is very useful to analyse the effect of the catalyst properties on the fuel cell performance, since an electrode with a lower activity will originate a larger arc. At the low-frequency region, the arc indicates the mass transfer losses and is characterized by an increase of the resistance with a decrease of the fuel cell voltage [211, 215–217, 225].

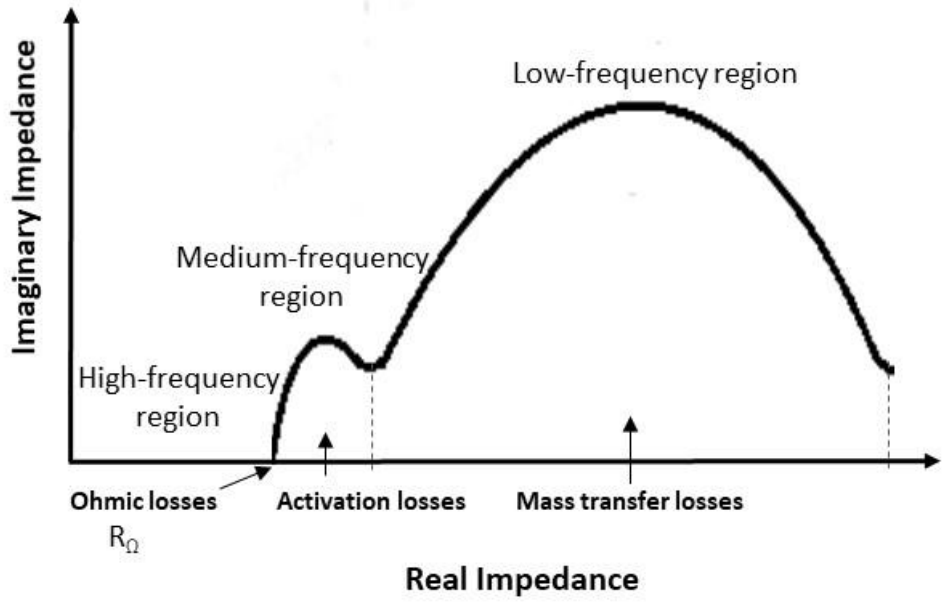

Figure 3.1. Representation of a typical Nyquist plot with the three major losses that negatively affect the fuel cell performance.

However, in some systems, such as in pDMFC systems, it is not possible to reach the mass transport region and therefore none of the resistances that negatively affects the fuel cell performance increases with a decrease of the voltage. In these conditions, the Nyquist plot may present an arc at the low-frequency region, which is not due to mass transport losses. Therefore, the arcs at the medium and lower frequency region are due to the activation losses, characterized by a decrease of the resistance with a decrease of the voltage. After verifying that, the great challenge is to link the different activation losses with the different phenomena/processes that characterize a working pDMFC. As already mentioned, the activation losses are due to the electrochemical reactions that occur in the fuel cell. In an ideal case, these include the methanol oxidation (anode side) and the oxygen reduction (cathode side).

3.2.3. Equivalent electric circuit (EEC)

The EIS data analysis is usually carried out by an equivalent electric circuit (EEC), which enables obtaining the electrochemical parameters of the system and estimating their most significant properties [225]. An EEC is a combination of different electric elements, such as resistors (R), which represent the ohmic resistances, capacitors (C), characterized by its capacitance, defined as the ratio between the stored electric charge and the voltage drop through the electrodes, and inductors (L). In a pDMFC the inductive behaviour comes from the slowness adsorption of different species, such as, the CO adsorption at the anode catalyst surface, and considers possible interferences due to wires or other sources of disturbance [86, 97]. As in fuel cell systems the capacitor has a non-ideal behaviour, due to a non-uniform distribution of the current, non-homogeneities of the reaction rates and surface roughness, it is usually replaced by a constant-phase element (CPE). Another additional element, commonly used in fuel cells systems, is the Warburg element (W), which is used to describe the diffusion processes occurring in a working fuel cell. This element can be identified through a linear response to changes in frequency, a line with an angle of 45º, and is observed at the low-frequency region [117, 217, 225, 226]. It should be here mentioned that whereas the ohmic resistance can be represented using a single element, a resistor, the other phenomena, such as activation and mass transfer losses, can only by represented using different elements linked together in series and/or parallel, depending on the characteristics and shape of each spectrum.

Additionally, the EEC should be as simple as possible but representing with accuracy the electrochemical system under study and this can be achieved through the analysis of the general pattern of the impedance spectrum, represented through the Nyquist plot. Reminding Figure 3.1, where a typical Nyquist plot for a fuel cell system is presented, it is possible to identify two arcs without diffusion as a rate determining step (since the presence of a Warburg element can be identified through a linear response to changes in frequency), which are represented by two parallel combinations of a resistor and a constant-phase element, as shown in Figure 3.2. Therefore, the equivalent circuit for the electrochemical system with the response presented in Figure 3.1, consists of two parallel R-CPE elements to model the activation and mass transport losses. Additionally, another resistor is needed to describe the ohmic losses represented by the point where the plot intersects the real impedance axis and an inductor to account the inductive behaviour that characterize these systems [211, 217,

225, 226]. After selecting the EEC based on the impedance spectrum, the EEC is fitted to the Nyquist plot and it is possible to estimate the value of each element used on the EEC, the most important ones are the ohmic (R_{Ohm}), activation (R_{act}) and mass transfer (R_{mt}) resistances.

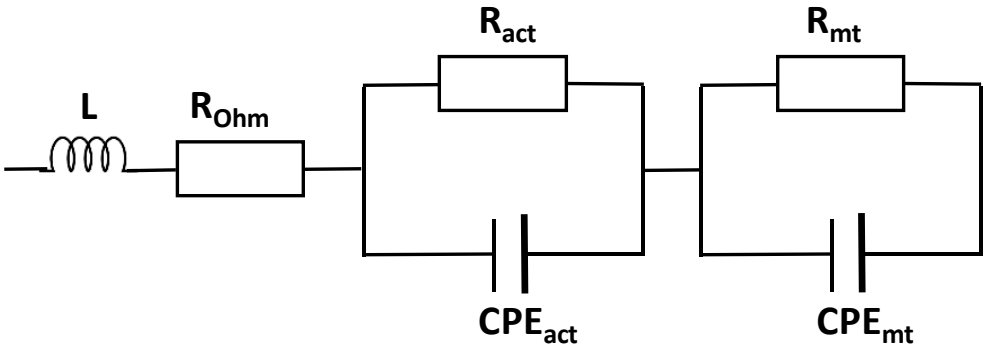

Figure 3.2. Equivalent electric circuit for a pDMFC considering the activation and mass transport losses.

3.3. EIS in passive DMFCs

Since the EIS technique provides significant information on the overall fuel cell performance and on the effect of each parameter, condition and component on the cell behaviour, it has been used in pDMFCs. This section provides an overview of the applications of the EIS technique in pDMFCs research, with emphasis on the *in-situ* measurements.

3.3.1. Diffusion layers

The diffusion layers play an important role in pDMFCs, since they are directly related to the different species transport. Therefore, different studies have been performed in order to improve the methanol [96, 99, 227] and oxygen [104, 148, 228] transport rates, by decreasing both the activation and mass transfer resistances. With this aim, Yuan et al. [96] prepared an anodic diffusion layer using graphene-carbon nanotubes (CNTs) as the anodic microporous layer (MPL). The proposed material, a new hybrid material, has a good hydrophilicity and a large pore volume, which can improve the methanol transfer and the carbon dioxide removal rate at the anode side. The impedance results, with a methanol concentration of 4 M and a DHE at the cathode, demonstrated that the addition of graphene-CNTs led to a decrease of

the activation resistance of the anodic reaction. The performance of the pDMFC showed an improvement due to the crack-free MPL, which also helped on decreasing the methanol crossover rate. The same author also investigated the effect of adding CNTs to the anodic MPL on the performance of a micro pDMFC [227], through EIS and cyclic voltammetry. The EIS tests were carried out using a DHE at the cathode side. The results showed a decrease of the activation and mass transfer resistances and an improvement of the catalyst utilization with the addition of the CNTs and consequently an enhancement of the fuel cell performance. Wu et al. [99] studied the use of polypyrrole nanowire networks (PPNNs) as anodic MPL in a pDMFC. EIS measurements were used as part of the electrochemical characterisation, feeding the cell with a methanol concentration of 4 M and using a DHE at the cathode. The results revealed that the use of PPNNs at the anode side allowed decreasing the anodic mass transfer resistance, enlarging the carbon fibre surface area, improving the catalyst utilisation and decreasing the anodic catalyst loading.

Cao et al. [104] proposed a novel MEA design using a double MPL at the cathode side of a pDMFC. The EIS results indicated that the use of this double MPL improved the cell performance due to a decrease of the activation transfer resistance of the oxygen reduction reaction (ORR). The results also showed an improvement of the oxygen transfer rate and a reduction of water crossover from the anode to the cathode. The same authors presented a new cathode diffusion layer (CDL) with mesoporous carbon (MC) applied on a pDMFC [148]. The EIS results showed a significant decrease on the activation and mass transport resistances with this new CDL. Moreover, this new layout promoted the water back diffusion, leading to an increase on the cell power density and an enhancement of its discharge stability. Chen and Zhao [228] proposed a novel architecture for the MEA of a pDMFC, using a porous metal structure for oxygen transport and electrons collection instead of the conventional cathode diffusion layer materials, carbon based materials. From the EIS results, it was possible to observe a decrease on the mass transfer resistance, which allowed an improvement of the oxygen transport, a higher performance and a more stable operation of the pDMFC.

3.3.2. Catalyst layers

Regarding the catalysts layers, the research work that has been done in pDMFCs aims to improve the catalyst activity [84, 88, 135, 162, 229] and/or decrease the catalyst loadings

[86, 97, 140], to reduce the overall system costs. Yuan et al. [135] evaluated the effect of decreasing the Nafion aggregate size within the anode catalyst layer on the performance of a pDMFC. The EIS measurements were performed with a DHE at the cathode and the results indicated a decrease on the activation resistance of the anodic reaction, with a decrease of the Nafion aggregation within the catalytic ink, which improved the catalyst and the Nafion ionomer utilisation, enhancing the performance of the pDMFC. Reshetenko et al. [229] studied the application of carbon nanotubes (CNT), with a filamentous morphology, as an additive to the cathode catalyst layer, based on a Pt black catalyst, towards the optimisation of the cathode structure. The EIS results indicated a decrease on both ohmic and activation resistances and therefore a faster oxygen reduction reaction. As a result, the power density of the pDMFC increased with the introduction of the CNT. Baglio et al. [162] used the impedance method to investigate different MEA configurations, with different hydrophobic-hydrophilic properties, in a pDMFC mini-stack. These properties were adjusted varying the amount of Nafion or replacing the ionomer in the catalytic layer with polytetrafluoroethylene (PTFE). Golmohammadi et al. [88] studied the use of a binary carbon supported Pd_3CO nanocatalyst by impregnation of multi-walled carbon nanotubes (MWCNTs) to improve the ORR in a pDMFC. The impedance results showed that the introduction of the MWCNTs as a secondary support decreased the activation resistance and increased the surface area, enhancing the ORR kinetics. Gharibi et al. [84] investigated an optimum Co amount in a Pd_xCo/C alloy nanoparticles as a new cathode for the ORR in pDMFCs, using the EIS measurements and an Ag/AgCl reference electrode. Considering that the Pd_xCo/C alloy electrocatalysts do not allow the adsorption and oxidation of methanol, it is expected that they can act as a methanol-tolerant ORR catalyst. The results indicated that the MEA with the Pd_3Co/C cathode showed a better performance, in terms of maximum power density and a lower activation resistance.

In an attempt to reduce the catalyst loading, Chen et al. [140] used a nanofiber network catalyst layer (NNCL) at the anode of a pDMFC, and the impedance measurements were conducted with a DHE at the cathode. The authors found that the anode catalyst layer with a 3D nanofiber network structure significantly increased the catalyst utilisation, allowing to reduce its loading, and decreased the anode activation resistance, leading to a great enhancement on the cell performance. Huang et al. [97] developed a porous anode structure by adding magnesium oxide (MgO) nanoparticles as a sacrificial template into the anode catalyst layer and anode MPL towards an improvement of the pDMFC performance. The

EIS measurements were used to perform the electrochemical characterisation of the anode, using a DHE at the cathode. The results showed that the addition of MgO lead to a decrease of the anode activation resistance, increasing the catalyst utilisation and thus allowing to decrease the catalyst loading. Pu et al. [86] aimed to reduce the catalyst loading of the cathode catalyst using Pt nanorod assemblies based on a double-layer cathode. For the EIS measurements, the cathode was used as the working electrode and the anode as counter and reference electrode, using a DHE at this side. The results showed an improvement of the cell performance due to an increase of the catalyst utilisation and a decrease of the activation resistance with the double-layer cathode. Therefore, the use of the Pt nanorod assemblies allowed a reduction of the cathode catalyst loading.

3.3.3. Membrane

The EIS technique has also been used to study the conductivity of the Nafion membranes for pDMFCs [129, 134]. Pu et al. [134] tried to improve the performance of a pDMFC using a surface-patterned Nafion® 115 membrane by thermal imprint lithography. The impedance measurements were performed with the anode as the working electrode and a DHE at the cathode. Through the EIS results, it was possible to observe that the anode activation and mass transfer resistances decreased with an increase of the roughness. Yuan et al. [129] studied a novel methanol-blocking Nafion® membrane prepared layer-by-layer with graphene oxide (GO) nanosheets in a pDMFC. For impedance measurements, the cathode was fed with pure nitrogen and the anode with a 2 M methanol solution. Results showed that this innovative membrane not only reduced the methanol crossover rate but also enhanced the membrane strength, which led to a higher power density and an improved energy efficiency of the pDMFC.

3.3.4. Current collector

Shrivastava et al. [150] investigated the feasibility of using a stainless steel wire mesh as CCs in pDMFCs, using the EIS measurements to analyse the fuel cell behaviour. EIS results indicated that the mesh made with thicker wires showed the lowest ohmic resistance and in-plane electrical resistance due to a better electrical contact between wires, leading to the best performance. Chen and Zhao [230] investigated the use of a porous metal foam as cathode

current collector in a pDMFC. The impedance results indicated a lower mass transfer resistance with the porous metal foam than when a perforated CC was used, due to a higher specific area. The results obtained also showed that the porous CC yielded a higher and more stable operation of the pDMFC even when the cell was fed with higher methanol concentrations. Mallick and Thombre [151] used expanded metal mesh current collectors (EMCCs) in pDMFCs with different combinations of the supporting plates. The results showed that the pDMFC with EMCCs achieved a better performance than the one with circular perforated CCs. In addition, the EIS measurements indicated a decrease of the mass transfer resistance using EMCCs with a larger open ratio, since it facilitates the reactants access to the catalyst layers. Xue et al. [231] examined the effect of using a stainless steel mesh as a methanol transfer barrier layer in a micro pDMFC. The experimental results revealed that the current collectors with the stainless steel mesh allowed to reduce the methanol crossover rate and the contact resistance.

3.3.5. Water crossover

Mass transport phenomena are crucial issues to overcome in fuel cells systems in order to improve their performance. Regarding the pDMFCs, the researchers have been studying the water crossover through the membrane using EIS as a diagnostic tool for a better understanding of these phenomena. Chen et al. [232] investigated the addition of fluorinated Vulcan XC-72R to the cathode MPL of a micro pDMFC to increase its hydrophobicity and promote the oxygen mass transfer and reduce the cathode flooding. The EIS results revealed a decrease on the activation resistance of the ORR with the new cathode structure, an improvement of the oxygen diffusion and a reduction of the water flooding, enhancing the performance of the micro pDMFC. Chen et al. [42] fabricated a new cathode catalyst layer with a discontinuous hydrophobicity distribution in order to favour the oxygen diffusion and water removal from the cathode. The impedance results showed a decrease on the activation resistance and an improvement of the pDMFC performance. It was concluded that the MEA with a stepwise hydrophobicity distribution at the cathode increased the oxygen transport in a thicker cathode catalyst layer and enhanced the water back diffusion from the cathode to the anode side. Xue et al. [113] fabricated a novel cathode diffusion layer, with reduced graphene oxide deposited in a stainless steel fibre felt (rGO-SSFF), to control the water management issues in micro pDMFCs and use higher methanol concentrations at the anode

side. The cell with this new cathode structure exhibited a higher performance even with higher methanol concentrations, due to a reduction of the cell internal resistances, estimated by the EIS measurements.
In the literature review was not verified the use of the EIS technique to analyse, directly, the effect of the methanol crossover phenomenon in the pDMFCs behaviour. The methanol that crosses the membrane to the cathode side leads to a parasite methanol oxidation reaction at this side, which can cause an extra loss in the fuel cell system.

3.3.6. Manufacturing method

As mentioned above, different factors and/or parameters can affect the fuel cell performance. For example, the clamping and compression of the different fuel cell layers in fuel cell assembly can have a significant impact on the overall performance. Mallick et al. [154] analysed the clamping effect on the performance of a pDMFC using the EIS as the main diagnostic tool. The pDMFC behaviour was evaluated for different clamping combinations (uniform, non-uniform) and different methanol concentrations. The impedance measurements were performed with the anode as the working electrode and the cathode as the counter and reference electrode. From the EIS studies, it was concluded that the non-uniform clamping caused a deterioration of the DMFC performance due to an increase on the ohmic and mass transfer resistances. Shrivastava et al. [48] investigated the effect of the diffusion layer compression rate on the performance of a pDMFC, for different methanol concentrations. The impedance results indicated a reduction of the ohmic losses with an increase of the compression rate, due to a decrease of the contact resistance between the DL and the CC and an increase of the bulk electrical conductivity, and consequently, an improvement of cell performance. This study revealed that the pDMFC working with a methanol concentration of 4 M and a compression rate of 32.5 % enhanced its performance in 200 % to 340 %.

3.3.7. Lifetime/durability

Another application of the EIS technique is to help on the evaluation of the fuel cell lifetime/durability, since the performance degradation is inevitable and is one of the key factors hindering the commercialisation of these systems, due to their lower autonomy.

Despite that, so far, studies on this issue were mostly performed in active DMFC systems. Jeon et al. [207] investigated the stability of a DMFC by keeping a constant current density, 150 mA/cm^2, for 435 h, and using the EIS measurements to quantitatively analyse the performance decay of each component. The EIS studies were carried out under two different conditions: a) analysis of the anode behaviour with a DHE used at the cathode and b) single cell, with oxygen fed to the cathode. The results showed that the internal resistance, which includes the membrane, electrode and interfacial resistances are responsible for 71 % of the performance lost, the cathode activation resistance 24 % and the anode activation resistance 5 %. Chen and Cha [209] presented a strategy to optimise the cathode operating conditions of a DMFC towards an improvement of its durability. In this work, the EIS technique was used to characterise the cell degradation mechanism, using an Ag/AgCl electrode as a reference electrode. Wang et al. [233] investigated the degradation factors in a DMFC, after a stability test of 50 h, using the EIS technique in a three-electrode system. The EIS measurements performed before and after the stability test indicated that the anode degradation was more severe than the cathode one, and the membrane swelling was one of the main factors for the performance degradation. In addition, the authors verified that the dispersion of Ru affected more the cell performance than the catalyst gathering, and cathode flooding was also a key factor on the performance degradation.

Escudero-Cid et al. [210] used a new long-term cycle test, called “start-run-stop-run” (SRSR) to simulate the DMFC performance under realistic operating conditions and understand its degradation mechanisms, using polarisation and EIS measurements. For the impedance tests, the anode was supplied with methanol and the cathode was first fed with oxygen and subsequently with hydrogen. The EIS results showed a lower MEA degradation, and proved that the anode reaction was the main cause for the loss of performance. Lai et al. [208] investigated through an accelerating test the degradation of a DMFC under a highly anodic potential, using the EIS measurements, carried out with this cell working under normal conditions (methanol fed to the anode and oxygen to the cathode). The impedance results indicated an increase in all the resistances with an increase of the degradation test time. The internal resistance increase was attributed to the damage in the ionomers, and the interfacial resistance increase to catalyst degradation, due to Ru dissolution on the anode side. Prabhuram et al. [234] conducted a long-term durability test (500 h) in a DMFC made of a hydrocarbon membrane and Nafion ionomer bonded electrodes. The impedance measurements were performed at the beginning and at the end of the durability test, in

galvanostatic mode and with methanol and air supplied, respectively, to the anode and cathode. Impedance measurements were also performed in potentiostatic mode with methanol at the anode and N_2 at the cathode. According to the EIS results, the internal resistance of the DMFC increased considerably during the 500 h of operation, due to an incompatibility between the polymeric materials, which lead to a performance degradation of 34 %. Bresciani et al. [235] investigated the temporary degradation of a DMFC in a 600 h test cycling and with periodic open circuit voltage interruptions and air-breaks. The results showed both membrane and cathode dehydration, which were responsible for the DMFC temporary degradation. However, this degradation was easily recovered during refresh cycles. The same authors also investigated the degradation mechanisms of each component of a DMFC, through *in-situ* EIS measurements conducted at the beginning and after a full refresh (performance recovery) and at the end of the DMFC lifetime [236]. The results allowed the authors to distinguish the effect of the active area loss at both anodic and cathodic electrodes, and it was verified an increase on the mass transport resistance, membrane degradation and reversible degradation during the operation time. Chen et al. [237] investigated the degradation of a DMFC with a running time above 3000 h with *in-situ* electrochemical tests, applied to analyse the different causes for the performance loss. The EIS data allowed to observe the cathode flooding phenomenon in the low-frequency region explaining the cell performance loss, due to decrease of the cathode catalyst active sites. The results also revealed that a higher operating temperature results in a rapid degradation of the catalyst activity, and a lower temperature causes an increase on the membrane resistance. Rabissi et al. [238, 239] used the EIS technique as a complementary tool to a locally resolved investigation on DMFC uneven components fading to analyse its degradation behaviour. In general, the local-EIS measurements revealed that the water distribution plays a crucial role on the local limitations, mainly at the cathode side, due to dehydration and/or flooding. These limitations are directly related to the local performance losses, making easy the understanding of the degradation behaviour in this case.

As most of the studies here presented were obtained in steady state conditions, which do not correspond to the real applications of these systems, it is mandatory to perform durability tests with active and passive DMFCs under realistic conditions, towards an accurate evaluation of its lifetime/durability.

3.4. Summary

The EIS technique has been considered as a fundamental tool in pDMFCs research and development, since it allows studying and understanding the different processes and/or phenomena that occur in these systems and their effect of the cell behaviour. This chapter intended, therefore to present the different studies done using the impedance diagnosis in these systems, as well as, to provide some fundamentals regarding this technique. As mentioned, the analyse of the impedance results in pDMFCs is very complex since these systems are affected by different processes that occur simultaneously in their normal operation. These include electrochemical reactions at both sides, methanol oxidation at the cathode side, due to methanol crossover, water crossover, heat management issues and two-phase flow phenomena, due to the formation of gaseous carbon dioxide at the anode and liquid water at the cathode. In addition, the selection of the EEC that will be used to represent these systems can lead to some misunderstanding due to an overlap of these phenomena in each frequency region. Therefore, the EEC elements should be selected accordingly to the impedance spectrum, and their combinations need to match with the phenomena observed on the spectrum. When the impedance spectra are well analysed and the EEC is properly chosen, the EIS measurements provide very useful information about the different fuel cell components (DL, membrane, catalyst and CC materials and properties), phenomena (methanol and water crossover, two-phase flow, mass transport, reaction rates) and fuel cell manufacturing (clamping and compression rate), since they allow to access the effect of each one on the fuel cell behaviour and lifetime.

CHAPTER 4

4. EXPERIMENTAL SETUP FOR A PASSIVE DMFC

A passive FC fed with a liquid fuel was used in the experimental studies. This chapter presents a description of its structure and components together with the different materials and designs tested. Furthermore, the features of the test station are presented and the experimental procedures adopted are described, regarding the polarisation curves and EIS measurements and electrical circuit fitting.

4.1. Fuel cell design

An in-house passive DMFC was developed using the standard state-of-the-art materials that are available in the market and with an easy refuelling and handling, regarding the assembly and connections. The passive DMFC is composed by a three-layer membrane (membrane and anode and cathode catalyst) and a diffusion layer, current collector, insulating plate and end plate in both sides, anode and cathode, as can be seen in Figure 4.1.

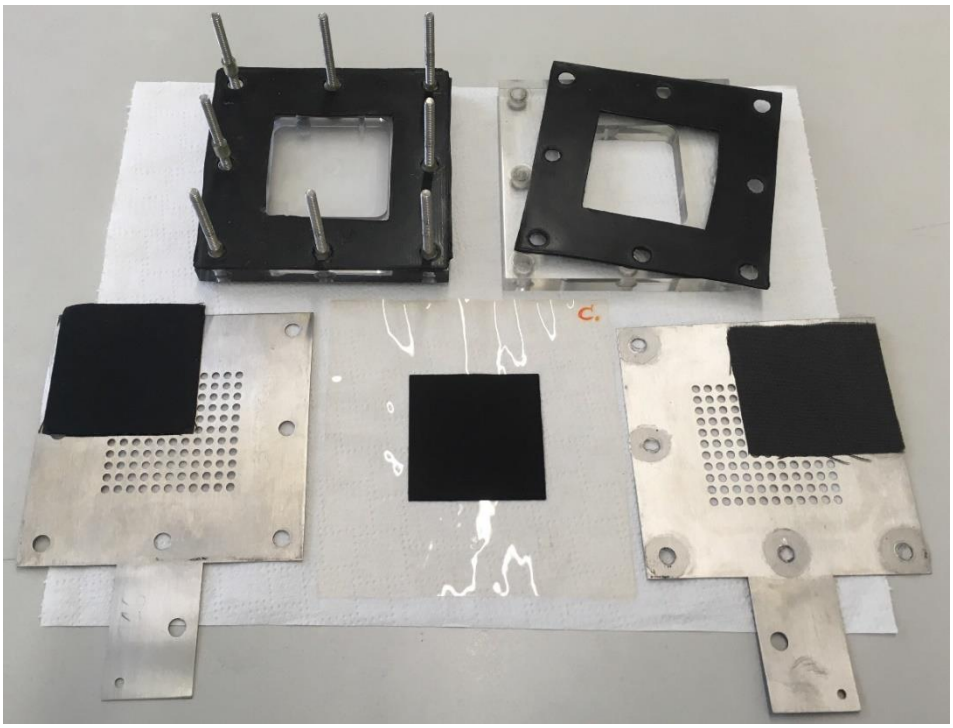

Figure 4.1. Components of the passive DMFC.

The passive DMFC, used in this work, (Figure 4.2) has a total area of 100 cm^2 and an active area of 25 cm^2.

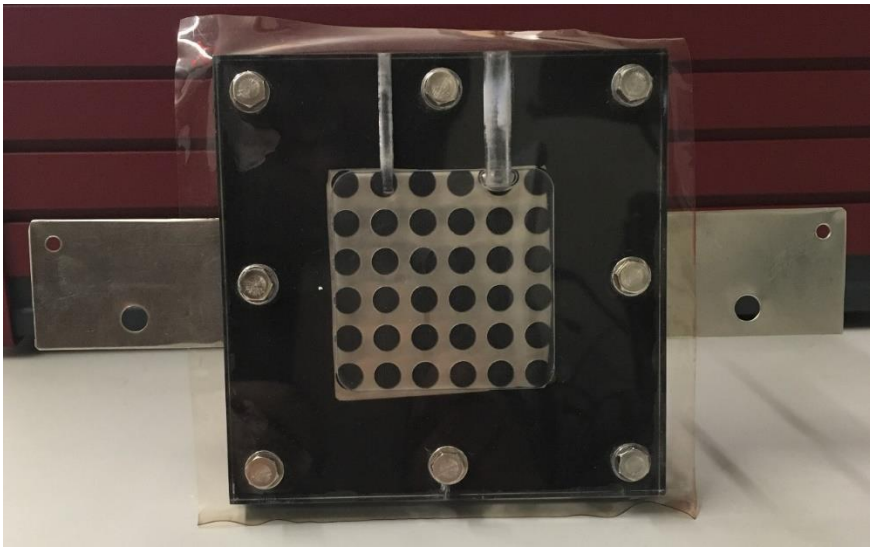

Figure 4.2. In-house passive DMFC.

4.1.1. End plates and insulating plates

The end plates are made of acrylic with 100 x 100 x 10 mm and are used to give mechanical support to the cell, bracing the cell and apply the desired tension on the different cell components. The end plates are connected by a total of eight bolts, with plastic bushes to prevent the electrical contact, and the cell is assembled applying a torque of 4 Nm on each bolt.

The anode end plate has a fuel reservoir of 12.5 cm^3, and the cathode end plate has an open window of 25 cm^2, as can be seen, respectively in Figure 4.3 a) and b).

Two rubber insulating plates are placed between the end plates and the current collectors to avoid the electrical contact between these layers. The insulating plates have an opening area of 25 cm^2 to allow the reactants flow to the active area and products removal.

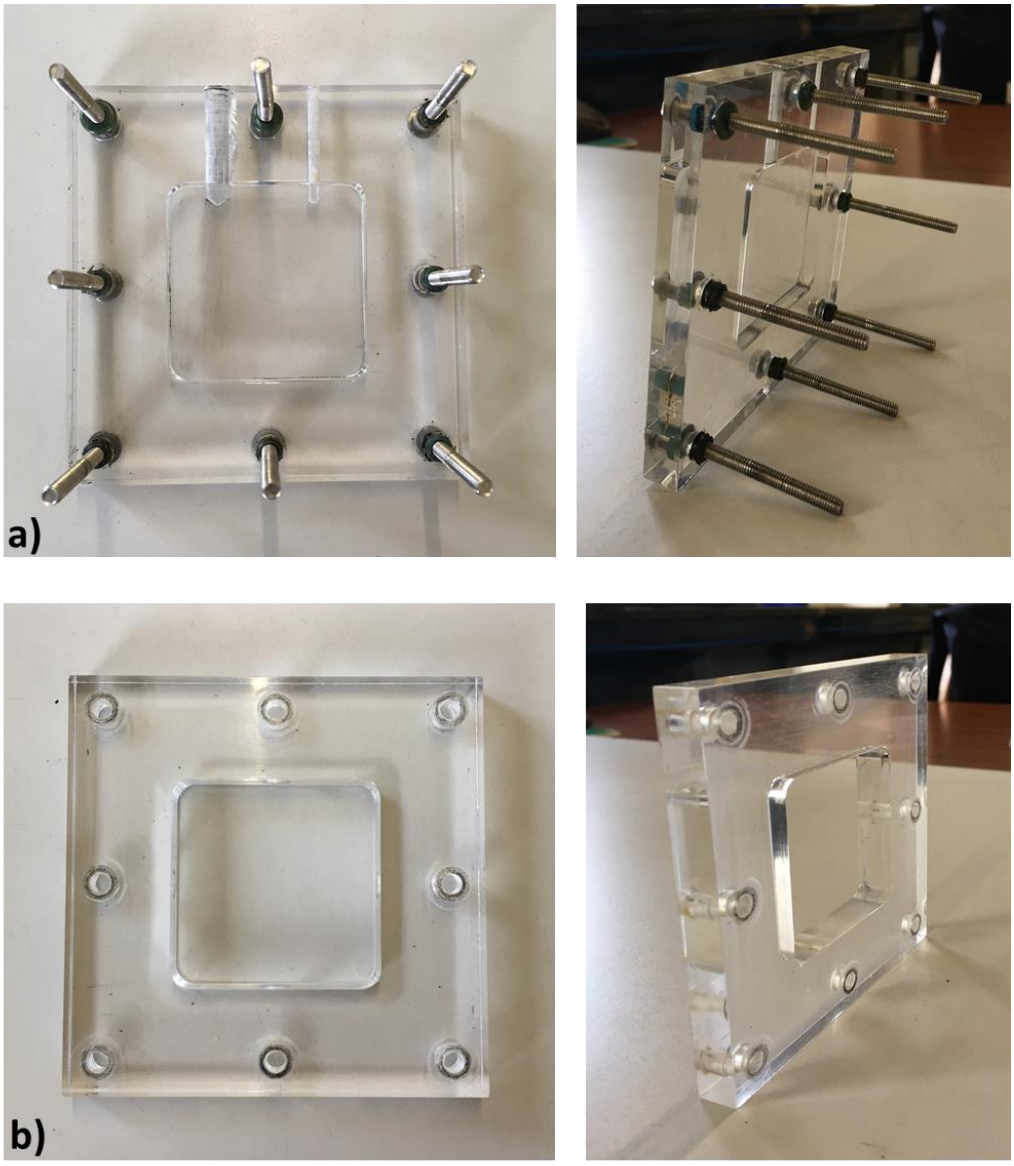

Figure 4.3. Acrylic end plates, a) anode and b) cathode.

4.1.2. Current collectors

Current collectors with different designs and materials were tested in this work. Figure 4.4 a), b) and c) show the different circular perforated current collectors tested, with different open ratio, and Figure 4.4 d) the open window current collector. The design characteristics of each CC and their open ratios are presented in Table 4.1. The different materials used for the CCs were stainless steel (SS), SS with a gold coating, aluminium and titanium.

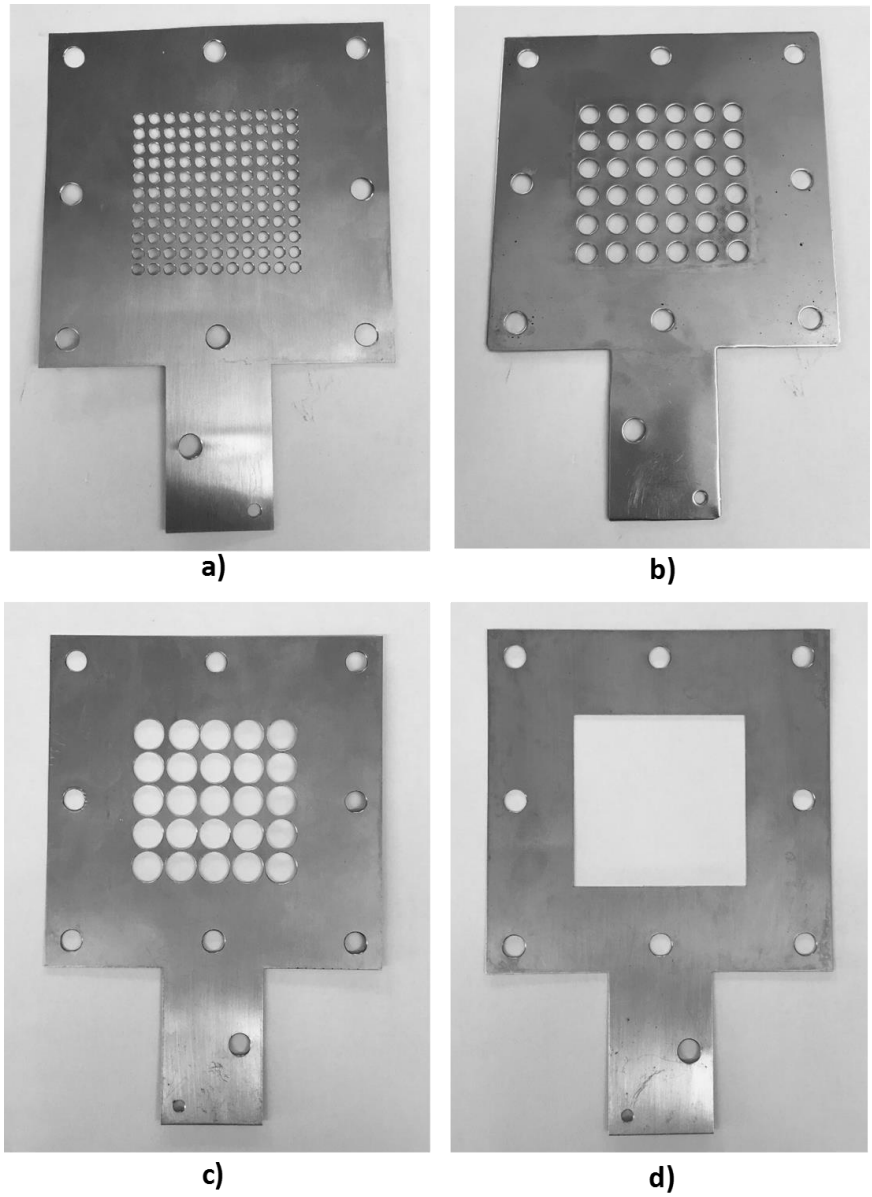

Figure 4.4. Perforated current collector with different open ratios: a) 34 % (CC_1); b) 41 % (CC_2); c) 64 % (CC_3) and d) open window frame current collector (CC_4).

Table 4.1. Design characteristics of the different current collectors tested.

Current collector design	Number of holes	Holes diameter (mm)	Open ratio (%)
CC_1	121	3	34
CC_2	36	6	41
CC_3	25	9	64
CC_4	Opened window frame		100

4.1.3. Membrane electrode assembly (MEA)

As mentioned before, the MEA is composed by a membrane and catalyst layers at the anode and the cathode side. The MEA has an active area of 25 cm^2, the membrane used was Nafion 117 and the catalyst at the anode was Pt/Ru (molar ratio 1:1) with a loading of 3 mg/cm^2 of and at the cathode Pt with a loading of 1.2 – 1.4 mg/cm^2, supplied by QuinTech.

4.1.4. Diffusion layers

While not participating directly in the electrochemical reactions, diffusion layers allow the reactants supply and products removal to the cell. Therefore, the physical and chemical properties of the diffusion layers (DLs), such as morphology, thickness, PTFE content and the existence of a microporous layer (MPL) determine their structure and characteristics (Figure 4.5). According to this important role in the FC operation, different carbon cloths and carbon papers, each one with a different thickness and surface treatment were tested. The characteristics of the different materials tested as anode and cathode diffusion layer are provided in Table 4.2. These materials were supplied by QuinTech, with the exception of CC_MPL_E that was acquired to Fuel Cells Etc. The diffusion layers were pressed by a non-bonded mode on the three-layer membrane when assembling the fuel cell.

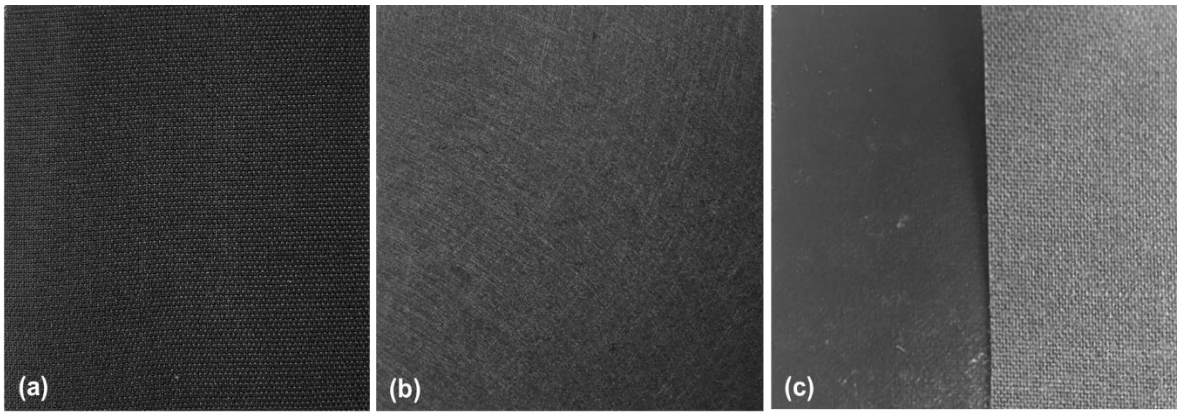

Figure 4.5. Diffusion layers used in this work: a) carbon cloth; b) carbon paper and c) carbon cloth with MPL (both sides).

Table 4.2. Properties of the materials used as diffusion layers.

Diffusion layer	Type	Thickness (mm)	Porosity	MPL
CC	Cloth	0.400	0.83	No
CC_T	Cloth	0.425	0.83	No
CC_MPL	Cloth	0.410	0.80	Yes
CC_MPL_E	Cloth	0.454	0.63	Yes
CP	Paper	0.110	0.78	No
CP_T	Paper	0.190	0.78	No
CP_MPL	Paper	0.240	0.80	Yes
CP_MPL_T	Paper	0.340	0.80	Yes

4.2. Test station

The experimental tests were performed with a commercial electrochemical test station Zahner Elektrik GmbH & Co.KG and the software used was Thales USB, as shown in Figure 4.6.

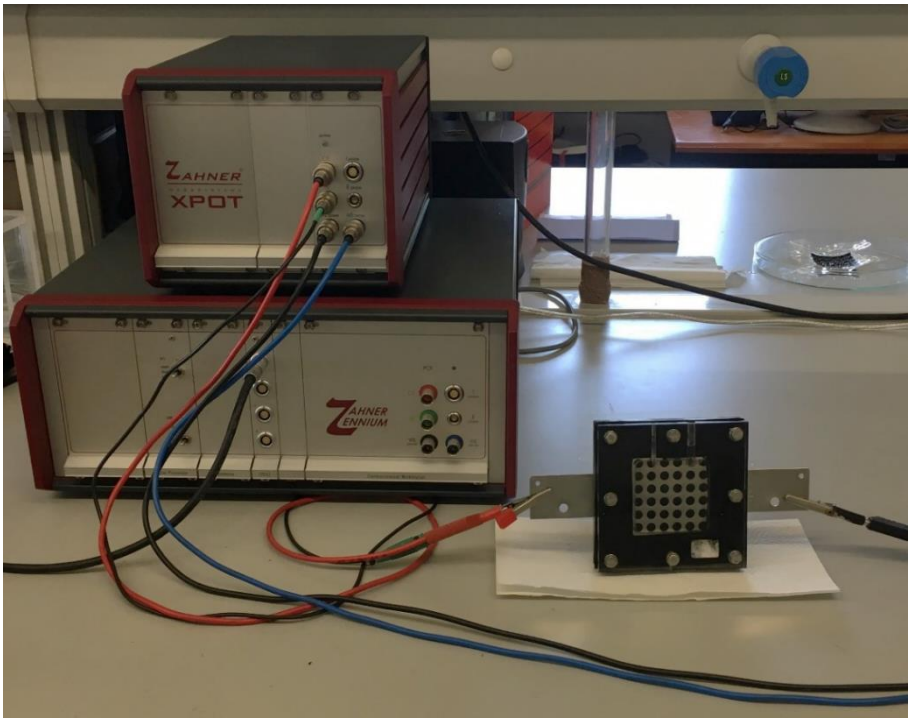

Figure 4.6. Zahner test station.

The polarisation measurements were conducted galvanostatically and the impedance curves were performed potentiostatically. The fuel cell was operated at ambient conditions (ambient pressure and temperature).

4.3. Experimental procedure

Different methanol concentrations, 1, 2, 3, 5, 7, 9 and 10 M, were used to carry out the experimental tests. Additionally, ethanol solutions with different concentrations were also used in the experiments with fuel mixtures. The methanol used had a purity of 99.99 % and was supplied by Fischer Chemical. Ethanol had a minimum purity of 99.5 % and was supplied by AGA.

4.3.1. Polarisation measurements

Polarisation or I-V curves were performed in galvanostatic mode, and the procedure adopted was the following:

1. Fill the anodic reservoir with the fuel;
2. Leave the cell at the open circuit conditions for fifteen minutes, to ensure its operation at steady state conditions;
3. As the cell was operated galvanostatically, the current applied range was from 0 to the maximum current allowed by the fuel cell, with a step of 10 mA until 100 mA and 50 mA after that. At each imposed current, the cell was operated for three minutes to reach steady state conditions;
4. For each value of current applied, the cell voltage was measured and its power calculated afterward.

For each set of conditions tested, experiments were performed until obtaining at least two similar results. Tests were accepted if the relative error between two readings was below 10 %.

4.3.2. EIS measurements and EEC fitting

The impedance measurements were performed right after obtaining the polarisation curves. The EIS tests were carried out with an amplitude of 10 mV, a frequency range from 10 mHz to 100 kHz, at different fuel cell voltages (0.45 V, 0.4 V, 0.35 V, 0.3 V and 0.2 V). The EIS measurements were performed in-situ to allow the measurement of the impedance of the fuel cell as a whole. This is the common procedure used to analyse a single fuel cell, since the information provided by this approach helps on the optimisation of the design parameters and operating conditions. As the use of a reference electrode in most of the fuel cell systems is difficult and unpractical, in this work, a dynamic hydrogen electrode (DHE) was used, by replacing the methanol or air supply by hydrogen. With this approach, it is assumed that the losses associated with the DHE are irrelevant and consequently all the measurements are attributed to the other electrode, the electrode under study. Therefore, when the DHE is used at the cathode, it is possible to study the anode behaviour and obtain the anode spectrum and when the DHE is used at the anode, it is possible to study the cathode behaviour and obtain the cathode spectrum. Then, performing the impedance measurements with the passive DMFC working with methanol and air, it is possible to obtain the overall passive DMFC spectrum and compare it with the single-cell ones, to separate the different electrode losses (anode and cathode) on the overall cell response. The impedance spectra were fitted to an equivalent electric circuit (EEC) by complex non-linear regression least squares fitting, using the Thales software from Zahner, and a maximum error up to 10% was accepted.

4.3.3. Durability test

The durability tests were performed at the end of this work and according to the following procedure:

1. Fill the anodic reservoir with the fuel;
2. Leave the cell at the open circuit conditions for fifteen minutes, to ensure its operation at steady state conditions;
3. Set the cell current at 10 mA/cm^2 and perform an EIS measurement at this condition;
4. Operate the cell at this current and measure the corresponding voltage behaviour/drop every fifteen minutes until reaching a voltage of 0.1 V;

5. Recharge the anode reservoir and verify if the cell recovers its performance;
6. If needed, repeat steps 4 and 5, otherwise repeat step 3 and end the durability test.

The durability tests were performed in duplicate and always with an EIS measurement at the beginning and at the end of each test to identify the different degradation and failure mechanisms, through the estimation of the different resistances that negatively affect the cell performance.

CHAPTER 5

5. EXPERIMENTAL RESULTS AND DISCUSSION

This chapter presents the experimental results obtained with a pDMFC, with an active area of 25 cm^2 working at ambient temperature and pressure, and explained under the light of the EIS data. The section starts with the interpretation of the EIS data using a selected set of values, which presents the same trends and patterns of the other results. Then, the effect of using different carbon based materials as anode and cathode DL on the fuel cell performance is presented. After that, the effect of the methanol concentration, methanol and ethanol ratio and the different CC materials and design, for the selected anode and cathode DLs, the ones that lead to the best power output, on the passive DMFC behaviour is discussed. The best configuration found on the studies regarding the optimisation of the design parameters was used to evaluate the pDMFC lifetime. In the durability tests, the cell was operated with a methanol concentration of 2 M at a constant current and the cell degradation behaviour was evaluated though the voltage drop over the time and the EIS data, which allow the identification of the different losses that lead to the cell degradation. An economic evaluation where the proposed MEA is compared with the conventional one is presented at the end of this chapter.

In each section of this chapter, due to a large number of tests performed and results obtained, a sub-set of conditions was selected and is presented. However, the remaining results can be found in Appendix A.

The contents of this chapter conducted to the paper: B. A. Braz, C. S. Moreira, V. B. Oliveira, and A. M. F. R. Pinto, "Effect of the current collector design on the performance of a passive direct methanol fuel cell", 2019, Electrochimica Acta, 300, 306-315 and the preparation and submission of the following papers: B. A. Braz, V. B. Oliveira and A. M. F. R. Pinto, "Experimental studies of the effect of cathode diffusion layer properties on a passive direct methanol fuel cell power output"; B. A. Braz, V. B. Oliveira and A. M. F. R. Pinto, "Analysis of the anode diffusion layer properties on the performance of a passive direct methanol fuel cell using electrochemical impedance spectroscopy"; B. A. Braz, V. B. Oliveira and A. M. F. R. Pinto, "Optimization of a passive direct methanol fuel cell with different current

collector materials"; B. A. Braz, C. S. Moreira, V. B. Oliveira and A. M. F. R. Pinto, "Performance of a passive direct alcohol fuel cell fed with a mixture of alcohols".

5.1. Electrochemical impedance spectroscopy

The results presented in this section were obtained using a pDMFC with carbon cloth as both anode and cathode diffusion layers (thickness of 0.400 mm), since this material is one of the most common used in literature and usually leads to good performances. As current collectors at the anode and cathode sides were used stainless steel plates, since according to the literature [23] this material is used in 76 % of the pDMFCs studies and having an open ratio of 41 % (CC_2). This was the layout employed by the researcher team in their previous works with pDMFCs, where they obtained very interesting results and performances [2, 101, 110].

As already mentioned, the EIS measurements can provide detailed information about the fuel cell system, enabling how to identify and quantify the different voltage losses that negatively affect the fuel cell performance: ohmic, activation and mass transport losses. The EIS data are usually represented by a Nyquist plot, such as the one shown in Figures 5.1, 5.2 and 5.3, where the real impedance (Z_{re}) and the imaginary impedance (Z_{im}) are plotted at the X and Y-axis, respectively. The characteristics and shape of each spectrum make possible identifying the different losses that affect the cell performance. Therefore, different combinations of several elements had to be considered on the equivalent circuit model that was used to model the impedance spectrum.

A typical Nyquist plot of a fuel cell can be divided into different regions according to its frequency range. At the high frequencies region, the imaginary impedance axis intercepts the real impedance one at a value called the high-frequency resistance (HFR), which represents the ohmic losses (as shown in Figures 5.1, 5.2 and 5.3). As is well known, the electrical resistance is time independent and is described through the Ohm's law. In electrical circuits, it is represented by a resistor (R) (R_{Ohm} in the EEC shown in Figure 5.4) and due to its frequency independency, its impedance has only a real part, identified by a single point the real axis (X-axis) of the Nyquist plot, with a value equal to R. The arc presented at the medium frequency region represents the activation losses and is characterized by a decrease of the resistance with a decrease of the voltage (as shown in Figures 5.2 and 5.3 and Table 5.1) [211]. The arc at the lower frequency region usually represents the mass transport losses

and is characterized by an increase of the resistance with a decrease of voltage (as shown in Figure 5.1) [211]. However, in some systems, it is not possible to reach the mass transport losses region and therefore the arcs, at the medium and lower frequency ranges, are due to the activation losses, characterized by a decrease of the resistance with a decrease of the voltage (as shown in Figure 5.2).

The first obtained results in the current work seemed to exhibit more than two arcs, suggesting that the system under study has an additional resistance that negatively affects its performance as shown in Figure 5.3. The plots in Figure 5.3 represent the spectrum of the pDMFC operating with methanol and air, and Table 5.1 displays the values for the four resistances obtained by adjusting the EEC shown in Figure 5.4 to the Nyquist plots. It is possible to notice that none of the resistances increases with a decrease of the cell voltage. This makes possible to perceive that under the operating conditions studied, the pDMFC does not suffer in a significant extent from concentration or mass transport losses and the activation ones are dominant for all the voltages studied. After this result, the next step was to link the different activation losses to the different phenomena/processes that occur in a working pDMFC.

It is known that the activation losses are due to the electrochemical reactions, usually the fuel oxidation (anode side) and the oxygen reduction (cathode side), which justify two of the arcs presented at the Nyquist plot. The other identified arc, the third one, which was not attributed to the mass transfer losses, should be due to an additional electrochemical reaction that occurs at the cathode side of these cells, the methanol oxidation due to methanol crossover and should be characteristic of the DMFCs. As was already emphasized along the text, the crossover is one of the major drawbacks of these systems owing to its strong negative impact on the cell power output, explained by the formation of a mixed potential at the cathode side, a loss of fuel at the anode side and cathode poisoning by the intermediate compounds formed due to the incomplete methanol oxidation reaction on the Pt catalyst (cathode catalyst). The resistance due to methanol crossover, which affects mainly the cathode side, can be clearly identified on the cathode spectrum, shown in Figure 5.2, where both resistances decrease with a decrease of the cell voltage, a normal behaviour of the activation losses. Therefore, both resistances presented on the cathode spectrum are due to the two reactions that occur at the cathode catalyst. Additionally, it is well known that the crossover decreases with a decrease of voltage [167], and accordingly, the crossover effect,

here estimated by the $R_{Crossover}$, decreases with a decrease of the voltage, as shown in Figures 5.2 and 5.3 and Table 5.1.

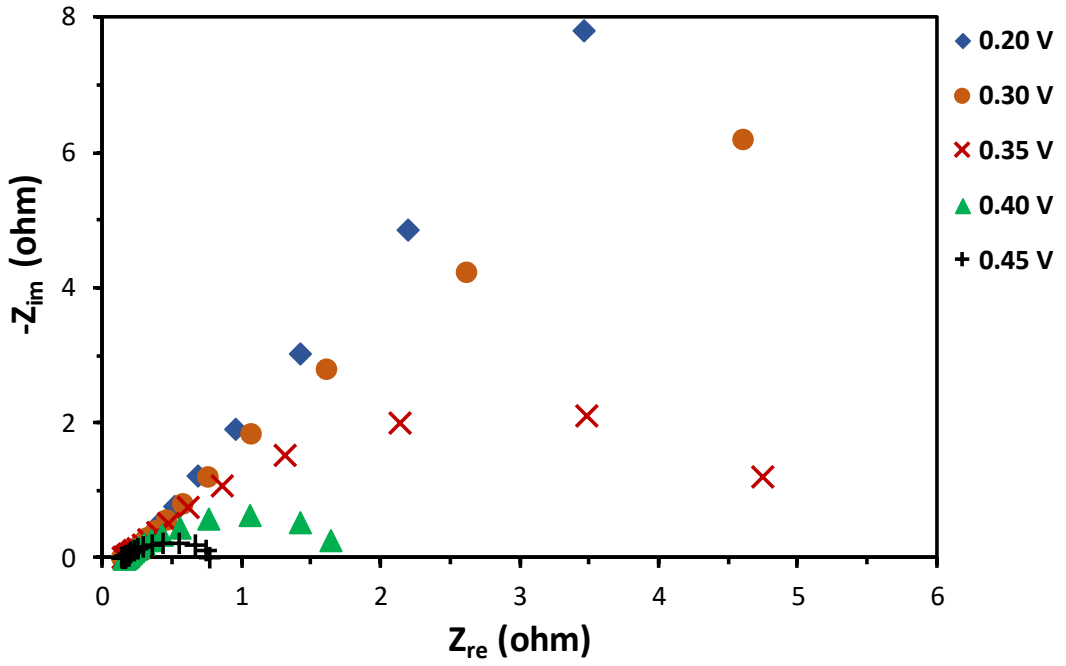

Figure 5.1. Nyquist plot of a pDMFC with the DHE at the cathode side and a methanol concentration of 1 M at the anode, for different cell voltages.

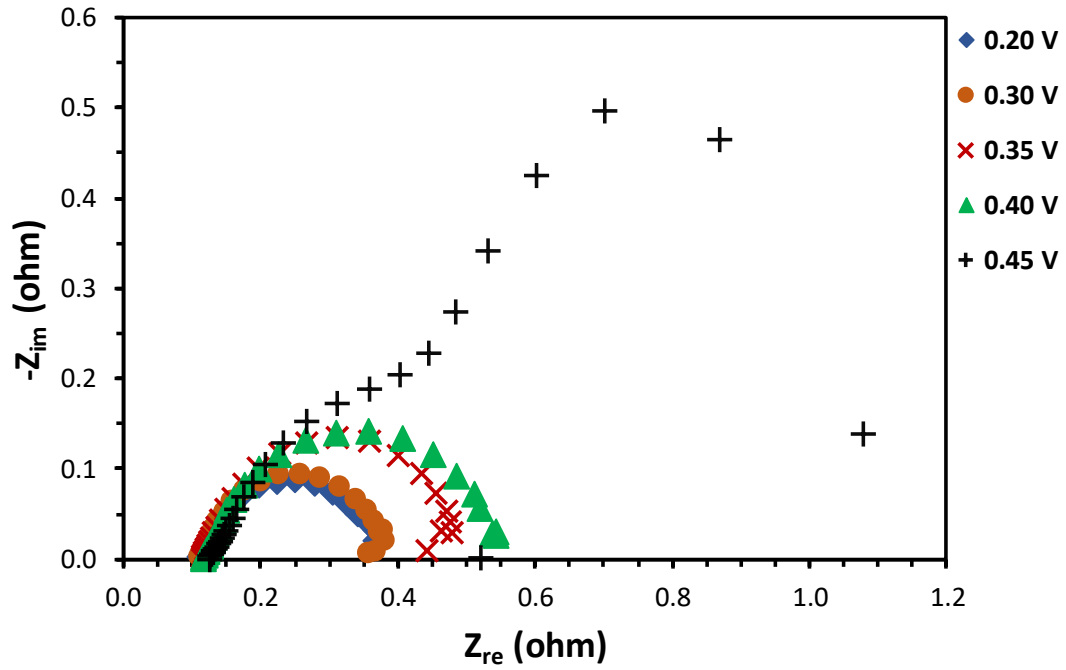

Figure 5.2. Nyquist plot of a pDMFC with the DHE at the anode side and air at the cathode side, for different cell voltages.

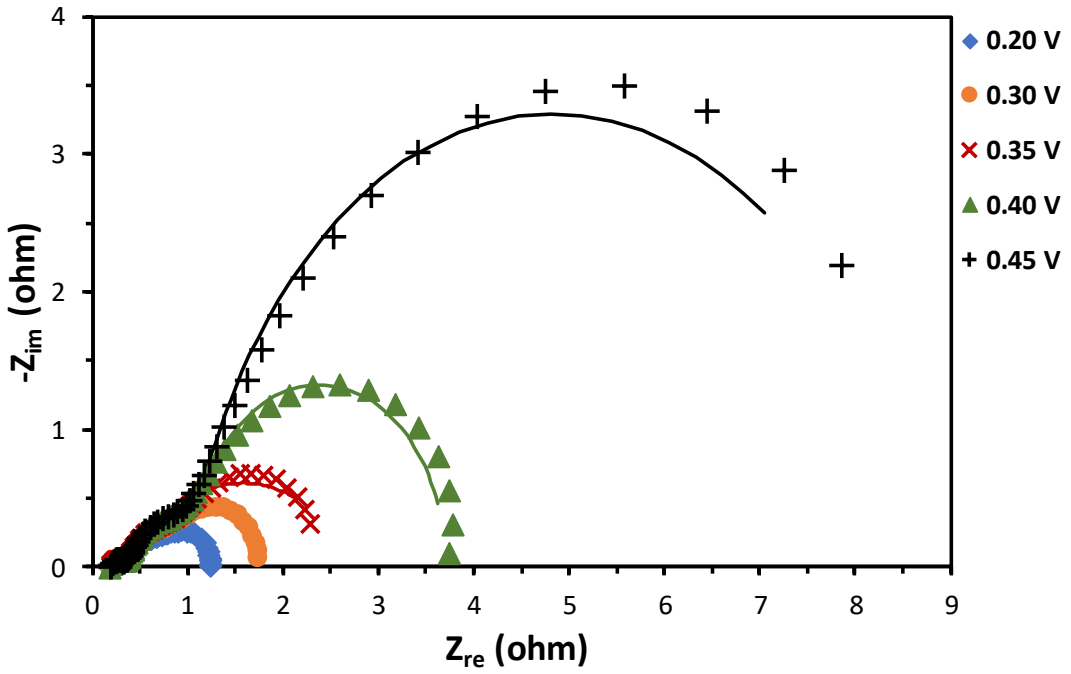

Figure 5.3. Nyquist plot of a pDMFC fed with methanol (1 M) at the anode and air at the cathode side, for different cell voltages.

Based on the EIS measurements performed for the pDMFC working with a DHE at the anode or cathode side with methanol and air and on the shape of each spectrum, the EEC used in this work, and presented in Figure 5.4, consists on a resistance, R_{Ohm} (ohmic resistance) connected in series with other three independent circuits. Each one comprising a resistance, R_A (activation losses due to the methanol oxidation at the anode), R_C (activation losses due to the oxygen reduction at the cathode) and $R_{Crossover}$ (activation losses due to the methanol oxidation at the cathode) in parallel with a constant phase element, CPE_A, CPE_C and $CPE_{Crossover}$, associated with the capacitance properties of the double-layer interfaces.

The plots depicted in Figure 5.3 for the pDMFC working with methanol and air show three semicircles for all the voltages tested, that decrease with a decrease of the cell voltage, indicating a reduction of the losses that negatively affect the cell performance with voltage. This can be also verified through the values of the different resistances presented in Table 5.1, which were obtained by fitting the EEC (Figure 5.4) to the EIS data presented in Figure 5.3. There is a good agreement between the EEC fitting and the experimental results, revealing that the EEC proposed reproduces with accuracy the system under study.

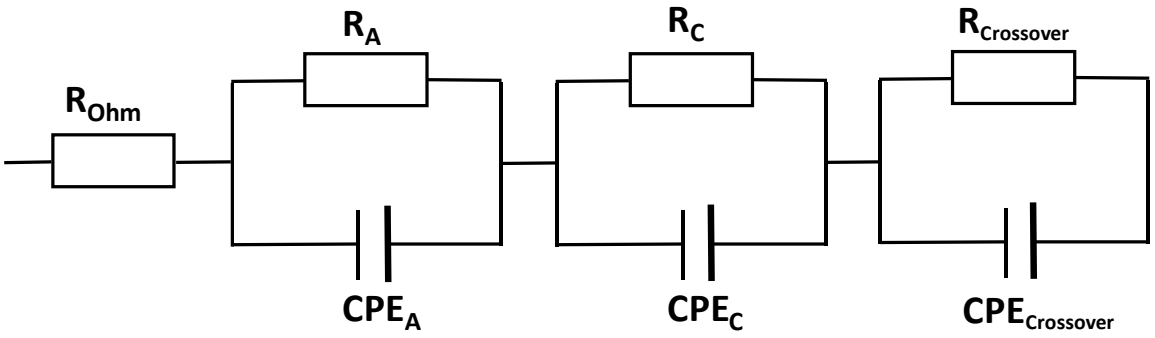

Figure 5.4. Equivalent electric circuit used to describe the EIS experimental data of a pDMFC with methanol and air.

Table 5.1. Values of the different resistances obtained by fitting the Nyquist plots of the pDMFC (Figure 5.3) with the EEC proposed in this work (Figure 5.4) for different fuel cell voltages.

Voltage (V)	R_{Ohm} (Ω)	R_A (Ω)	R_C (Ω)	$R_{Crossover}$ (Ω)
0.45	0.18	0.15	0.47	7.2
0.40	0.18	0.15	0.47	3.1
0.35	0.18	0.15	0.47	1.5
0.30	0.18	0.15	0.32	1.2
0.20	0.18	0.15	0.17	0.7

The approach used in this work is new, since as the authors are aware no other work, regarding a pDMFC used this methodology and the EEC here proposed. Therefore, these results are ground-breaking, identifying the different phenomena that affect the pDMFC power output.

It should be here highlighted, that the impedance spectra obtained for the other conditions studied followed the same pattern as those presented in this section, with similar results for the EEC fitting and resistance values (the remaining results can be found in Appendix A). The EIS data for a voltage of 0.2 V, near the voltage corresponding to the optimum power density for each condition, were selected to be presented in the following sections and will be used to explain the polarisation results and the pDMFC behaviour.

5.2. Effect of anode diffusion layer properties

Although the DLs do not have a direct contribution on the electrochemical reactions that occur in a working pDMFC, they allow the reactants access to the catalyst layers and the heat removal, electrically connect the catalyst layers to the current collectors, provide the products removal from the cell and the mechanical support to the MEA. Therefore, these layers should be electrically and thermally conductive and sufficiently porous to allow the flow of reactants and products and rigid to support the MEA, but at the same time must have some flexibility to maintain a good electrical contact. Carbon-based materials, such as carbon paper and carbon cloth, have been widely used as DL materials in pDMFCs, since they met all the DL requirements. Additionally, the DLs can have a single-layer structure, typically made of carbon-based materials, or a dual-layer structure, where one layer is known as backing layer (BL), which is similar to the one of the single-layer structure, and the second layer is a MPL. The BL acts as flow diffuser and give mechanical support and the MPL is used to decrease the contact resistance between the catalyst layer and the BL and to uniformly distribute the reactants over the catalyst layer surface. Therefore, the MPL should be porous to promote the reactants transport and the products removal and electrically and thermally conductive.

It is commonly accepted that the structural parameters of DLs that have a clearly effect on the pDMFC performance are its thickness (linked to the transport resistances), porosity (related to the species transport) and its wettability and roughness (responsible for the droplet/bubble attachment or coverage on the DL surface). Therefore, layers with different structures, thicknesses, porosities, permeability and surface wettability, will result in different transport characteristics and fuel cell behaviour [13, 34, 41, 93, 96, 101, 102, 110, 121, 126, 146, 149, 194, 227, 240].

In this section, the experimental results regarding the effect of the ADL properties on the fuel cell behaviour are analysed through polarisation and EIS measurements. The results were obtained with stainless steel current collectors, with an open ratio of 41 % (CC_2), at the anode and cathode sides and with carbon cloth with a thickness of 0.400 mm (CC) as cathode DL. At the ADL, different carbon-based materials were tested with a different structure, thickness and surface treatment as displayed in Table 4.2. As can be seen, CC and CC_T have the same porosity (0.83) but CC_T has a slightly higher thickness (0.425 mm instead of 0.400 mm). The carbon cloths with a microporous layer present lower porosities

than the untreated ones (0.80 and 0.63) and the CC_MPL_E a higher thickness than the CC_MPL (0.540 mm and 0.410 mm).

5.2.1. Effect of carbon cloth as anode DL

Figure 5.5 shows the polarisation curves of a pDMFC using four different carbon cloths, with different properties (Table 4.2), as anode diffusion layer (ADL) for different methanol concentrations. The values for the ohmic and activation resistances, at 0.2 V, as well as the maximum power density achieved for each configuration are shown in Table 5.2. The plots presented in Figure 5.5 put in evidence that it was only possible to operate the cell with higher methanol concentrations, 7 M, without a significant loss of performance, when using carbon cloth with a dual-layer structure, CC_MPL and CC_MPL_E. The MPL favours the fuel distribution on the catalyst surface increasing the anode electrochemical rate and therefore decreasing the anode overpotential (R_A). Additionally, as more methanol reacts at the anode side, less methanol crosses the membrane towards the cathode side, decreasing the methanol crossover rate and consequently the cathode activation losses due to methanol crossover ($R_{Crossover}$), as can be seen in Table 5.2. This also leads to a reduction of the cathode activation losses (R_C), since the cathode catalyst poisoning by the undesired methanol oxidation reaction is less severe, leading to more available active sites for the oxygen reduction reaction. Regarding the carbon cloths with a single structure tested, for lower methanol concentrations (1 M and 2 M) better performances were achieved with the carbon cloth with the lower thickness (CC), which showed lower $R_{Crossover}$ values (Table 5.2). However, with an increase of the methanol concentration the performance increases when a carbon cloth with a higher thickness (CC_T) was used as ADL. As already mentioned, the thickness and porosity of the DLs are very important parameters that have a remarkable effect on the cell performance, since are responsible for the different species transport towards the catalyst layer and out of the cell. As expected a higher thickness will lead to a higher transport resistance through this layer, but will also lead to a more uniform distribution of the fuel along the catalyst layer. This will conduct to an increase of the fuel oxidation rate, a decrease of the anode activation losses (R_A) and of the methanol crossover rate ($R_{Crossover}$), as can be verified in Table 5.2. Despite the fact that the methanol crossover rate increases with an increase of the methanol concentration, which can be confirmed by a decrease of the open circuit-voltage with the methanol concentration (Figure 5.5), an

increase of the methanol concentration until a maximum value (in this work was 5 M), also lead to an increase of the amount of fuel that reaches the catalyst layer, increasing its oxidation rate and consequently decreasing the anode activation losses (R_A). Under these conditions, the cathode activation losses (R_C) also decrease, since less methanol crosses the membrane towards the cathode side and reacts at this side ($R_{Crossover}$).

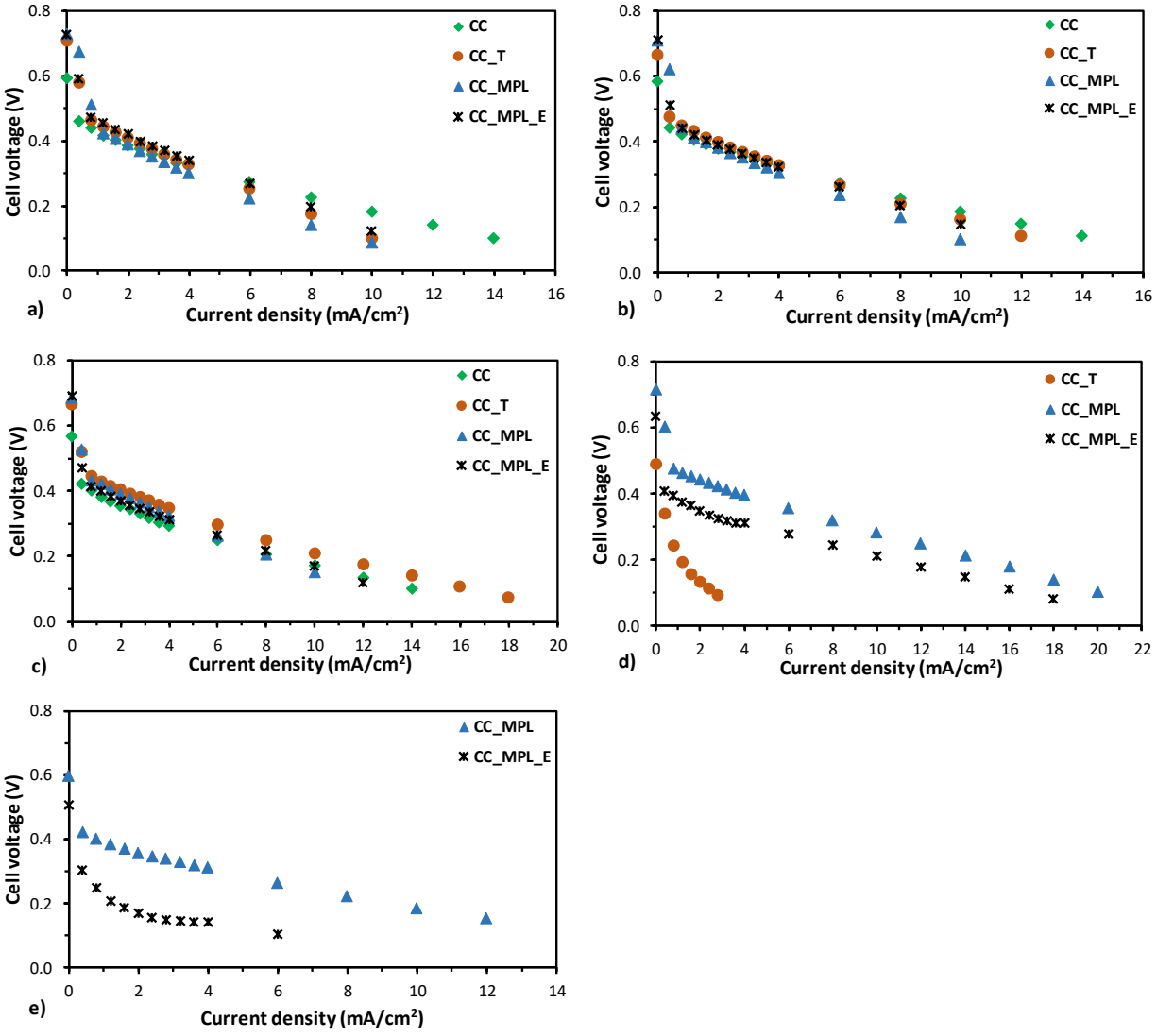

Figure 5.5. Effect of using different carbon cloths as ADL on the cell performance for different methanol concentrations: a) 1 M, b) 2 M, c) 3 M, d) 5 M and e) 7 M.

Based on the results presented in this section (Figure 5.5 and Table 5.2) the best performance, 3.00 mW/cm^2, was achieved using a carbon cloth with a dual-layer structure, CC_MPL, as ADL and with a methanol concentration of 5 M.

Table 5.2. Values for the different resistances of the EEC for the different carbon cloths tested as ADL and its maximum power density.

Diffusion layer	Methanol concentration	R_{Ohm} (Ω)	R_A (Ω)	R_C (Ω)	$R_{Crossover}$ (Ω)	Maximum Power density (mW/cm^2)
CC	1 M	0.26	0.03	0.24	0.41	1.84
	2 M	0.42	0.03	0.16	0.43	1.89
	3 M	0.26	0.02	0.12	0.43	1.72
CC_T	1 M	0.46	0.01	0.05	0.81	1.53
	2 M	0.64	0.02	0.04	0.65	1.70
	3 M	0.37	0.01	0.03	0.61	2.12
	5 M	0.48	0.01	0.03	3.25	0.27
CC_MPL	1 M	0.47	0.03	0.39	0.63	1.34
	2 M	0.46	0.02	0.30	0.47	1.43
	3 M	0.42	0.03	0.28	0.30	1.66
	5 M	0.41	0.02	0.13	0.24	3.00
	7 M	0.57	0.03	0.12	0.38	1.87
CC_MPL_E	1 M	0.25	0.02	0.38	0.55	1.63
	2 M	0.33	0.02	0.28	0.46	1.65
	3 M	0.30	0.03	0.14	0.36	1.74
	5 M	0.34	0.02	0.17	0.32	2.15
	7 M	0.40	0.02	0.33	3.35	0.63

5.2.2. Effect of carbon paper as anode DL

The effect of carbon paper as ADL in a passive DMFC was also studied in this work, using four different types of carbon papers with different properties, as detailed in Table 4.2. Figure 5.6 shows the polarisation curves for the different carbon papers tested and for different methanol concentrations. Likewise, in the previous section, regarding the carbon cloth properties, CC was used as cathode DL for all the conditions tested. The different resistances of the EEC, at a voltage of 0.2 V, and the maximum power density achieved for each configuration are presented in Table 5.3.

As happened when carbon cloth was used as ADL, the best results were achieved with a carbon paper with a dual-layer structure, CP_MPL and CP_MPL_T. These results are in

accordance to what is expected, since as can be seen in Table 5.3, this dual-layer structure allowed increasing the carbon paper porosity, which favours the methanol supply and distribution on the catalyst layer surface, increasing its oxidation rate on de anode catalyst (R_A), decreasing its crossover rate and the overall cathode activation losses (R_C and $R_{Crossover}$). Additionally, the carbon papers with MPL presented lower ohmic losses, R_{Ohm}, (Table 5.3), since a MPL is also used to decrease the contact resistance between the BL and the catalyst layer. The results also showed that the use of a carbon paper with a dual-layer structure and a higher thickness, CP_MPL_T is preferable, since despite a higher thickness leads to a higher methanol transport resistance, it will also limit the amount of methanol that reaches the membrane and crosses it towards the cathode side.

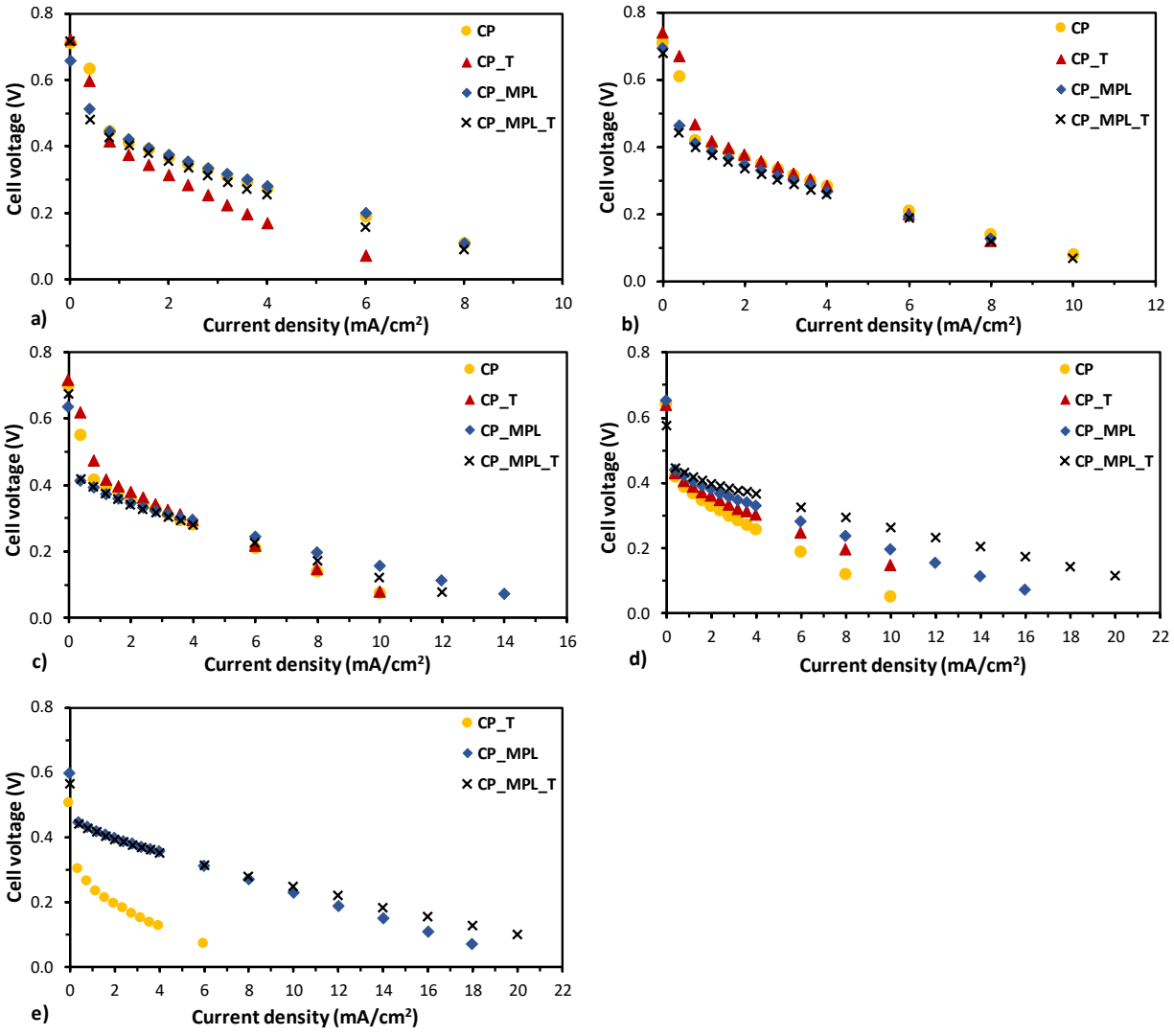

Figure 5.6. Effect of using different carbon papers as ADL on cell performance for different methanol concentrations: a) 1 M, b) 2 M, c) 3 M, d) 5 M and e) 7 M.

Table 5.3. Values for the different resistances of the EEC for the different carbon papers tested as ADL and its maximum power density.

Diffusion layer	Methanol concentration	R_{Ohm} (Ω)	R_A (Ω)	R_C (Ω)	$R_{Crossover}$ (Ω)	Maximum Power density (mW/cm^2)
CP	1 M	0.55	0.03	0.37	0.61	0.67
	2 M	0.84	0.02	0.29	0.53	1.14
	3 M	0.87	0.04	0.24	0.45	1.27
	5 M	0.80	0.02	0.03	0.93	1.12
CP_T	1 M	0.85	0.01	0.12	1.35	0.72
	2 M	0.69	0.02	0.27	0.58	1.14
	3 M	0.66	0.08	0.27	0.54	1.32
	5 M	0.66	0.08	0.18	0.44	1.56
	7 M	0.44	0.02	0.24	1.20	0.50
CP_MPL	1 M	0.37	0.02	0.39	0.62	1.19
	2 M	0.50	0.03	0.20	0.56	1.16
	3 M	0.66	0.02	0.20	0.52	1.58
	5 M	0.49	0.02	0.16	0.31	1.96
	7 M	0.36	0.03	0.21	0.30	2.28
	9 M	0.42	0.03	0.20	0.55	1.75
CP_MPL_T	1 M	0.35	0.01	0.32	0.78	1.02
	2 M	0.34	0.01	0.13	0.64	1.13
	3 M	0.29	0.02	0.15	0.55	1.39
	5 M	0.32	0.02	0.20	0.46	2.82
	7 M	0.32	0.01	0.15	0.32	2.63

As can be seen by the results presented in this section, the use of CP_MPL as ADL allowed running the pDMFC with a methanol concentration of 9 M. However, the power density was lower than the one achieved with 7 M and the same ADL, and the best one achieved with CP_MPL_T, due to an increase of the methanol crossover rate that leads to an increase of the cathode activation resistance due to methanol crossover ($R_{Crossover}$). From the plots presented in Figure 5.6 and the data shown in Table 5.3, it can be concluded that when carbon paper was used as ADL, the best performance, 2.82 mW/cm^2, was achieved using the carbon paper with MPL and a higher thickness, CP_MPL_T, and a methanol concentration of 5 M.

5.3. Effect of cathode diffusion layer properties

A similar study to the one performed for the anode side was conducted for the cathode side in order to evaluate the effect of the CDL properties on the pDMFC power output. Therefore, four different carbon cloths and carbon papers, each one with a different thickness and surface treatment (Table 4.2) were tested at the cathode side. The results were obtained with stainless steel current collectors, with an open ratio of 41 % (CC_2), at the anode and cathode sides and with carbon cloth with a microporous layer (CC_MPL) as anode DL, since, as was verified in the previous section, this was the material that led to the best performance.

5.3.1. Effect of carbon cloth as cathode DL

Figure 5.7 shows the polarisation curves for the different carbon cloths tested on the cathode side, feeding the cell with three different methanol concentration, 1 M, 2 M and 3 M. A carbon cloth with microporous layer (CC_MPL) was used as anode DL for all the experiments. The values for the ohmic and activation resistances at 0.2 V, as well as, the maximum power density achieved for each configuration are presented in Table 5.4.

As the methanol crossover is a major drawback in DMFCs optimisation, it is expected that the values of $R_{Crossover}$ should represent the major negative contribution to decrease the cell performance, even when tailoring the cathode. This happens because in fact, the parasitic methanol oxidation reaction occurs at the cathode catalyst layer using a non-adequate catalyst. The results presented in Figure 5.7 and Table 5.4 confirm these expectations.

Generally, for all the concentrations tested, better performances are achieved using carbon cloth generating the lower values of $R_{Crossover}$ representing by far the largest resistance for all the conditions tested. The best performances were obtained with the CC for all the methanol concentrations tested and with the CC_T type carbon cloth for the lower concentration. As found in previous work [91, 241], thicker cathodes usually conduct to better results due to a low methanol crossover generated with the higher MEA thickness.

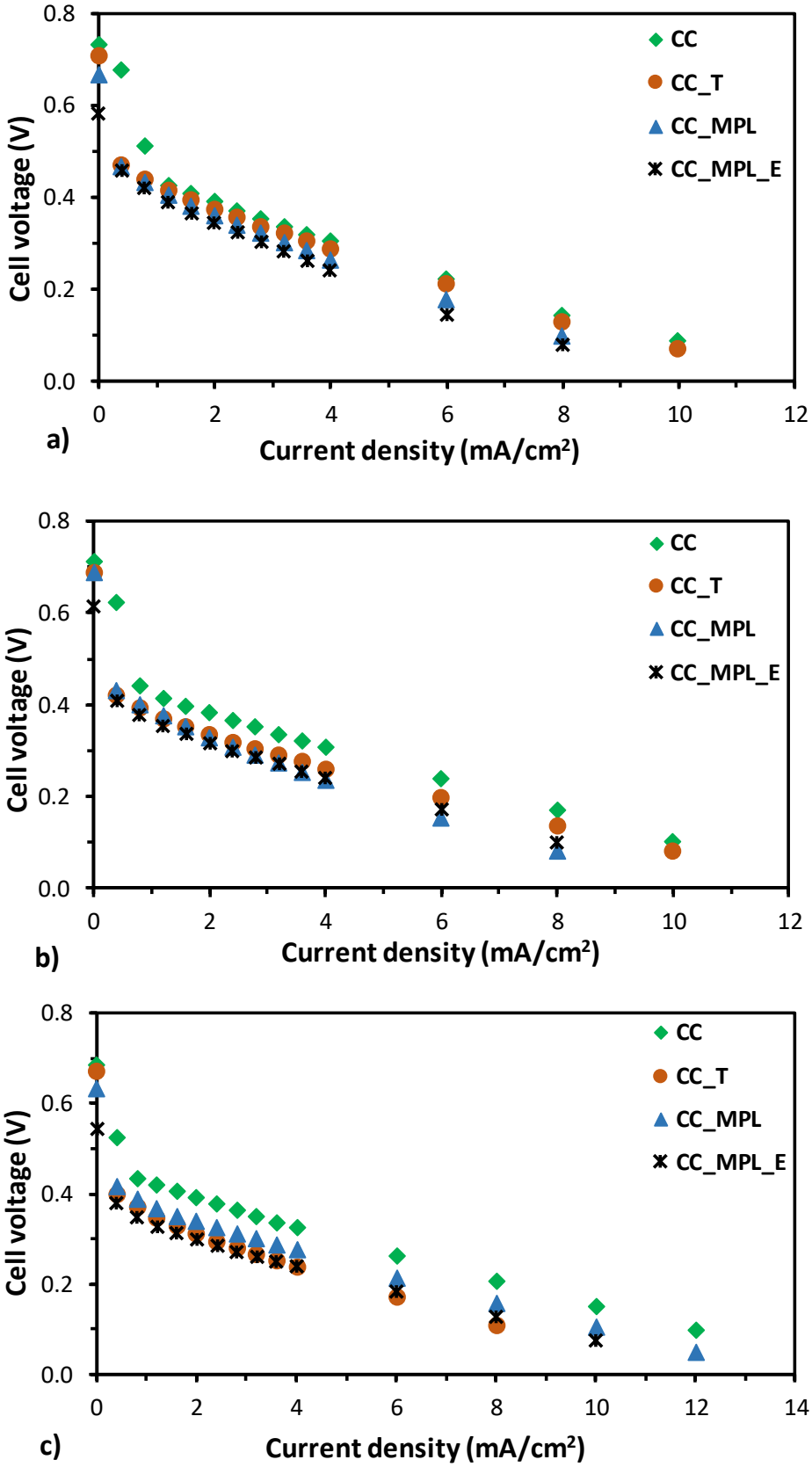

Figure 5.7. Effect of using different carbon cloths as CDL on cell performance for different methanol concentrations: a) 1 M, b) 2 M and c) 3 M.

Table 5.4. Values for the different resistances of the EEC for the different carbon cloths tested as CDL and its maximum power density.

Diffusion layer	Methanol concentration	R_{Ohm} (Ω)	R_A (Ω)	R_C (Ω)	$R_{Crossover}$ (Ω)	Maximum Power density (mW/cm^2)
CC	1 M	0.47	0.03	0.39	0.63	1.34
	2 M	0.46	0.02	0.30	0.47	1.43
	3 M	0.42	0.03	0.28	0.30	1.66
CC_T	1 M	0.45	0.01	0.34	0.59	1.26
	2 M	0.68	0.02	0.29	0.55	1.19
	3 M	0.40	0.02	0.18	0.48	1.04
CC_MPL	1 M	0.55	0.01	0.44	0.87	1.06
	2 M	0.56	0.01	0.27	0.62	0.95
	3 M	0.60	0.02	0.19	0.56	1.30
CC_MPL_E	1 M	0.60	0.01	0.45	1.03	0.96
	2 M	0.42	0.015	0.29	0.57	1.03
	3 M	0.45	0.01	0.19	0.52	1.12

Accordingly, in this work care was taken to select carbon cloths with a relatively high thickness as displayed in Table 4.2. The main question was to check if when using a relatively thick cathode DL, it is worthwhile the use of a MPL which usually contributes to an increase in the MEA cost. As can be concluded from the values displayed at Table 5.4, the cell configurations using carbon cloth with a MPL (CC_MPL and CC_MPL_E) do not generate, in most of the conditions tested, higher performances, when compared to the carbon cloth cathodes without this extra-layer and operating at the same methanol concentration level.

It would be expected that using a MPL at the cathode DL would be beneficial for the fuel cell performance due to an enhanced water management and a more uniform reactant distribution at the electrode surface. However, the use of a MPL has a negative impact on the cathode porosity (0.80 for the CC_MPL and 0.63 for the CC_MPL _T). The decrease of the porosity of the DL, negatively affects the oxygen and water diffusion rates to and from the catalyst layer, due to a blocking of the diffusion layer pores [98]. This leads to a lower oxygen concentration at the reaction zone and more active sites available for the methanol oxidation with the available water for this reaction. A relatively high methanol gradient is

maintained, contributing for a high level of methanol crossover which is responsible for the reasonably high levels of fuel crossover. Figures 5.7 a) - c) put in evidence the impact of this relatively lower oxygen concentration in a lower limiting current obtained in particular for the two lower methanol concentrations, when using carbon cloth with MPL.

5.3.2. Effect of carbon paper as cathode DL

A similar study was performed using carbon paper as cathode DL, with four different materials considered: two carbon papers PTFE treated (porosity of 0.78) with different thicknesses, CP and CP_T (0.110 mm and 0.190 mm) and two carbon papers with MPL, CP_MPL and CP_MPL_T, which have a slightly higher porosity (0.80), and thickness of 0.240 mm and 0.340 mm, respectively. The polarisation curves are depicted in Figure 5.8 and the resistance values and maximum power output displayed in Table 5.5. Likewise, in the study concerning the use of carbon cloth, three different methanol concentrations (1 M, 2 M and 3 M) were tested and a carbon cloth with a microporous layer (CC_MPL) was used as the anode DL.

As can be seen in Figure 5.8 and Table 5.5, for all the concentration values tested, better performances were achieved using CP_MPL as cathode DL. These results are expected for this relatively thick carbon paper with a MPL with a slightly higher porosity than the two thinner carbon paper materials (Table 4.2). Carbon paper is less porous than carbon cloth.

The introduction of the MPL layer tends to generate an increase in its average porosity, which is favourable for the oxygen diffusion and water removal. Therefore, more oxygen reaches the catalyst layer, which represents less active sites available on the platinum catalyst for the methanol oxidation.

In fact, at the cathode catalyst both methanol and oxygen compete for available sites for the oxidation and reduction reactions, respectively. A relatively low methanol gradient is maintained which tends to generate lower levels of methanol crossover. The enhanced water removal promoted by the MPL layer, helps to alleviate the cathode from the excess water formed avoiding cathode flooding.

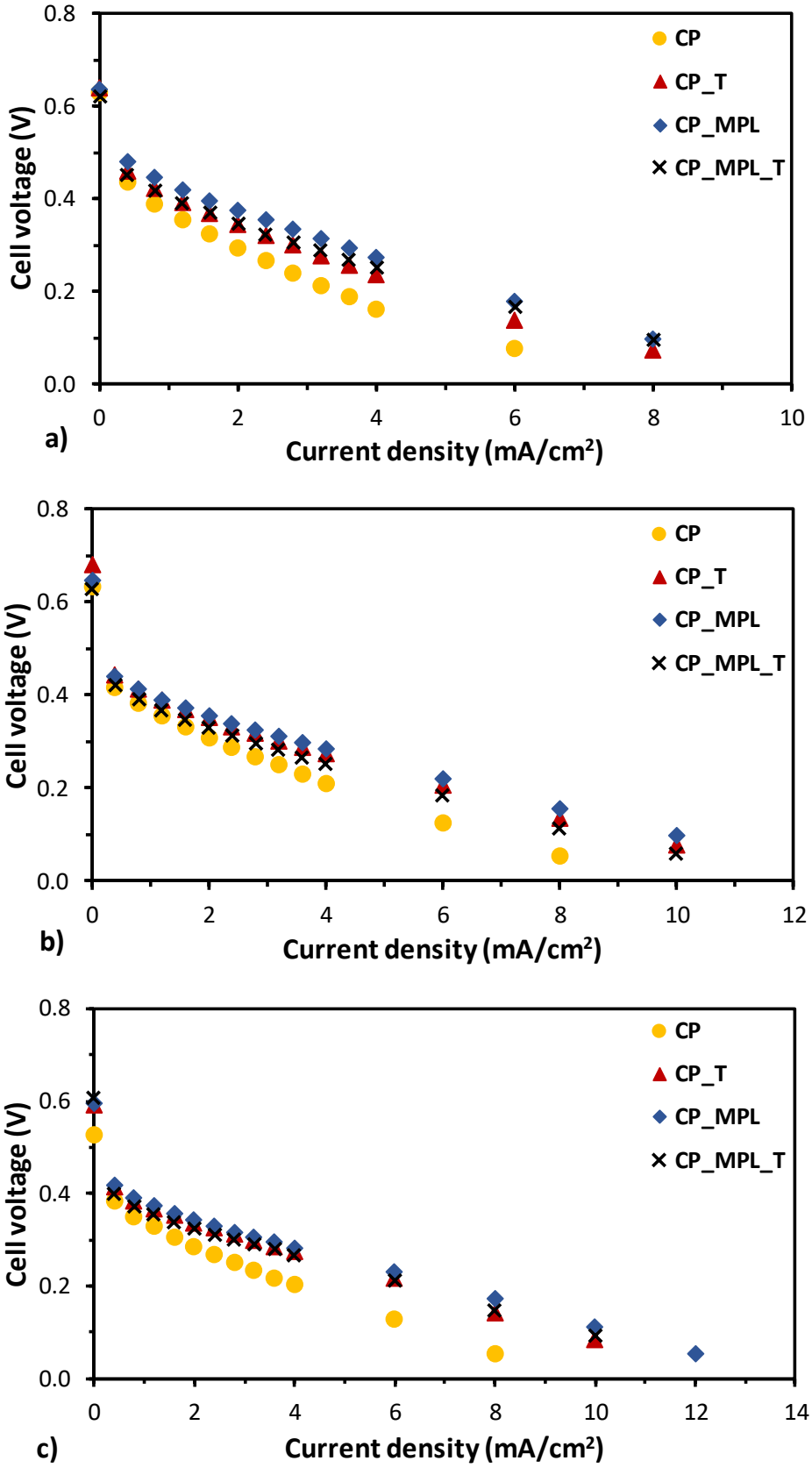

Figure 5.8. Effect of using different carbon papers as CDL on cell performance for different methanol concentrations: a) 1 M, b) 2 M and c) 3 M.

Despite its slightly lower porosity, the CP_T, surprisingly, showed similar power outputs when compared to those obtained with the carbon paper with a MPL. The two PTFE treated carbon papers – CP and CP_T – differ mainly in their thickness (0.110 cm and 0.190 cm, respectively). The presence of the PTFE helps for both materials in the water removal. The greater thickness of CP_T ensures a higher water concentration at the cathode catalyst layer which contributes, as expected, to lower levels of methanol crossover when comparing the performance of these two materials.

Table 5.5. Values for the different resistances of the EEC for the different carbon papers tested as CDL and its maximum power density.

Diffusion layer	Methanol concentration	R_{Ohm} (Ω)	R_A (Ω)	R_C (Ω)	$R_{Crossover}$ (Ω)	Maximum Power density (mW/cm^2)
CP	1 M	0.55	0.01	0.38	1.01	0.68
	2 M	0.63	0.02	0.35	0.76	0.84
	3 M	0.76	0.01	0.30	0.91	0.80
CP_T	1 M	0.54	0.02	0.36	0.82	0.95
	2 M	0.54	0.02	0.22	0.61	1.23
	3 M	0.66	0.02	0.21	0.58	1.28
CP_MPL	1 M	0.42	0.01	0.45	0.84	1.09
	2 M	0.52	0.02	0.28	0.61	1.33
	3 M	0.72	0.02	0.21	0.53	1.38
CP_MPL_T	1 M	0.50	0.02	0.42	0.92	1.01
	2 M	0.37	0.015	0.32	0.65	1.10
	3 M	0.45	0.01	0.28	0.44	1.25

5.4. Effect of methanol concentration

In the previous sections, better performances were obtained when CC_MPL was used as anode DL and CC as cathode DL. Therefore, in this section these materials were used as DLs to study the effect of the methanol concentration on the pDMFC performance towards a further increase of its performance. Stainless steel current collectors with an open ratio of 41 % (CC_2) were also used at the anode and cathode sides. The corresponding polarisation curves are showed in Figure 5.9 and the different resistances, as well as, the maximum power

density achieved for each concentration tested, 1 M, 2 M, 3 M, 5 M and 7 M, are depicted in Table 5.6.

As can be seen in Figure 5.9, the open circuit voltage is much lower that the ideal voltage due to methanol crossover towards the cathode side, and decreases with an increase of the methanol concentration. This is explained by an increase of the concentration gradient between the anode and the cathode side with an increase of the methanol concentration, which lead to a higher crossover rate through the membrane [211].

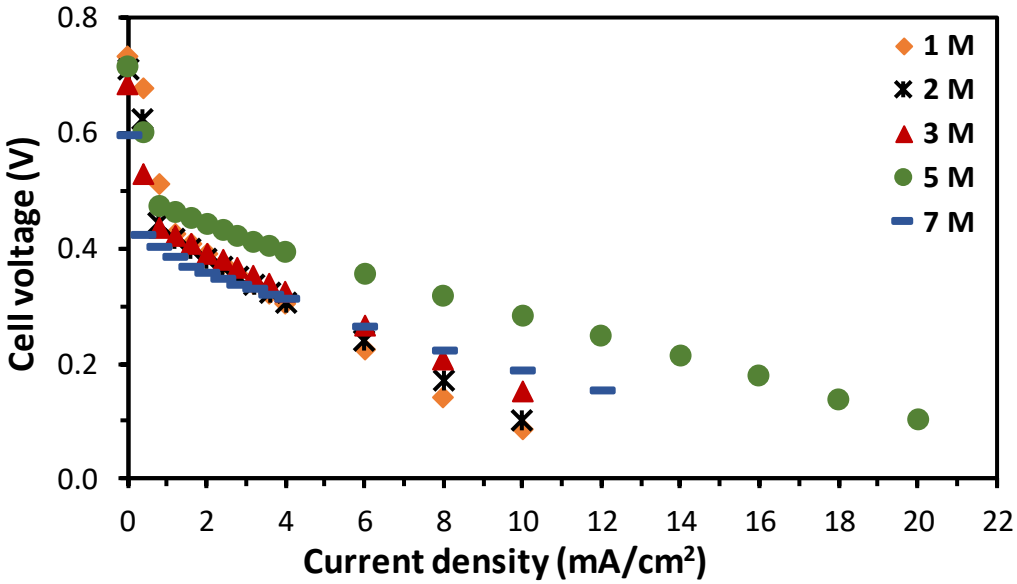

Figure 5.9. Effect of methanol concentration on the pDMFC performance with the tailored MEA.

Even though, as can be seen by the plots presented in Figure 5.9 and the power outputs achieved for each concentration (Table 5.6), the best performance was obtained with a methanol concentration of 5 M. This is due to the fact that despite an increase on the methanol concentration generates an increase of the methanol crossover rate it also increases the methanol diffusion through the anode layers, due to a higher concentration gradient between them, increasing the amount of methanol that reaches the reaction zone and therefore increasing the methanol oxidation rate. A higher oxidation rate will lead to a lower activation loss on the anode side (R_A) and a lower methanol crossover, since the availability of methanol at the catalyst layer is lower, and therefore its concentration gradient, which is the driven force for its crossover, is also lower. A decrease of the methanol crossover rate will also generate higher cathode performances and therefore lower activation losses for both

cathode electrochemical reactions: oxygen reduction (R_C) and methanol oxidation ($R_{Crossover}$).

Additionally, a higher methanol concentration at the anode side leads to a lower water concentration at this side, increasing the water back diffusion towards the anode [110, 167]. This will avoid cathode flooding and will allow a more efficient water management on the cathode side, increasing the oxygen diffusion towards the catalyst sites, with a consequent increase on the oxygen reduction rate and a decrease of the cathode activation losses (R_C). However, the results showed that when the methanol concentration is too high, 7 M, the beneficial effect of a higher methanol concentration at the anode and cathode reactions (R_A and R_C) is lower than the negative effect of an increase of the methanol crossover rate with an increase of the activation losses of the parasitic oxidation reaction ($R_{Crossover}$). Therefore, in these conditions the cell loses performance (Figure 5.9 and Table 5.6).

Table 5.6. Values for the different resistances of the EEC for the different methanol concentrations tested and its maximum power density.

Methanol concentration	R_{Ohm} (Ω)	R_A (Ω)	R_C (Ω)	$R_{Crossover}$ (Ω)	Maximum Power density (mW/cm^2)
1 M	0.47	0.03	0.39	0.63	1.34
2 M	0.46	0.02	0.30	0.47	1.43
3 M	0.42	0.03	0.28	0.30	1.66
5 M	0.41	0.02	0.13	0.24	3.00
7 M	0.57	0.03	0.12	0.38	1.87

5.5. Effect of methanol:ethanol ratio

As already mentioned, the passive DAFCs can be supplied with different alcohols, but the most used and studied ones are methanol and ethanol. Methanol has the highest energy to carbon ratio of any other alcohol, but is toxic for humans and is non-renewable. Ethanol emerges as an alternative and promising fuel due to its non-toxicity, natural availability and renewability. Nevertheless, the performance of direct ethanol fuel cells (DEFCs) is lower than the DMFCs (direct methanol fuel cells), due to the sluggish ethanol electrochemical oxidation, since it is very difficult to cleavage the carbon-carbon bond presented on the ethanol structure. A novel idea, to achieve higher performances with passive DAFCs, is to

explore the possibility of using mixtures of methanol and ethanol, since it is expected to obtain the best characteristics of each alcohol. However, this is still a less explored research field. Therefore, in order to combine the advantages of both fuels, the present section presents a study with the in-house pDMFC fed with a mixture of methanol and ethanol with different concentrations and volume ratios (Table 5.7), towards its optimisation. The results were obtained with stainless steel current collectors, with an open ratio of 41 % (CC_2), at the anode and cathode sides and with carbon cloth with a MPL (CC_MPL) as anode DL and carbon cloth (CC) as cathode DL.

Table 5.7. Methanol and ethanol ratios for the different fuel concentrations: 2 M, 3 M and 5 M

Methanol/Ethanol ratio	Methanol volume (%)	Ethanol volume (%)
75:25	75	25
50:50	50	50
25:75	25	75
0:100	0	100

The polarisation curves are presented in Figure 5.10 and the values for the different resistances of the EEC, at 0.2 V, and the maximum power density achieved for each condition tested can be found in Table 5.8.

As can be seen in Figure 5.10 and Table 5.8, the best results were achieved with a lower amount of ethanol, lower volume ratio, for the higher fuel concentrations tested, 3 M and 5 M. However, for 2 M similar performances were achieved until an ethanol ratio of 50 %. These results can be explained by the fact that the anode activation losses increase with an increase of the ethanol ratio due to its slow reaction rate, to the fact that the catalyst used, in this work, Pt/Ru, is not the adequate one for this reaction and to the misplaced adsorption of ethanol on Pt/Ru [242]. Additionally, a higher ethanol ratio will lead to a lower anode catalyst activity due to its poisoning by the by-products from the incomplete ethanol oxidation reaction, leading to a decrease of the active sites for the methanol oxidation reaction. Therefore, less methanol reacts on the anode side and more methanol reaches the membrane and crosses it towards the cathode side (higher $R_{Crossover}$).

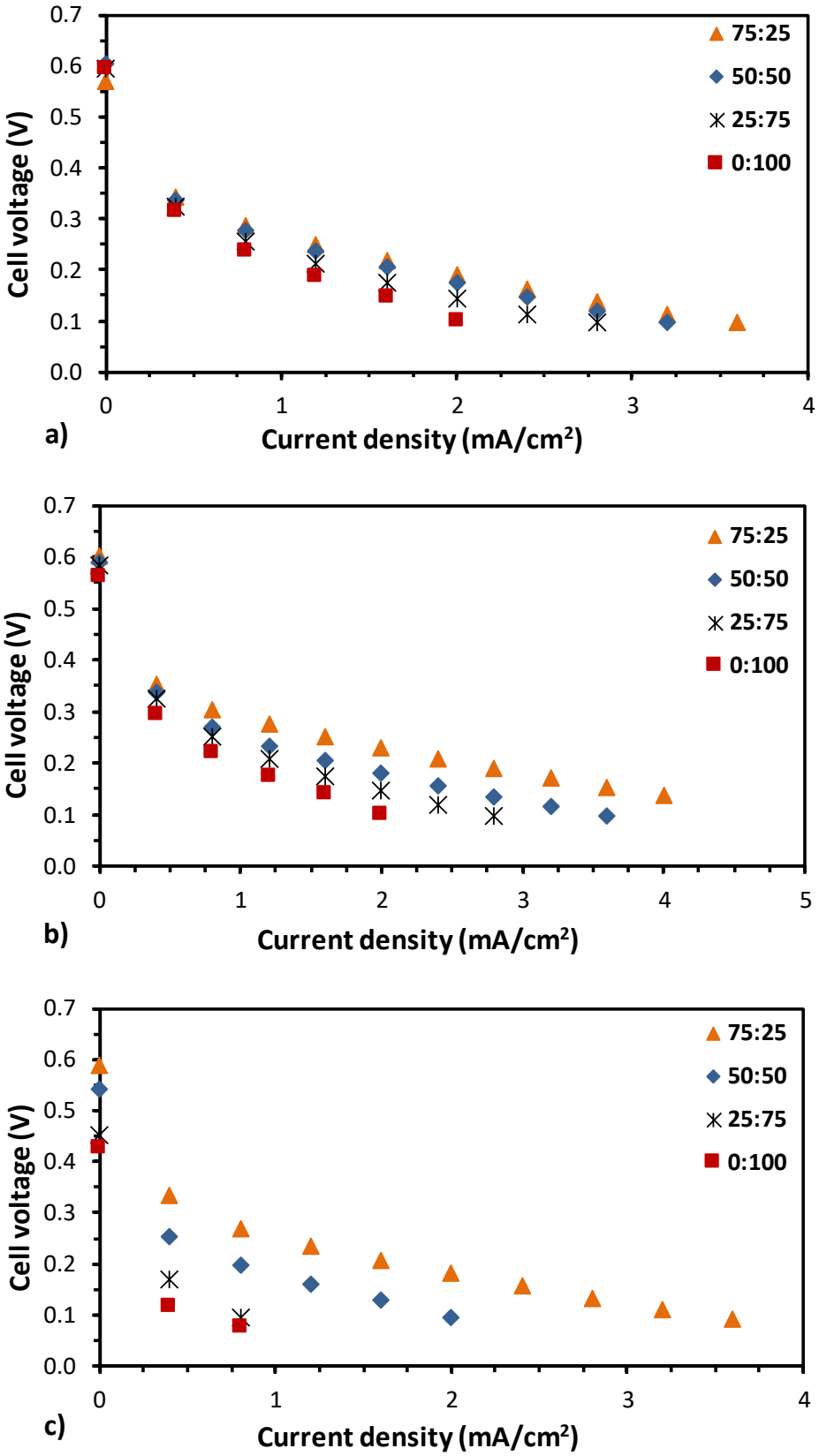

Figure 5.10. Effect of methanol:ethanol ratio on the pDMFC performance for different methanol concentration of a) 2 M, b) 3 M and c) 5 M.

This will increase the cathode activation losses due to cathode poisoning by the methanol oxidation at this side, which will decrease the oxygen reduction rate and therefore increase the cathode activation losses due to this reaction (R_C) and to the undesired one ($R_{Crossover}$). As expected, and as can be seen by the resistance values presented in Table 5.8, the crossover effect is more severe for higher ethanol ratios and fuel concentrations.

Table 5.8. Values for the different resistances of the EEC for the pDMFC tested with different methanol:ethanol ratio and its maximum power density.

Fuel Concentration	Methanol:Ethanol Ratio	R_{Ohm} (Ω)	R_A (Ω)	R_C (Ω)	$R_{Crossover}$ (Ω)	Maximum Power density (mW/cm^2)
2 M	75:25	0.29	0.02	0.53	2.70	0.39
	50:50	0.30	0.02	0.68	3.95	0.35
	25:75	0.35	0.02	0.83	5.93	0.29
	0:100	0.33	0.02	1.20	9.68	0.23
3 M	75:25	0.29	0.02	0.52	2.07	0.55
	50:50	0.29	0.03	0.60	4.02	0.38
	25:75	0.30	0.02	0.92	5.95	0.29
	0:100	0.25	0.06	0.76	10.4	0.23
5 M	75:25	0.57	0.04	0.89	2.67	0.37
	50:50	0.52	0.09	1.73	5.16	0.21
	25:75	0.53	0.10	4.80	18.2	0.08
	0:100	0.54	0.10	8.36	31.3	0.06

The best performance was achieved for a methanol:ethanol ratio of 75:25 and a fuel concentration of 3 M (Figure 5.10 and Table 5.8). However, this value is much lower than the one obtained with 100 % of methanol (Table 5.6). For the ethanol oxidation, a binary catalyst of Pt/Sn would be more appropriate [243, 244], since it would increase the electrocatalytic activity and the ethanol oxidation rate. In this case, to attend the oxidation

requirements of each alcohol, it would be preferable to use a mixed catalyst, which is not commercially available.

5.6. Effect of current collector design

As already mentioned in chapter 2, due to their roles in the fuel cell systems, the current collectors design has an important effect on the performance of a pDMFC. Different designs will induce different mass, heat and charge transport phenomena, with a direct effect on the reactants supply, products removal and electrons recovery and transport. According to its configuration, the CCs can be categorized in perforated CCs and metal mesh ones, being the perforated CCs the most widely used in the passive fuel cell systems. Besides the perforation design, its open ratio, defined as the ratio between the CC open area and the cell active area, also has a significant effect on the cell performance. It would be expected that higher open ratios will be beneficial for the reactants supply and products removal leading to higher performances. However, higher open ratios also lead to higher interfacial contact resistances and lower areas for electrons collection/recovery.

The study reported in this section intends to assess the effect of the anode and cathode CC design on the power output of a pDMFC. Three different perforated CCs, each one with a different open ratio, and an open window frame CC were tested at both anode and cathode sides (Table 4.1). As in the previous sections, the results were obtained with stainless steel current collectors. Carbon cloth with a MPL (CC_MPL) was used as anode DL and carbon cloth (CC) as cathode DL, since as can be seen in sections 5.2. and 5.3, these materials lead to the best performances.

5.6.1. Effect of anode current collector design

Figure 5.11 shows the polarisation curves of a pDMFC with four different CCs designs (CC_1, CC_2, CC_3 and CC_4 – please recall Table 4.1) at the anode side and using three different methanol concentrations, 1 M, 2 M and 3 M. The values for the ohmic and activation resistances ($R_{A,}$ $R_{C,}$ $R_{Crossover}$) at 0.2 V, as well as, the maximum power density achieved for each CC tested are displayed in Table 5.9. The cathode current collector, CC_2, was kept the same in all the experiments regarding the effect of the anode current collector on the performance of a pDMFC. The results showed that, for all the concentrations tested,

a better performance was achieved with the CC with the lower open ratio (34 %) at the anode side (CC_1). This can be concluded based on the I-V curves, on the resistance values, which are lower, and on the maximum power density achieved that is higher. As can be seen in Table 5.9, CC_1 presents lower ohmic resistances due to its higher metallic area, which favours the electrons collection/recovery, the compression rate and the MEA support, decreasing the cell contact resistances and consequently the ohmic resistance (R_{Ohm}). In opposition, the current collector with the open window frame (CC_4) presents the higher ohmic resistances.

Despite the fact that the diffusion of reactants towards the anode catalyst layer is enhanced using CCs with a higher open ratio, due to its higher open area for reactants supply and products removal, the methanol crossover, here represented as $R_{Crossover}$, also increases.

Additionally, as expected and as can be seen by the results presented in Figure 5.11 and Table 5.9, this increase is more meaningful for the open frame current collector (CC_4).

The presence of methanol on the cathode side leads to the formation of a mixed potential at this side, due to its oxidation on the cathode catalyst active sites, to catalyst/cathode poisoning by this reaction by-products, due to the incomplete methanol oxidation on Pt catalysts and hinders the oxygen access to the catalyst layer and catalyst active sites. This will lead to a decrease on the oxygen reduction rate and an increase on the cathode activation losses (R_C), a decrease of the cathode performance and consequently the overall cell performance.

Therefore, the use of a current collector with a lower open ratio at the anode would be beneficial to control the amount of methanol that reaches the membrane and consequently crosses it towards the cathode side, decreasing the cathode losses (R_C and $R_{Crossover}$) and consequently increasing the cell performance (Fig. 5.11 and Table 5.9).

The results presented regarding the effect of the anode CC design, showed that the selection of the optimal design would depend on the methanol concentration and on achieving the right balance between the positive and negative effects of each design on the cell performance/power output. In this study, the maximum power output, 2.92 mW/cm^2, was achieved with the current collector with the lowest open ratio, CC_1, and a methanol concentration of 3 M.

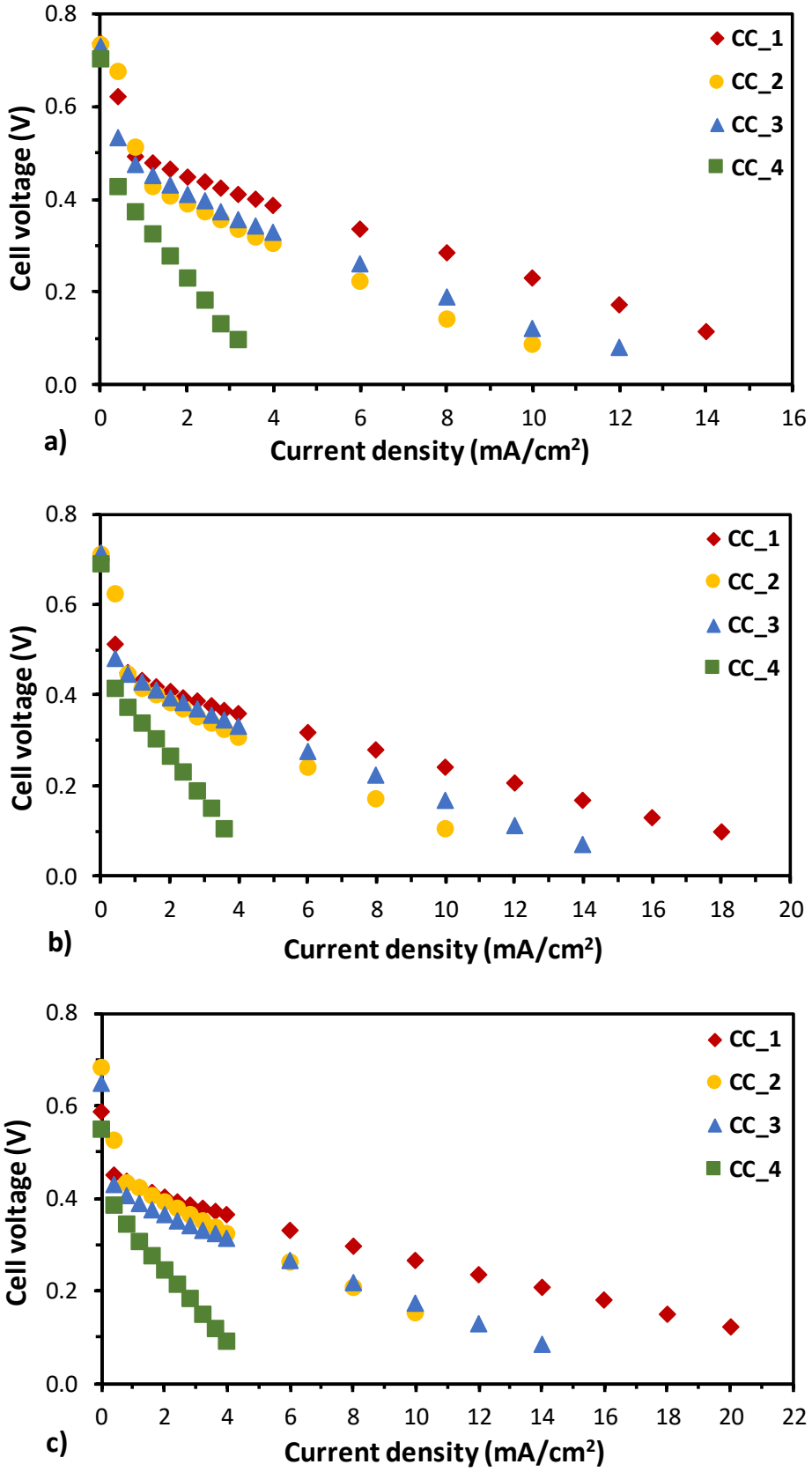

Figure 5.11. Effect of the anode CC design on the performance of a pDMFC for different methanol concentrations: a) 1 M, b) 2 M and c) 3 M; cathode CC_2.

Table 5.9. Values for the different resistances of the EEC for the different CC designs tested on the anode side and its maximum power density; cathode CC_2.

CC design	Methanol concentration	R_{Ohm} (Ω)	R_A (Ω)	R_C (Ω)	$R_{Crossover}$ (Ω)	Maximum Power density (mW/cm^2)
CC_1	1 M	0.23	0.01	0.27	0.46	2.30
	2 M	0.25	0.01	0.15	0.30	2.45
	3 M	0.31	0.01	0.10	0.32	2.92
CC_2	1 M	0.47	0.03	0.39	0.63	1.34
	2 M	0.46	0.02	0.30	0.47	1.43
	3 M	0.42	0.03	0.28	0.30	1.66
CC_3	1 M	0.32	0.02	0.39	0.58	1.55
	2 M	0.35	0.015	0.25	0.40	1.77
	3 M	0.35	0.01	0.13	0.47	1.76
CC_4	1 M	0.71	0.01	1.50	2.26	0.46
	2 M	0.76	0.02	0.12	2.91	0.55
	3 M	0.77	0.01	0.09	2.65	0.52

5.6.2. Effect of cathode current collector design

It is well known that the cathode current collector is responsible for the oxygen supply and products removal from the cell, for providing the electrons needed for the oxygen reduction reaction, transported through the external circuit from the anode side, and for the MEA support. Therefore, the cathode CC design will also have an important role on the cathode performance and consequently on the overall cell performance. A similar study to the one performed for the anode side, was performed for the cathode, where four different CCs with different designs (CC_1, CC_2, CC_3 and CC_4) were employed on the cathode side and a current collector with an open ratio of 41 % (CC_2) was used on the other side, anode. Three different methanol concentrations, 1 M, 2 M and 3 M were tested.

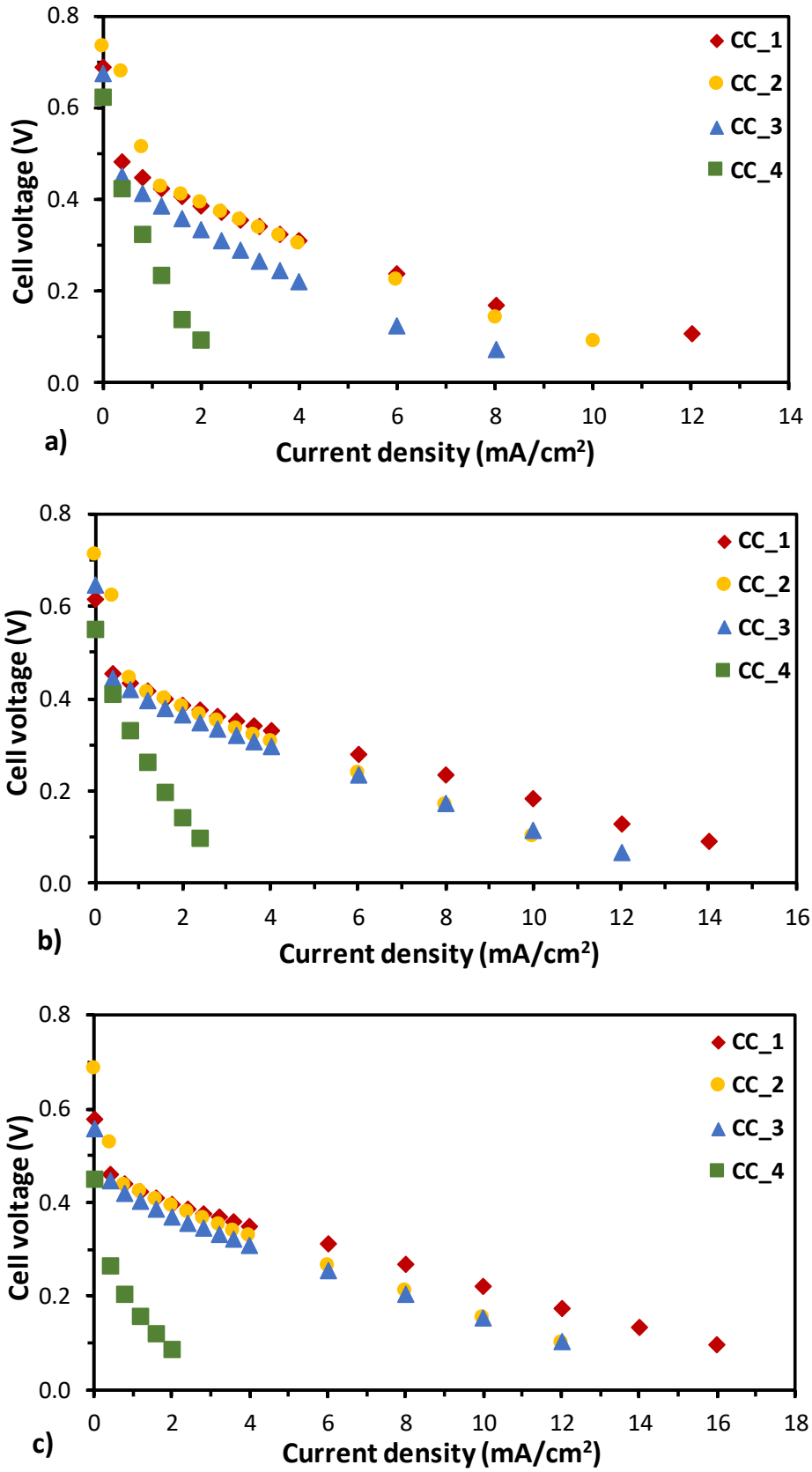

Figure 5.12. Effect of the cathode CC design on the performance of a pDMFC for different methanol concentrations: a) 1 M, b) 2 M and c) 3 M; anode CC_2.

The effect of the cathode CC on the cell performance can be analysed through the polarisation curves exhibited in Figure 5.12, and the values for the different resistances that affect the cell performance and its maximum power density, presented in Table 5.10.
The results demonstrated that the best performance was achieved with CC_1 and the worst with the open window frame, CC_4. These results can be explained by the fact that despite a higher open ratio allows a more efficient oxygen deliver to the reaction zone and therefore a higher oxygen reduction rate (lower R_C) it also leads to a higher water removal rate, which is beneficial to avoid cathode flooding but has a negative impact on methanol crossover ($R_{Crossover}$).

Table 5.10. Values for the different resistances of the EEC for the different CC designs tested on the cathode side and its maximum power density; anode CC_2.

CC design	Methanol concentration	R_{Ohm} (Ω)	R_A (Ω)	R_C (Ω)	$R_{Crossover}$ (Ω)	Maximum Power density (mW/cm^2)
CC_1	1 M	0.36	0.01	0.26	0.62	1.43
	2 M	0.31	0.02	0.20	0.41	1.88
	3 M	0.29	0.02	0.13	0.35	2.20
CC_2	1 M	0.47	0.03	0.39	0.63	1.34
	2 M	0.46	0.02	0.30	0.47	1.43
	3 M	0.42	0.03	0.28	0.30	1.66
CC_3	1 M	0.44	0.03	0.42	0.89	0.88
	2 M	0.41	0.03	0.24	0.60	1.19
	3 M	0.35	0.03	0.17	0.52	1.62
CC_4	1 M	0.64	0.02	0.17	6.15	0.28
	2 M	0.64	0.02	0.14	4.40	0.32
	3 M	0.64	0.02	0.14	5.62	0.19

The presence of a higher amount of water on the cathode side decreases the water concentration gradient between the anode and cathode side and therefore the water crossover rate. As reported by Xu et al. [91] in their work, where they investigated the characteristics

of the methanol and water crossover in a pDMFC, this will also decrease the methanol crossover rate, increasing the fuel efficiency. In addition, the open window frame CC (CC_4) will lead to a lower MEA support and compression rate increasing the electrical contact resistance between the different fuel cell layers, clearly perceived by the higher ohmic resistances (R_{Ohm}) presented in Table 5.10.

Consequently, the best power output, 2.20 mW/cm^2, was achieved with CC_1 as cathode current collector and a methanol concentration of 3 M, due to its lower open ratio. This design conducted to an enhancement of the electrical connection and a decrease of the cell contact resistances (R_{Ohm}).

Additionally, this design presented the lowest activation losses due to the methanol oxidation reaction on the cathode side due to methanol crossover ($R_{Crossover}$). This was achieved due to a lower water removal rate on the cathode side that conducted to a lower water crossover rate from the anode to the cathode and consequently lower methanol crossover rate [91].

5.7. Effect of current collector material

It is known that CCs play a significant role in the cell total weight and cost as they are responsible for about 80 % of the cell total weight [26]. Consequently, to achieve the pDMFC technology goals, small, compact, low cost and weight and high durability and power, the CCs should have: high electrical conductivity and mechanical and corrosion resistance, should be easily manufactured and have a low weight and cost [23, 26]. Based on that, different metallic materials have been used as CCs in pDMFCs, such as stainless steel (SS) [40, 51–59], titanium [60], aluminium [44], copper [167], printed circuit board [39, 61, 62] and porous metals [163, 230]. However, as documented by Yousefi and Zohoor [23] 76 % of the CCs used in pDMFCs are made from stainless steel. The major problem of using this material is that after a long-term operation SS suffers corrosion, increasing the contact resistance between the CC and the membrane and leading to the presence and accumulation of the corrosion products on the different fuel cell layers, poisoning them [13]. The presence of these compounds on the membrane leads to a decrease of its conductivity and hinders the protons transport towards the cathode side [167]. Therefore, to avoid corrosion, the CCs are usually coated with a thin layer of a high conductive metal, such as platinum, gold and titanium [26, 61]. However, this coating increases significantly the CC costs and consequently the system overall costs. The development of low-cost materials and an

optimisation of the CCs coating in order to ensure an optimal balance between the corrosion resistance and its cost are key factors towards the commercialization of pDMFC systems. Having this in mind, the effect of the current collector material of the anode and cathode sides on the cell performance was evaluated with three different materials, SS, SS+Au and Ti, as shown in Table 5.11. These materials were selected based on its unique properties and towards a cost and weight reduction. All of them have a thickness of 0.5 mm and a perforated circular-hole-array pattern with an open ratio of 34 % (CC_1), the design that conduced to the best performance. As DLs, carbon cloth with a MPL (CC_MPL) was used on the anode and carbon cloth (CC) on the cathode, since these materials showed the best performance, section 5.2 and 5.3.

Table 5.11. Values of the electrical conductivity and costs of the different materials used as CCs.

Material	Electrical conductivity (S/m)	Cost (€)/CC
Stainless steel	$1.33x10^7$	0.50
Gold	$4.30x10^7$	73.50
Titanium	$1.79x10^7$	4.70

The pDMFC was operated with three different methanol concentrations, 1 M, 2 M and 3 M. On the studies regarding this effect on the anode side, SS was used as CC at the cathode side. Then, the best material found for the anode side (Ti) was used on this side and the three different materials (SS, SS+Au and Ti) were tested at the cathode side. The polarisation curves regarding the anode side can be found in Figure 5.13 while those for the cathode side in Figure 5.14. The values for different resistances of the EEC (ohmic and the three activation resistances) at 0.2 V, as well as, the maximum power density achieved for each configuration are presented in Table 5.12.

As can be seen in Figure 5.13 and Table 5.12, on the overall higher performances were achieved using Ti as anode CC. The use of Ti as material of CCs promotes the advance of this technology in portable applications, since it the lightest material of all, reducing the weight of the cell.

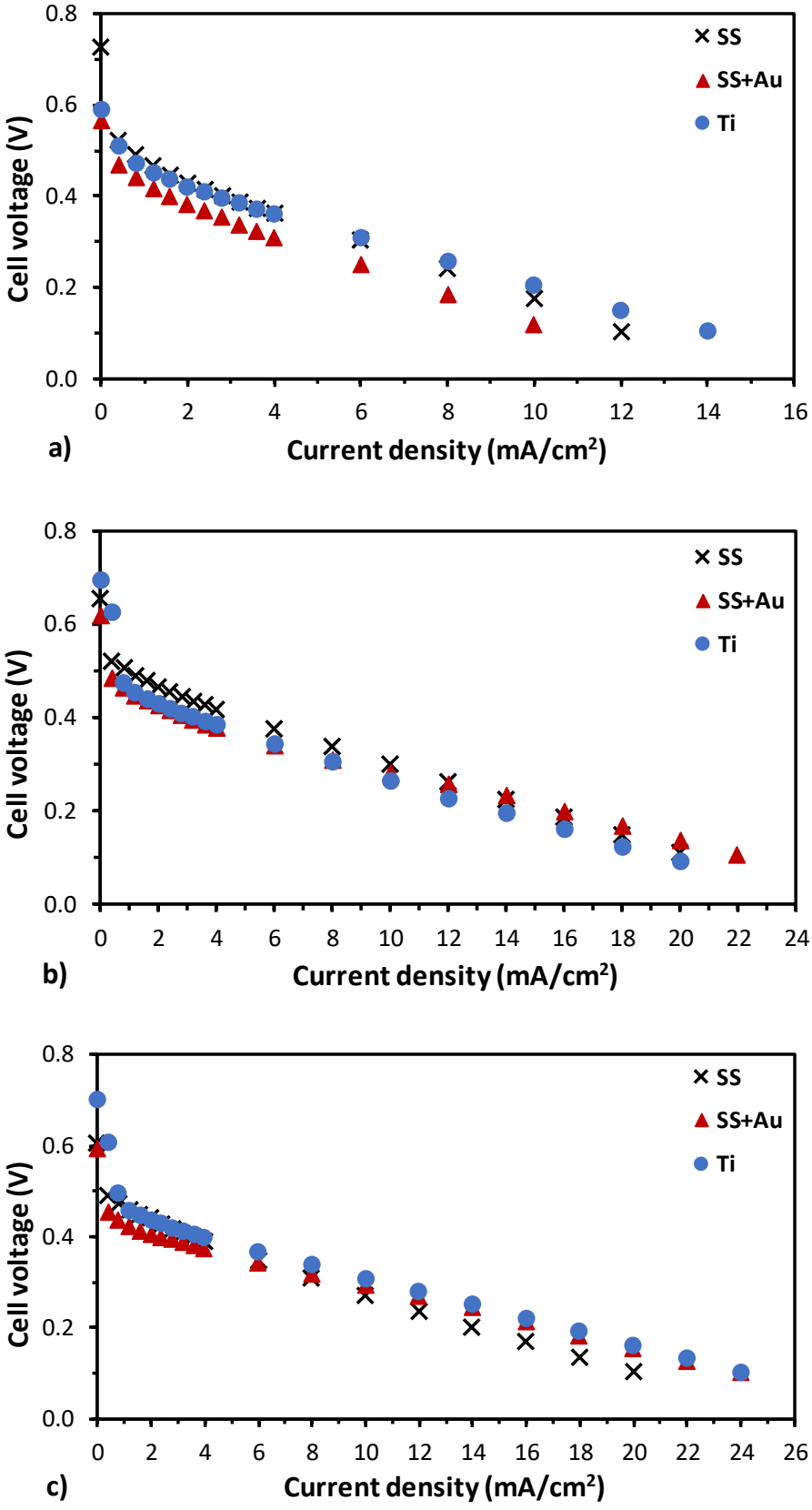

Figure 5.13. Effect of the CC material on the anode side on cell performance for different methanol concentrations: a) 1 M, b) 2 M and c) 3 M; cathode CC_1.

Table 5.12. Values for the different resistances of the EEC for the different materials tested as CCs on both anode and cathode sides and its maximum power density.

CC Material (Anode/Cathode)	**Methanol concentration**	**R_{Ohm} (Ω)**	**R_A (Ω)**	**R_C (Ω)**	**$R_{Crossover}$ (Ω)**	**Maximum Power density (mW/cm^2)**
SS/SS	1 M	0.30	0.01	0.05	0.77	1.93
	2 M	0.35	0.01	0.04	0.34	3.14
	3 M	0.32	0.01	0.09	0.28	2.83
SS+Au/SS	1 M	0.09	0.02	0.005	0.67	1.50
	2 M	0.09	0.01	0.005	0.43	3.25
	3 M	0.09	0.02	0.005	0.34	3.41
Ti/SS	1 M	0.14	0.02	0.37	0.65	2.05
	2 M	0.16	0.02	0.30	0.51	2.74
	3 M	0.12	0.01	0.17	0.27	3.54
Ti/SS+Au	1 M	0.12	0.02	0.005	1.02	1.15
	2 M	0.13	0.03	0.005	0.65	1.87
	3 M	0.11	0.03	0.005	0.50	2.30
Ti/Ti	1 M	0.12	0.06	0.005	1.00	1.26
	2 M	0.16	0.07	0.005	0.95	1.30
	3 M	0.16	0.06	0.005	0.99	1.25

These results can be explained by the fact that, as shown in Table 5.12, when using Ti the cell presented lower ohmic resistances (R_{Ohm}) than when using SS, due to its higher electrical conductivity (Table 5.11), and, for almost all the concentrations tested, slightly lower activation losses at the cathode side due to methanol crossover ($R_{Crossover}$) than SS+Au. As the methanol crossover is one of the major drawbacks in pDMFCs, it is expected that lower $R_{Crossover}$ values lead to higher fuel cell performances. As expected lower ohmic losses were obtained when SS+Au was used as CC, due to its higher electrical conductivity and corrosion

resistance and a lower contact resistance between the CC and the diffusion layer, achieved by coating the SS surface with a thin Au layer [60]. A lower ohmic resistance leads to an enhancement of both electronic and ionic transport. Additionally, this material, SS+Au, has a much higher cost than the other two tested and the power outputs achieved with this material as CC were only higher than those obtained with Ti for a methanol concentration of 2 M. Therefore, the advantages of using SS+Au do not overcome its higher cost.

As already referred, as Ti presented the best overall performance when used as anode CC, was used as anode CC on the tests regarding the evaluation of the effect of the cathode CC material on the pDMFC behaviour. According to the polarisation curves, depicted in Figure 5.14, and the maximum power density achieved, shown in Table 5.12, for all the concentrations tested, better performances were achieved using SS as cathode CC.

Despite the use of SS+Au and Ti as cathode CC lead to lower ohmic and cathode activation resistances (R_{Ohm} and R_C), due to their higher electrical conductivity (Table 5.11), these materials led to higher losses due to the undesired methanol oxidation reaction at the cathode side ($R_{Crossover}$). This can be explained by the fact that CCs with higher electrical conductivities will lead to an enhancement of the electrons recovery on the cathode side and its availability for the cathode electrochemical reactions, oxygen reduction and methanol oxidation due to methanol crossover. As more methanol reacts on the cathode side its concentration decreases on this side and therefore the concentration gradient between the anode and cathode side increases, increasing the methanol crossover rate towards the cathode. As the methanol crossover is one of the major losses that negatively affect the DMFC systems, higher activation losses due to the methanol oxidation at the cathode side ($R_{Crossover}$) will lead to lower power outputs (Figure 5.14 and Table 5.12).

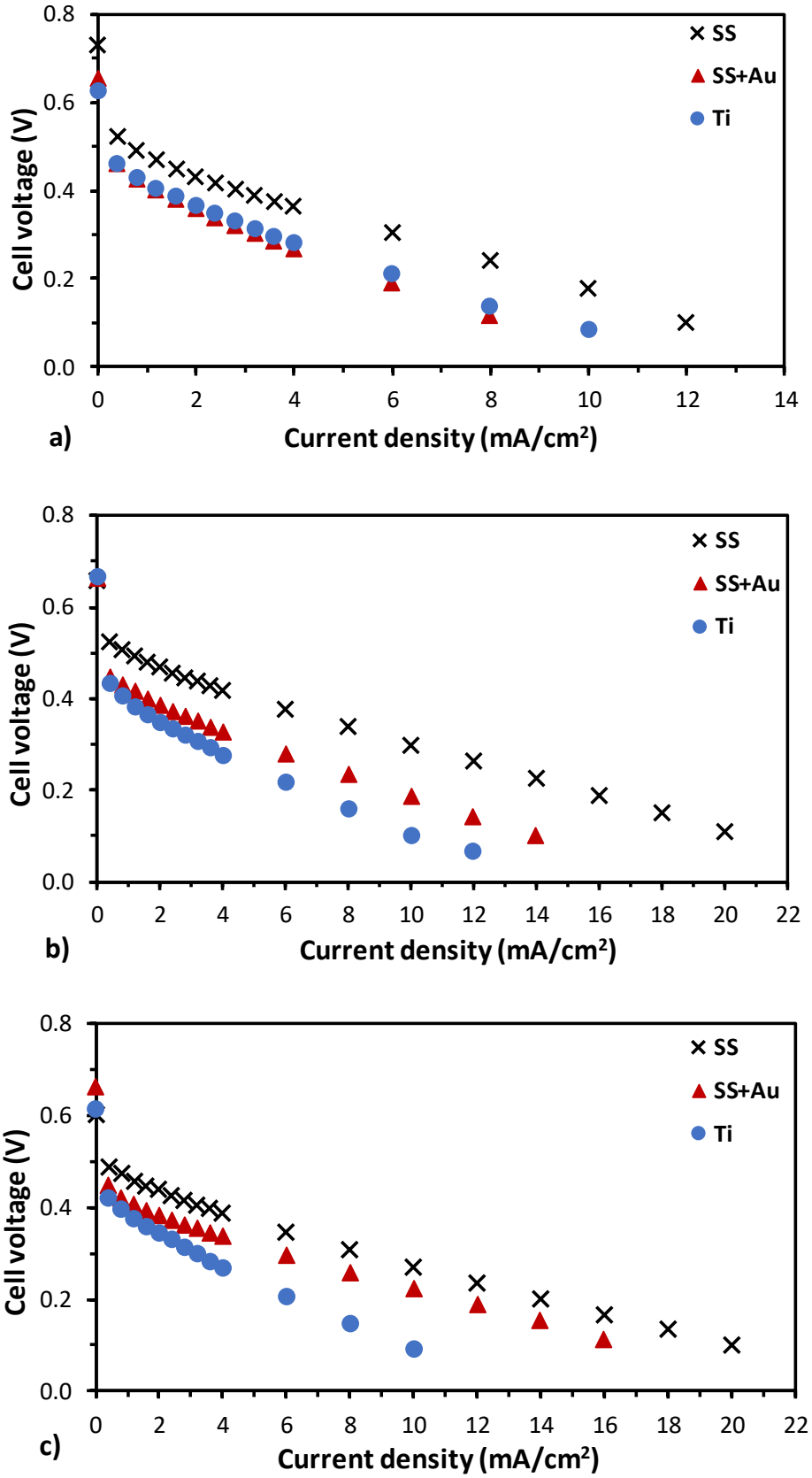

Figure 5.14. Effect of the CC material on the cathode side on cell performance for different methanol concentrations: a) 1 M, b) 2 M and c) 3 M; anode CC_1.

5.8. Durability

As mentioned, the fuel cell lifetime is another important challenge to overcome on pDMFC systems, since despite the fact that the loss of efficiency during the fuel cell operation is unavoidable it can be minimized through an understanding of the different types of degradation and failure mechanisms. Therefore, at the end of this work, the best configuration found on the studies regarding the effect of design parameters on the performance of a pDMFC was used to evaluate the cell lifetime.

The durability tests were carried out with the best design configuration on each side, CC_MPL as anode DL and Ti as anode current collector, with an open ratio of 34 % (CC_1) and CC as cathode DL and SS as cathode current collector with an open ratio of 34 % (CC_1). As the methanol concentration likely influence the cell durability over its operating time, usually, in the durability tests, it is used a dilute methanol solution and a higher current density in order to minimize the methanol crossover rate [202]. Therefore, in this work, the durability tests were realized with a methanol concentration of 2 M and a current density of 10 mA/cm^2. The tests were performed with two identical pDMFCs and the results presented in this section are an average of the values of the two cells. As the durability of the cell was analysed through the voltage decay over the time, a polarisation curve was recorded at the beginning and at the end of the lifetime test and these results provided the degradation rate, which was estimated by the voltage drop measured. EIS measurements were performed at the beginning and at the end of the lifetime test to evaluate the degradation rate, through the assessment of the different resistances that negatively affect the cell performance (ohmic and activation losses). Towards that, the EEC presented in Figure 5.4 was fitted to the EIS data. Figure 5.15 presents the average values of the polarisation data at the beginning and at the end of each test and Table 5.13 shows the average values for the ohmic and activation resistances at 0.2 V, as well as, an average value of the maximum power density at the beginning and at the end of each test. The cells lifetime was determined by the point where it was not possible to recover its performance (voltage below 0.1 V), evaluated by its voltage drop over the time.

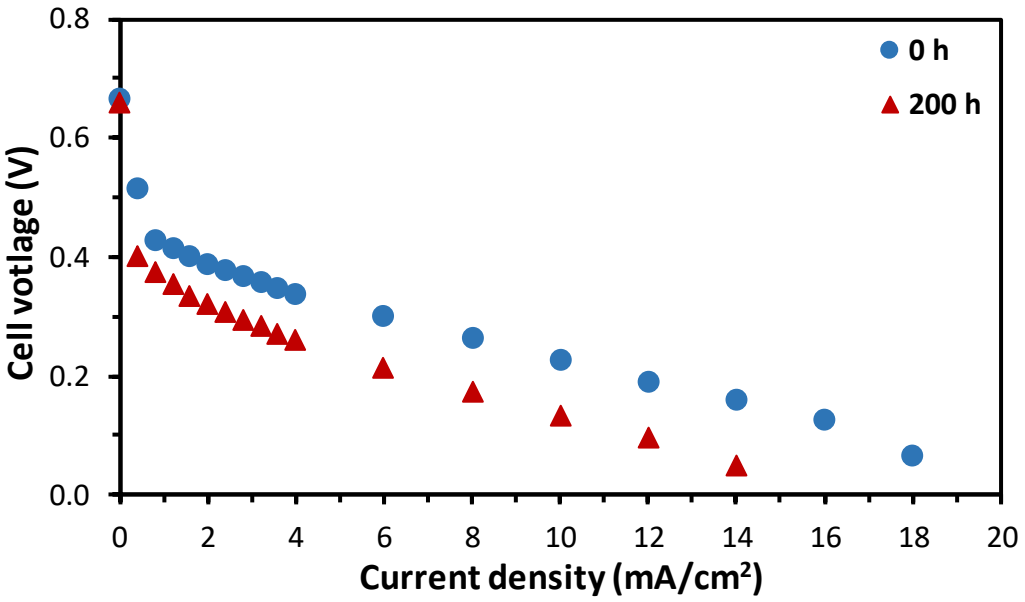

Figure 5.15. Polarisation curves at the beginning (0 h) and at the end (200 h) of the durability tests.

The results showed that the performance lost was irreversible for a running time higher than 200 h. Therefore, this value was pointed out as the pDMFC lifetime. Additionally, as verified by the maximum power density achieved on the polarisation measurements at the beginning and at the end of the durability tests, presented in Table 5.12, the loss of performance was 41 %. As this value is higher that the targets defined by the U.S. Department of Energy (DOE) for a DMFC, loss of efficiency until 20 % [202], EIS measurements were performed as a complementary diagnostic technique to access and quantify the losses that negatively affect the cell behaviour, in order to adopt measures to avoid or reduce them. As can be seen in Table 5.12 the ohmic losses (R_{Ohm}), the anode activation losses (R_A) and the cathode activation losses (R_C and $R_{Crossover}$) increased with the cell operating time. Therefore, it can be concluded that the performance degradation was mainly due to a degradation of the membrane and anode catalyst [147]. The increase of the R_{Ohm} may be justified by a decrease of the electrical contact between the catalyst layer and the membrane and catalyst layer and diffusion layer, caused by the migration of noble metals and degradation of these layers and degradation of the polymer membrane [204]. The increase of R_C and $R_{Crossover}$ are related to the increase of the R_A, since an increase on the anode activation losses indicate a deterioration of the anode catalyst, reducing its activity and consequently increasing the anode overpotential losses. As the methanol oxidation rate decreases, more methanol is

available to cross the membrane towards the cathode side, reacting on this side, and increasing the cathode activation losses.

Table 5.13. Values for the different resistances of the EEC at the beginning (0 h) and at the end (200 h) of the durability tests and its maximum power density.

Operating time	R_{Ohm} (Ω)	R_A (Ω)	R_C (Ω)	$R_{Crossover}$ (Ω)	Maximum Power density (mW/cm^2)
0 h	0.13	0.02	0.14	0.44	2.30
200 h	0.16	0.03	0.17	0.57	1.38

5.9. Economic evaluation

To reach its commercialization and massive use, the pDMFC systems must be cost competitive and have similar investment and manufacturing costs than the conventional technologies that they will replace: batteries. These systems overall costs include material, manufacturing and operating and maintenance costs, where the material ones are responsible for the major fraction on the overall costs. Regarding them, it is known and accepted that the major components/layers responsible for its higher value are the catalyst layers. The pDMFCs efficiency is limited by the electrochemical reactions occurring at both anode and cathode sides, since the slow kinetics of these reactions lead to significant potential losses. Therefore, to achieve the efficiencies needed for these systems real implementation, the catalyst loadings recommended are approximately 4 mg/cm^2 of Pt-based catalyst at the anode and 4 mg/cm^2 of Pt at the cathode, which are very expensive. However, for some specific applications, where the power requirements are not so demanding, a sustainable solution towards the reduction of the system costs is to use lower amounts of the noble metals, such as Pt and Pt/Ru. Having this approach in mind, one of the goals of this work was to optimise the performance of a pDMFC by testing different carbon-based materials as anode and cathode DL, with different properties and costs, and using a 3-layer membrane with lower loadings on both catalyst layers.

In the previous sections, two carbon based materials, carbon paper and carbon cloth, with different characteristics, where employed as anode and cathode DL and their effects on the fuel cell power output were evaluated. Concerning the costs of the materials commonly used

as DLs in these systems, as can be seen in Table 5.14, CP has a price per cm^2 usually higher than the carbon cloth one, however the two best materials in the present study (CC and CP_MPL) have similar prices.

Regarding the current collector, the best materials found for the anode and cathode sides, respectively Ti and SS have lower costs (Table 5.11) allowing to achieve an optimal balance between the cell performance and costs.

Table 5.14. Costs of the different materials tested as anode and cathode DLs (values obtained from QuinTech and Fuel Cells Etc) and total DLs cost (25 cm^2).

Material	**Cost (€)**	**Size (cm^2)**	**Cost (€)/cm^2**	**DL cost (€) (25 cm^2)**
CC	95	900	0.120	3.00
CC_T	108	900	0.106	2.65
CC_MPL	45	400	0.113	2.83
CC_MPL_E	12	25	0.480	12.0
CP	127	361	0.352	8.80
CP_T	99	361	0.274	6.85
CP_MPL	45	400	0.113	2.83
CP_MPL_T	45	400	0.113	2.83

As can be seen in Table 5.15, the use of a 3-layer MEA with lower loadings (3 mg/cm^2 Pt/Ru and 1.3 mg/cm^2 Pt), when compared to the common loadings used for this type of fuel cells (4 mg/cm^2 Pt/Ru and 4 mg/cm^2 Pt) allowed a reduction of 13 % on the fuel cell costs.

Table 5.15. Cost of a 3-layer MEA for pDMFC systems.

MEA	**Characteristic**	**Cost (€)**
Commercial MEA	Nafion 117; Anode 4 mg/cm^2 Pt/Ru; Cathode 4 mg/cm^2 Pt	151
Low Cost MEA	Nafion 117; Anode 3 mg/cm^2 Pt/Ru; Cathode 1.3 mg/cm^2 Pt	132

5.10. Summary

The experimental results obtained regarding the effect of the different operating (methanol concentration and methanol/ethanol ratio) and design conditions (different diffusion layer materials and current collectors design and materials) on the performance of a pDMFC were presented throughout this chapter. The durability tests performed with the optimised pDMFC and an economic evaluation, where the cost reduction achieved with the optimised pDMFC, can also be found in this chapter.

The cell performance and lifetime were evaluated through the polarisation curves and the results were explained under the light of the EIS data by modelling it with an innovative electric equivalent circuit, consisting of four resistances and three constant phase elements. This was the first work on this field performed by current research group. Therefore, the first section of this chapter is devoted to the EIS data analysis and EEC fitting, where it was explained the EEC used in this work, based on the impedance spectrum obtained from the overall cell and half-cell measurements. This procedure allowed the identification of the different losses that negatively affect the cell performance and their quantification through the estimation of its corresponding resistances: ohmic and anode and cathode activation resistances. The cathode resistance comprises the cathode activation losses due to oxygen reduction reaction and the parasitic methanol oxidation reaction at this side, due to methanol crossover and these two contributions were quantified. The latter was, as far as the author is aware, for the first time identified for a pDMFC. The EEC employed in this study showed a good agreement with the EIS data, revealing that the EEC reproduces with accuracy the system under study.

The results, concerning the effect of the anode DL on the cell performance, revealed that better performances were achieved using anode DLs with a dual-layer structure mainly due to an improvement of the methanol transport and methanol oxidation rate on the anode side, oxygen reduction on the cathode side and a reduction of the contact resistance between the BL and the catalyst layer and on the methanol crossover rate. Additionally, the use of CCs with a dual-layer structure showed slightly higher performances that the CP ones.

Among the two different carbon based materials studied (carbon paper and carbon cloth) as cathode DL, better results were achieved using carbon cloth, mainly due to its higher porosity which conducted to higher oxygen and water diffusion rates and therefore lower cathode activation losses. Regarding the addition of a MPL to the cathode DL structure, it

was verified that this is only advantageous when carbon paper is used as backing layer due to an enhancement of its porosity, which is beneficial for the oxygen diffusion and water management.

Very high methanol concentrations lead to lower performances, since the advantages of using higher methanol concentrations on the anode reaction rate and anode performance were lower than its negative effect on the methanol crossover rate, which lead to lower cathode performances due to a higher methanol oxidation rate on this side.

Regarding the study using methanol:ethanol mixtures, a higher ethanol ratio in the fuel solution lead to higher methanol crossover rates and lower cathode performances due to the anode catalyst poisoning by the ethanol oxidation reaction by-products.

Using the current collector with the lower open ratio (34 %) on both anode and cathode sides allowed achieving the best performance. A lower open ratio at the anode side lead to a lower methanol crossover rate, a lower contact resistance and a higher area for electron collection/recovery. Similarly, a cathode current collector with a lower open ratio, allowed a higher metallic area for electron recovery and MEA support and a higher compression rate, which a decrease of the contact resistance between the different fuel cell layers. Additionally, a lower open ration on the cathode side allowed increasing the water back diffusion rate and consequently decreasing the water and methanol crossover rates from the anode to the cathode side.

Regarding the CCs materials tested for the anode side the best performances were achieved with Ti as anode CC, due to lower ohmic resistances than SS and lower cathode activation resistances due to methanol crossover than SS+Au. Regarding the cathode side, better performances were achieved using SS current collectors, since this configuration generally resulted in lower cathode activation resistances due to methanol crossover than the other two materials tested, SS and gold plated SS.

The durability tests carried out with the best configuration showed a fuel cell lifetime of 200 hours and a loss of performance with the operating time of 41 %, explained by a degradation of the membrane and the anode catalyst layer.

Comparing the maximum power output achieved in this work, 5.23 mW/cm^2, with the ones presented in literature and more specifically with the ones obtained by the researcher group in their previous work [101], it can be verified that the current one is much lower. However, this result is explained by the fact that, in this work, lower catalyst loadings than the conventional ones were used towards a reduction of the systems costs. The use of these

reduced loadings allowed a reduction of 13 % on the 3-layer MEA cost and consequently on the pDMFC device.

CHAPTER 6

6. CONCLUSIONS AND FUTURE WORK

This section presents the conclusions of this research work, whose main goal was the optimisation of a passive DMFC, using the materials commercially available, towards its optimisation in terms of performance and costs. Some recommendations for future work are also presented.

6.1. Conclusions

A major challenge on the development of pDMFC systems towards its implementation in the market is to use cost-effective materials with lower weights and attractive performances. Therefore, it is mandatory to use lower catalyst loadings, since the noble metals used as catalysts in these systems have higher costs, and operate de cell with higher methanol concentrations without significant losses of methanol to the cathode side. Based on that and on the fact that the CCs are responsible for about 80 % of these systems weight, different materials, with different costs, weights and designs, were tested as CC in the anode and cathode sides of an in-house pDMFC, towards a cost and weight reduction. Additionally, as the catalyst are responsible for a major fraction on the pDMFC costs, a MEA with lower catalyst loadings (3 mg/cm^2 Pt/Ru and 1.3 mg/cm^2 Pt), was used in this work, to decrease even more these systems cost. Different carbon-based materials with different characteristics were tested as anode and cathode diffusion layers, towards an optimisation of the anode and cathode performances and consequently the cell performance. The best configuration, the one that produced an optimal balance between the cell performance, costs and weight, was used to perform a durability test to evaluate the lifetime of the pDMFC proposed in this work. To take the advantages of using both ethanol and methanol as fuels in DAFCs, different methanol and ethanol ratios in the fuel feed solution of the pDMFC, were tested.
Most of the works, regarding the experimental diagnosis of pDMFCs have been limited to the use of polarisation measurements. Despite this technique gives very useful information and point out the various losses that negatively affect the cell performance, it does not allow to evaluate its contribution independently, since the information provided is the sum of the various losses. To solve this limitation, in this study, EIS measurements were performed as

a complementary diagnostic tool to evaluate the performance and identify and quantify the different voltage losses that negatively affect the pDMFC under study: ohmic and activation losses. Additionally, an innovative EEC was fitted to the EIS data, showing a good agreement with the experimental results and reproducing with accuracy the system under study. A major finding of this work was the ability of identifying the activation of the methanol oxidation parasitic reaction which gives an indirect measure of the methanol crossover. As this is a major drawback of these systems, this new approach enables to optimize conditions leading to lower non-desirable fuel crossover.

The results showed that, in general, higher performances were obtained using carbon cloth as DL due to an enhanced diffusion rates, leading to lower activation losses. Despite its higher thickness, carbon cloth has, in most cases, a porosity higher than carbon paper enhancing the species diffusion towards the catalyst layer, which will improve the electrochemical reaction rates and consequently the cell performance.

Higher methanol and ethanol ratios on the fuel solution lead to lower power outputs mainly due to an increase of the cathode activation losses, due to an increase of the methanol oxidation rate at this side, which lead to cathode poisoning and a decrease of the catalyst active sites for the oxygen reduction reaction.

Using perforated current collectors with a lower open ratio on both sides is more advantageous than the open frame and the ones with a higher open ratio since presented lower contact resistances and activation losses due to the methanol oxidation reaction on the cathode side and higher compression rates and metallic area for electron recovery/collection.

The use of Ti as anode CC and SS as cathode CC lead to lower cathode activation resistances due to methanol crossover and therefore higher cathode performances and higher power outputs. The use of Ti is advantageous since it has a higher corrosion resistance and is lighter that the other two materials tested, allowing to work with a device with low weigh.

For this specific cell design and conditions tested, the maximum power density, 5.23 mW/cm^2, was achieved using Ti as anode current collector and SS as cathode current collector both with an open ratio of 34 %, carbon cloth with a MPL as anode DL and carbon cloth as cathode DL and a methanol concentration of 7 M. The durability tests carried out with the best configuration showed a fuel cell lifetime of 200 hours.

Despite the power output and cell lifetime obtained in this work is below the desirable, may be high enough for some specific applications, where the power requirements are not so demanding. Moreover, the use of a 3 layer-MEA with lower loadings allowed a cost

reduction of 13 %. Additionally, in this work, it was proposed a pDMFC with lower costs and weight that allowed working with high methanol concentrations and lower methanol crossover rates.

Through this work, it can be highlighted that the configuration of a pDMFC play an important role on its performance/behaviour, therefore it is mandatory to select the best options towards the optimisation of these devices and achieve the power outputs, costs and lifetime needed for its implementation and commercialization.

6.2. Future work

As the main target of a pDMFC is its effective introduction in the market to replace the conventional batteries in portable electronic devices, further efforts should be directed towards the development of a prototype of a pDMFC that can be used to charge a mobile phone. However, as a pDMFC is a multiphase system involving simultaneous mass, charge and energy transfer, the development of a 1D+3D mathematical model considering the effects of two-phase flow, heat and mass transfer along with the electrochemical reactions would be very helpful to provide pivotal information to further optimise these devices.

Additionally, it would be very interesting the design, development and optimisation of a micro pDMFC, aiming its application in smaller portable electronic devices such as hearing heads.

In other hand, the introduction of ethanol as fuel or a full replace of methanol by ethanol in passive DAFCs would be also very interesting, since ethanol is less toxic and can be obtained from renewable sources. Therefore, it is needed to develop more active and efficient catalyst for the ethanol oxidation reaction with lower cost, preferably Pt-free ones, towards an increase of the anode performance and consequently the DEFCs power outputs.

REFERENCES

[1] F. Barbir. "PEM Fuel Cells: Theory and Practice", 2nd ed., Elsevier Academic Press, USA, 2013.

[2] V.B. Oliveira. "Transport Phenomena in Direct Methanol Fuel Cells : Modelling and Experimental studies", PhD Thesis, University of Porto, 2009.

[3] F. O`Hayre, R., Cha, S., Cotella W., Prinz.Fuel Cell Fundamentals, 3rd ed., John Wiley & Sons, USA, 2006.

[4] K. Sundmacher. "Fuel cell engineering: Toward the design of efficient electrochemical power plants" *Ind. Eng. Chem. Res.*, 49 (2010) 10159–10182.

[5] U.B. Demirci. "Direct liquid-feed fuel cells: Thermodynamic and environmental concerns" *J. Power Sources*, 169 (2007) 239–246.

[6] S.K. Kamarudin, F. Achmad, W.R.W. Daud. "Overview on the application of direct methanol fuel cell (DMFC) for portable electronic devices" *Int. J. Hydrogen Energy*, 34 (2009) 6902–6916.

[7] R. Rashidi, I. Dincer, G.F.F. Naterer, P. Berg. "Performance evaluation of direct methanol fuel cells for portable applications" *J. Power Sources*, 187 (2009) 509–516.

[8] X. Zhao, M. Yin, L. Ma, L. Liang, C. Liu, J. Liao, T. Lu, W. Xing. "Recent advances in catalysts for direct methanol fuel cells" *Energy Environ. Sci.*, 4 (2011) 2736–2753.

[9] N.A. Karim, S.K. Kamarudin. "An overview on non-platinum cathode catalysts for direct methanol fuel cell" *Appl. Energy*, 103 (2013) 212–220.

[10] J.N. Tiwari, R.N. Tiwari, G. Singh, K.S. Kim. "Recent progress in the development of anode and cathode catalysts for direct methanol fuel cells" *Nano Energy*, 2 (2013) 553–578.

[11] R.N. Singh, R. Awasthi, C.S. Sharma. "Review: An overview of recent development of platinum-based cathode materials for direct methanol fuel cells" *Int. J. Electrochem. Sci.*, 9 (2014) 5607–5639.

[12] A.M. Zainoodin, S.K. Kamarudin, W.R.W. Daud. "Electrode in direct methanol fuel cells" *Int. J. Hydrogen Energy*, 35 (2010) 4606–4621.

[13] S.S. Munjewar, S.B. Thombre, R.K. Mallick. "Approaches to overcome the barrier issues of passive direct methanol fuel cell - Review" *Renew. Sustain. Energy Rev.*, 67 (2017) 1087–1104.

[14] S.S. Munjewar, S.B. Thombre, R.K. Mallick. "A comprehensive review on recent material development of passive direct methanol fuel cell" *Ionics*, 23 (2017) 1–18.

[15] S.K. Kamarudin, N. Hashim. "Materials, morphologies and structures of MEAs in DMFCs" *Renew. Sustain. Energy Rev.*, 16 (2012) 2494–2515.

[16] H. Ahmad, S.K. Kamarudin, U.A. Hasran, W.R.W. Daud. "Overview of hybrid membranes for direct-methanol fuel-cell applications" *Int. J. Hydrogen Energy*, 35 (2010) 2160–2175.

[17] F. Lufrano, V. Baglio, P. Staiti, V. Antonucci, A.S. Aricò. "Performance analysis of polymer electrolyte membranes for direct methanol fuel cells" *J. Power Sources*, 243 (2013) 519–534.

[18] M. Ahmed, I. Dincer. “A review on methanol crossover in direct methanol fuel cells : challenges and achievements” *Int. J. Energy Res.,* 35 (2011) 1213–1228.

[19] T.S. Zhao, W.W. Yang, R. Chen, Q.X. Wu. “Towards operating direct methanol fuel cells with highly concentrated fuel” *J. Power Sources,* 195 (2010) 3451–3462.

[20] A. Faghri, X. Li, H. Bahrami. “Recent advances in passive and semi-passive direct methanol fuel cells” *Int. J. Therm. Sci.,* 62(2012) 12–18.

[21] X. Li, A. Faghri. “Review and advances of direct methanol fuel cells (DMFCs) part I: Design, fabrication, and testing with high concentration methanol solutions” *J. Power Sources,* 226 (2013) 223–240.

[22] M.Z.F. Kamaruddin, S.K. Kamarudin, W.R.W. Daud, M.S. Masdar. “An overview of fuel management in direct methanol fuel cells” *Renew. Sustain. Energy Rev.,* 24 (2013) 557–565.

[23] S. Yousefi, M. Zohoor. “Conceptual design and statistical overview on the design of a passive DMFC single cell” *Int. J. Hydrogen Energy,* 39 (2014) 5972–5980.

[24] P. Kumar, K. Dutta, S. Das, P.P. Kundu. “An overview of unsolved deficiencies of direct methanol fuel cell technology : factors and parameters affecting its widespread use” *Int. J. Energy Res.,* 38 (2014) 1367–1390.

[25] A. Ismail, S.K. Kamarudin, W.R.W. Daud, S. Masdar, M.R. Yosfiah. “Mass and heat transport in direct methanol fuel cells” *J. Power Sources,* 196 (2011) 9847–9855.

[26] R.K. Mallick, S.B. Thombre, N.K. Shrivastava. “A critical review of the current collector for passive direct methanol fuel cells” *J. Power Sources,* 285 (2015) 510–529.

[27] N.K. Shrivastava, S.B. Thombre, R.B. Chadge. “Liquid feed passive direct methanol fuel cell: challenges and recent advances” *Ionics,* 22 (2016) 1–23.

[28] S. Basri, S.K. Kamarudin. “Process system engineering in direct methanol fuel cell” *Int. J. Hydrogen Energy,* 36 (2011) 6219–6236.

[29] H. Bahrami, A. Faghri. “Review and advances of direct methanol fuel cells: Part II: Modeling and numerical simulation” *J. Power Sources,* 230 (2013) 303–320.

[30] T.S. Zhao, C. Xu, R. Chen, W.W. Yang. “Mass transport phenomena in direct methanol fuel cells” *Prog. Energy Combust. Sci.,* 35 (2009) 275–292.

[31] S.-L. Chen, C.-T. Lin, C.-C. Chieng, F.-G. Tseng. “Highly efficient CO_2 bubble removal on carbon nanotube supported nanocatalysts for direct methanol fuel cell” *J. Power Sources,* 195 (2010) 1640–1646.

[32] W. Yuan, Y. Tang, X. Yang, B. Liu, Z. Wan. “Structural diversity and orientation dependence of a liquid-fed passive air-breathing direct methanol fuel cell” *Int. J. Hydrogen Energy,* 37 (2012) 9298–9313.

[33] O. Gholami, S.J. Imen, M. Shakeri. “Effect of non-uniform parallel channel on performance of passive direct methanol fuel cell” *Int. J. Hydrogen Energy*, 38 (2013) 3395–3400.

[34] W. Yuan, B. Zhou, J. Hu, J. Deng, Z. Zhang, Y. Tang. “Passive direct methanol fuel cell using woven carbon fiber fabric as mass transfer control medium” *Int. J. Hydrogen Energy,* 40 (2015) 2326–2333.

[35] D.S. Falcão, J.P. Pereira, A.M.F.R. Pinto. “Effect of stainless steel meshes on the performance of passive micro direct methanol fuel cells” *Int. J. Hydrogen Energy*, 41 (2016) 13859–13867.

[36] W. Chen, W. Yuan, G. Ye, F. Han, Y. Tang. “Utilization and positive effects of produced CO_2 on the performance of a passive direct methanol fuel cell with a composite anode structure” *Int. J. Hydrogen Energy*, 42 (2017) 15613–15622.

[37] W. Zheng, A. Suominen, H. Lagercrantz, A. Tuominen. “A two-dimensional model for CO_2/fuel multiphase flow on the anode side of a DMFC” *J. Fuel Cell Sci. Technol.*, 9 (2012) 11009-1-11009–7.

[38] W. Liu, W. Cai, C. Liu, S. Sun, W. Xing. “Magnetic coupled passive direct methanol fuel cell: Promoted CO_2 removal and enhanced catalyst utilization” *Fuel*, 139 (2015) 308–313.

[39] Y. Zhou, X. Wang, X. Guo, X. Qiu, L. Liu. “A water collecting and recycling structure for silicon-based micro direct methanol fuel cells” *Int. J. Hydrogen Energy*, 37 (2012) 967–976.

[40] C. Xu, A. Faghri. “Effect of the capillary property of porous media on the water transport characteristics in a passive liquid-feed DMFC” *J. Fuel Cell Sci. Technol.*, 7 (2010) 61007-1-61007–14.

[41] X. Li, A. Faghri, C. Xu. “Water management of the DMFC passively fed with a high-concentration methanol solution” *Int. J. Hydrogen Energy*, 35 (2010) 8690–8698.

[42] M. Chen, J. Chen, Y. Li, Q. Huang, H. Zhang, X. Xue, Z. Zou, H. Yang. “Cathode catalyst layer with stepwise hydrophobicity distribution for a passive direct methanol fuel cell” *Energy & Fuels*, 26 (2012) 1178–1184.

[43] S. Yousefi, M. Shakeri, K. Sedighi. “The effect of cell orientations and environmental conditions on the performance of a passive DMFC single cell” *Ionics*, 19 (2013) 1637–1647.

[44] Z. Wang, X. Zhang, L. Nie, Y. Zhang, X. Liu. “Elimination of water flooding of cathode current collector of micro passive direct methanol fuel cell by superhydrophilic surface treatment” *Appl. Energy*, 126 (2014) 107–112.

[45] X. Zhang, Y. Li, H. Chen, Z. Wang, Z. Zeng, M. Cai, Y. Zhang, X. Liu. “A water management system for metal-based micro passive direct methanol fuel cells” *J. Power Sources*, 273 (2015) 375–379.

[46] H. Bahrami, A. Faghri. “Water management in a passive DMFC using highly concentrated methanol solution” *J. Fuel Cell Sci. Technol.*, 8 (2011) 21011-1-21011–15.

[47] C.E. Perles. “Propriedades físico-químicas relacionadas ao desenvolvimento de membranas de Nafion® para aplicações em células a combustível do tipo PEMFC” *Polímeros Ciência E Tecnol.*, 18 (2008) 281–288.

[48] N.K. Shrivastava, S.B. Thombre, R.K. Mallick. “Effect of diffusion layer compression on passive DMFC performance” *Electrochim. Acta*, 149 (2014) 167–175.

[49] X. Li, I. Sabir. “Review of bipolar plates in PEM fuel cells: Flow-field designs” *Int. J. Hydrogen Energy*, 30 (2005) 359–371.

[50] A. Hermann, T. Chaudhuri, P. Spagnol. “Bipolar plates for PEM fuel cells: A review” *Int. J. Hydrogen Energy,* 30 (2005) 1297–1302.

[51] Y.H. Chan, T.S. Zhao, R. Chen, C. Xu. “A small mono-polar direct methanol fuel cell stack with passive operation” *J. Power Sources,* 178 (2008) 118–124.

[52] Y. Tang, W. Yuan, M. Pan, B. Tang, Z. Li, Z. Wan. “Effects of structural aspects on the performance of a passive air-breathing direct methanol fuel cell” *J. Power Sources,* 195 (2010) 5628–5636.

[53] Y.-D. Kuan, J.-Y. Chang, S.-M. Lee. “Experimental investigation of the effect of free openings of current collectors on a direct methanol fuel cell” *J. Power Sources,* 196 (2011) 717–728.

[54] W. Yuan, Y. Tang, Q. Wang, Z. Wan. “Dominance evaluation of structural factors in a passive air-breathing direct methanol fuel cell based on orthogonal array analysis” *Appl. Energy,* 88 (2011) 1671–1680.

[55] C. Yang, J. Wang, X. Xie, S. Wang, Z. Mao, H. Wang. “Electrochemical behavior of surface treated metal bipolar plates used in passive direct methanol fuel cell” *Int. J. Hydrogen Energy,* 37 (2012) 867–872.

[56] S. Yousefi, D.D. Ganji. “Experimental investigation of a passive direct methanol fuel cell with 100cm2 active areas” *Electrochim. Acta,* 85(2012) 693–699.

[57] W. Yuan, Y. Tang, X. Yang, Z. Wan. “Toward using porous metal-fiber sintered plate as anodic methanol barrier in a passive direct methanol fuel cell” *Int. J. Hydrogen Energy,* 37 (2012) 13510–13521.

[58] W. Yuan, J. Deng, Z. Zhang, X. Yang, Y. Tang. “Study on operational aspects of a passive direct methanol fuel cell incorporating an anodic methanol barrier” *Renew. Energy,* 62 (2014) 640–648.

[59] A. Calabriso, L. Cedola, L. Del Zotto, F. Rispoli, S.G. Santori, L. Del Zotto, F. Rispoli, S.G. Santori. “Performance investigation of passive direct methanol fuel cell in different structural configurations” *J. Clean. Prod.,* 88 (2015) 23–28.

[60] H. Wu, H. Zhang, P. Chen, J. Guo, T. Yuan, J. Zheng, H. Yang. “Integrated anode structure for passive direct methanol fuel cells with neat methanol operation” *J. Power Sources,* 248 (2014) 1264–1269.

[61] J.-W. Guo, X.-F. Xie, J.-H. Wang, Y.-M. Shang. “Effect of current collector corrosion made from printed circuit board (PCB) on the degradation of self-breathing direct methanol fuel cell stack” *Electrochim. Acta,* 53 (2008) 3056–3064.

[62] S.H. Kim, H.Y. Cha, C.M. Miesse, J.H. Jang, Y.S. Oh, S.W. Cha. “Air-breathing miniature planar stack using the flexible printed circuit board as a current collector” *Int. J. Hydrogen Energy,* 34 (2009) 459–466.

[63] G. Lu, C.-Y. Wang. "Two-phase microfluidics, heat and mass transport in direct methanol fuel cells", in: Transport Phenomena Fuel Cells, WIT Press, 2005, 317–358.

[64] R. Parsons, T. Vandernoot. “The oxidation of small organic molecules - A survey of recent fuel cell related research” *J. Electroanal. Chem.,* 257 (1988) 9–45.

[65] A. Hamnett. “Mechanism and electrocatalysis in the direct methanol fuel cell” *Catal. Today,* 38 (1997) 445–457.

[66] A.O. Neto, M. Linardi, E.R. Gonzalez. "Oxidação eletroquímica do metanol sobre partículas de PtRu e PtMo suportadas em carbono de alta área superficial" *Eclética Química*, 28 (2003) 55–62.

[67] J.P. Meyers, J. Newman. "Simulation of the direct methanol fuel cell - II. Modeling and data analysis of transport and kinetic phenomena" *J. Electrochem. Soc.*, 149 (2002) A718–A728.

[68] X. Yue, W. Yang, X. Liu, Y. Wang, C. Liu, Q. Zhang, J. Jia. "A facile method to prepare Pt/C/TiO_2 nanotubes electrode for electro-oxidation of methanol" *Electrochim. Acta*, 174 (2015) 667–671.

[69] X. Lou, J. Chen, M. Wang, J. Gu, P. Wu, D. Sun, Y. Tang. "Carbon nanotubes supported cerium dioxide and platinum nanohybrids : Layer-by-layer synthesis and enhanced electrocatalytic activity for methanol oxidation" *J. Power Sources*, 287 (2015) 203–210.

[70] X. Li, J. Wei, Y. Chai, S. Zhang. "Carbon nanotubes/tin oxide nanocomposite-supported Pt catalysts for methanol electro-oxidation" *J. Colloid Interface Sci.*, 450 (2015) 74–81.

[71] S. Ali, R. Ahmed, M. Sohail, M. Shahid. "Co@Pt core – shell nanoparticles supported on carbon nanotubes as promising catalyst for methanol electro-oxidation" *J. Ind. Eng. Chem.*, 28 (2015) 344–350.

[72] E. Lee, S. Kim, J. Jang, H. Park, A. Matin, Y. Kim, Y. Kwon. "Effects of particle proximity and composition of Pt-M (M = Mn, Fe, Co) nanoparticles on electrocatalysis in methanol oxidation reaction" *J. Power Sources*, 294 (2015) 75–81.

[73] X. Zhang, L. Ma. "Electrochemical fabrication of platinum nanoflakes on fulleropyrrolidine nanosheets and their enhanced electrocatalytic activity and stability for methanol oxidation reaction" *J. Power Sources*, 286 (2015) 400–405.

[74] J. Ma, L. Wang, X. Mu, Y. Cao. "Enhanced electrocatalytic activity of Pt nanoparticles supported on functionalized graphene for methanol oxidation and oxygen reduction" *J. Colloid Interface Sci.*, 457 (2015) 102–107.

[75] C. Lu, W. Kong, H. Zhang, B. Song, Z. Wang. "Gold e platinum bimetallic nanotubes templated from tellurium nanowires as efficient electrocatalysts for methanol oxidation reaction" *J. Power Sources*, 296 (2015) 102–108.

[76] C. Hu, X. Wang. "Highly dispersed palladium nanoparticles on commercial carbon black with significantly high electro-catalytic activity for methanol and ethanol oxidation" *Int. J. Hydrogen Energy*, 40 (2015) 12382–12391.

[77] A. Serrà, E. Gómez, E. Vallés. "Novel electrodeposition media to synthesize CoNi-Pt Core@Shell stable mesoporous nanorods with very high active surface for methanol" *Electrochim. Acta*, 174(2015) 630–639.

[78] Y.-W. Lee, J. Lee, D. Kwak, E. Hwang, J.I. Sohn, K. Park. "Pd@Pt core–shell nanostructures for improved electrocatalytic activity in methanol oxidation reaction" *Appl. Catal. B Environ.*, 179 (2015) 178–184.

[79] Y. Zheng, H. Chen, Y. Dai, N. Zhang, W. Zhao, S. Wang, Y. Lou, Y. Li, Y. Sun. "Preparation and characterization of Pt/TiO_2 nanofibers catalysts for methanol electro-oxidation" *Electrochim. Acta*, 178 (2015) 74–79.

[80] D. Chen, Y. Zhao, X. Peng, X. Wang, W. Hu, C. Jing, S. Tian, J. Tian. "Star-like PtCu nanoparticles supported on graphene with superior activity for methanol electro-oxidation." *Electrochim. Acta*, 177 (2015) 86–92.

[81] H. Mao, T. Huang, A. Yu. "Surface Palladium rich Cu_xPd_y/carbon catalysts for methanol and ethanol oxidation in alkaline media" *Electrochim. Acta*, 174 (2015) 1–7.

[82] Y. Fan, P. Liu, Z. Zhang, Y. Cui, Y. Zhang. "Three-dimensional hierarchical porous platinum e copper alloy networks with enhanced catalytic activity towards methanol and ethanol electro-oxidation" *J. Power Sources*, 296 (2015) 282–289.

[83] G. Yang, Y. Zhou, H. Pan, C. Zhu, S. Fu, C.M. Wai, D. Du, J. Zhu, Y. Lin. "Ultrasonic-assisted synthesis of Pd–Pt/carbon nanotubes nanocomposites for enhanced electro-oxidation of ethanol and methanol in alkaline medium" *Ultrason. Sonochem.*, 28 (2016) 192–198.

[84] H. Gharibi, F. Golmohammadi, M. Kheirmand. "Fabrication of MEA based on optimum amount of Co in Pd_xCo/C alloy nanoparticles as a new cathode for oxygen reduction reaction in passive direct methanol fuel cells" *Electrochim. Acta*, 89 (2013) 212–221.

[85] H. Gharibi, F. Golmohammadi, M. Kheirmand. "Palladium/cobalt coated on multi-walled carbon nanotubes as an electro-catalyst for oxygen reduction reaction in passive direct methanol fuel cells" *Fuel Cells*, 13 (2013) 987–1004.

[86] L. Pu, H. Zhang, T. Yuan, Z. Zou, L. Zou, X.-M.M. Li, H. Yang. "High performance platinum nanorod assemblies based double-layered cathode for passive direct methanol fuel cells" *J. Power Sources*, 276 (2015) 95–101.

[87] M. Asteazaran, G. Cespedes, S. Bengió, M.S. Moreno, W.E. Triaca, A.M. Castro Luna. "Research on methanol-tolerant catalysts for the oxygen reduction reaction" *J. Appl. Electrochem.*, 45 (2015) 1187–1193.

[88] F. Golmohammadi, H. Gharibi, S. Sadeghi. "Synthesis and electrochemical characterization of binary carbon supported Pd_3Co nanocatalyst for oxygen reduction reaction in direct methanol fuel cells" *Int. J. Hydrogen Energy*, 41 (2016) 7373–7387.

[89] F. Dehghani Sanij, H. Gharibi. "Preparation of bimetallic alloyed palladium-nickel electro-catalysts supported on carbon with superior catalytic performance towards oxygen reduction reaction" *Colloids Surfaces A Physicochem. Eng. Asp.*, 538 (2018) 429–442.

[90] B. Xiao, H. Bahrami, A. Faghri. "Analysis of heat and mass transport in a miniature passive and semi passive liquid-feed direct methanol fuel cell" *J. Power Sources*, 195 (2010) 2248–2259.

[91] C. Xu, A. Faghri, X. Li, T. Ward. "Methanol and water crossover in a passive liquid-feed direct methanol fuel cell" *Int. J. Hydrogen Energy*, 35(2010) 1769–1777.

[92] L. Feng, J. Zhang, W. Cai, W. Xing, C. Liu. "Single passive direct methanol fuel cell supplied with pure methanol" *J. Power Sources*, 196 (2011) 2750–2753.

[93] Y.-C. Park, D.-H. Kim, S. Lim, S.-K. Kim, D.-H. Peck, D.-H. Jung. "Design of a MEA with multi-layer electrodes for high concentration methanol DMFCs" *Int. J. Hydrogen Energy*, 37 (2012) 4717–4727.

[94] F. Zhang, J. Jiang, Y. Zhou, J. Xu, Q. Huang, Z. Zou, J. Fang, H. Yang. "A neat methanol fed passive DMFC with a new anode structure" *Fuel Cells*, 17 (2017) 315–320.

[95] W. Yuan, Y. Tang, X. Yang, B. Liu, Z. Wan. "Manufacture, characterization and application of porous metal-fiber sintered felt used as mass-transfer controlling medium for direct methanol fuel cells" *Trans. Nonferrous Met. Soc. China*, 23 (2013) 2085–2093.

[96] T. Yuan, J. Yang, Y. Wang, H. Ding, X. Li, L. Liu, H. Yang. "Anodic diffusion layer with graphene-carbon nanotubes composite material for passive direct methanol fuel cell" *Electrochim. Acta*, 147 (2014) 265–270.

[97] Q. Huang, J. Jiang, J. Chai, T. Yuan, H. Zhang, Z. Zou, X. Zhang, H. Yang. "Construction of porous anode by sacrificial template for a passive direct methanol fuel cell" *J. Power Sources*, 262 (2014) 213–218.

[98] M.A. Abdelkareem, E.T. Kasem, N. Nakagawa, E.A.M. Abdelghani, A.A. Elzatahry, K.A. Khalil, N.A.M. Barakat. "Enhancement of the passive direct methanol fuel cells performance by modification of the cathode microporous layer using carbon nanofibers" *Fuel Cells*, 14 (2014) 607–613.

[99] H. Wu, T. Yuan, Q. Huang, H. Zhang, Z. Zou, J. Zheng, H. Yang. "Polypyrrole nanowire networks as anodic micro-porous layer for passive direct methanol fuel cells" *Electrochim. Acta*, 141 (2014) 1–5.

[100] Y. Zhang, R. Xue, X. Zhang, J. Song, X. Liu. "RGO deposited in stainless steel fiber felt as mass transfer barrier layer for μ-DMFC" *Energy*, 91 (2015) 1081–1086.

[101] V.B. Oliveira, J.P. Pereira, A.M.F.R. Pinto. "Effect of anode diffusion layer (GDL) on the performance of a passive direct methanol fuel cell (DMFC)" *Int. J. Hydrogen Energy*, 41 (2016) 19455–19462.

[102] X.H. Yan, P. Gao, G. Zhao, L. Shi, J.B. Xu, T.S. Zhao. "Transport of highly concentrated fuel in direct methanol fuel cells" *Appl. Therm. Eng.*, 126 (2017) 290–295.

[103] C.E. Shaffer, C.-Y. Wang. "Role of hydrophobic anode MPL in controlling water crossover in DMFC" *Electrochim. Acta*, 54 (2009) 5761–5769.

[104] J. Cao, M. Chen, J. Chen, S. Wang, Z. Zou, Z. Li, D.L. Akins, H. Yang. "Double microporous layer cathode for membrane electrode assembly of passive direct methanol fuel cells" *Int. J. Hydrogen Energy*, 35(2010) 4622–4629.

[105] C.E. Shaffer, C.-Y. Wang. "High concentration methanol fuel cells: Design and theory" *J. Power Sources*, 195 (2010) 4185–4195.

[106] Q.X. Wu, T.S. Zhao, R. Chen, W.W. Yang. "Enhancement of water retention in the membrane electrode assembly for direct methanol fuel cells operating with neat methanol" *Int. J. Hydrogen Energy*, 35 (2010) 10547–10555.

[107] H.-C.C. Peng, P.-H.H. Chen, H.-W.W. Chen, C.-C.C. Chieng, T.-K.K. Yeh, C. Pan, F.-G.G. Tseng. "Passive cathodic water/air management device for micro-direct methanol fuel cells" *J. Power Sources*, 195 (2010) 7349–7358.

[108] Q.X. Wu, T.S. Zhao, W.W. Yang. "Effect of the cathode gas diffusion layer on the water transport behavior and the performance of passive direct methanol fuel cells

operating with neat methanol" *Int. J. Heat Mass Transf.,* 54 (2011) 1132–1143.

[109] J. Zhang, L. Feng, W. Cai, C. Liu, W. Xing. "The function of hydrophobic cathodic backing layers for high energy passive direct methanol fuel cell" *J. Power Sources,* 196 (2011) 9510–9515.

[110] V.B. Oliveira, D.S. Falcão, C.M. Rangel, A.M.F.R. Pinto. "Water management in a passive direct methanol fuel cell" *Int. J. Energy Res.,* 37 (2013) 991–1001.

[111] H. Deng, Y. Zhang, X. Zheng, Y. Li, X. Zhang, X. Liu. "A CNT (carbon nanotube) paper as cathode gas diffusion electrode for water management of passive μ-DMFC (micro-direct methanol fuel cell) with highly concentrated methanol" *Energy,* 82 (2015) 236–241.

[112] X.H. Yan, T.S. Zhao, G. Zhao, L. An, X.L. Zhou. "A hydrophilic-hydrophobic dual-layer microporous layer enabling the improved water management of direct methanol fuel cells operating with neat methanol" *J. Power Sources,* 294 (2015) 232–238.

[113] R. Xue, Y. Zhang, X. Liu. "A novel cathode gas diffusion layer for water management of passive μ-DMFC" *Energy,* 139(2017) 535–541.

[114] Q.X. Wu, T.S. Zhao, R. Chen, W.W. Yang. "A microfluidic-structured flow field for passive direct methanol fuel cells operating with highly concentrated fuels" *J. Micromechanics Microengineering,* 20 (2010) 045014–045023.

[115] W. Cai, S. Li, L. Feng, J. Zhang, D. Song, W. Xing, C. Liu. "Transient behavior analysis of a new designed passive direct methanol fuel cell fed with highly concentrated methanol" *J. Power Sources,* 196(2011) 3781–3789.

[116] W. Yuan, Y. Tang, Z. Wan, M. Pan. "Operational characteristics of a passive air-breathing direct methanol fuel cell under various structural conditions" *Int. J. Hydrogen Energy,* 36(2011) 2237–2249.

[117] X. Li, A. Faghri. "Development of a direct methanol fuel cell stack fed with pure methanol" *Int. J. Hydrogen Energy,* 37 (2012) 14549–14556.

[118] W. Yuan, Y. Tang, X. Yang. "High-concentration operation of a passive air-breathing direct methanol fuel cell integrated with a porous methanol barrier" *Renew. Energy,* 50(2013) 741–746.

[119] J. Guo, H. Zhang, J. Jiang, Q. Huang, T. Yuan, H. Yang. "Development of a self-adaptive direct methanol fuel cell fed with 20 M methanol" *Fuel Cells,* 13 (2013) 1018–1023.

[120] X.H. Yan, T.S. Zhao, L. An, G. Zhao, L. Zeng. "A micro-porous current collector enabling passive direct methanol fuel cells to operate with highly concentrated fuel" *Electrochim. Acta,* 139 (2014) 7–12.

[121] Q.X. Wu, L. An, X.H. Yan, T.S. Zhao. "Effects of design parameters on the performance of passive direct methanol fuel cells fed with concentrated fuel" *Electrochim. Acta,* 133 (2014) 8–15.

[122] M.A. Abdelkareem, T. Yoshitoshi, T. Tsujiguchi, N. Nakagawa. "Vertical operation of passive direct methanol fuel cell employing a porous carbon plate" *J. Power Sources,* 195 (2010) 1821–1828.

[123] S. Yousefi, M. Shakeri, K. Sedighi. "The effect of operating parameters on the perfomance of a passive DMFC single cell" *World Appl. Sci. J.,* 22 (2013) 516–522.

[124] J. Huang, T. Ward, A. Faghri. “Optimizing the anode structure of a passive tubular-shaped direct methanol fuel cell to operate with high concentration methanol” *J. Fuel Cell Sci. Technol.*, 9 (2012) 51008-1-51008–6.

[125] X. Liu, S. Fang, Z. Ma, Y. Zhang. “Structure design and implementation of the passive μ-DMFC” *Micromachines*, 6 (2015) 230–238.

[126] D.S. Falcão, J.P. Pereira, C.M. Rangel, A.M.F.R. Pinto. “Development and performance analysis of a metallic micro-direct methanol fuel cell for portable applications” *Int. J. Hydrogen Energy*, 40 (2015) 5408–5415.

[127] L.D. Tsai, H.C. Chien, W.H. Huang, C.P. Huang, C.Y. Kang, J.N. Lin, F.C. Chang. “Novel bilayer composite membrane for passive direct methanol fuel cells with pure methanol” *Int. J. Electrochem. Sci.*, 8 (2013) 9704–9713.

[128] H.S. Thiam, W.R.W. Daud, S.K. Kamarudin, A.B. Mohamad, A.A.H. Kadhum, K.S. Loh, E.H. Majlan. “Performance of direct methanol fuel cell with a palladium–silica nanofibre/Nafion composite membrane” *Energy Convers. Manag.*, 75 (2013) 718–726.

[129] T. Yuan, L. Pu, Q. Huang, H. Zhang, X. Li, H. Yang. “An effective methanol-blocking membrane modified with graphene oxide nanosheets for passive direct methanol fuel cells” *Electrochim. Acta*, 117 (2014) 393–397.

[130] Q. He, J. Zheng, S. Zhang. “Preparation and characterization of high performance sulfonated poly(p-phenylene-co-aryl ether ketone) membranes for direct methanol fuel cells” *J. Power Sources*, 260 (2014) 317–325.

[131] M. Cui, Z. Zhang, T. Yuan, H. Yang, L. Wu, E. Bakangura, T. Xu. “Proton-conducting membranes based on side-chain-type sulfonated poly(ether ketone/ether benzimidazole)s via one-pot condensation” *J. Memb. Sci.*, 465 (2014) 100–106.

[132] J. Zheng, J. Wang, S. Zhang, T. Yuan, H. Yang. “Synthesis of novel cardo poly(arylene ether sulfone)s with bulky and rigid side chains for direct methanol fuel cells” *J. Power Sources*, 245 (2014) 1005–1013.

[133] J. Zheng, Q. He, N. Gao, T. Yuan, S. Zhang, H. Yang. “Novel proton exchange membranes based on cardo poly(arylene ether sulfone/nitrile)s with perfluoroalkyl sulfonic acid moieties for passive direct methanol fuel cells” *J. Power Sources*, 261 (2014) 38–45.

[134] L. Pu, J. Jiang, T. Yuan, J. Chai, H. Zhang, Z. Zou, X.-M.M. Li, H. Yang. “Performance improvement of passive direct methanol fuel cells with surface-patterned Nafion® membranes” *Appl. Surf. Sci.*, 327 (2015) 205–212.

[135] T. Yuan, Y. Kang, J. Chen, C. Du, Y. Qiao, X. Xue, Z. Zou, H. Yang. “Enhanced performance of a passive direct methanol fuel cell with decreased Nafion aggregate size within the anode catalytic layer” *Int. J. Hydrogen Energy*, 36 (2011) 10000–10005.

[136] J. Zheng, Q. He, C. Liu, T. Yuan, S. Zhang, H. Yang. “Nafion-microporous organic polymer networks composite membranes” *J. Memb. Sci.*, 476 (2015) 571–579.

[137] Z. Jiang, Z.-J. Jiang. “Plasma-polymerized membranes with high proton conductivity for a micro semi-passive direct methanol fuel cell” *Plasma Process. Polym.*, 13 (2016) 105–115.

[138] J. Zheng, W. Bi, X. Dong, J. Zhu, H. Mao, S. Li, S. Zhang. "High performance tetra-sulfonated poly(p-phenylene-co-aryl ether ketone) membranes with microblock moieties for passive direct methanol fuel cells" *J. Memb. Sci.*, 517 (2016) 47–56.

[139] X.H. Yan, R. Wu, J.B. Xu, Z. Luo, T.S. Zhao. "A monolayer graphene - Nafion sandwich membrane for direct methanol fuel cells" *J. Power Sources*, 311 (2016) 188–194.

[140] P. Chen, H. Wu, T. Yuan, Z. Zou, H. Zhang, J. Zheng, H. Yang. "Electronspun nanofiber network anode for a passive direct methanol fuel cell" *J. Power Sources*, 255 (2014) 70–75.

[141] E.C.L. Ferreira, F.M.. Quadros, J.P.I. Souza. "Desenvolvimento de um conjunto membrana-eletrodos para célula a combustível de metanol direto passiva" *Quim. Nova*, 33 (2010) 1313–1319.

[142] J. Chai, Y. Zhou, J. Fan, J. Jiang, T. Yuan, H. Zhang, Z. Zou, H. Qian, H. Yang. "Fabrication of nano-network structure anode by zinc oxide nanorods template for passive direct methanol fuel cells" *Int. J. Hydrogen Energy*, 40 (2015) 6647–6654.

[143] M. Amani, M. Kazemeini, M. Hamedanian, H. Pahlavanzadeh, H. Gharibi. "Investigation of methanol oxidation on a highly active and stable Pt-Sn electrocatalyst supported on carbon-polyaniline composite for application in a passive direct methanol fuel cell" *Mater. Res. Bull.*, 68 (2015) 166–178.

[144] Y. Wang, Q. Cheng, T. Yuan, Y. Zhou, H. Zhang, Z. Zou, J. Fang, H. Yang. "Controllable fabrication of ordered Pt nanorod array as catalytic electrode for passive direct methanol fuel cells" *Chinese J. Catal.*, 37 (2016) 1089–1095.

[145] G. Wang, L. Lei, J. Jiang, Y. Zhou, Q. Huang, Z. Zou, S.P. Jiang, H. Yang. "An ordered structured cathode based on vertically aligned Pt nanotubes for ultra-low Pt loading passive direct methanol fuel cells" *Electrochim. Acta*, 252 (2017) 541–548.

[146] A.M. Zainoodin, S.K. Kamarudin, M.S. Masdar, W.R.W. Daud, A.B. Mohamad, J. Sahari. "High power direct methanol fuel cell with a porous carbon nanofiber anode layer" *Appl. Energy*, 113 (2014) 946–954.

[147] A.M.M. Zainoodin, S.K.K. Kamarudin, M.S.S. Masdar, W.R.W.R.W. Daud, A.B.B. Mohamad, J. Sahari. "Investigation of MEA degradation in a passive direct methanol fuel cell under different modes of operation" *Appl. Energy*, 135 (2014) 364–372.

[148] J. Cao, L. Wang, L. Song, J. Xu, H. Wang, Z. Chen, Q. Huang, H. Yang. "Novel cathodal diffusion layer with mesoporous carbon for the passive direct methanol fuel cell" *Electrochim. Acta*, 118 (2014) 163–168.

[149] B.C. Ong, S.K. Kamarudin, M.S. Masdar, U.A. Hasran. "Applications of graphene nano-sheets as anode diffusion layers in passive direct methanol fuel cells (DMFC)" *Int. J. Hydrogen Energy*, 42 (2017) 9252–9261.

[150] N.K. Shrivastava, S.B. Thombre, R. V. Motghare. "Wire mesh current collectors for passive direct methanol fuel cells" *J. Power Sources*, 272(2014) 629–638.

[151] R.K. Mallick, S.B. Thombre. "Performance of passive DMFC with expanded metal mesh current collectors" *Electrochim. Acta*, 243(2017) 299–309.

[152] A. Wang, W. Yuan, S. Huang, Y. Tang, Y. Chen. "Structural effects of expanded metal mesh used as a flow field for a passive direct methanol fuel cell" *Appl. Energy*,

208 (2017) 184–194.

[153] O. Gholami, S.J. Imen, M. Shakeri. “Effect of anode and cathode flow field geometry on passive direct methanol fuel cell performance” *Electrochim. Acta*, 158 (2015) 410–417.

[154] R.K. Mallick, S.B. Thombre, R. V. Motghare, R.R. Chillawar. “Analysis of the clamping effects on the passive direct methanol fuel cell performance using electrochemical impedance spectroscopy” *Electrochim. Acta*, 215 (2016) 150–161.

[155] R. Hashemi, S. Yousefi, M. Faraji. “Experimental studying of the effect of active area on the performance of passive direct methanol fuel cell” *Ionics*, 21 (2015) 2851–2862.

[156] W. Zheng, A. Suominen, J. Kankaanranta, A. Tuominen. “A new structure of a passive direct methanol fuel cell” *Chem. Eng. Sci.*, 76 (2012) 188–191.

[157] T. Ward, X. Li, A. Faghri. “Performance characteristics of a novel tubular-shaped passive direct methanol fuel cell” *J. Power Sources*, 196 (2011) 6264–6273.

[158] Z. Wu, X. Kuang, L. Liu, X. Wang. “A flexible foldable tubular μDMFC for powering wearable devices” *J. Microelectromechanical Syst.*, 26(2017) 1147–1154.

[159] T. Tsujiguchi, M.A. Abdelkareem, T. Kudo, N. Nakagawa, T. Shimizu, M. Matsuda. “Development of a passive direct methanol fuel cell stack for high methanol concentration” *J. Power Sources*, 195 (2010) 5975–5979.

[160] F. Achmad, S.K. Kamarudin, W.R.W. Daud, E.H. Majlan. “Passive direct methanol fuel cells for portable electronic devices” *Appl. Energy*, 88 (2011) 1681–1689.

[161] L. Feng, W. Cai, C. Li, J. Zhang, C. Liu, W. Xing. “Fabrication and performance evaluation for a novel small planar passive direct methanol fuel cell stack” *Fuel*, 94 (2012) 401–408.

[162] V. Baglio, A. Stassi, F.V. Matera, H. Kim, V. Antonucci, A.S. Aricò. “AC-impedance investigation of different MEA configurations for passive-mode DMFC mini-stack applications” *Fuel Cells*, 10 (2010) 124–131.

[163] L. Wang, M. He, Y. Hu, Y. Zhang, X. Liu, G. Wang. “A ‘4-cell’ modular passive DMFC (direct methanol fuel cell) stack for portable applications” *Energy*, 82 (2015) 229–235.

[164] W. Yuan, X. Zhang, S. Zhang, J. Hu, Z. Li, Y. Tang. “Lightweight current collector based on printed-circuit-board technology and its structural effects on the passive air-breathing direct methanol fuel cell” *Renew. Energy*, 81 (2015) 664–670.

[165] O. Barbera, A. Stassi, D. Sebastian, J.L. Bonde, G. Giacoppo, C. D’Urso, V. Baglio, A.S. Aricò. “Simple and functional direct methanol fuel cell stack designs for application in portable and auxiliary power units” *Int. J. Hydrogen Energy*, 41 (2016) 12320–12329.

[166] M.S. Masdar, Dedikarni, A.M. Zainoodin, M.I. Rosli, S.K. Kamarudin, W.R.W. Daud. “Performance and stability of single and 6-cell stack passive direct methanol fuel cell (DMFC) for long-term operation” *Int. J. Hydrogen Energy*, 42 (2017) 9230–9242.

[167] V.B. Oliveira, C.M. Rangel, A.M.F.R. Pinto. “One-dimensional and non-isothermal model for a passive DMFC” *J. Power Sources*, 196 (2011) 8973–8982.

[168] M. Guarnieri, V. Di Noto, F. Moro. “A dynamic circuit model of a small direct methanol fuel cell for portable electronic devices” *IEEE Trans. Ind. Electron.*, 57 (2010) 1865–1873.

[169] H. Bahrami, A. Faghri. “Exergy analysis of a passive direct methanol fuel cell” *J. Power Sources*, 196 (2011) 1191–1204.

[170] N.S. Rosenthal, S.A. Vilekar, R. Datta. “A comprehensive yet comprehensible analytical model for the direct methanol fuel cell” *J. Power Sources*, 206 (2012) 129–143.

[171] N.K. Shrivastava, S.B. Thombre, K.L. Wasewar. “Nonisothermal mathematical model for performance evaluation of passive direct methanol fuel cells” *J. Energy Eng.*, 139 (2013) 266–274.

[172] J. Ko, P. Chippar, H. Ju. “A one-dimensional, two-phase model for direct methanol fuel cells – Part I: Model development and parametric study” *Energy*, 35 (2010) 2149–2159.

[173] W.W. Yang, T.S. Zhao, Q.X. Wu. “Modeling of a passive DMFC operating with neat methanol” *Int. J. Hydrogen Energy*, 36 (2011) 6899–6913.

[174] W. Cai, S. Li, L. Yan, L. Feng, J. Zhang, L. Liang, W. Xing, C. Liu. “Design and simulation of a liquid electrolyte passive direct methanol fuel cell with low methanol crossover” *J. Power Sources*, 196 (2011) 7616–7626.

[175] W. Cai, S. Li, C. Li, L. Liang, W. Xing, C. Liu. “A model based thermal management of DMFC stack considering the double-phase flow in the anode” *Chem. Eng. Sci.*, 93 (2013) 110–123.

[176] K.M. Yin. “One-dimensional steady state algebraic model on the passive direct methanol fuel cell with consideration of the intermediate liquid electrolyte” *J. Power Sources*, 282 (2015) 368–377.

[177] N.K. Shrivastava, S.B. Thombre, K.L. Wasewar. “A real-time simulating non-isothermal mathematical model for the passive feed direct methanol fuel cell” *Int. J. Green Energy*, 13 (2016) 213–228.

[178] S. Basri, S.K. Kamarudin, W.R.W. Daud, Z. Yaakub, M.M. Ahmad, N. Hashim, U. a. Hasran. “Unsteady-state modelling for a passive liquid-feed DMFC” *Int. J. Hydrogen Energy*, 34 (2009) 5759–5769.

[179] S. Basri, S.K. Kamarudin, W.R.W. Daud, M.M. Ahmad. “Non-linear optimization of passive direct methanol fuel cell (DMFC)” *Int. J. Hydrogen Energy*, 35 (2010) 1759–1768.

[180] D. Ye, X. Zhu, Q. Liao, J. Li, Q. Fu. “Two-dimensional two-phase mass transport model for methanol and water crossover in air-breathing direct methanol fuel cells” *J. Power Sources*, 192 (2009) 502–514.

[181] C. Xu, A. Faghri. “Water transport characteristics in a passive liquid-feed DMFC” *Int. J. Heat Mass Transf.*, 53 (2010) 1951–1966.

[182] H. Bahrami, A. Faghri. “Transport phenomena in a semi-passive direct methanol fuel cell” *Int. J. Heat Mass Transf.*, 53 (2010) 2563–2578.

[183] X. Li, A. Faghri. “Local entropy generation analysis on passive high-concentration DMFCs (direct methanol fuel cell) with different cell structures” *Energy*, 36 (2011)

403–414.

[184] T. Ward, C. Xu, A. Faghri. “Performance and design analysis of tubular-shaped passive direct methanol fuel cells” *Int. J. Hydrogen Energy,* 36 (2011) 9216–9230.

[185] G. Jewett, A. Faghri, B. Xiao. “Optimization of water and air management systems for a passive direct methanol fuel cell” *Int. J. Heat Mass Transf.,* 52 (2009) 3564–3575.

[186] D. Gerteisen. “Transient and steady-state analysis of catalyst poisoning and mixed potential formation in direct methanol fuel cells” *J. Power Sources,* 195 (2010) 6719–6731.

[187] L. Wang, Y. Zhang, Z. An, S. Huang, Z. Zhou, X. Liu. “Non-isothermal modeling of a small passive direct methanol fuel cell in vertical operation with anode natural convection effect” *Energy,* 58 (2013) 283–295.

[188] X.Y. Li, W.W. Yang, Y.L. He, T.S. Zhao, Z.G. Qu. “Effect of anode micro-porous layer on species crossover through the membrane of the liquid-feed direct methanol fuel cells” *Appl. Therm. Eng.,* 48 (2012) 392–401.

[189] Z. Miao, J.-L. Xu, Y.-L. He. “Modeling of the transport phenomena in passive direct methanol fuel cells using a two-phase anisotropic model” *Adv. Mech. Eng.,* 2014 (2014) 1–15.

[190] H. Guo, Y.P. Chen, Y.Q. Xue, F. Ye, C.F. Ma. “Three-dimensional transient modeling and analysis of two-phase mass transfer in air-breathing cathode of a fuel cell” *Int. J. Hydrogen Energy,* 38 (2013) 11028–11037.

[191] T. Guo, J. Sun, H. Deng, K. Jiao, X. Huang. “Transient analysis of passive direct methanol fuel cells with different operation and design parameters” *Int. J. Hydrogen Energy,* 40 (2015) 14978–14995.

[192] Z. Yuan, J. Yang, N. Ye, Z. Li, Y. Sun, H. Shen. “Analysis of the capillary-force-based μDMFC (micro direct methanol fuel cell) supplied with pure methanol” *Energy,* 89 (2015) 858–863.

[193] G. Ting, J. Sun, H. Deng, X. Xie, K. Jiao, X. Huang. “Investigation of cell orientation effect on transient operation of passive direct methanol fuel cells” *Int. J. Hydrogen Energy,* 41 (2016) 6493–6507.

[194] M. Zago, A. Casalegno, F. Bresciani, R. Marchesi. “Effect of anode MPL on water and methanol transport in DMFC: Experimental and modeling analyses” *Int. J. Hydrogen Energy,* 39 (2014) 21620–21630.

[195] J. Sun, T. Guo, H. Deng, K. Jiao, X. Huang. “Effect of electrode variable contact angle on the performance and transport characteristics of passive direct methanol fuel cells” *Int. J. Hydrogen Energy,* 40 (2015) 10568–10587.

[196] P.A. García-Salaberri, M. Vera. “On the effects of assembly compression on the performance of liquid-feed DMFCs under methanol-limiting conditions: A 2D numerical study” *J. Power Sources,* 285 (2015) 543–558.

[197] Y.Q. Xue, H. Guo, H.H. Shang, F. Ye, C.F. Ma. “Simulation of mass transfer in a passive direct methanol fuel cell cathode with perforated current collector” *Energy,* 81 (2015) 501–510.

[198] M.Z.F. Kamaruddin, S.K. Kamarudin, M.S. Masdar, W.R.W. Daud. “Investigating design parameter effects on the methanol flux in the passive storage of a direct methanol fuel cell” *Int. J. Hydrogen Energy*, 40 (2015) 11931–11942.

[199] T. Guo, J. Sun, J. Zhang, H. Deng, X. Xie, K. Jiao, X. Huang. “Transient analysis of passive vapor-feed DMFC fed with neat methanol” *Int. J. Hydrogen Energy*, 42 (2017) 3222–3239.

[200] S. Fang, Y. Zhang, Y. Zou, S. Sang, X. Liu. “Structural design and analysis of a passive DMFC supplied with concentrated methanol solution” *Energy*, 128 (2017) 50–61.

[201] K.P. Kothekar, S.B. Thombre, R.K. Mallick. “Estimation of kinetic and electric parameters of liquid feed passive DMFCs” *Int. J. Hydrogen Energy*, 42 (2017) 24358–24371.

[202] A. Mehmood, M.A. Scibioh, J. Prabhuram, M.G. An, H.Y. Ha. “A review on durability issues and restoration techniques in long-term operations of direct methanol fuel cells” *J. Power Sources*, 297 (2015) 224–241.

[203] S.D. Knights, K.M. Colbow, J. St-Pierre, D.P. Wilkinson. “Aging mechanisms and lifetime of PEFC and DMFC” *J. Power Sources*, 127 (2004) 127–134.

[204] W. Chen, G. Sun, J. Guo, X. Zhao, S. Yan, J. Tian, S. Tang, Z. Zhou, Q. Xin. “Test on the degradation of direct methanol fuel cell” *Electrochim. Acta*, 51 (2006) 2391–2399.

[205] H.-C. Cha, C.-Y. Chen, J.-Y. Shiu. “Investigation on the durability of direct methanol fuel cells” *J. Power Sources*, 192 (2009) 451–456.

[206] F. Bresciani, C. Rabissi, M. Zago, R. Marchesi, A. Casalegno. “On the effect of gas diffusion layers hydrophobicity on direct methanol fuel cell performance and degradation” *J. Power Sources*, 273 (2015) 680–687.

[207] M.K. Jeon, J.Y. Won, K.S. Oh, K.R. Lee, S.I. Woo. “Performance degradation study of a direct methanol fuel cell by electrochemical impedance spectroscopy” *Electrochim. Acta*, 53 (2007) 447–452.

[208] C.-M. Lai, J. Lin, K. Hsueh, C.-P. Hwang, K.-C. Tsay, L.-D. Tsai, Y.-M. Peng. “On the accelerating degradation of DMFC at highly anodic potential” *J. Electrochem. Soc.*, 155 (2008) B843–B851.

[209] C.Y. Chen, H.C. Cha. “Strategy to optimize cathode operating conditions to improve the durability of a direct methanol fuel cell” *J. Power Sources*, 200 (2012) 21–28.

[210] R. Escudero-Cid, J.C. Pérez-Flores, E. Fatás, P. Ocón. “Degradation of DMFC using a new long-term stability cycle” *Int. J. Green Energy*, 12 (2016) 641–653.

[211] P. Piela, R. Fields, P. Zelenay. “Electrochemical impedance spectroscopy for direct methanol fuel cell diagnostics” *J. Electrochem. Soc.*, 153 (2006) A1902–A1913.

[212] P. Joghee, J.N. Malik, S. Pylypenko, R. O’Hayre. “A review on direct methanol fuel cells – In the perspective of energy and sustainability” *MRS Energy Sustain.*, 2 e 3 (2015) 1–31.

[213] N. Hashim, S.K. Kamarudin, W.R.W. Daud. “Design, fabrication and testing of a PMMA-based passive single-cell and a multi-cell stack micro-DMFC” *Int. J. Hydrogen Energy*, 34 (2009) 8263–8269.

[214] B.A. Braz, V.B. Oliveira, A.M.F.R. Pinto. "Recent developments in passive direct methanol fuel cells", in: Direct Methanol Fuel Cells Applications, Performance and Technology, Nova Science Publishers, 2017, 143–203.

[215] J.T. Mueller, P.M. Urban. “Characterization of direct methanol fuel cells by ac impedance spectroscopy” *J. Power Sources*, 75 (1998) 139–143.

[216] J. Wu, X. Zi, H. Wang, M. Blanco, J.J. Martin, J. Zhang, X.Z. Yuan, H. Wang, M. Blanco, J.J. Martin, J. Zhang. “Diagnostic tools in PEM fuel cell research: Part I Electrochemical techniques” *Int. J. Hydrogen Energy*, 33 (2008) 1735–1746.

[217] S.M. Rezaei Niya, M. Hoorfar. “Study of proton exchange membrane fuel cells using electrochemical impedance spectroscopy technique - A review” *J. Power Sources*, 240 (2013) 281–293.

[218] C.Y. Du, T.S. Zhao, W.W. Yang. “Effect of methanol crossover on the cathode behavior of a DMFC: A half-cell investigation” *Electrochim. Acta*, 52 (2007) 5266–5271.

[219] Z. Wang, G. Yin, Y. Shao, B. Yang, P. Shi, P. Feng. “Electrochemical impedance studies on carbon supported PtRuNi and PtRu anode catalysts in acid medium for direct methanol fuel cell” *J. Power Sources*, 165 (2007) 9–15.

[220] L. Wang, B. Kang, N. Gao, X. Du, L. Jia, J. Sun. “Corrosion behaviour of austenitic stainless steel as a function of methanol concentration for direct methanol fuel cell bipolar plate” *J. Power Sources*, 253 (2014) 332–341.

[221] H. Deng, Z. Ma, X. Zhang, Y. Zhang, X. Liu. “Corrosion resistance in simulated DMFC environment of plasma electrolytic oxidation coating prepared on aluminum alloy” *Surf. Coatings Technol.*, 269 (2015) 108–113.

[222] N. Huang, W. Li, C. Liang, L. Xu, X. Wang, T. Sun, M. Sun. “Using localized impedance spectroscopy to study the effect of loading potential variation on DMFC anode performance” *Mater. Sci. Forum*, 852 (2016) 785–791.

[223] B. Ma, J. Bai, L. Dong. “Electrochemical impedance analysis of methanol oxidation on carbon nanotube-supported Pt and Pt-Ru nanoparticles” *J. Solid State Electrochem.*, 17 (2013) 2783–2788.

[224] A. Döner, G. Kardas, G. Kardaş. “A novel , effective and low cost electrocatalyst for direct methanol fuel cells applications” *Int. J. Hydrogen Energy*, 40 (2015) 4840–4849.

[225] X. Yuan, H. Wang, J. Colin Sun, J. Zhang. “AC impedance technique in PEM fuel cell diagnosis-A review” *Int. J. Hydrogen Energy*, 32 (2007) 4365–4380.

[226] X.Z. Yuan, C. Song, H. Wang, J. Zhang. "Electrochemical impedance spectroscopy in PEM fuel cells - Fundamentals and applications", Springer, 2010.

[227] T. Yuan, Z. Zou, M. Chen, Z. Li, B. Xia, H. Yang. “New anodic diffusive layer for passive micro-direct methanol fuel cell” *J. Power Sources*, 192 (2009) 423–428.

[228] R. Chen, T.S. Zhao. “A novel electrode architecture for passive direct methanol fuel cells” *Electrochem. Commun.*, 9 (2007) 718–724.

[229] T. V. Reshetenko, H.T. Kim, H.J. Kweon. “Modification of cathode structure by introduction of CNT for air-breathing DMFC” *Electrochim. Acta*, 53 (2008) 3043–

3049.

[230] R. Chen, T.S. Zhao. “Porous current collectors for passive direct methanol fuel cells” *Electrochim. Acta*, 52 (2007) 4317–4324.

[231] R. Xue, Y. Zhang, X. Li, X. Liu. “Performance investigation and effect of temperature on a passive μDMFC with stainless steel mesh” *Appl. Therm. Eng.*, 141 (2018) 642–647.

[232] M. Chen, S. Wang, Z. Zou, T. Yuan, Z. Li, D.L. Akins, H. Yang. “Fluorination of Vulcan XC-72R for cathodic microporous layer of passive micro direct methanol fuel cell” *J. Appl. Electrochem.*, 40 (2010) 2117–2124.

[233] Y. Wang, G.G. Liu, M. Wang, G.G. Liu, J. Li, X. Wang. “Study on stability of self-breathing DFMC with EIS method and three-electrode system” *Int. J. Hydrogen Energy*, 38 (2013) 9000–9007.

[234] J. Prabhuram, N.N. Krishnan, B. Choi, T.H. Lim, H.Y. Ha, S.K. Kim. “Long-term durability test for direct methanol fuel cell made of hydrocarbon membrane” *Int. J. Hydrogen Energy*, 35 (2010) 6924–6933.

[235] F. Bresciani, C. Rabissi, A. Casalegno, M. Zago, R. Marchesi. “Experimental investigation on DMFC temporary degradation” *Int. J. Hydrogen Energy*, 39 (2014) 21647–21656.

[236] F. Bresciani, C. Rabissi, M. Zago, P. Gazdzicki, M. Schulze, L. Guétaz, S. Escribano, J.L. Bonde, R. Marchesi, A. Casalegno. “A combined in-situ and post-mortem investigation on local permanent degradation in a direct methanol fuel cell” *J. Power Sources*, 306 (2016) 49–61.

[237] M. Chen, M. Wang, Z. Yang, X. Ding, X. Wang. “Long-term degradation behaviors research on a direct methanol fuel cell with more than 3000 h lifetime” *Electrochim. Acta*, 282 (2018) 702–710.

[238] C. Rabissi, P. Gazdzicki, L. Guétaz, S. Escribano, L. Grahl-Madsen, A. Baricci, A. Casalegno. “A locally resolved investigation on direct methanol fuel cell uneven components fading: Steady state and degradation local analysis” *J. Power Sources*, 397 (2018) 361–373.

[239] C. Rabissi, M. Zago, P. Gazdzicki, L. Guétaz, S. Escribano, L. Grahl-Madsen, A. Casalegno. “A locally resolved investigation on direct methanol fuel cell uneven components fading: Local cathode catalyst layer tuning for homoegeneous operation and reduced degradation rate” *J. Power Sources*, 404 (2018) 135–148.

[240] Q.X. Wu, T.S. Zhao, R. Chen, W.W. Yang. “Effects of anode microporous layers made of carbon powder and nanotubes on water transport in direct methanol fuel cells” *J. Power Sources*, 191 (2009) 304–311.

[241] D.S. Falcão, R.A. Silva, C.M. Rangel, A.M.F.R. Pinto. “Performance of an active micro direct methanol fuel cell using reduced catalyst loading MEAs” *Energies*, 10 (2017) 1–9.

[242] N. Wongyao, A. Therdthianwong, S. Therdthianwong. “Performance of direct alcohol fuel cells fed with mixed methanol/ethanol solutions” *Energy Convers. Manag.*, 52 (2011) 2676–2681.

[243] W.J. Zhou, B. Zhou, W.Z. Li, Z.H. Zhou, S.Q. Song, G.Q. Sun, Q. Xin, S.

Douvartzides, M. Goula, P. Tsiakaras. “Performance comparison of low-temperature direct alcohol fuel cells with different anode catalysts” *J. Power Sources*, 126 (2004) 16–22.

[244] S.Q. Song, W.J. Zhou, Z.H. Zhou, L.H. Jiang, G.Q. Sun, Q. Xin, V. Leontidis, S. Kontou, P. Tsiakaras. “Direct ethanol PEM fuel cells: The case of platinum based anodes” *Int. J. Hydrogen Energy*, 30 (2005) 995–1001.

Appendix A: Polarisation and EIS data

In this chapter, all the polarisation and EIS data obtained with the in-house developed pDMFC are presented. These results are very relevant to evaluate the effect of the different design conditions and methanol concentrations on the cell behaviour and for the assessment of the different losses that negatively affect these systems. Some of the results here presented were already showed in the different sections of Chapter 5.

A.1. Effect of anode diffusion layer properties

All the results presented in this section were obtained with stainless steel current collectors, with an open ratio of 41 % (CC_2), at the anode and cathode sides and with carbon cloth with a thickness of 0.400 mm (CC) as cathode DL.

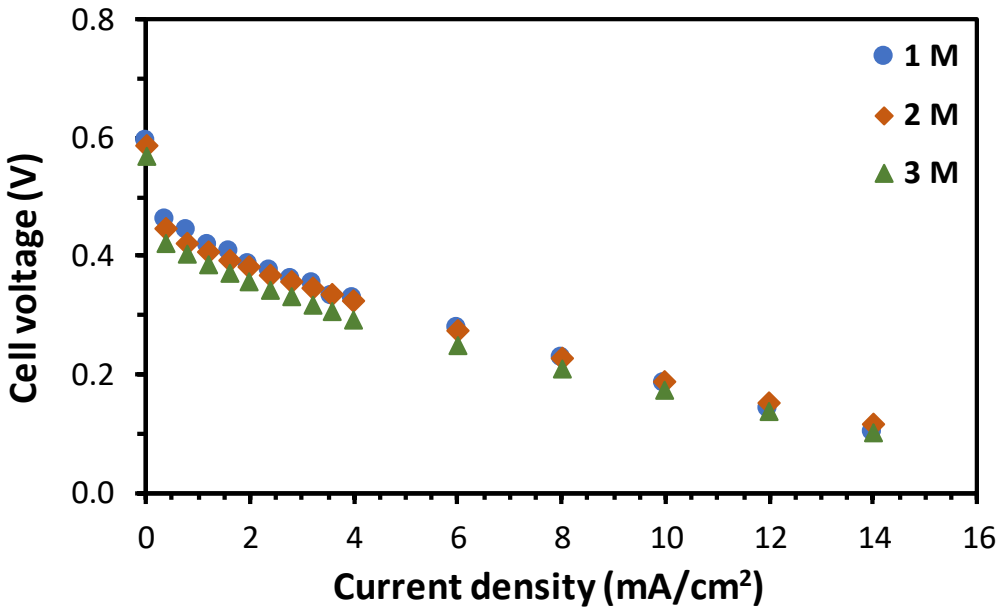

Figure A.1. Effect of methanol concentration on the cell performance using CC as ADL.

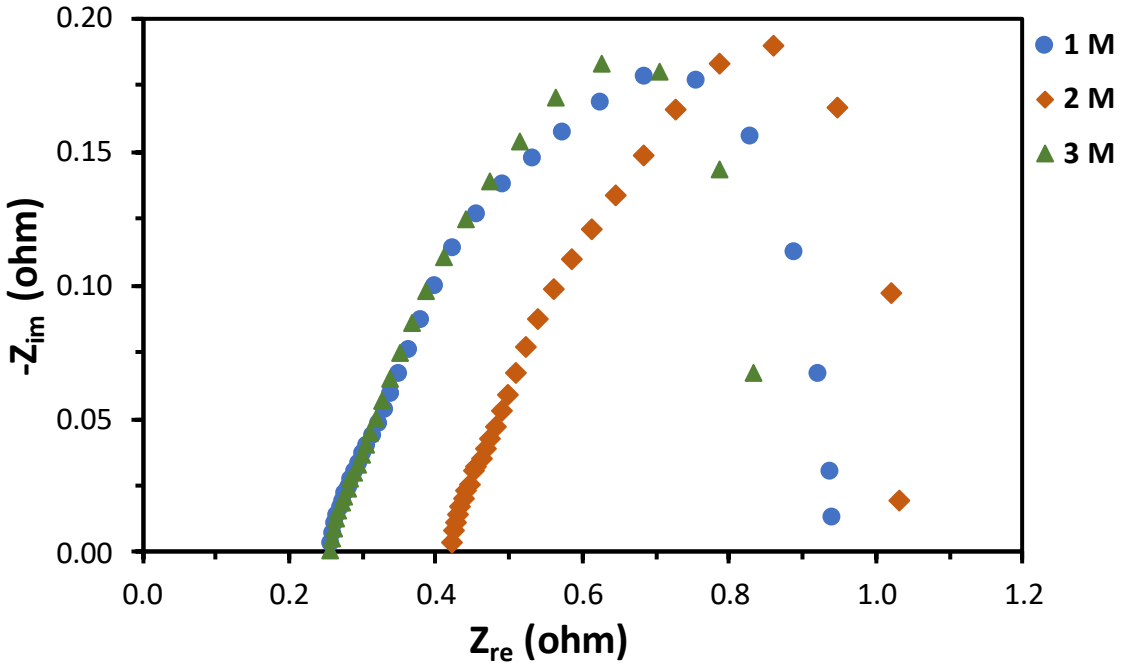

Figure A.2. Nyquist plot of a pDMFC for different methanol concentrations and 0.2 V using CC as ADL.

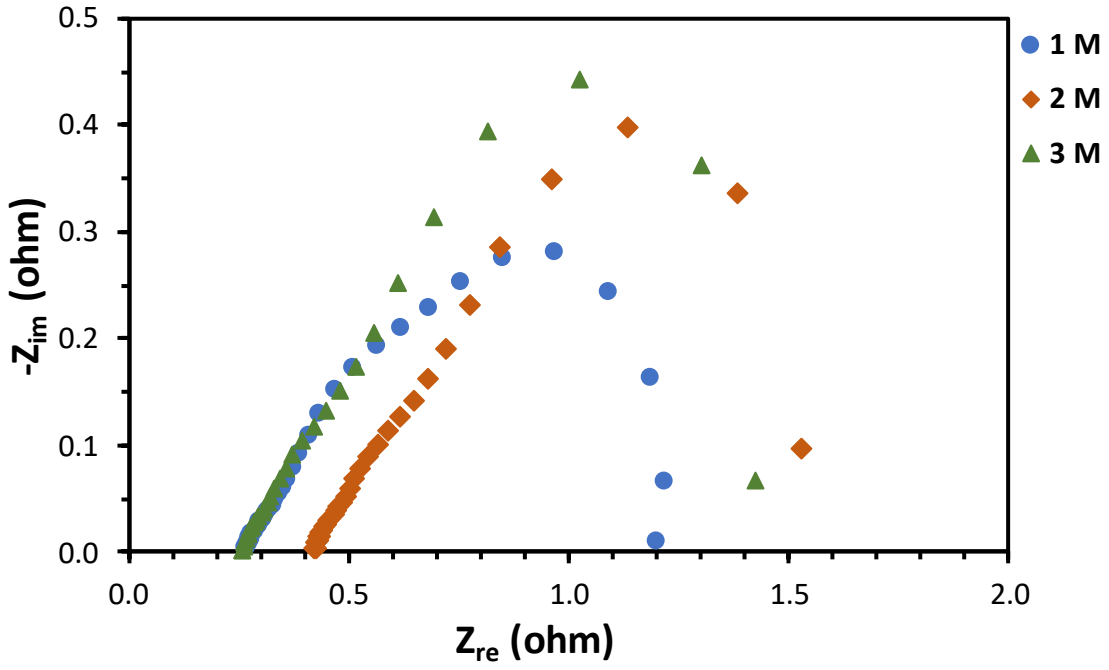

Figure A.3. Nyquist plot of a pDMFC for different methanol concentrations and 0.3 V using CC as ADL.

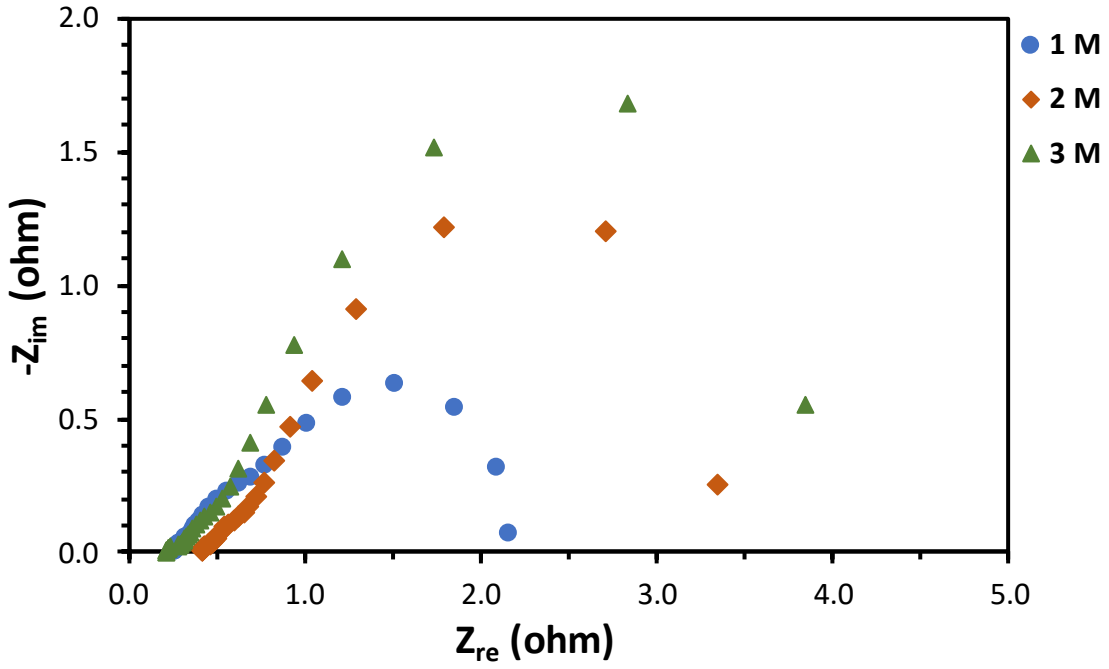

Figure A.4. Nyquist plot of a pDMFC for different methanol concentrations and 0.4 V using CC as ADL.

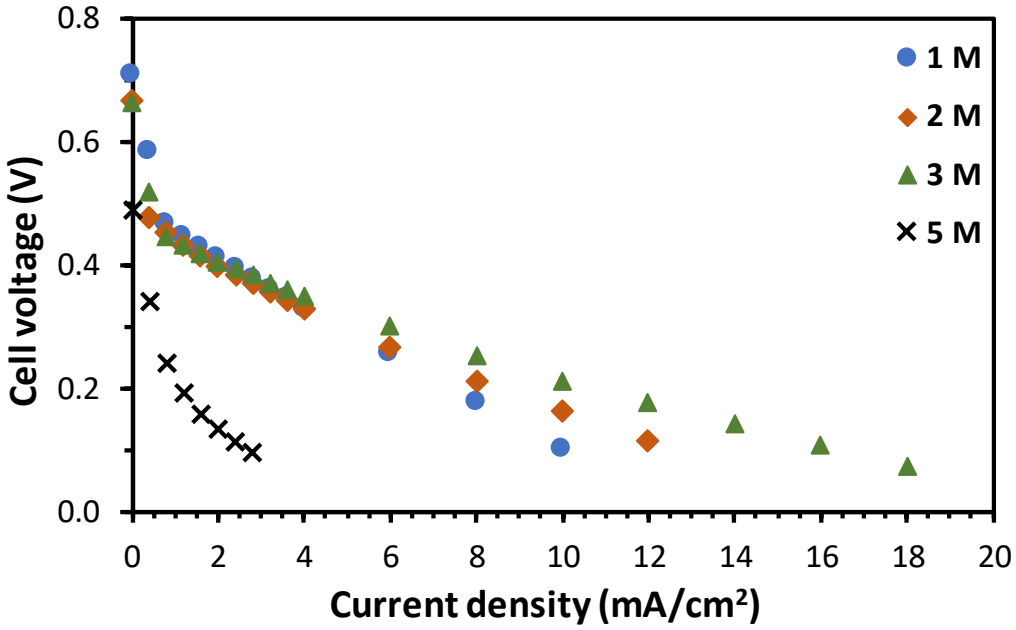

Figure A.5. Effect of methanol concentration on the cell performance using CC_T as ADL.

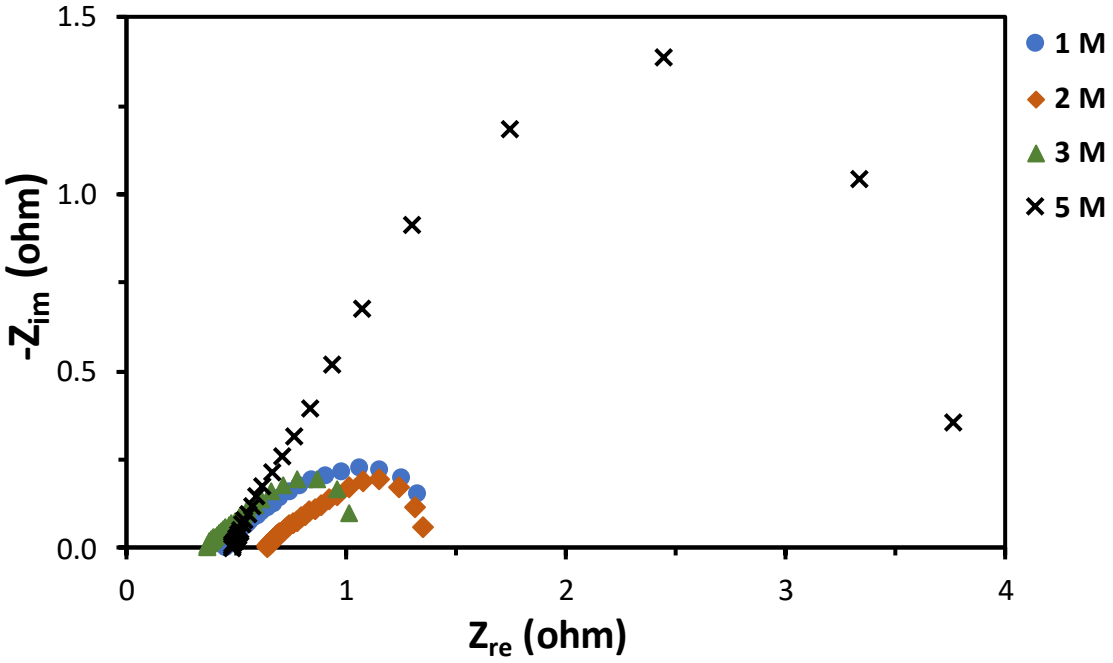

Figure A.6. Nyquist plot of a pDMFC for different methanol concentrations and 0.2 V using CC_T as ADL.

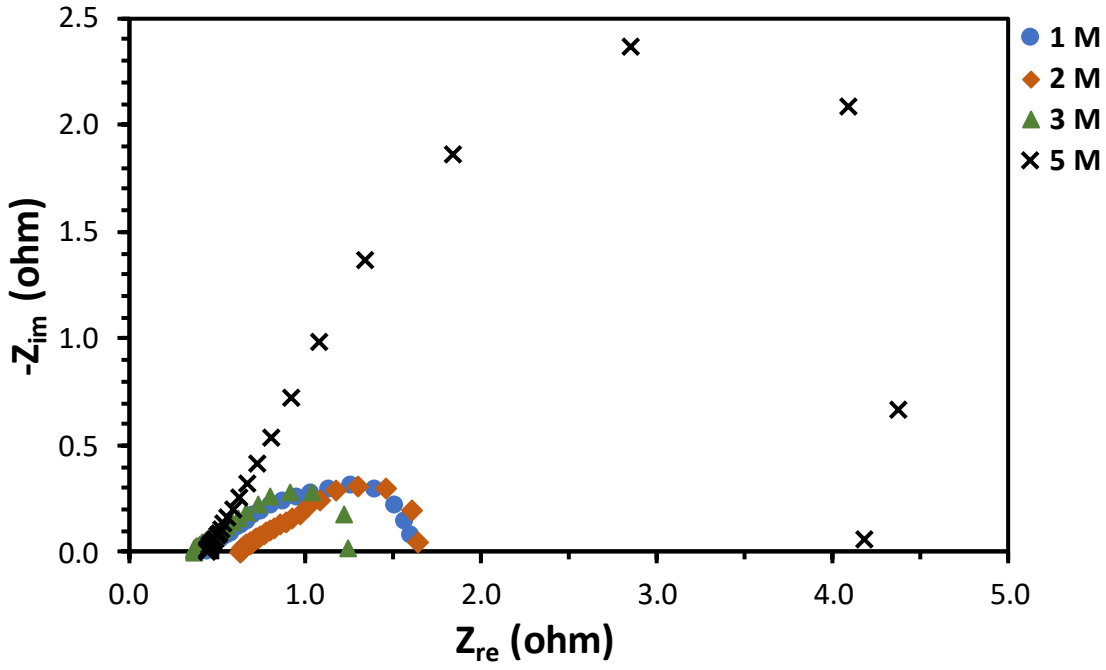

Figure A.7. Nyquist plot of a pDMFC for different methanol concentrations and 0.3 V using CC_T as ADL.

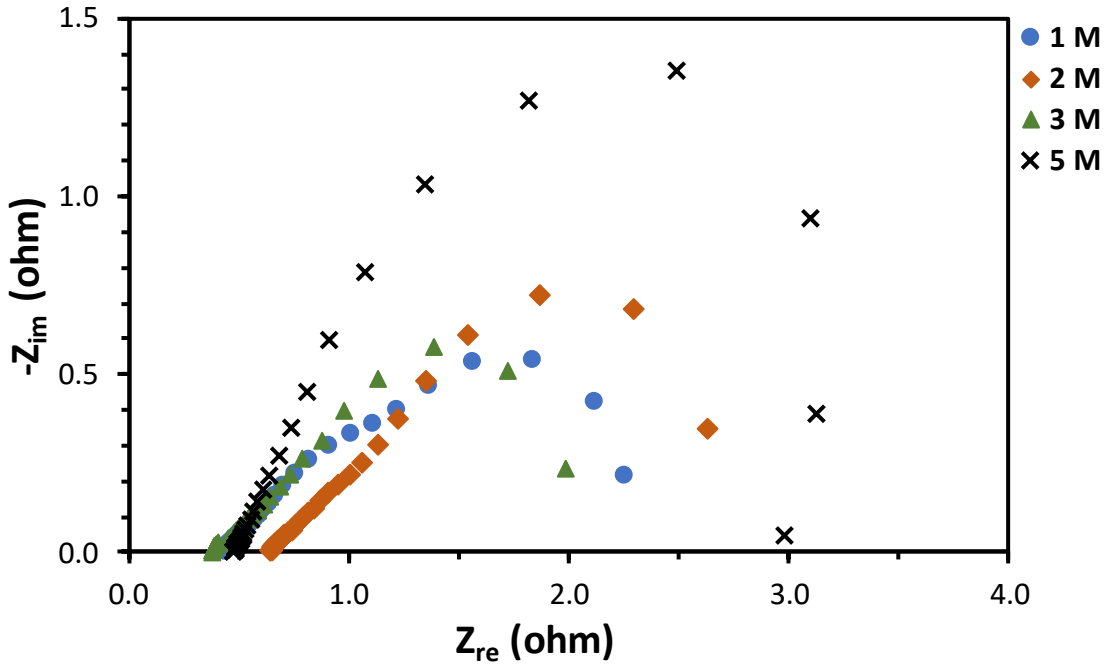

Figure A.8. Nyquist plot of a pDMFC for different methanol concentrations and 0.4 V using CC_T as ADL.

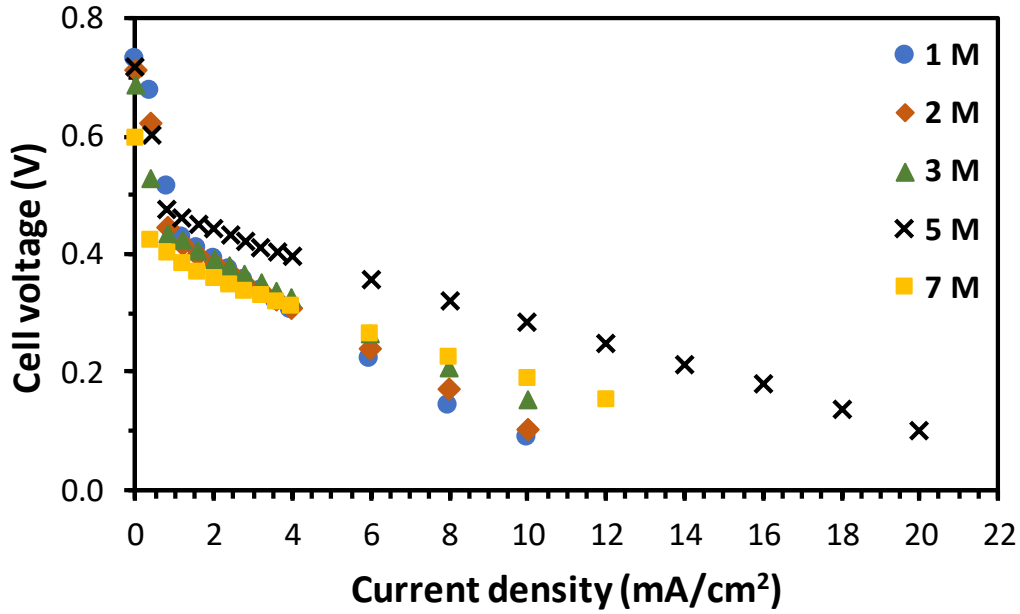

Figure A.9. Effect of methanol concentration on the cell performance using CC_MPL as ADL.

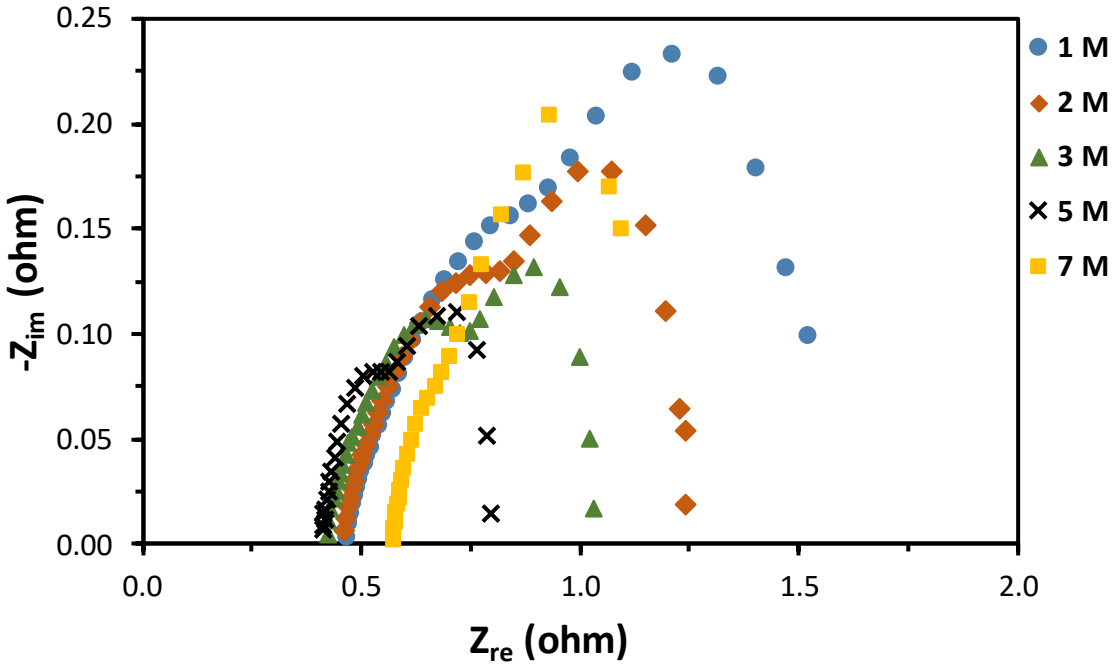

Figure A.10. Nyquist plot of a pDMFC for different methanol concentrations and 0.2 V using CC_MPL as ADL.

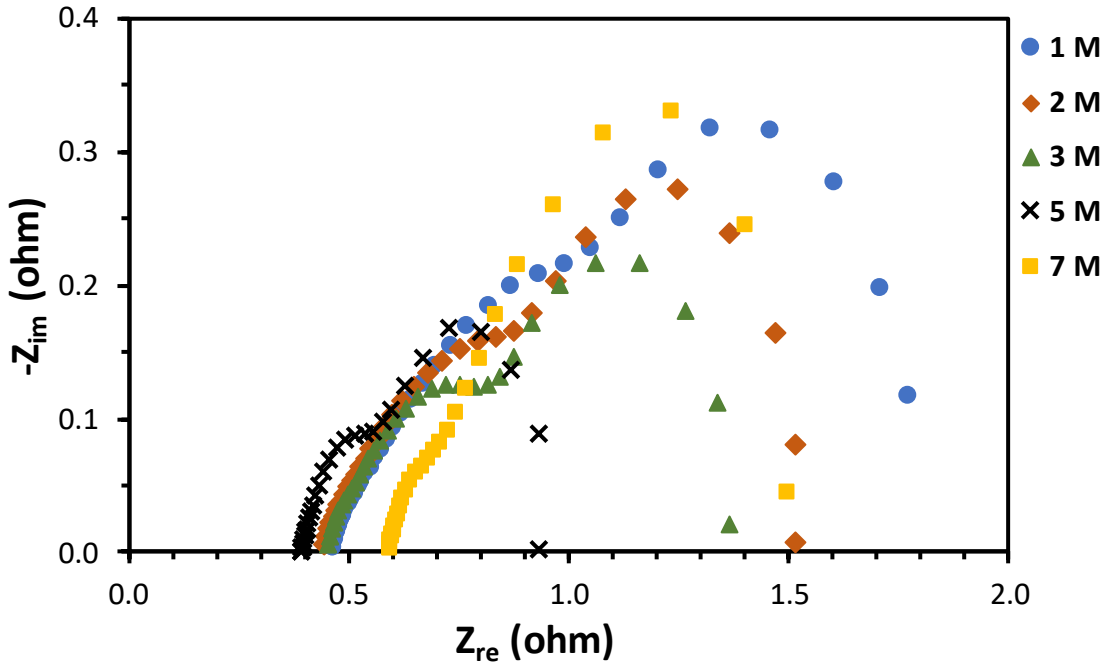

Figure A.11. Nyquist plot of a pDMFC for different methanol concentrations and 0.3 V using CC_MPL as ADL.

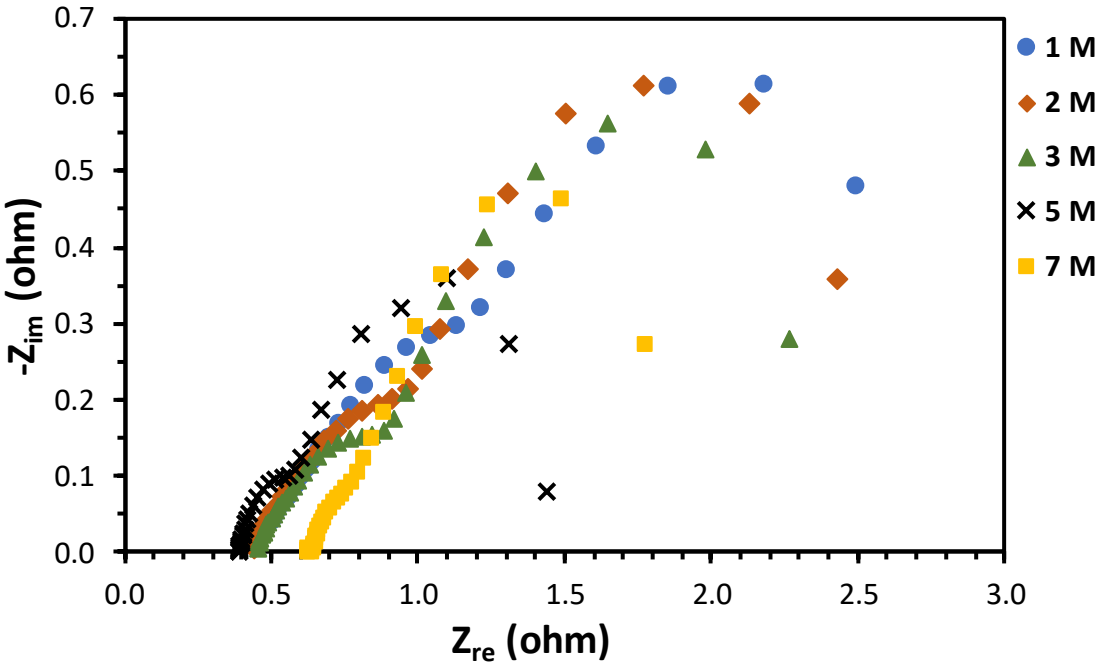

Figure A.12. Nyquist plot of a pDMFC for different methanol concentrations and 0.4 V using CC_MPL as ADL.

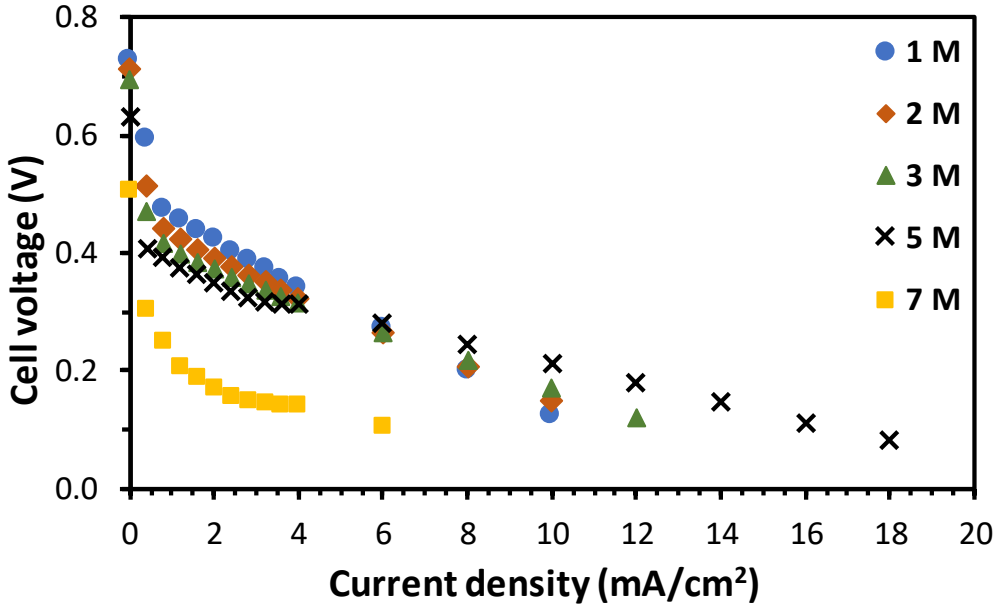

Figure A.13. Effect of methanol concentration on the cell performance using CC_MPL_E as ADL.

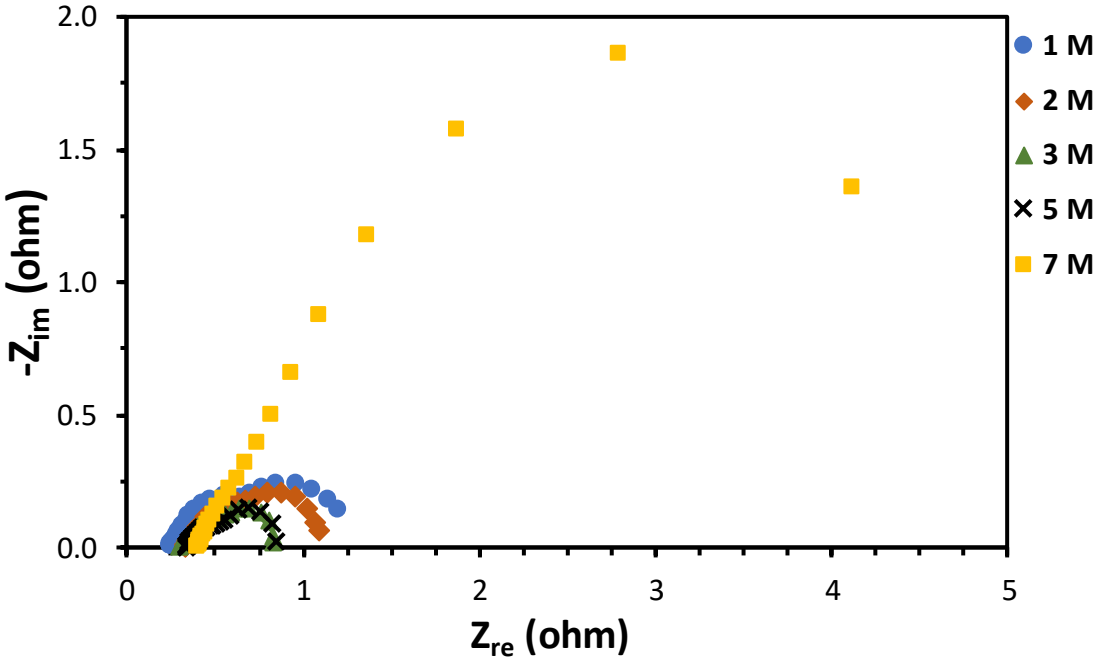

Figure A.14. Nyquist plot of a pDMFC for different methanol concentrations and 0.2 V using CC_MPL_E as ADL.

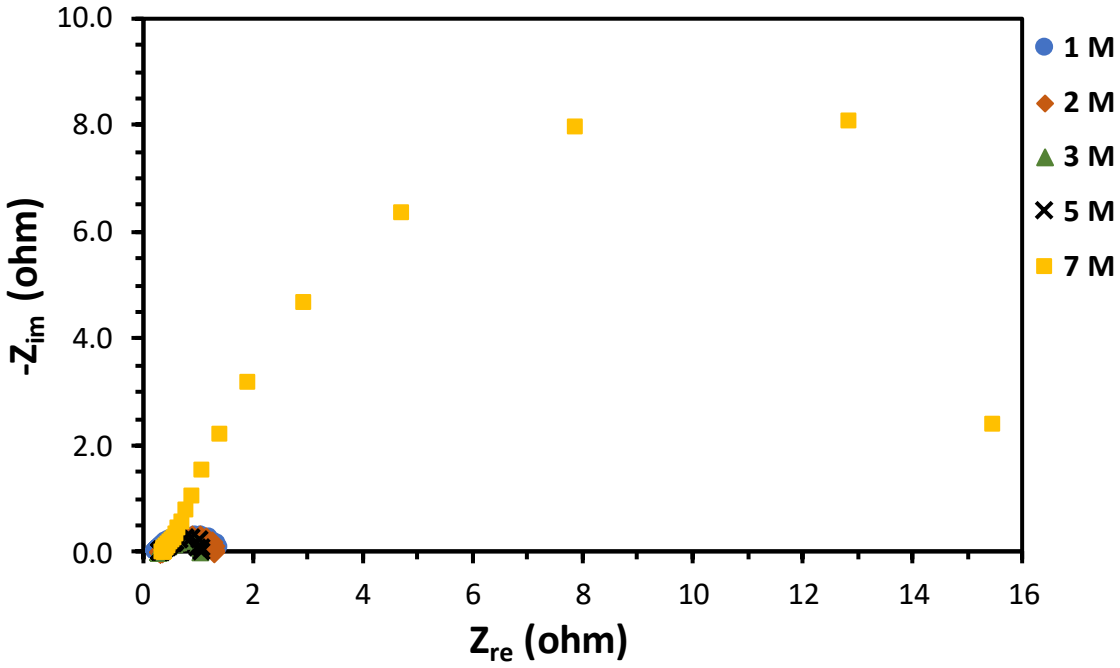

Figure A.15. Nyquist plot of a pDMFC for different methanol concentrations and 0.3 V using CC_MPL_E as ADL.

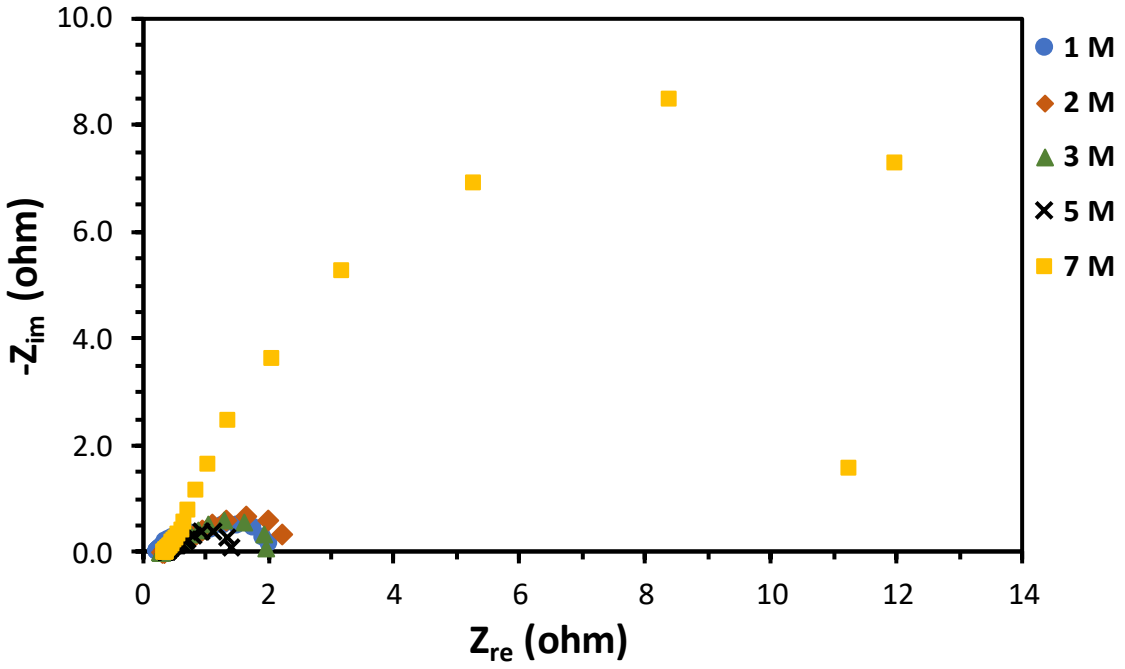

Figure A.16. Nyquist plot of a pDMFC for different methanol concentrations and 0.4 V using CC_MPL_E as ADL.

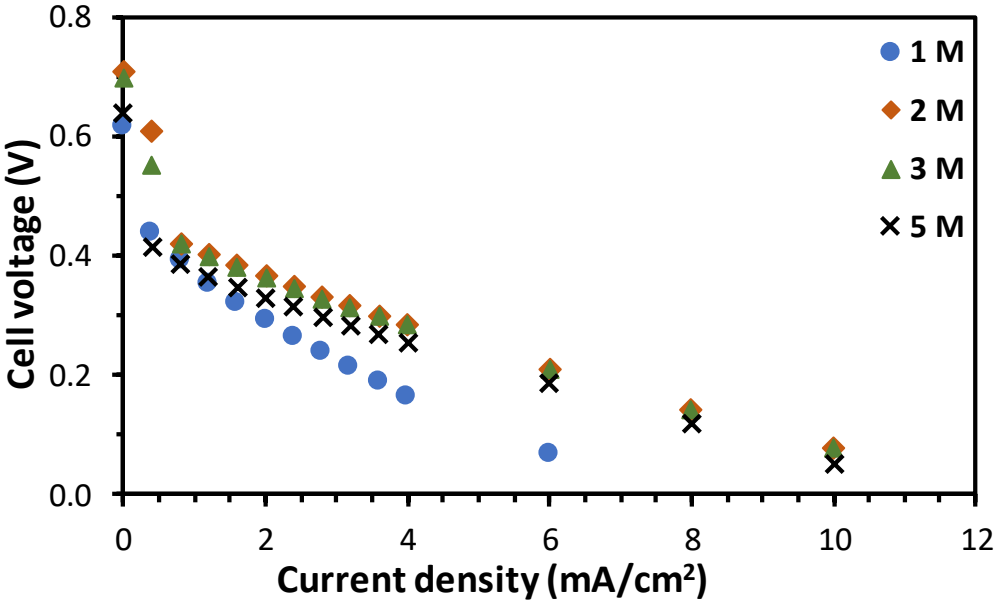

Figure A.17. Effect of methanol concentration on the cell performance using CP as ADL.

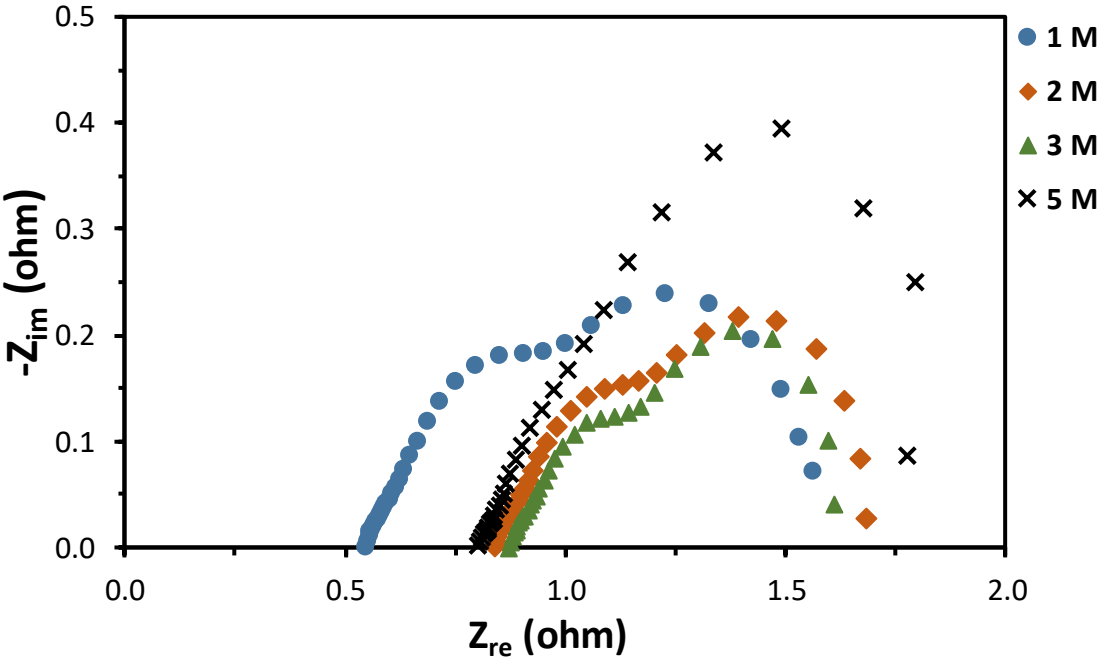

Figure A.18. Nyquist plot of a pDMFC for different methanol concentrations and 0.2 V using CP as ADL.

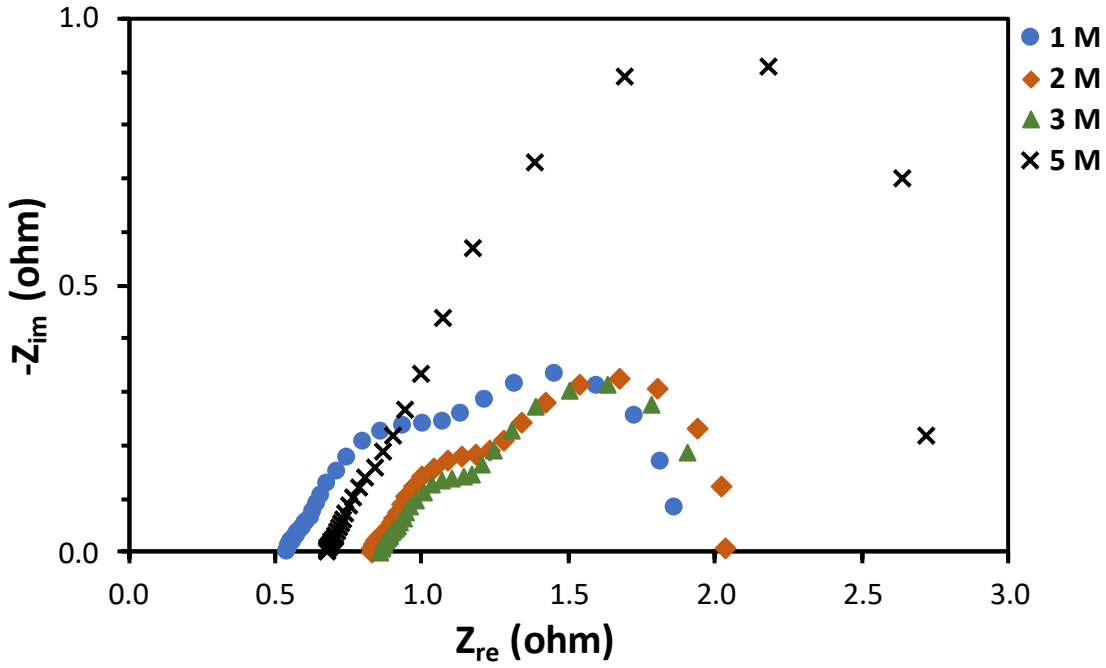

Figure A.19. Nyquist plot of a pDMFC for different methanol concentrations and 0.3 V using CP as ADL.

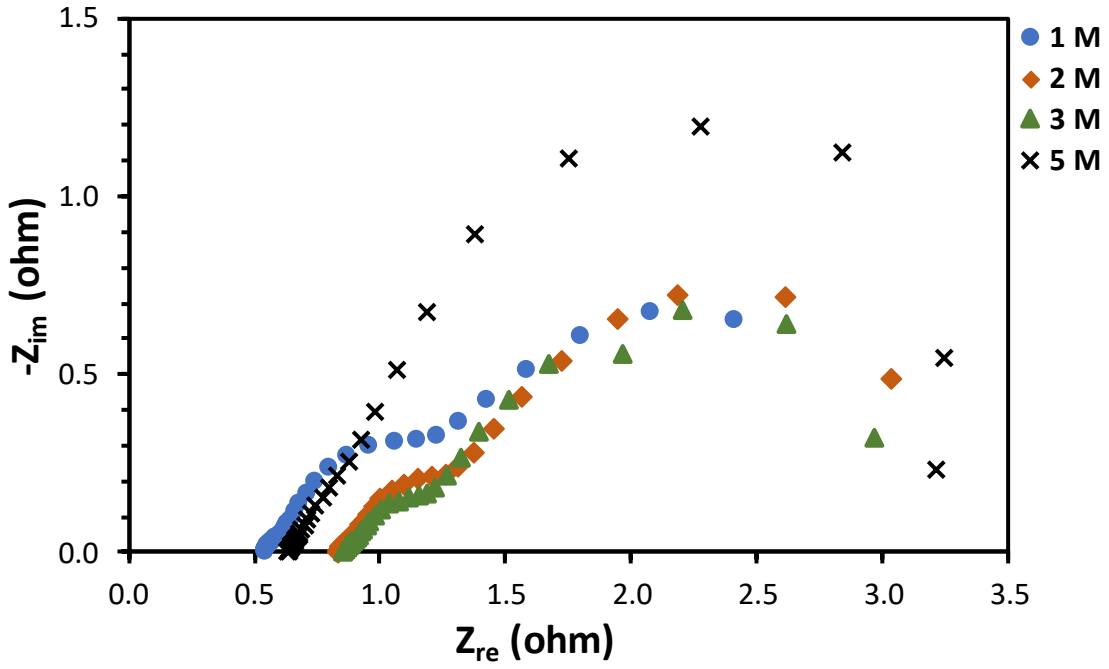

Figure A.20. Nyquist plot of a pDMFC for different methanol concentrations and 0.4 V using CP as ADL.

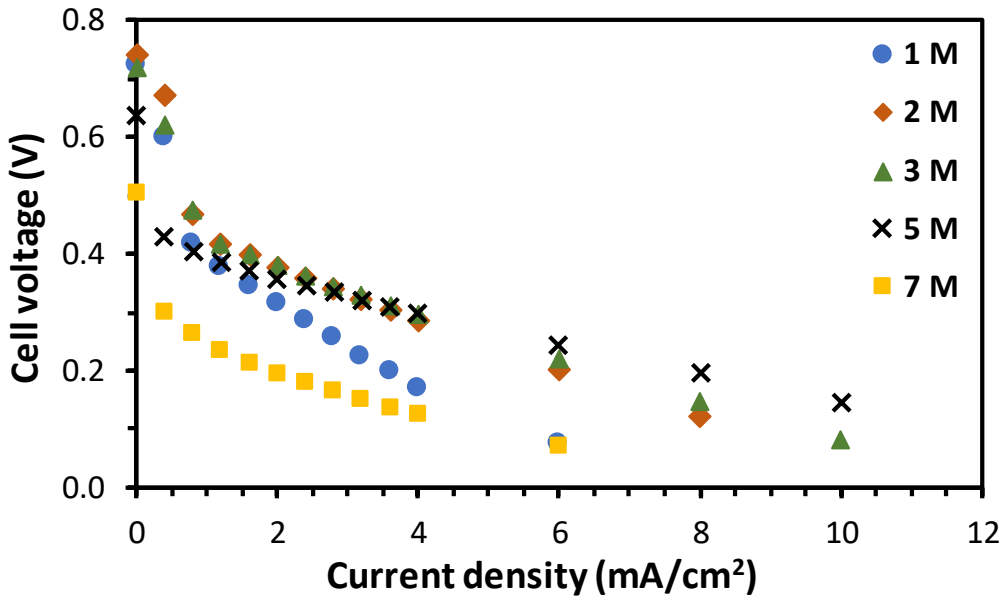

Figure A.21. Effect of methanol concentration on the cell performance using CP_T as ADL.

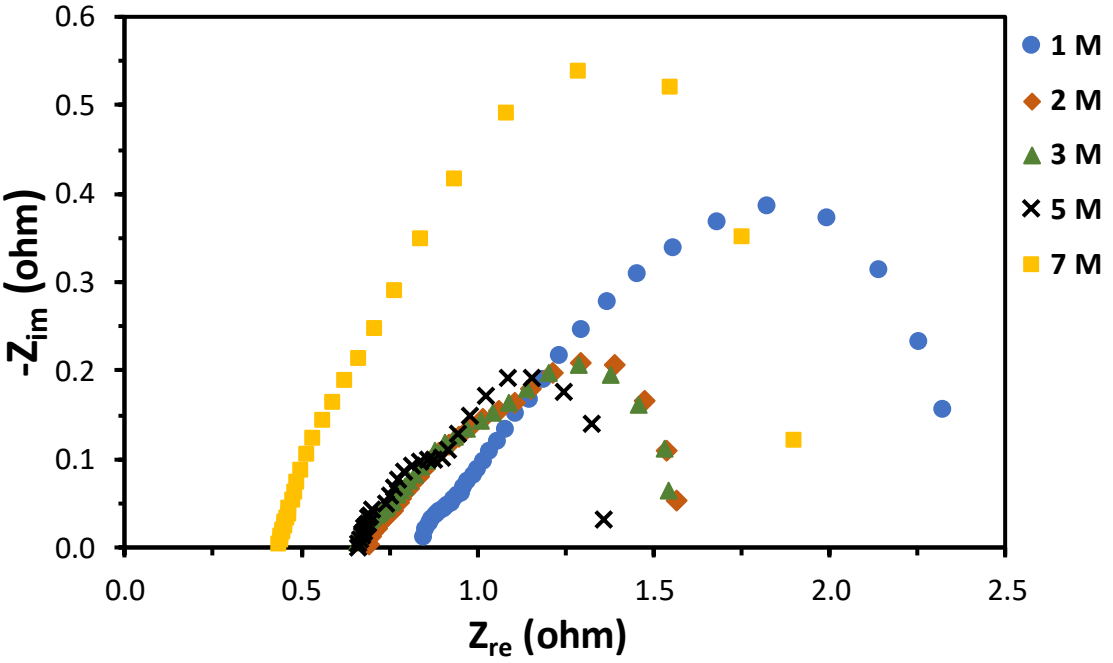

Figure A.22. Nyquist plot of a pDMFC for different methanol concentrations and 0.2 V using CP_T as ADL.

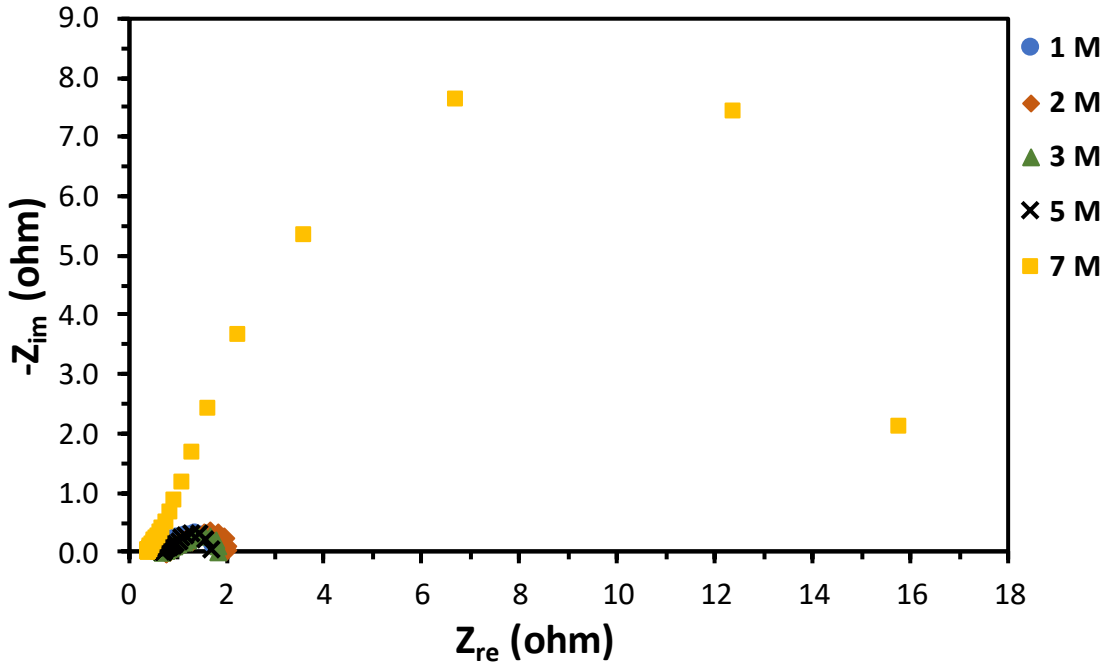

Figure A.23. Nyquist plot of a pDMFC for different methanol concentrations and 0.3 V using CP_T as ADL.

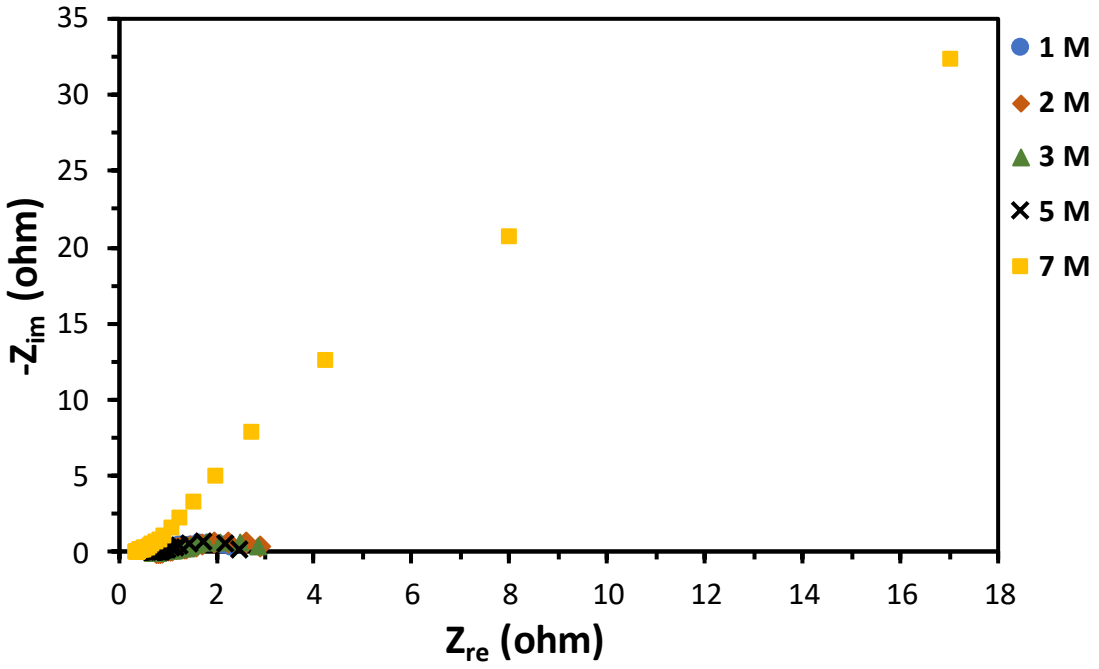

Figure A.24. Nyquist plot of a pDMFC for different methanol concentrations and 0.4 V using CP_T as ADL.

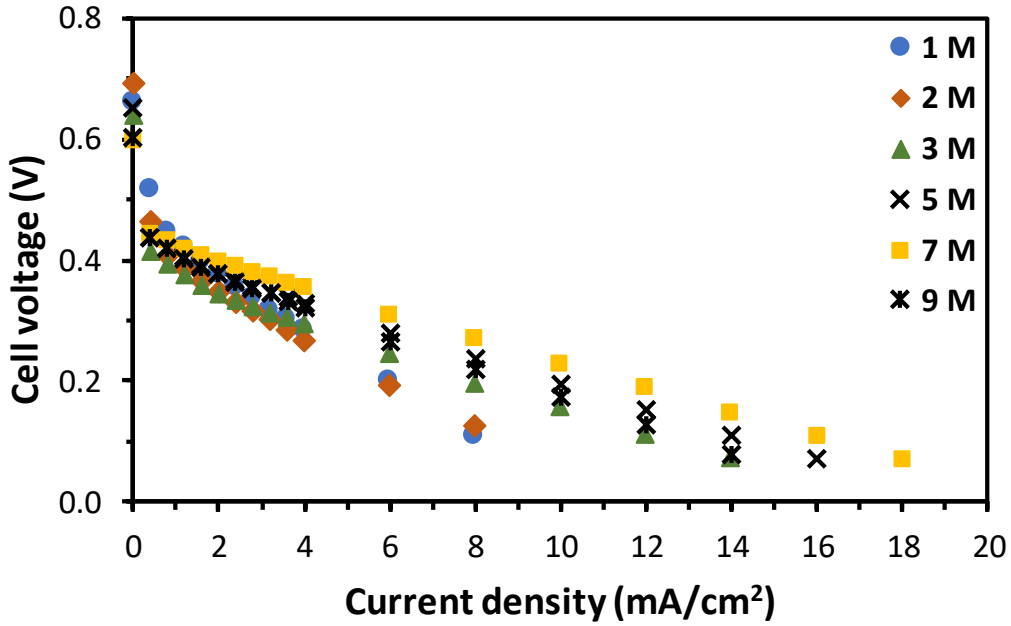

Figure A.25. Effect of methanol concentration on the cell performance using CP_MPL as ADL.

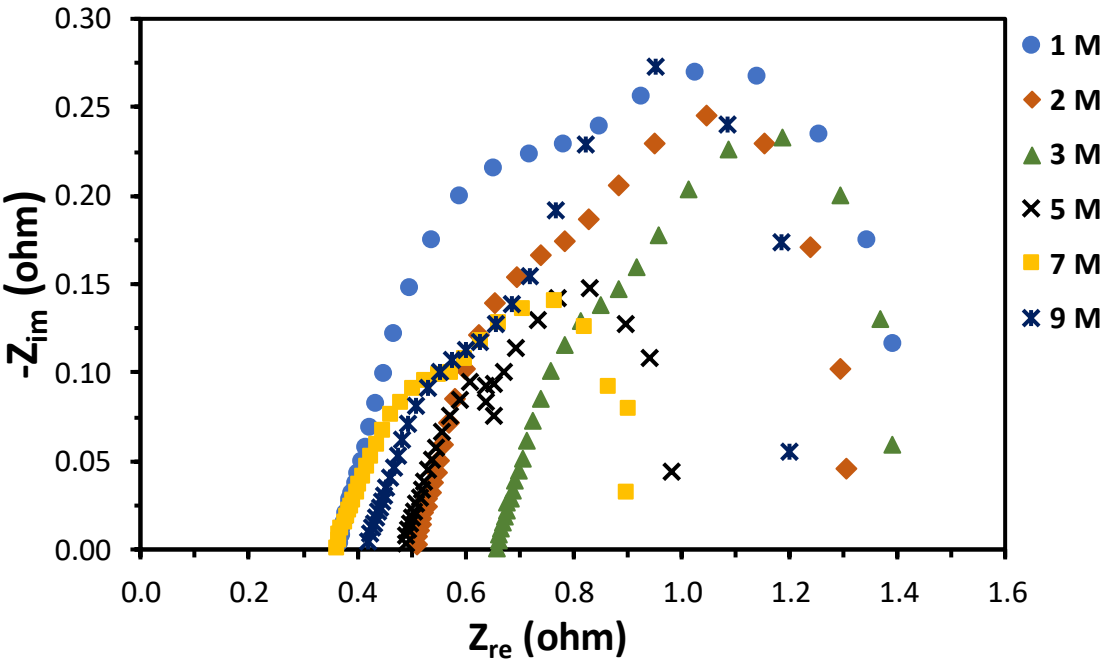

Figure A.26. Nyquist plot of a pDMFC for different methanol concentrations and 0.2 V using CP_MPL as ADL.

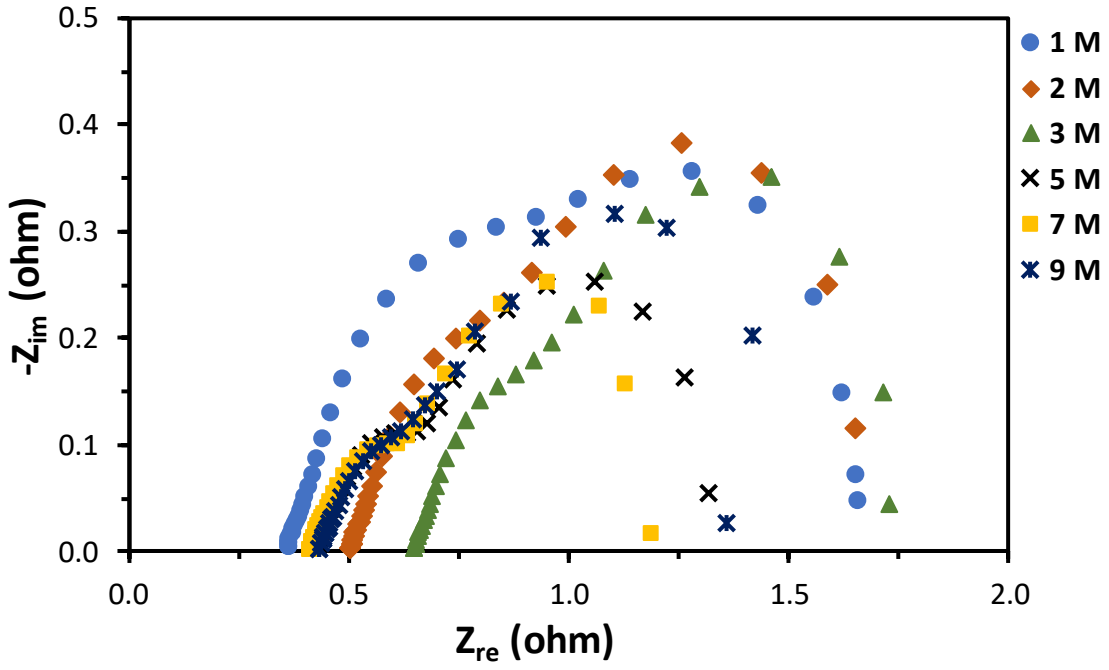

Figure A.27. Nyquist plot of a pDMFC for different methanol concentrations and 0.3 V using CP_MPL as ADL.

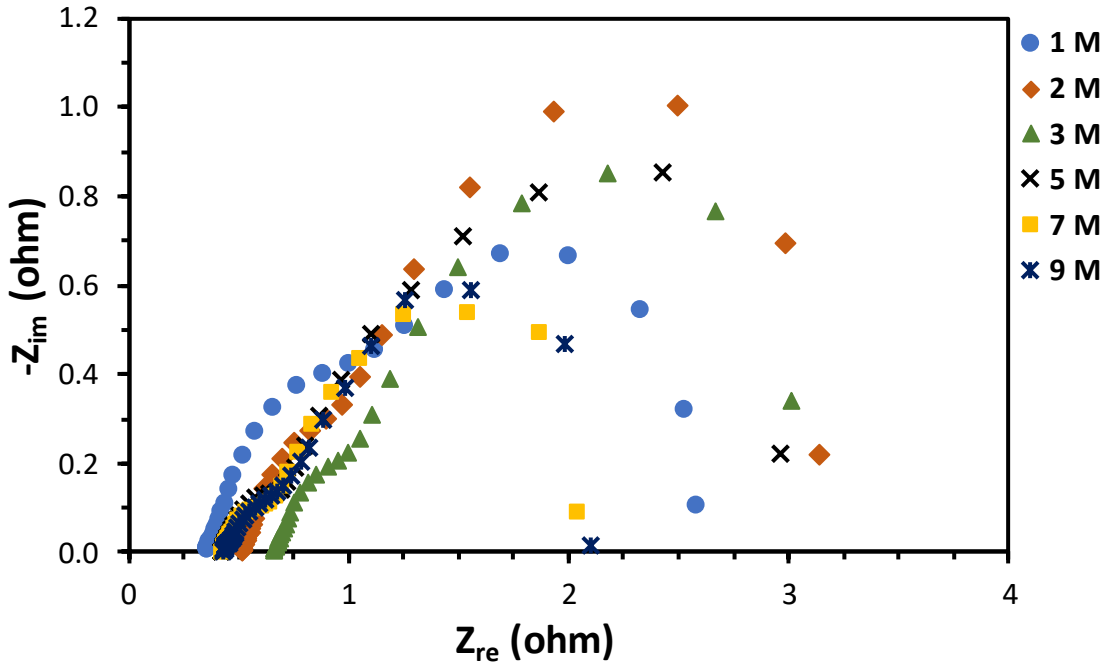

Figure A.28. Nyquist plot of a pDMFC for different methanol concentrations and 0.4 V using CP_MPL as ADL.

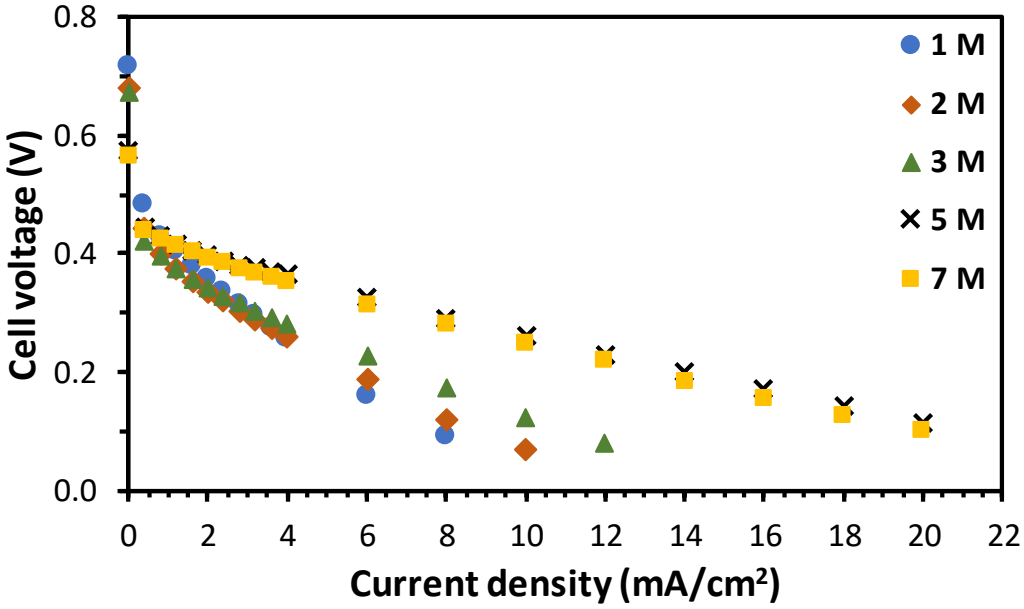

Figure A.29. Effect of methanol concentration on the cell performance using CP_MPL_T as ADL.

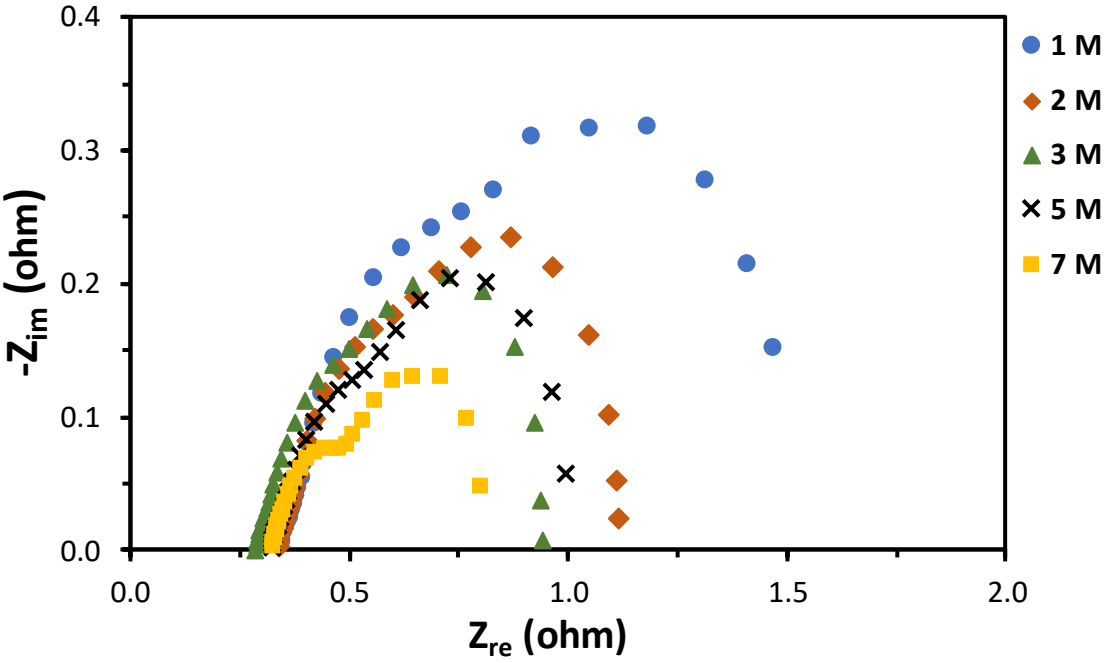

Figure A.30. Nyquist plot of a pDMFC for different methanol concentrations and 0.2 V using CP_MPL_T as ADL.

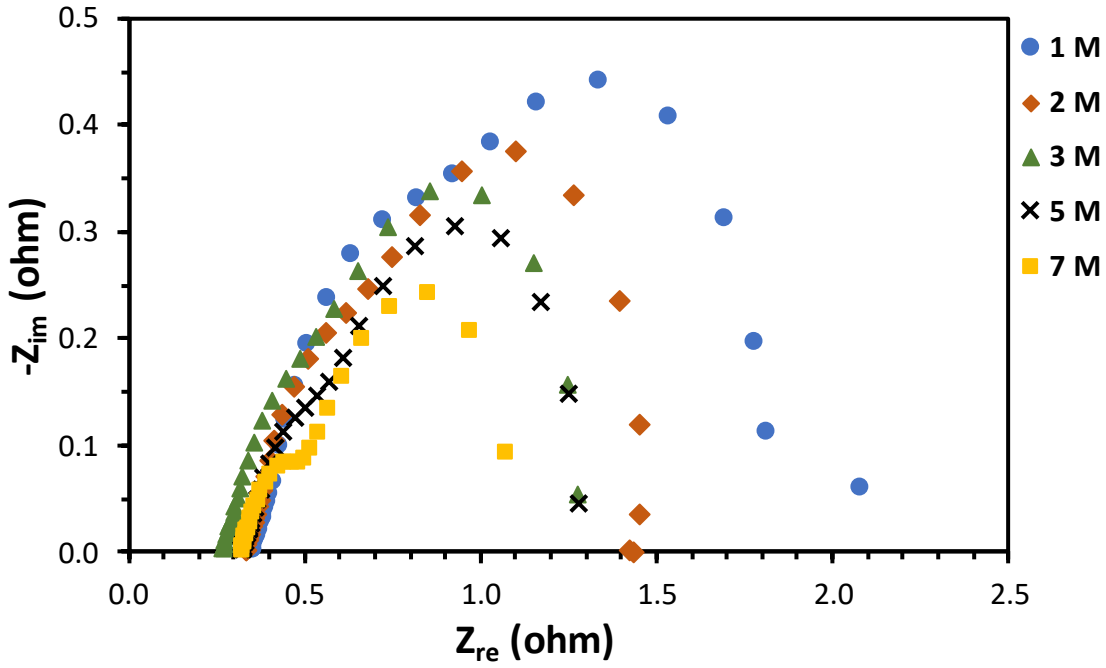

Figure A.31. Nyquist plot of a pDMFC for different methanol concentrations and 0.3 V using CP_MPL_T as ADL.

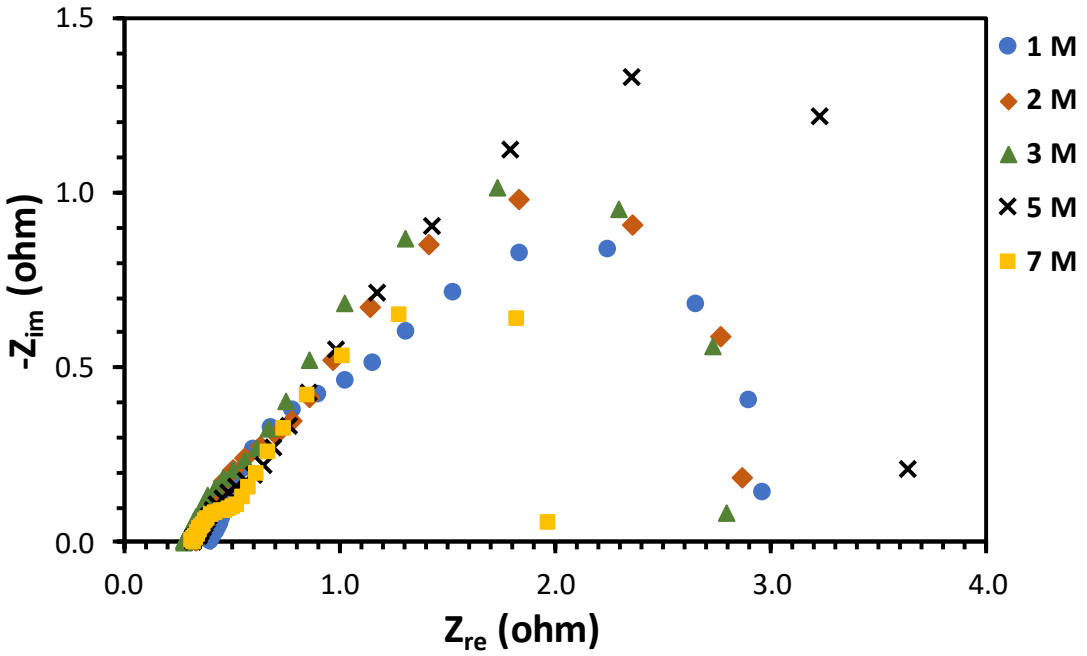

Figure A.32. Nyquist plot of a pDMFC for different methanol concentrations and 0.4 V using CP_MPL_T as ADL.

A.2. Effect of cathode diffusion layers properties

All the results presented in this section were obtained with stainless steel current collectors, with an open ratio of 41 % (CC_2), at the anode and cathode sides and with CC_MPL as anode DL.

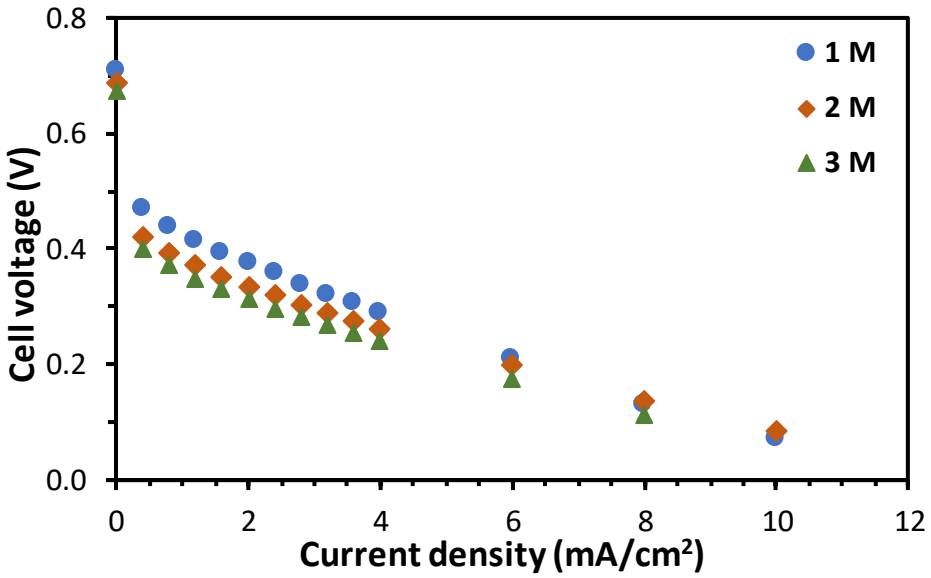

Figure A.33. Effect of methanol concentration on the cell performance using CC_T as CDL.

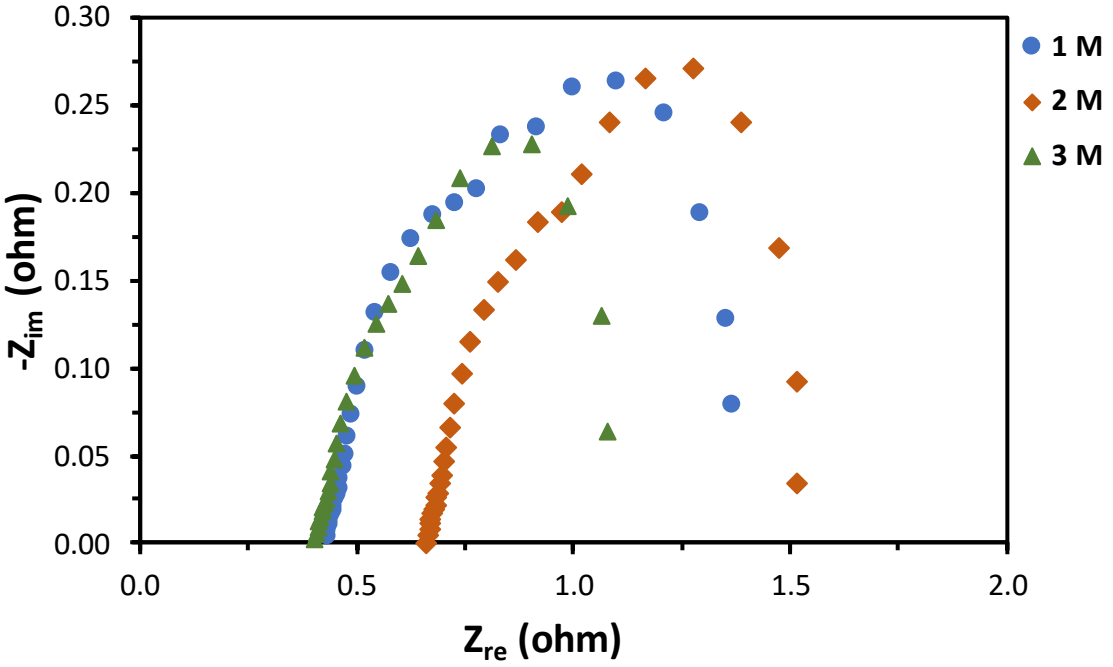

Figure A.34. Nyquist plot of a pDMFC for different methanol concentrations and 0.2 V using CC_T as CDL.

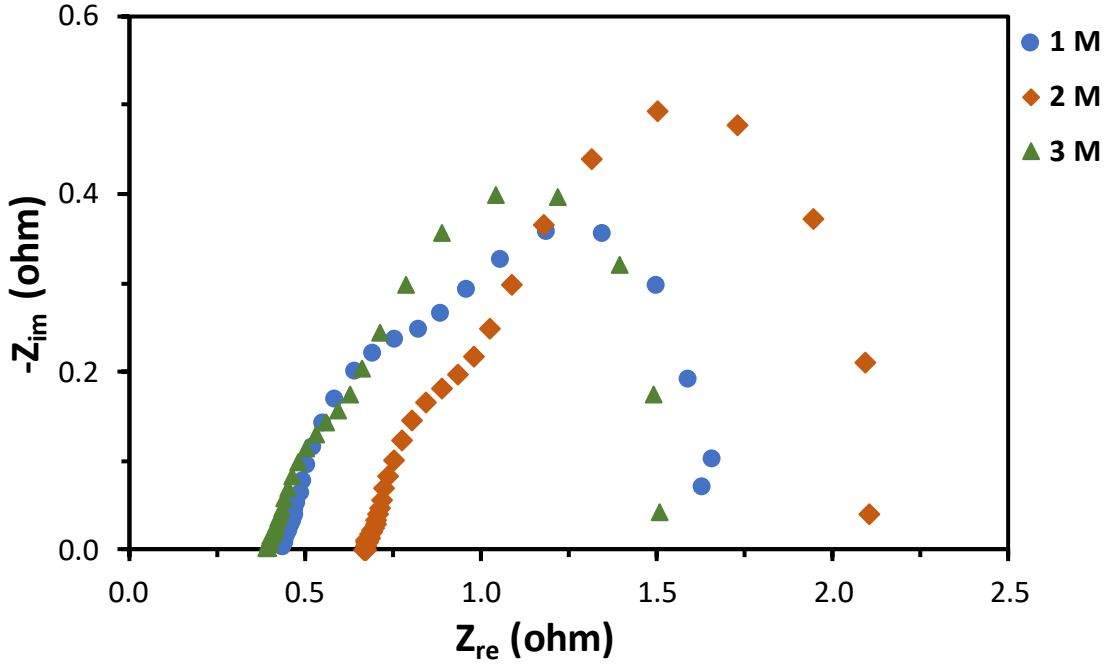

Figure A.35. Nyquist plot of a pDMFC for different methanol concentrations and 0.3 V using CC_T as CDL.

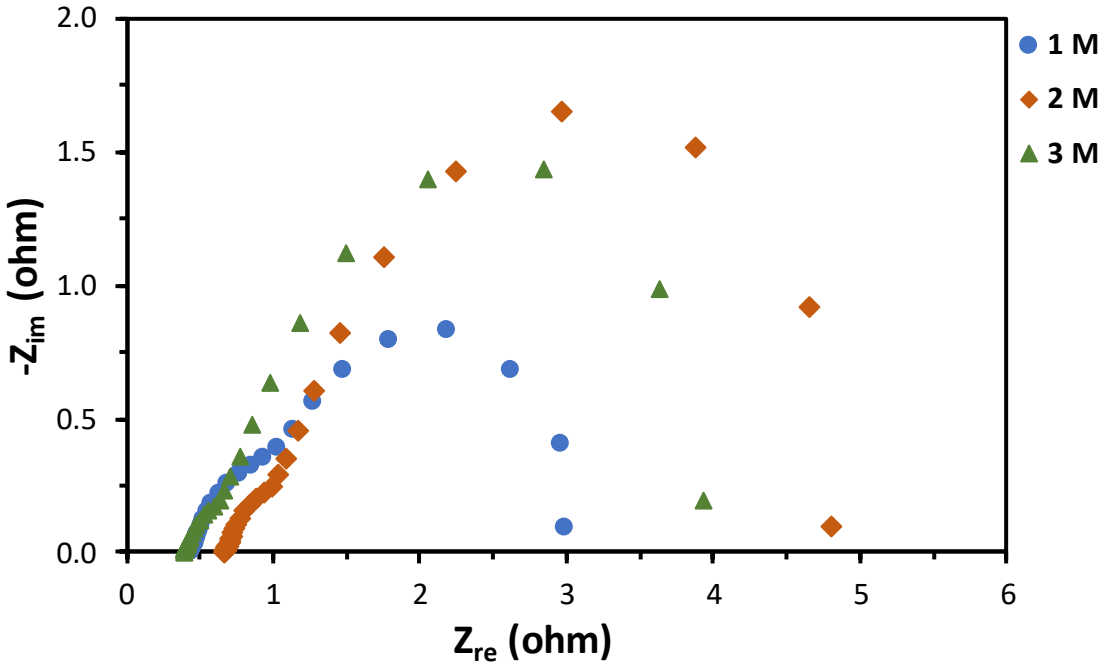

Figure A.36. Nyquist plot of a pDMFC for different methanol concentrations and 0.4 V using CC_T as CDL.

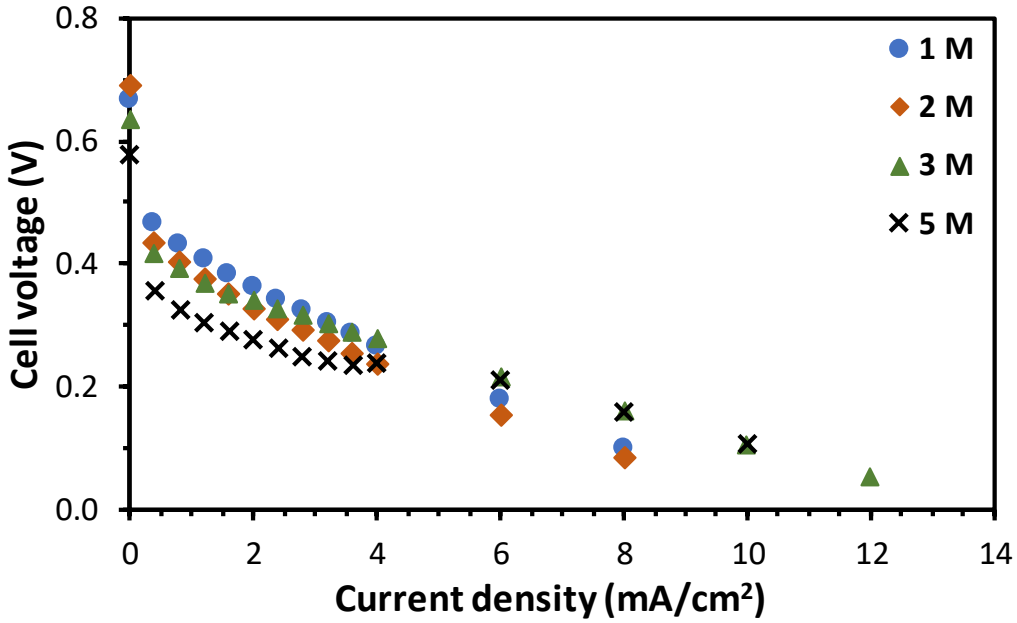

Figure A.37. Effect of methanol concentration on the cell performance using CC_MPL as CDL.

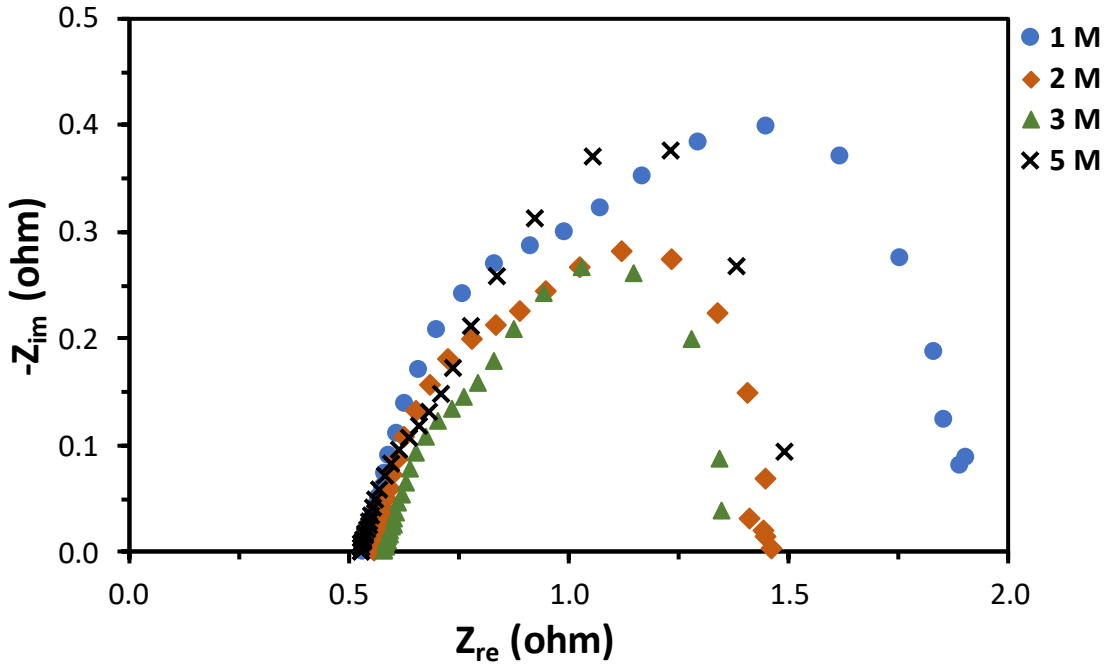

Figure A.38. Nyquist plot of a pDMFC for different methanol concentrations and 0.2 V using CC_MPL as CDL.

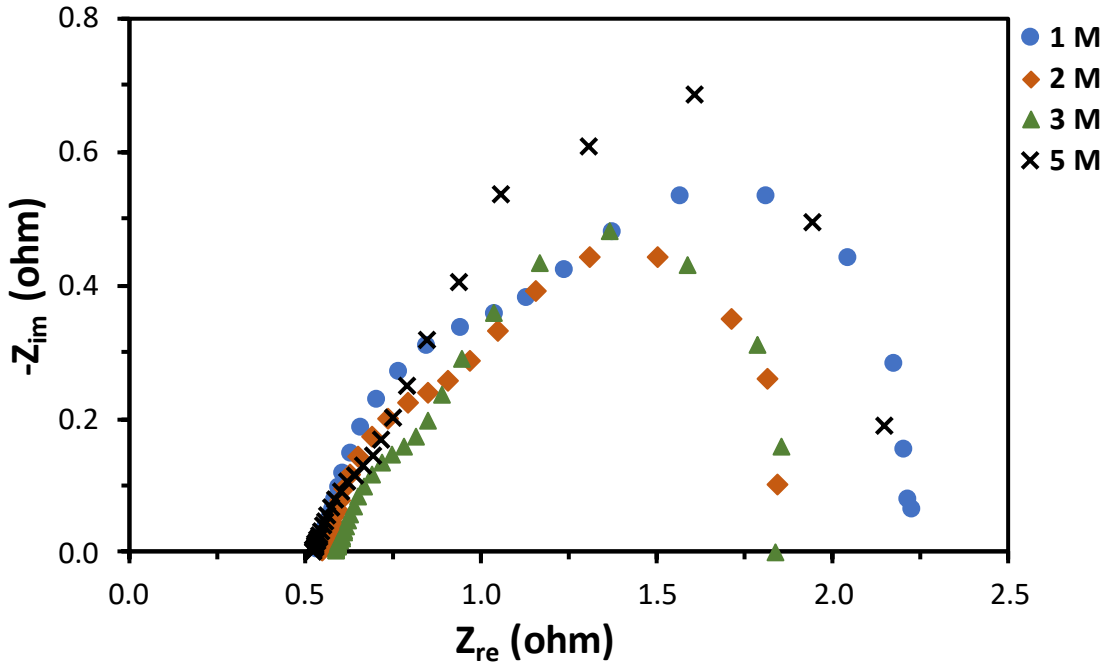

Figure A.39. Nyquist plot of a pDMFC for different methanol concentrations and 0.3 V using CC_MPL as CDL.

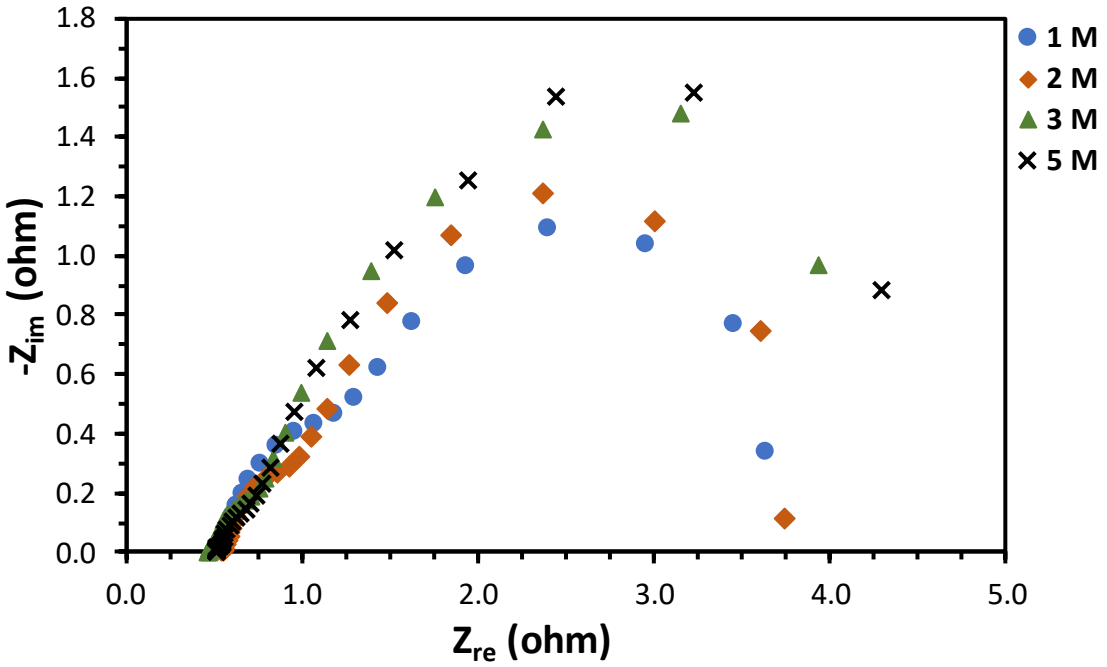

Figure A.40. Nyquist plot of a pDMFC for different methanol concentrations and 0.4 V using CC_MPL as CDL.

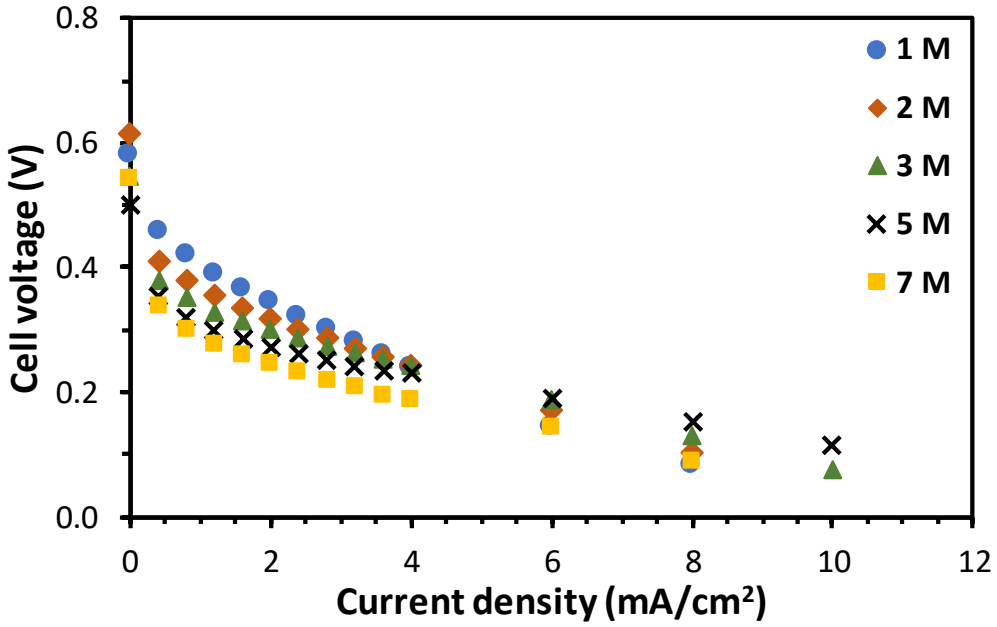

Figure A.41. Effect of methanol concentration on the cell performance using CC_MPL_E as CDL.

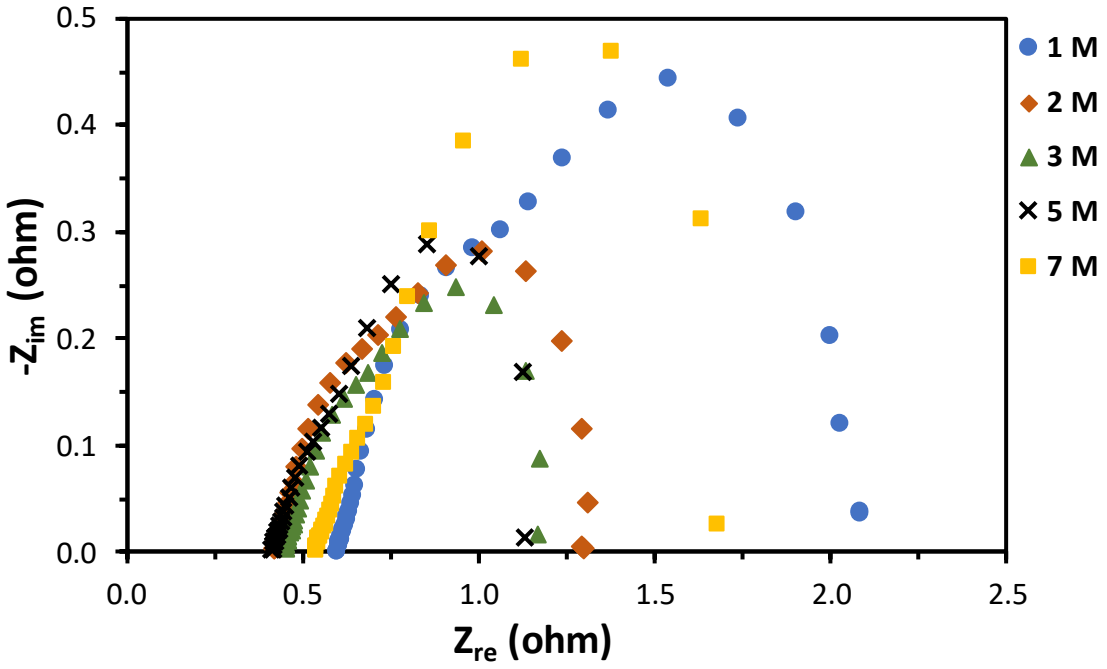

Figure A.42. Nyquist plot of a pDMFC for different methanol concentrations and 0.2 V using CC_MPL_E as CDL.

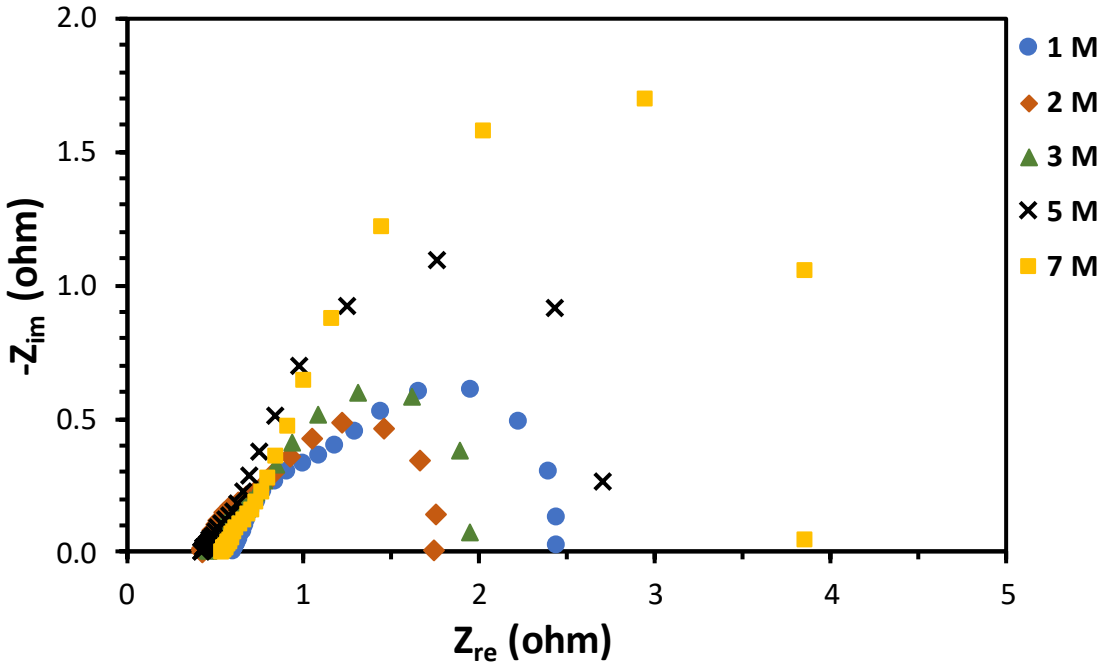

Figure A.43. Nyquist plot of a pDMFC for different methanol concentrations and 0.3 V using CC_MPL_E as CDL.

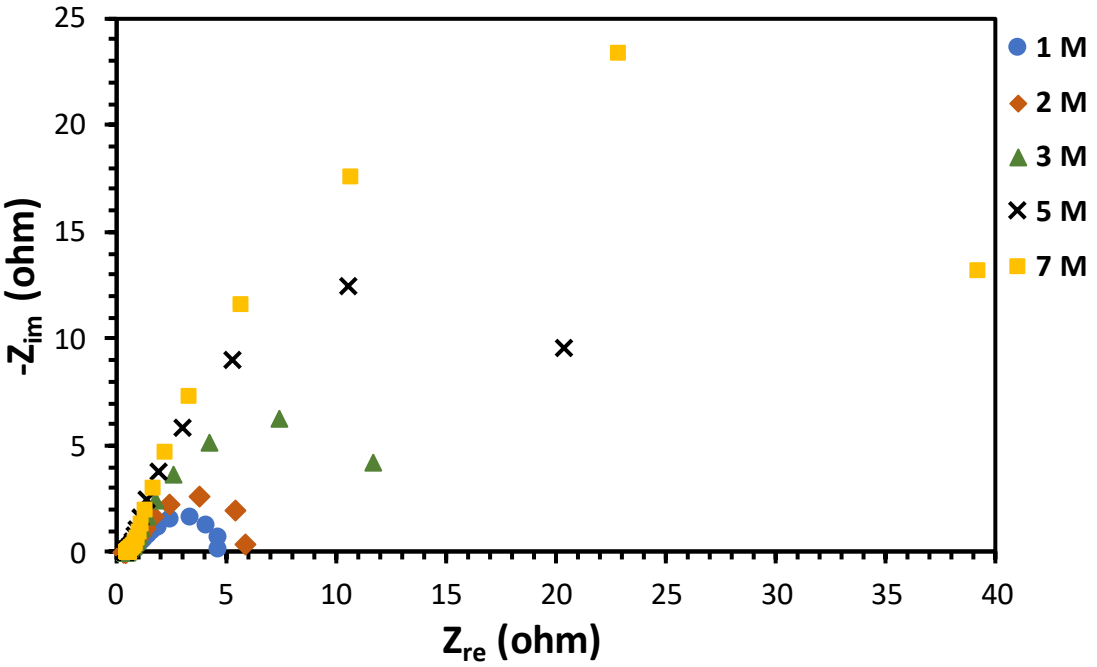

Figure A.44. Nyquist plot of a pDMFC for different methanol concentrations and 0.4 V using CC_MPL_E as CDL.

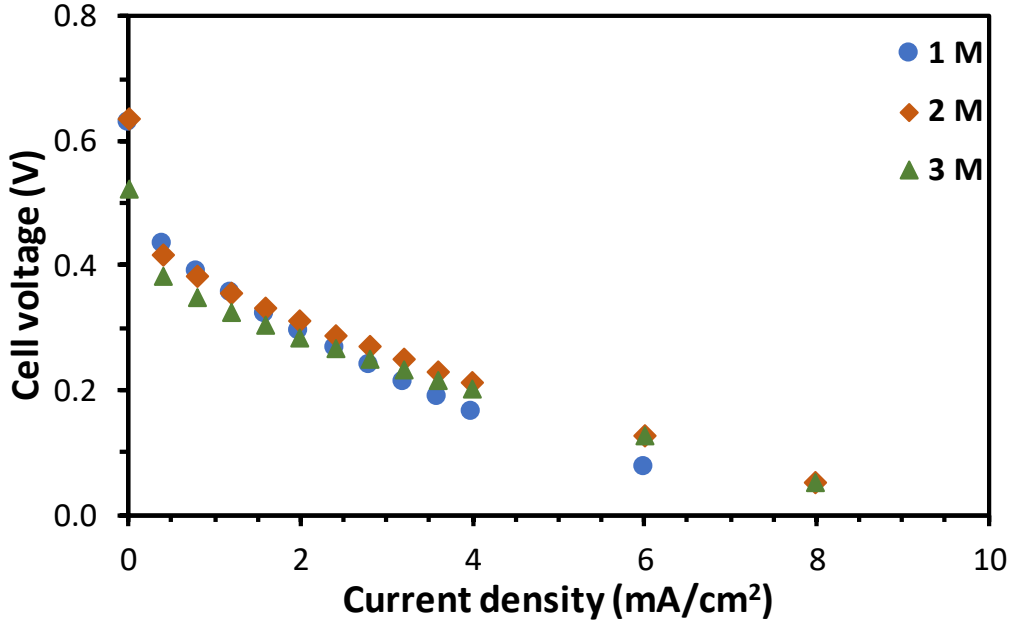

Figure A.45. Effect of methanol concentration on the cell performance using CP as CDL.

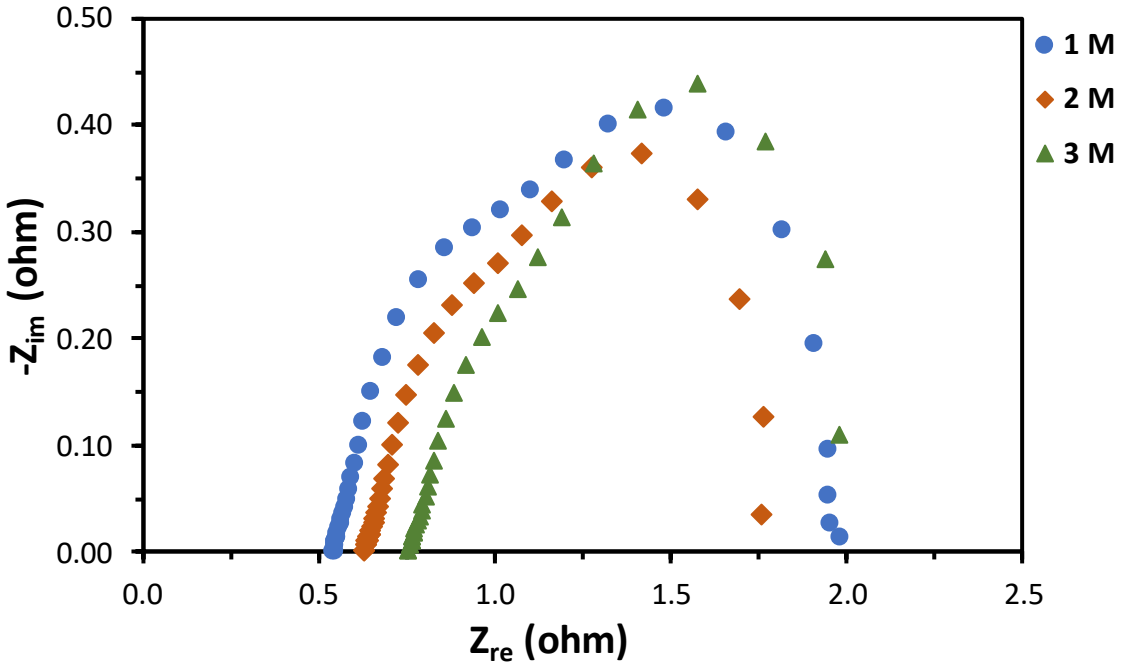

Figure A.46. Nyquist plot of a pDMFC for different methanol concentrations and 0.2 V using CP as CDL.

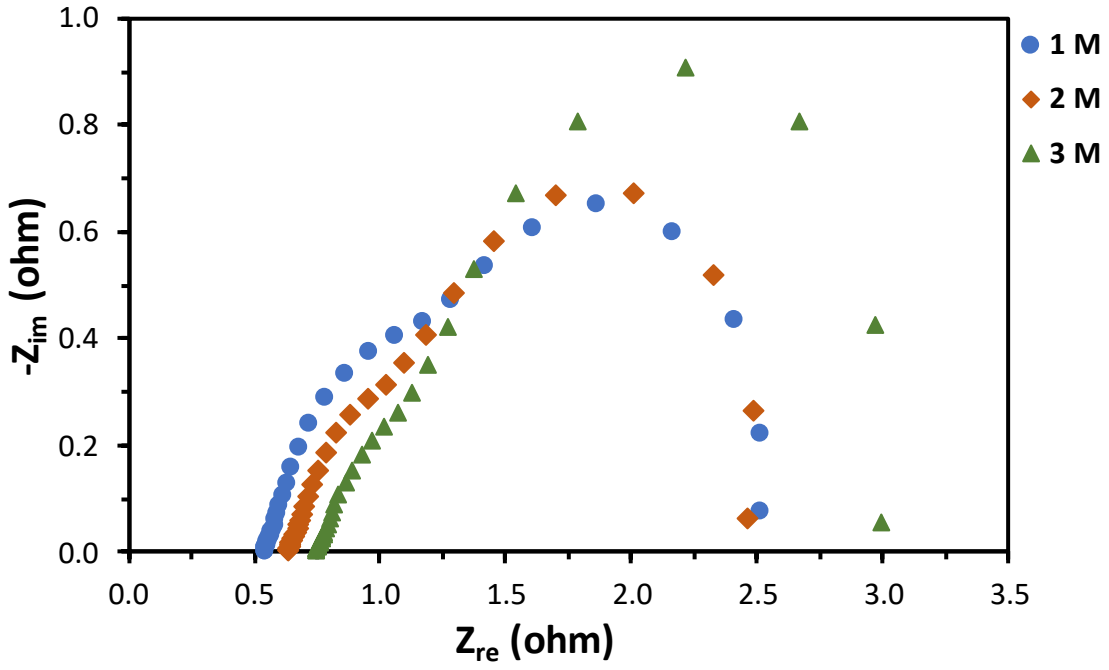

Figure A.47. Nyquist plot of a pDMFC for different methanol concentrations and 0.3 V using CP as CDL.

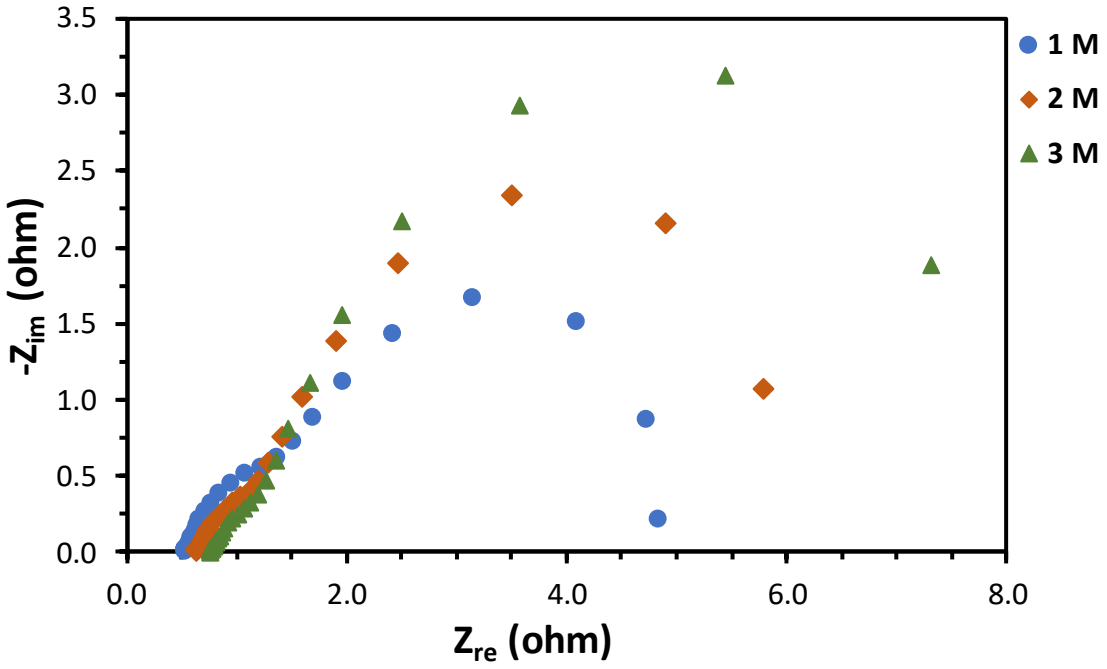

Figure A.48. Nyquist plot of a pDMFC for different methanol concentrations and 0.4 V using CP as CDL.

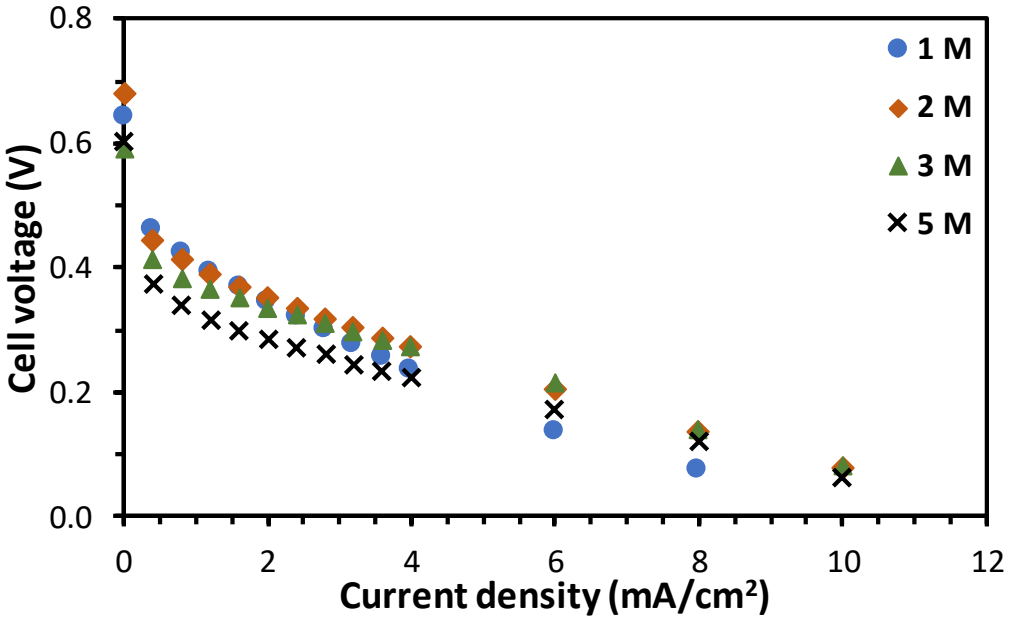

Figure A.49. Effect of methanol concentration on the cell performance using CP_T as CDL.

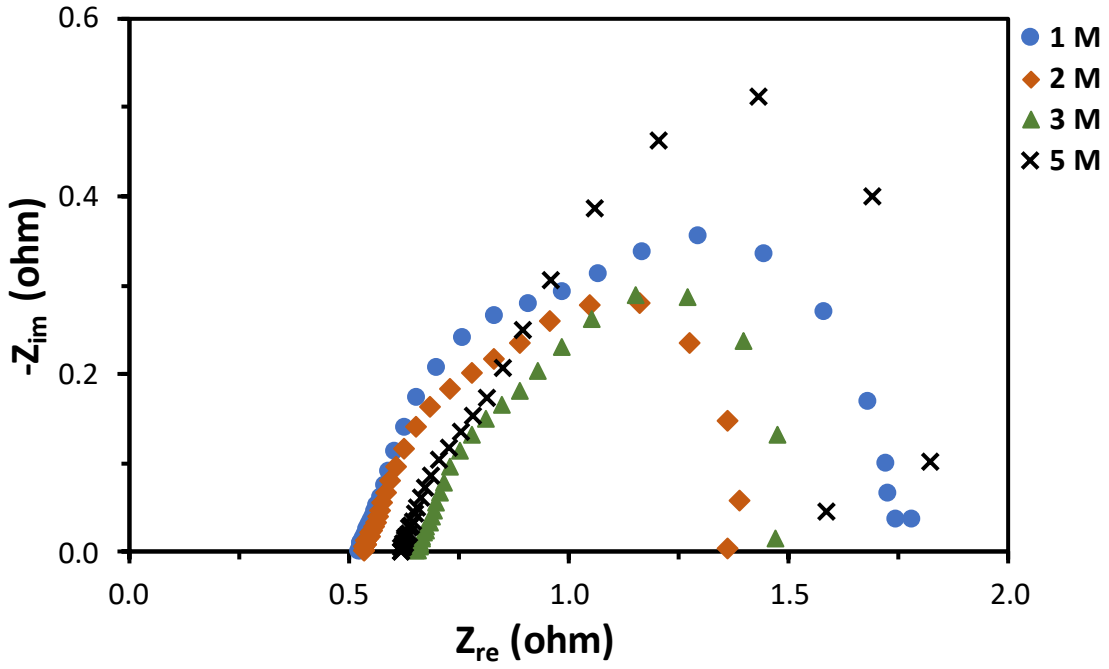

Figure A.50. Nyquist plot of a pDMFC for different methanol concentrations and 0.2 V using CP_T as CDL.

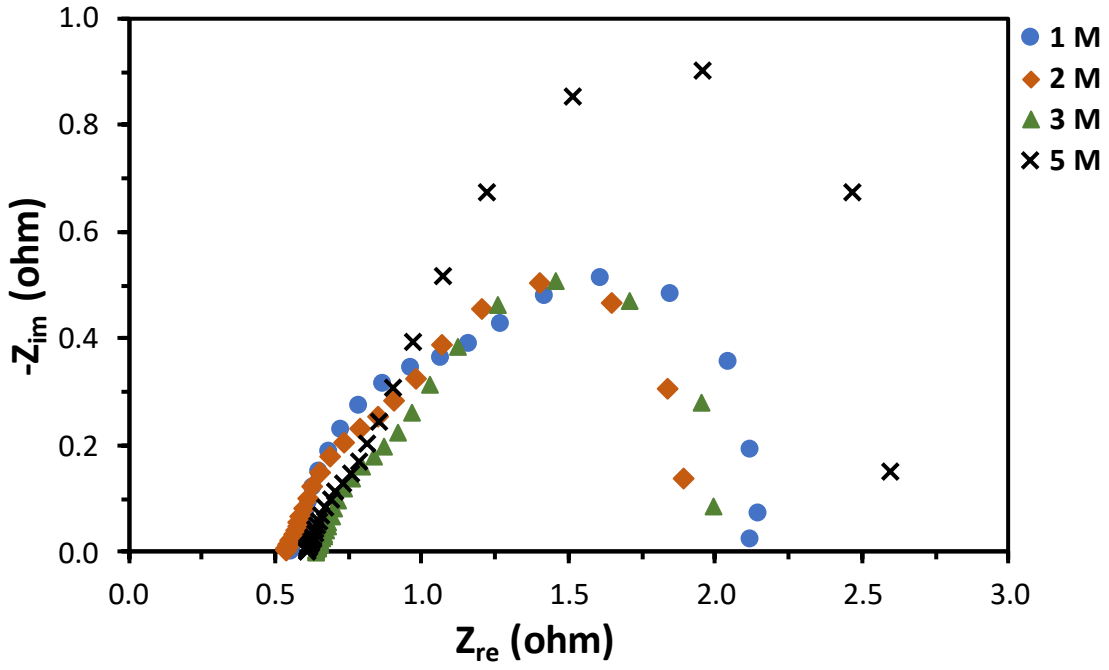

Figure A.51. Nyquist plot of a pDMFC for different methanol concentrations and 0.3 V using CP_T as CDL.

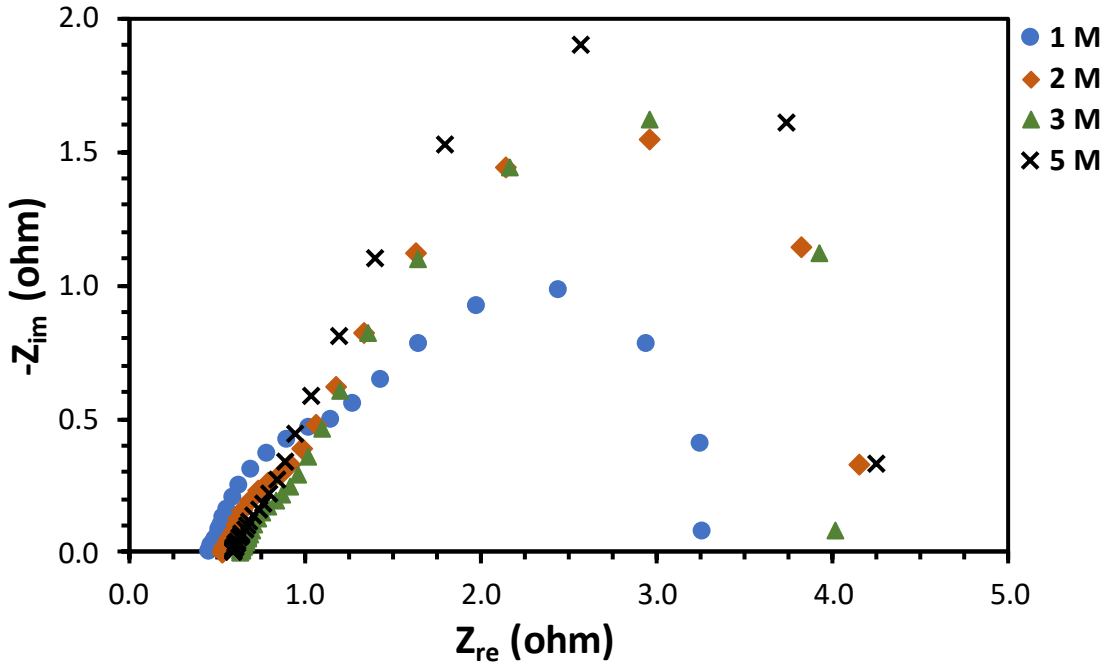

Figure A.52. Nyquist plot of a pDMFC for different methanol concentrations and 0.4 V using CP_T as CDL.

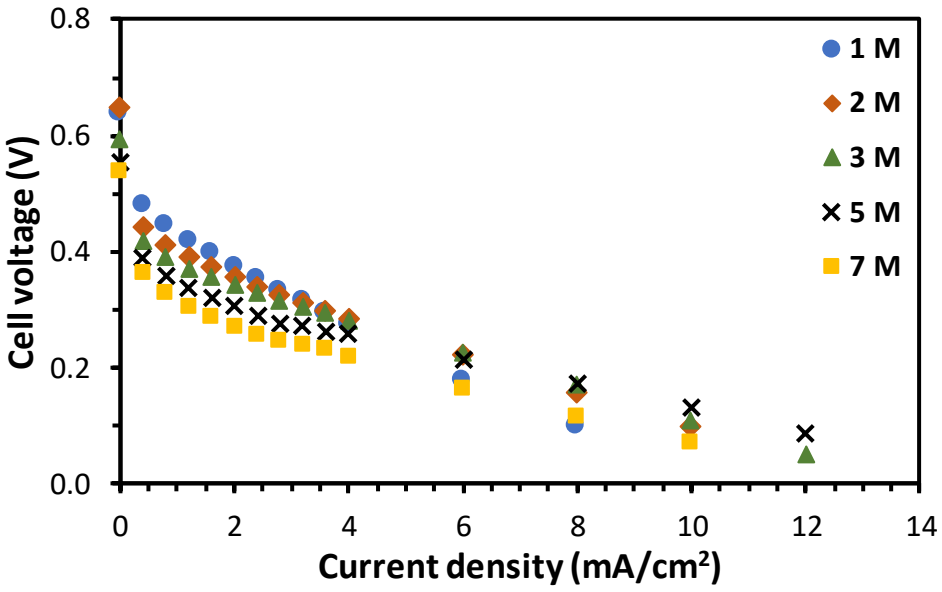

Figure A.53. Effect of methanol concentration on the cell performance using CP_MPL as CDL.

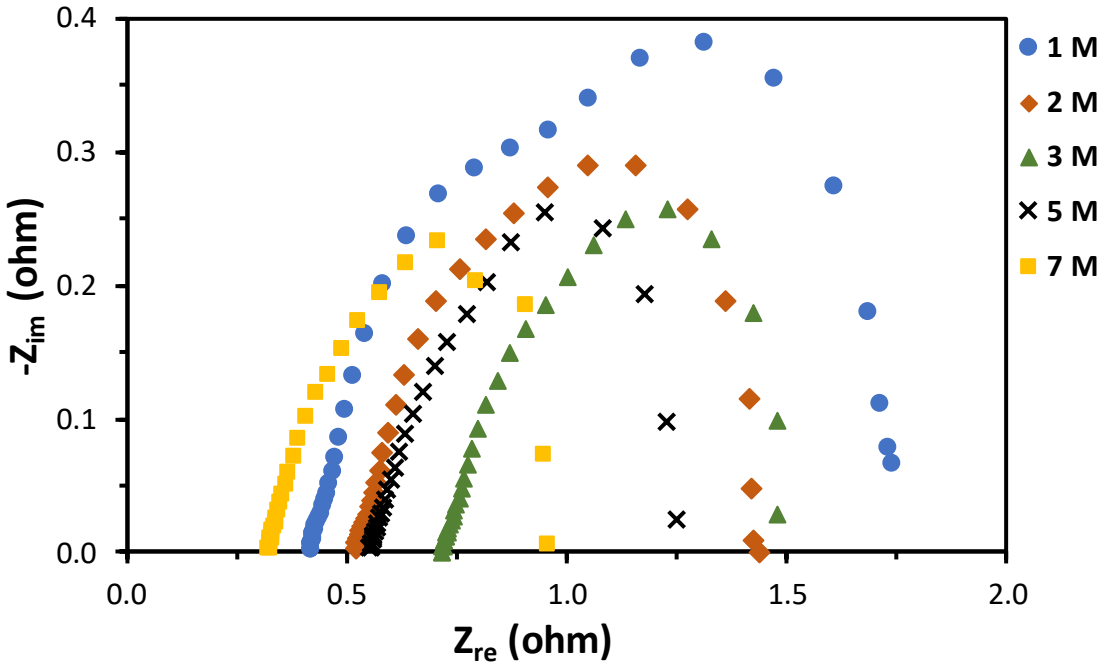

Figure A.54. Nyquist plot of a pDMFC for different methanol concentrations and 0.2 V using CP_MPL as CDL.

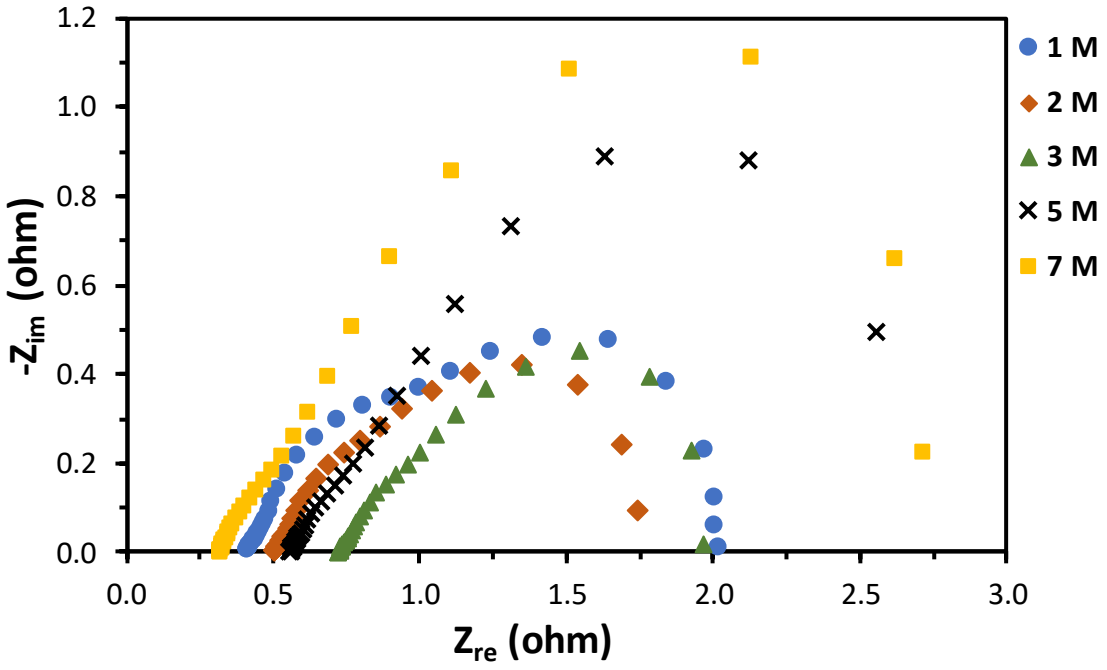

Figure A.55. Nyquist plot of a pDMFC for different methanol concentrations and 0.3 V using CP_MPL as CDL.

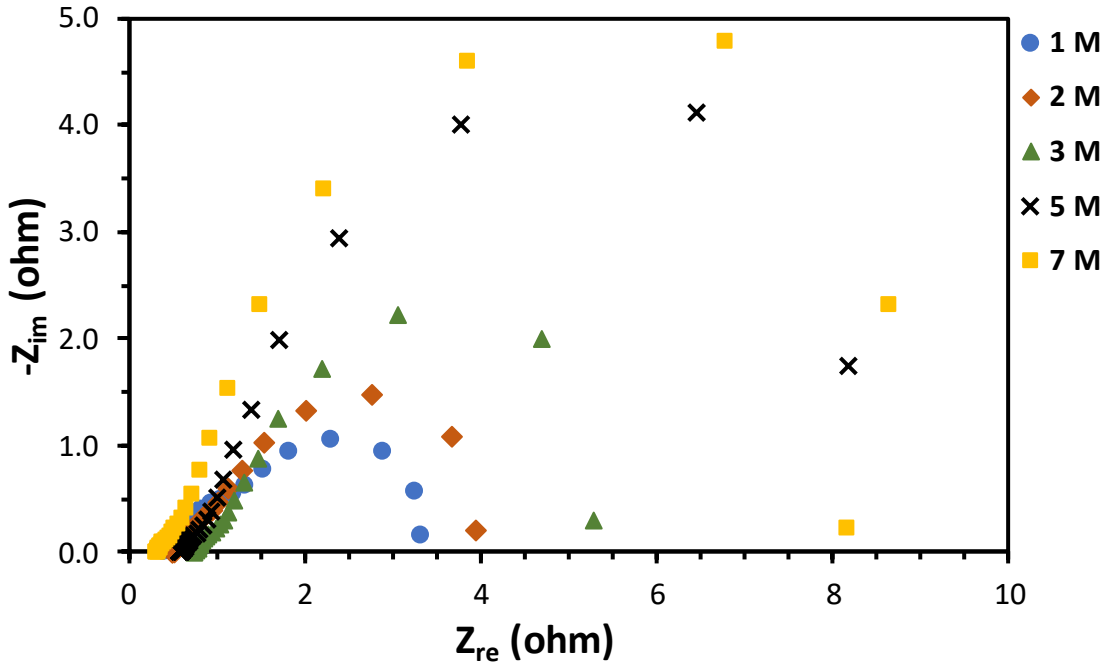

Figure A.56. Nyquist plot of a pDMFC for different methanol concentrations and 0.4 V using CP_MPL as CDL.

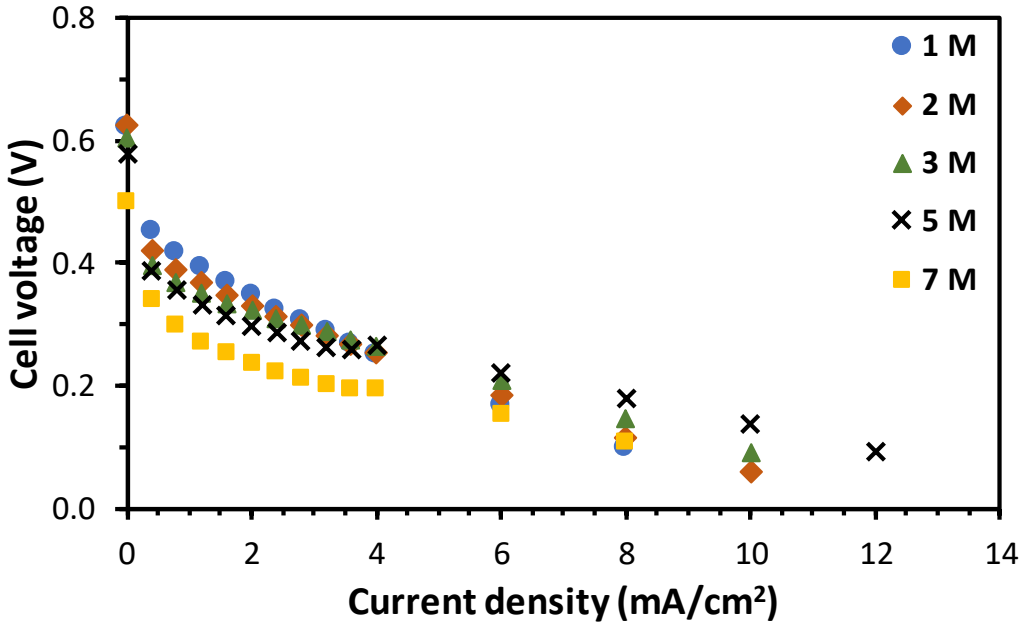

Figure A.57. Effect of methanol concentration on the cell performance using CP_MPL_T as CDL.

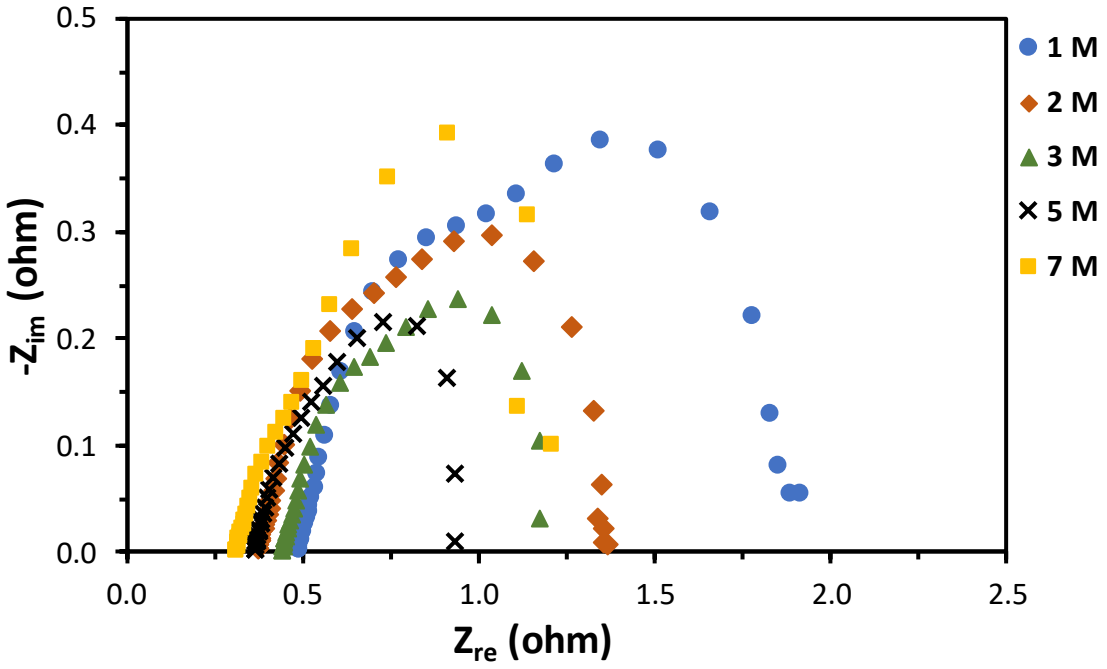

Figure A.58. Nyquist plot of a pDMFC for different methanol concentrations and 0.2 V using CP_MPL_T as CDL.

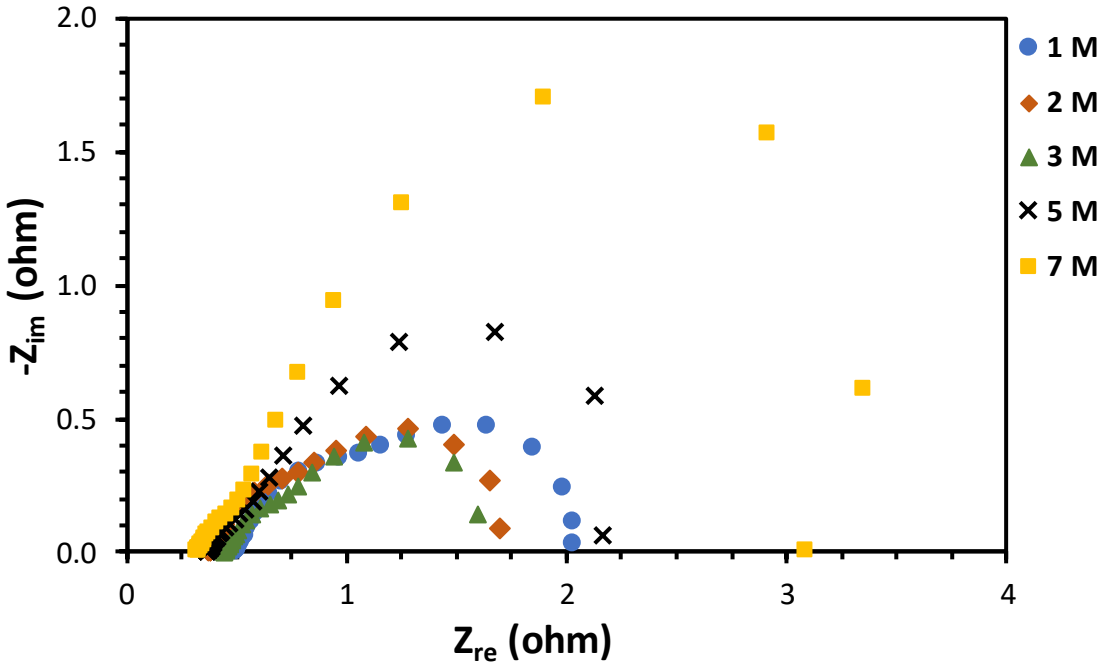

Figure A.59. Nyquist plot of a pDMFC for different methanol concentrations and 0.3 V using CP_MPL_T as CDL.

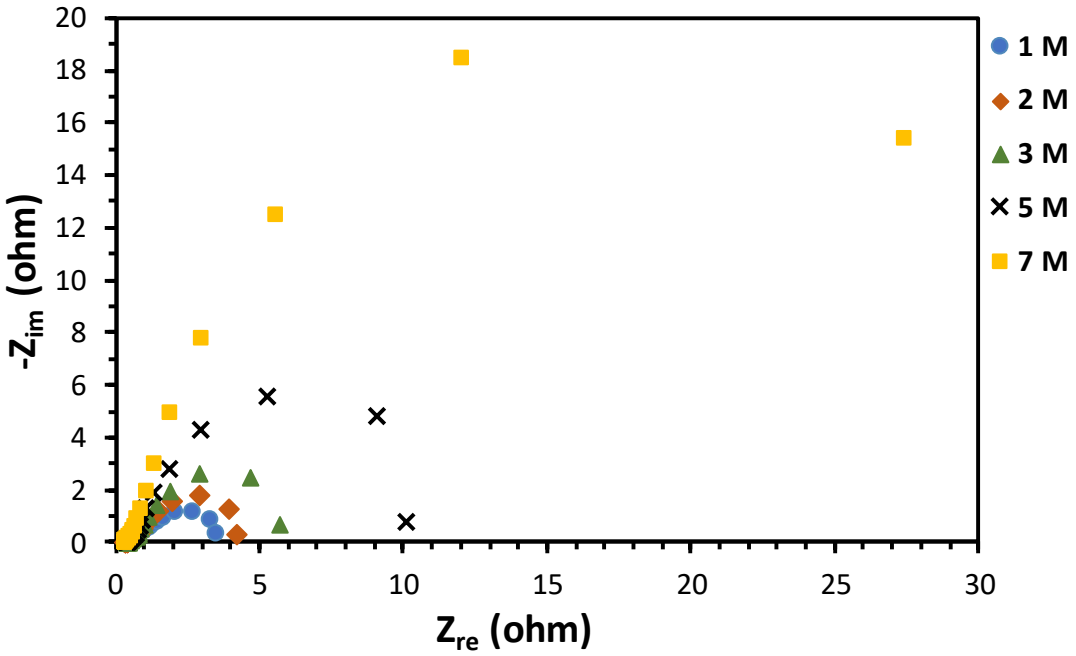

Figure A.60. Nyquist plot of a pDMFC for different methanol concentrations and 0.4 V using CP_MPL_T as CDL.

A.3. Effect of anode current collector design

All the results presented in this section were obtained with a stainless steel current collector, with an open ratio of 41 % (CC_2), at the cathode side and with CC_MPL as anode DL and CC as cathode DL.

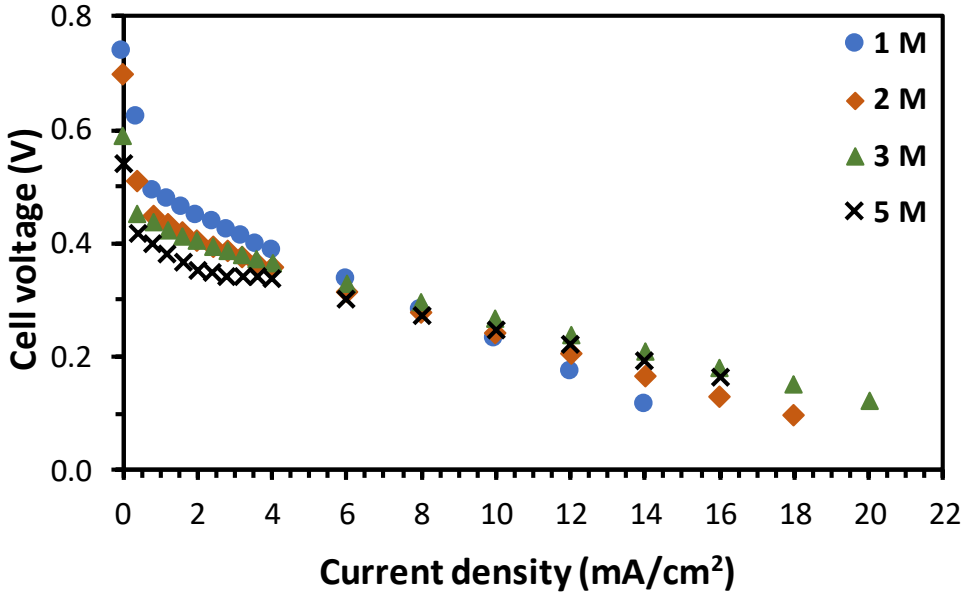

Figure A.61. Effect of methanol concentration on the cell performance using CC_1 as anode CC.

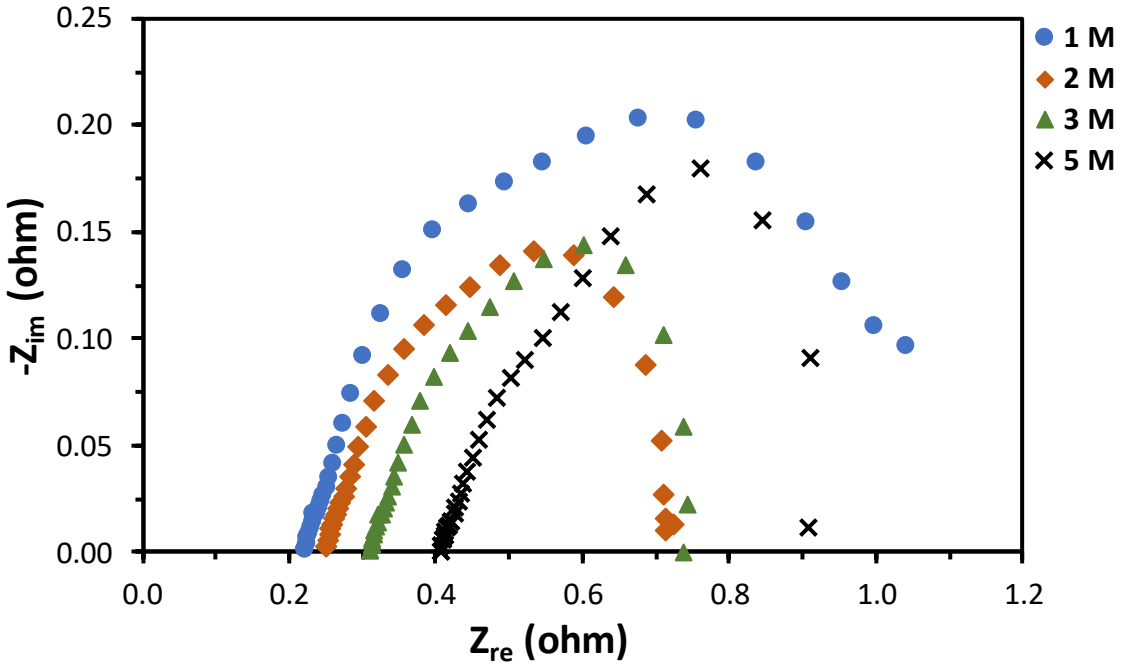

Figure A.62. Nyquist plot of a pDMFC for different methanol concentrations and 0.2 V using CC_1 as anode CC.

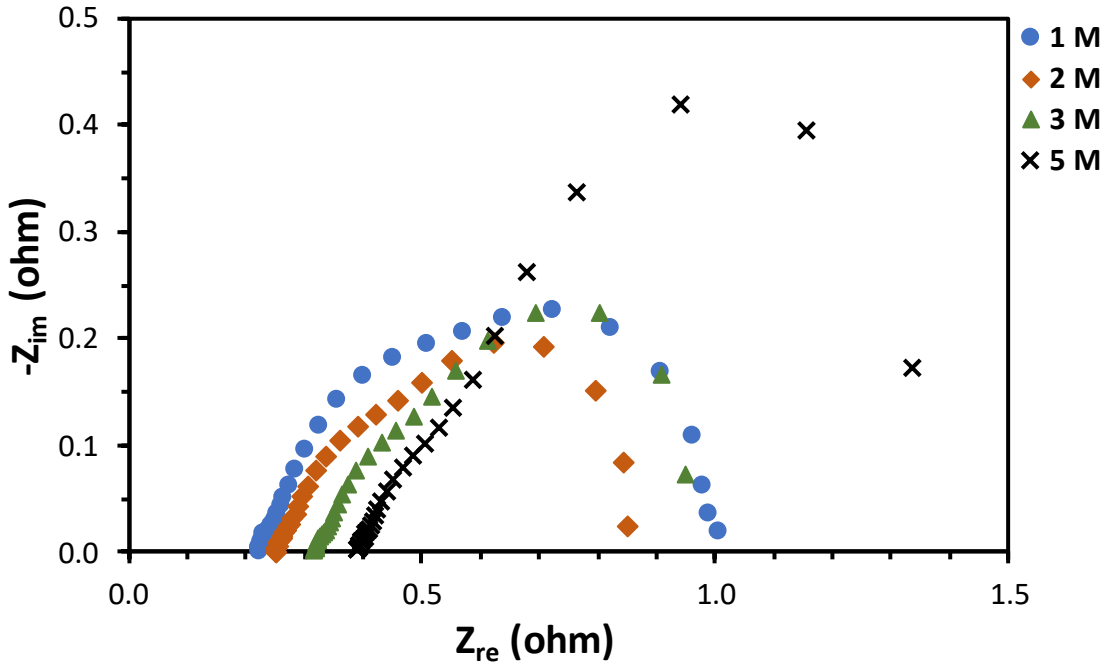

Figure A.63. Nyquist plot of a pDMFC for different methanol concentrations and 0.3 V using CC_1 as anode CC.

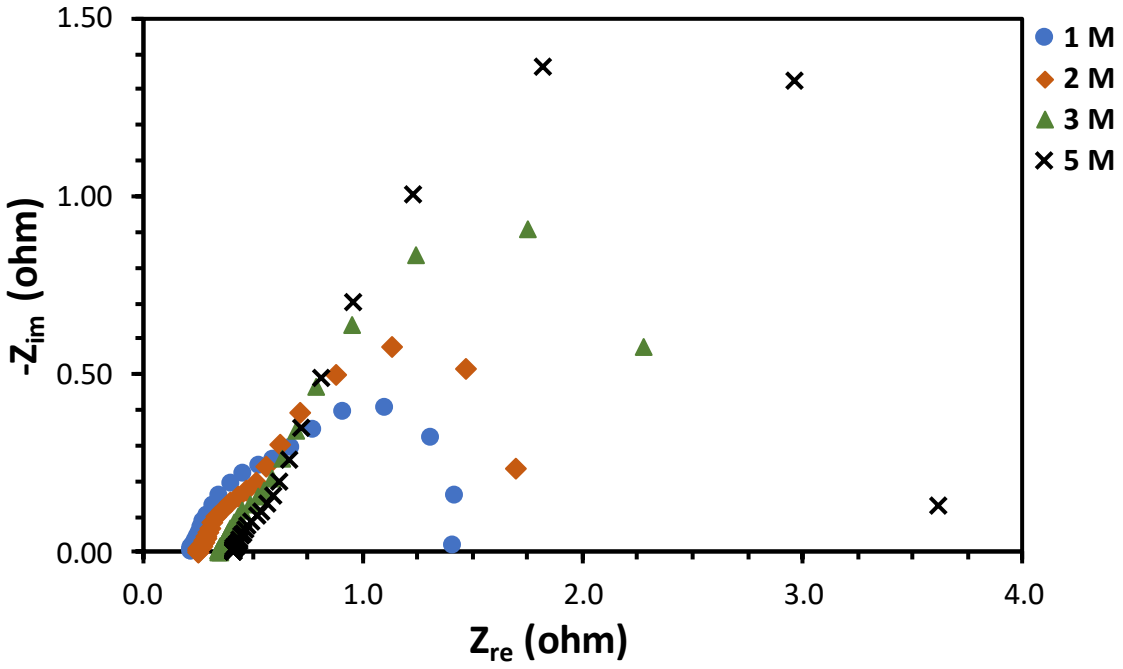

Figure A.64. Nyquist plot of a pDMFC for different methanol concentrations and 0.4 V using CC_1 as anode CC.

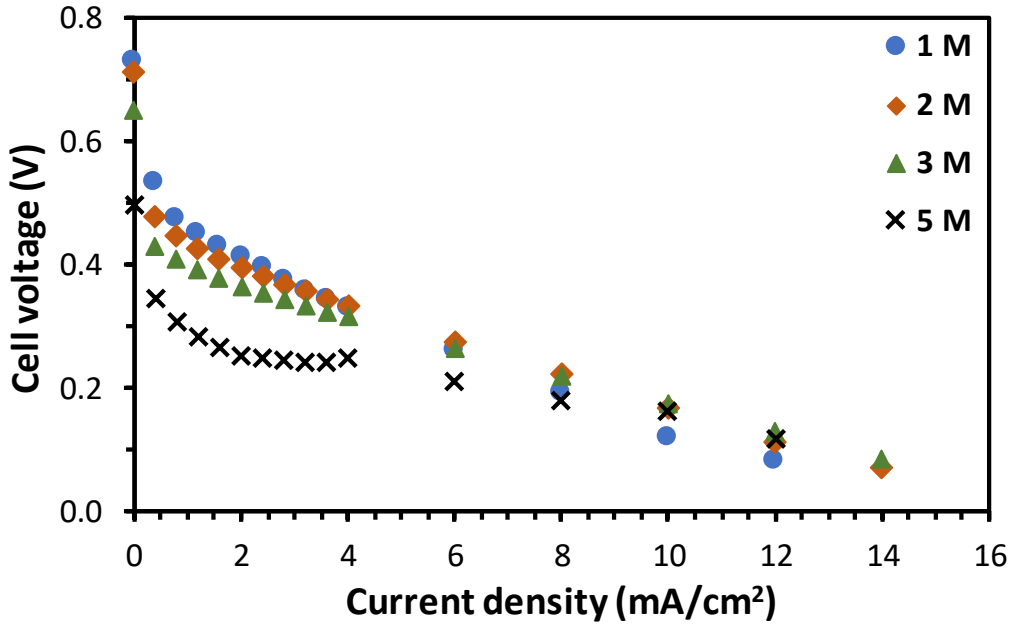

Figure A.65. Effect of methanol concentration on the cell performance using CC_3 as anode CC.

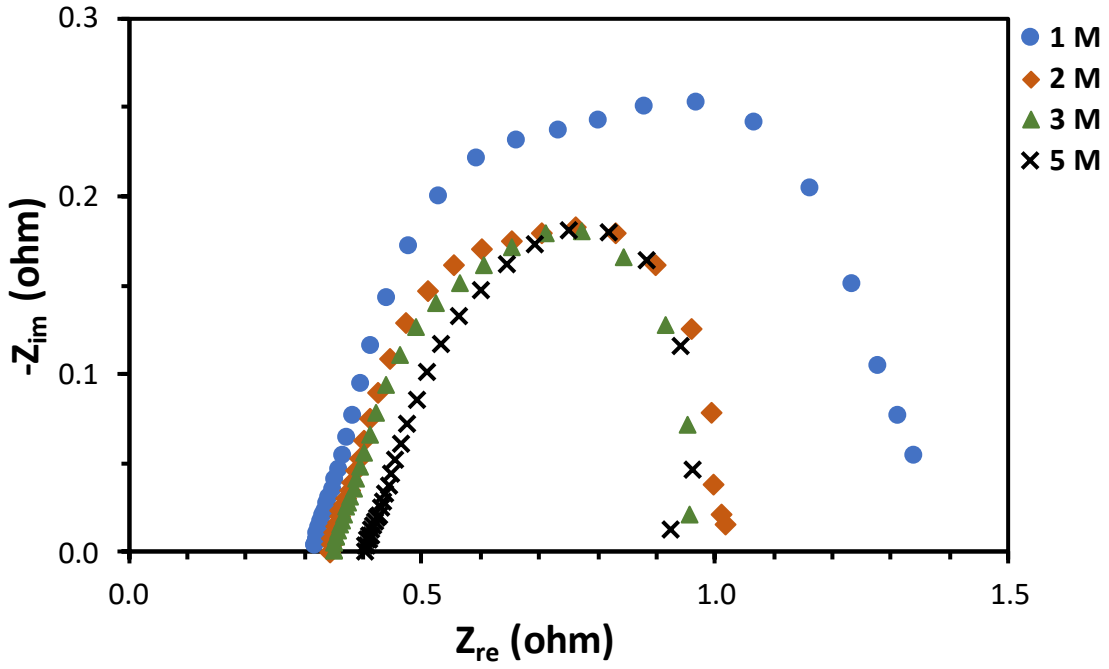

Figure A.66. Nyquist plot of a pDMFC for different methanol concentrations and 0.2 V using CC_3 as anode CC.

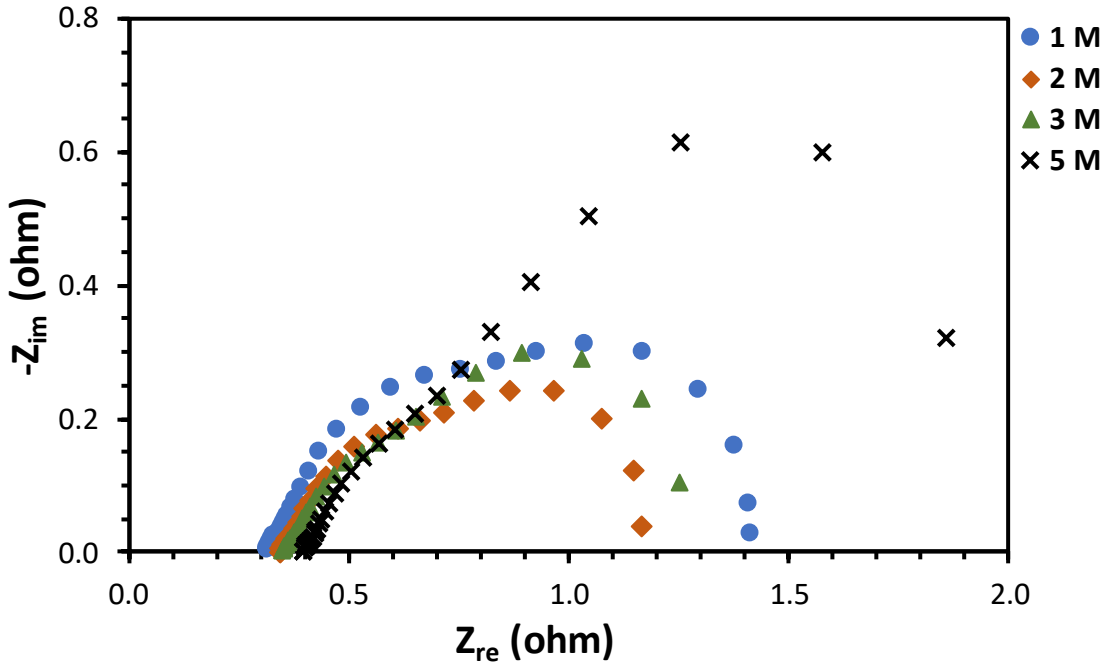

Figure A.67. Nyquist plot of a pDMFC for different methanol concentrations and 0.3 V using CC_3 as anode CC.

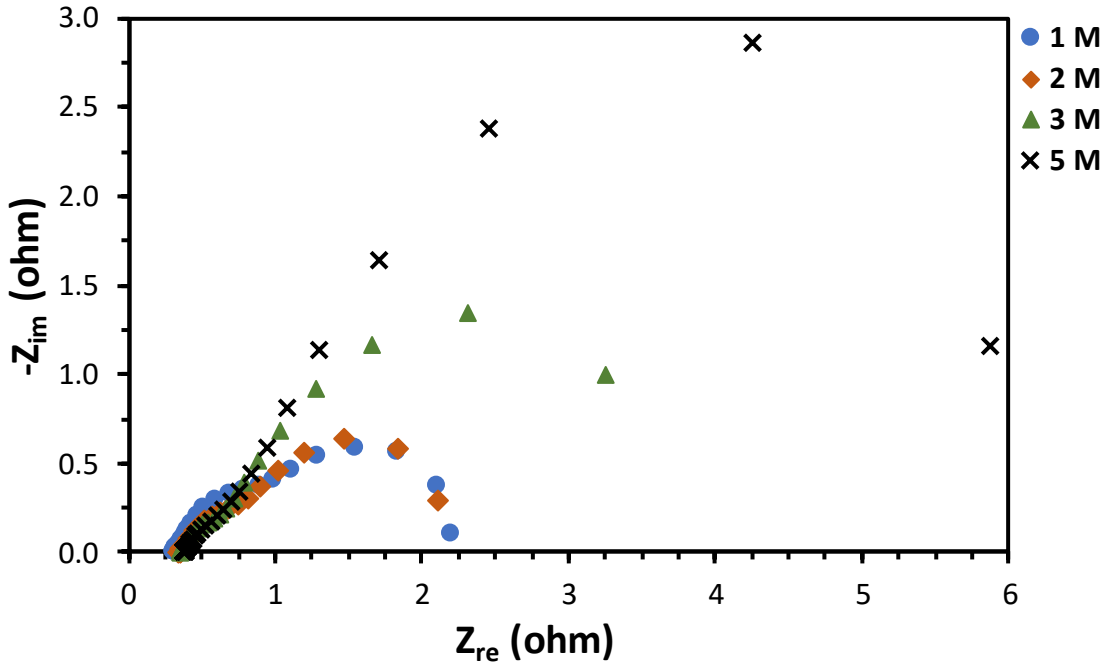

Figure A.68. Nyquist plot of a pDMFC for different methanol concentrations and 0.4 V using CC_3 as anode CC.

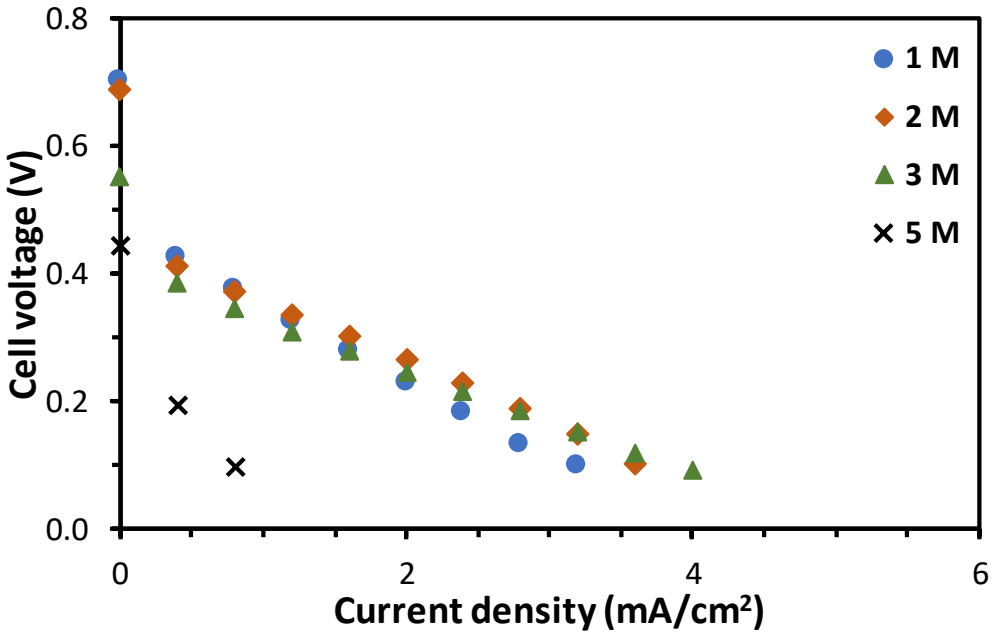

Figure A.69. Effect of methanol concentration on the cell performance using CC_4 as anode CC.

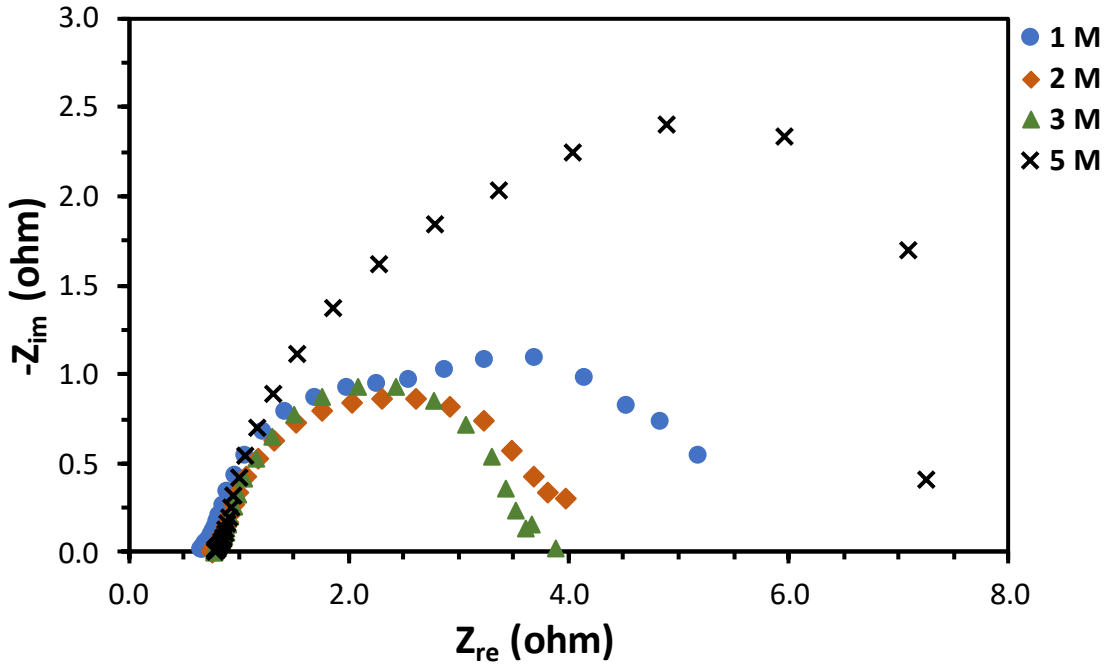

Figure A.70. Nyquist plot of a pDMFC for different methanol concentrations and 0.2 V using CC_4 as anode CC.

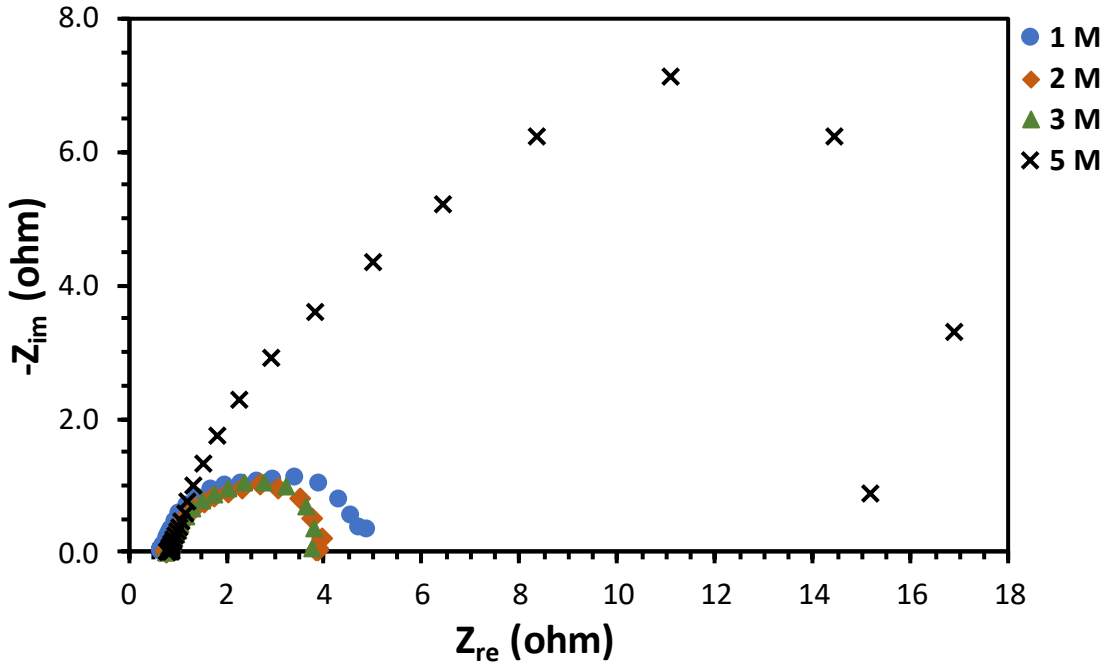

Figure A.71. Nyquist plot of a pDMFC for different methanol concentrations and 0.3 V using CC_4 as anode CC.

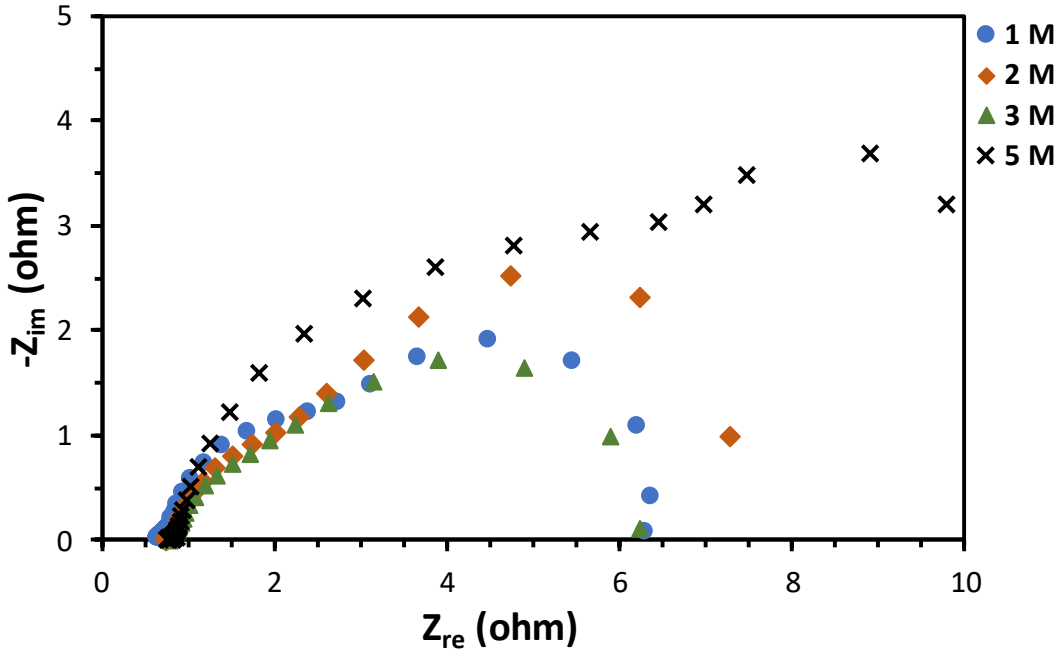

Figure A.72. Nyquist plot of a pDMFC for different methanol concentrations and 0.4 V using CC_4 as anode CC.

A.4. Effect of cathode current collector design

All the results presented in this section were obtained with a stainless steel current collector, with an open ratio of 41 % (CC_2), at the anode side and with CC_MPL as anode DL and CC as cathode DL.

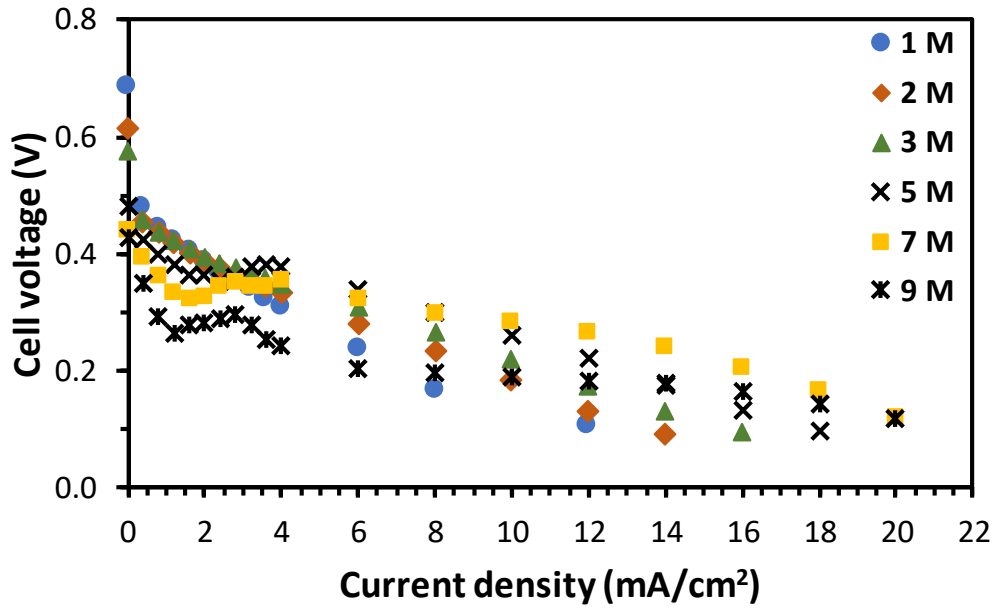

Figure A.73. Effect of methanol concentration on the cell performance using CC_1 as cathode CC.

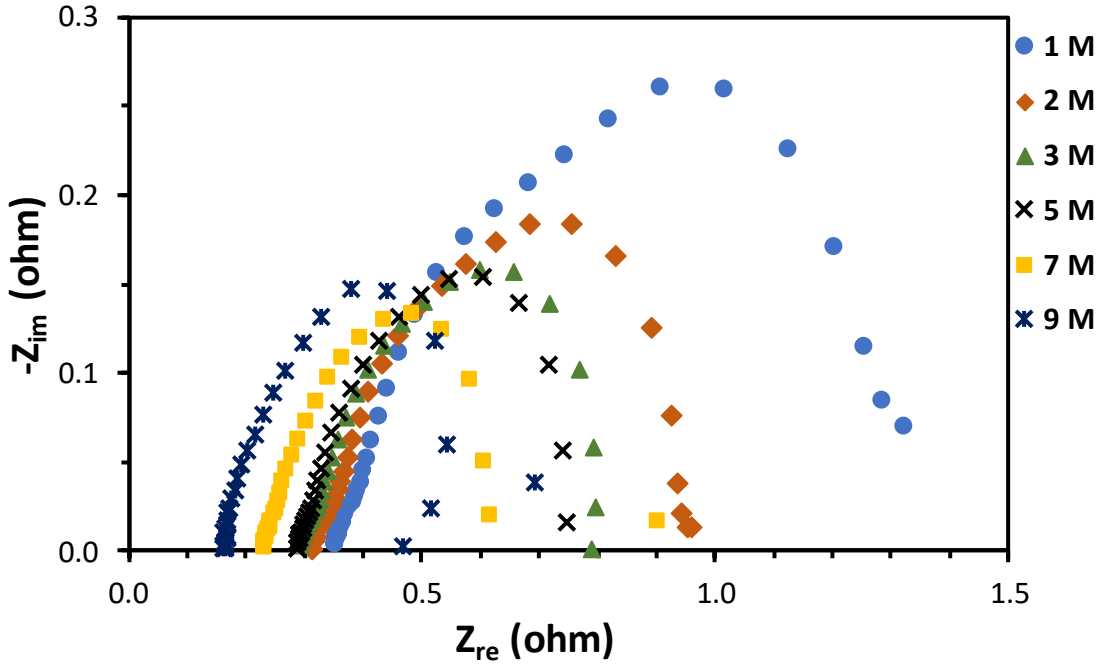

Figure A.74. Nyquist plot of a pDMFC for different methanol concentrations and 0.2 V using CC_1 as cathode CC.

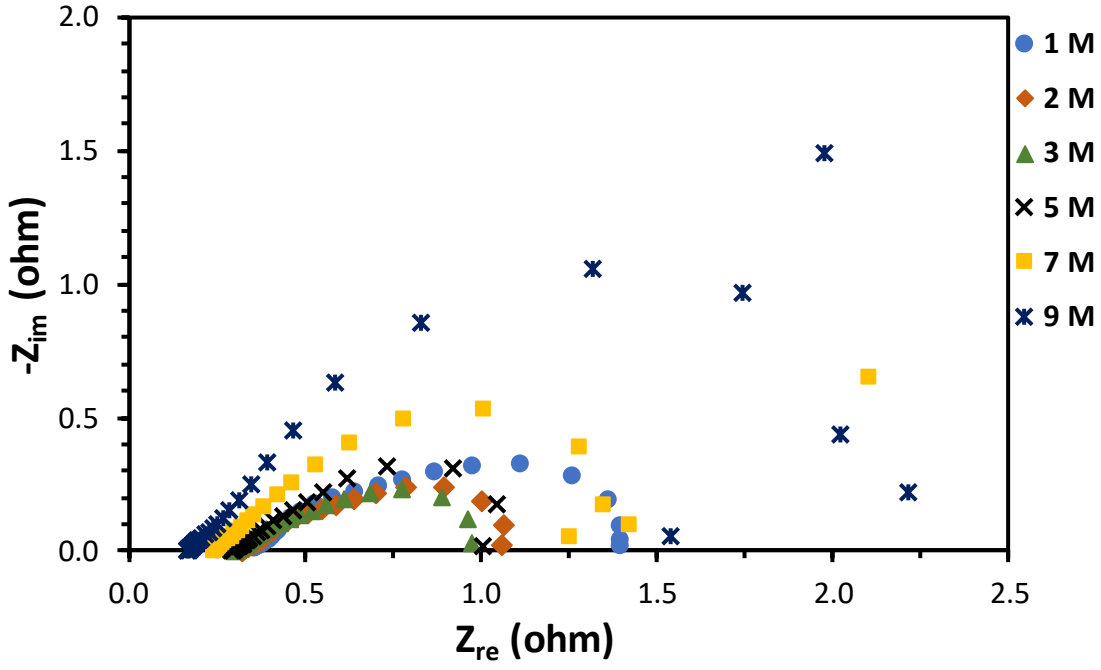

Figure A.75. Nyquist plot of a pDMFC for different methanol concentrations and 0.3 V using CC_1 as cathode CC.

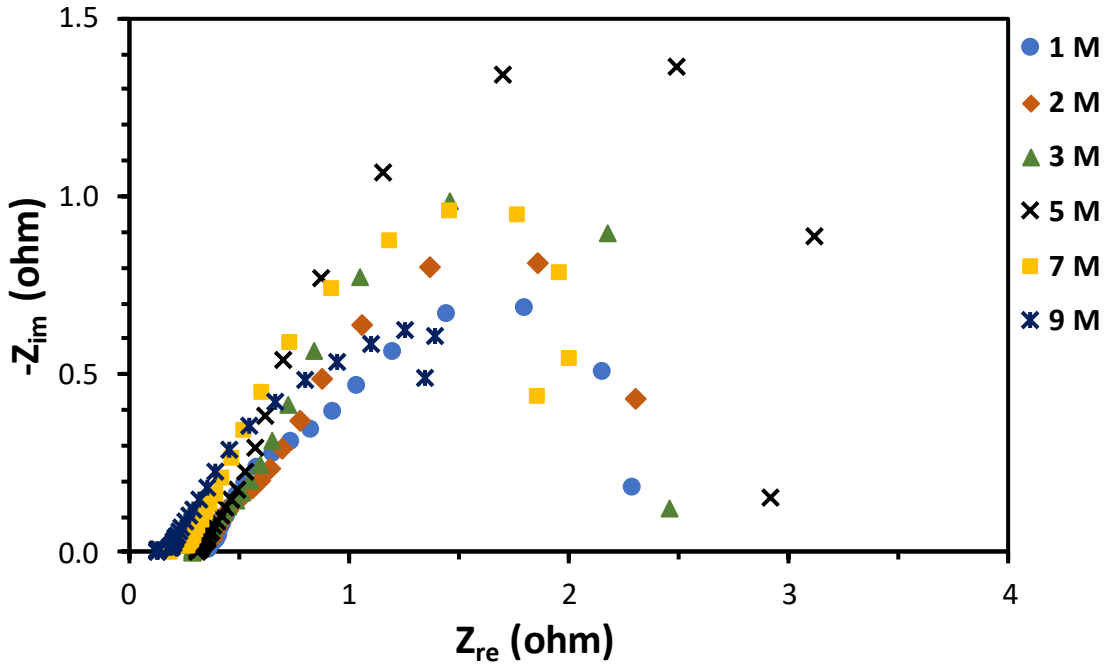

Figure A.76. Nyquist plot of a pDMFC for different methanol concentrations and 0.4 V using CC_1 as cathode CC.

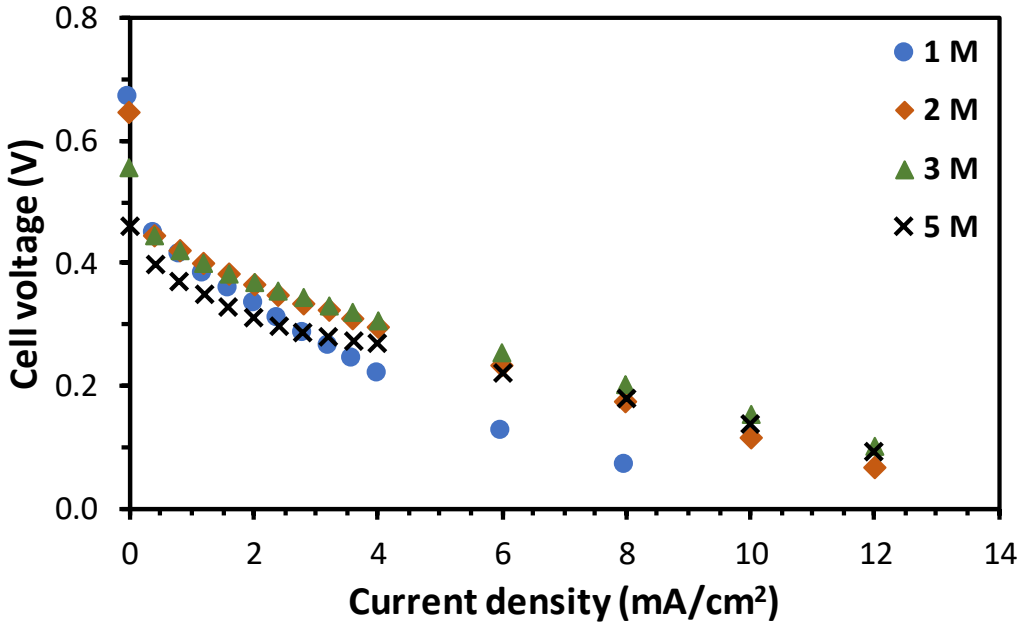

Figure A.77. Effect of methanol concentration on the cell performance using CC_3 as cathode CC.

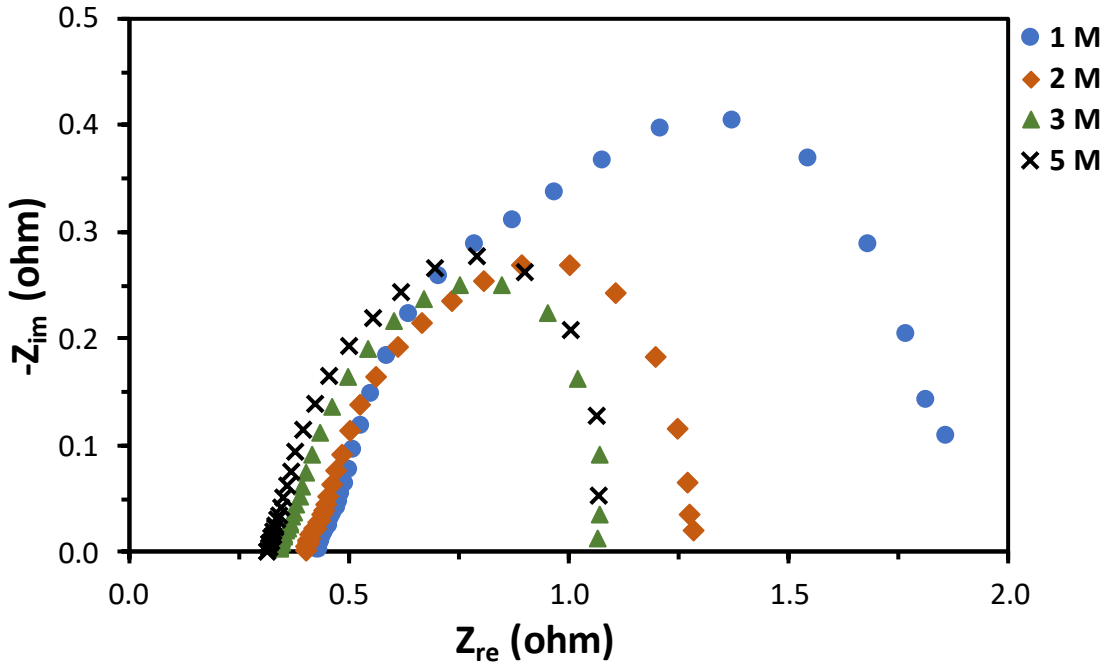

Figure A.78. Nyquist plot of a pDMFC for different methanol concentrations and 0.2 V using CC_3 as cathode CC.

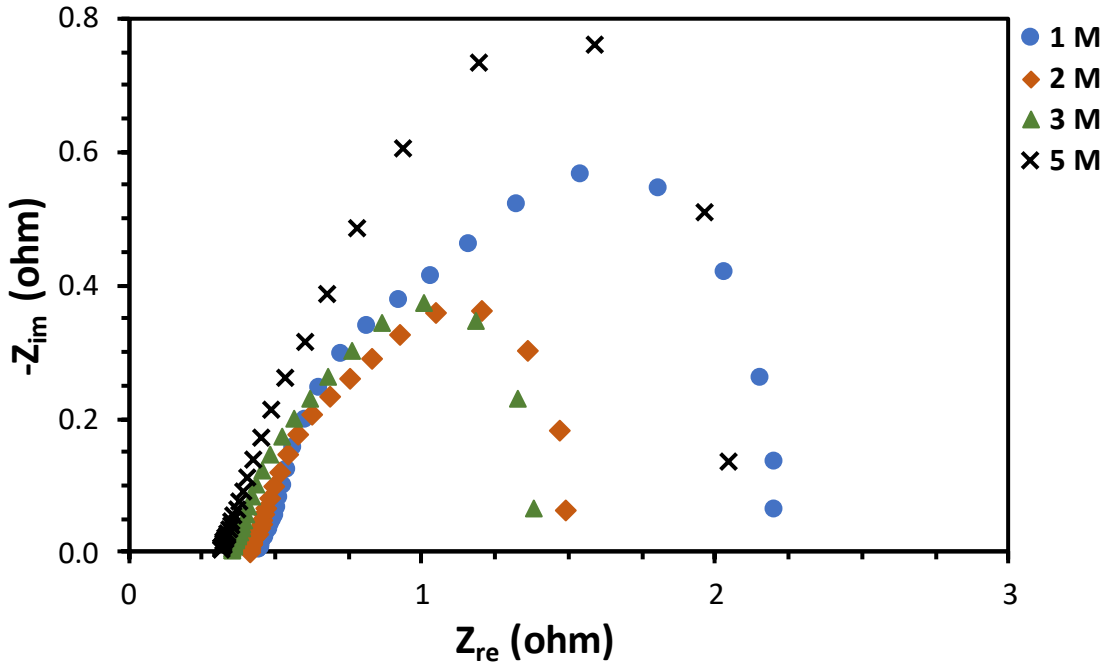

Figure A.79. Nyquist plot of a pDMFC for different methanol concentrations and 0.3 V using CC_3 as cathode CC.

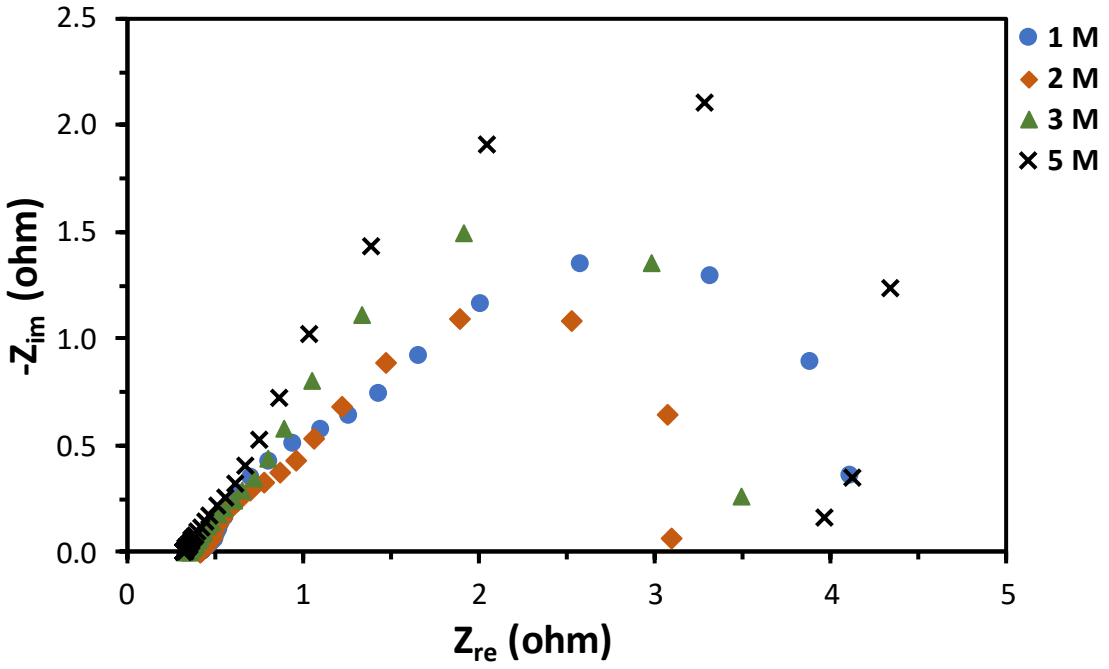

Figure A.80. Nyquist plot of a pDMFC for different methanol concentrations and 0.4 V using CC_3 as cathode CC.

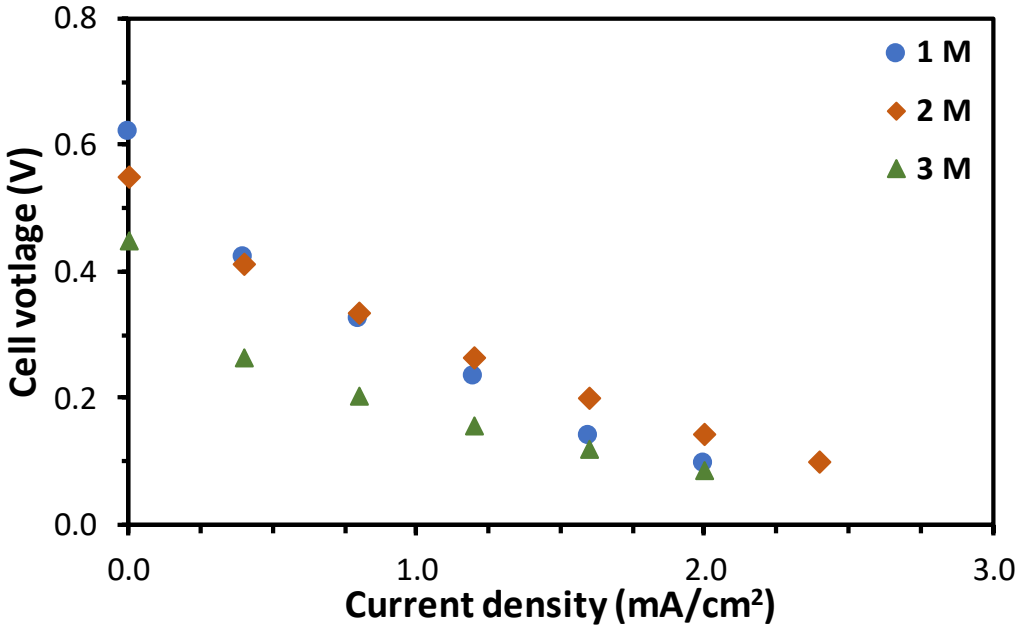

Figure A.81. Effect of methanol concentration on the cell performance using CC_4 as cathode CC.

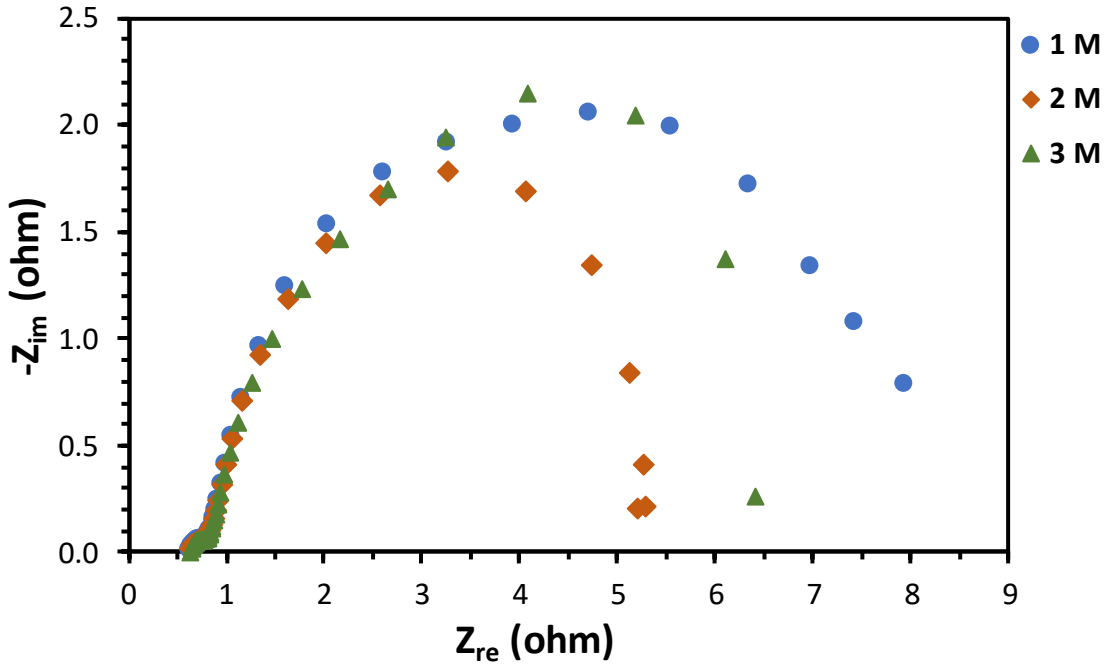

Figure A.82. Nyquist plot of a pDMFC for different methanol concentrations and 0.2 V using CC_4 as cathode CC.

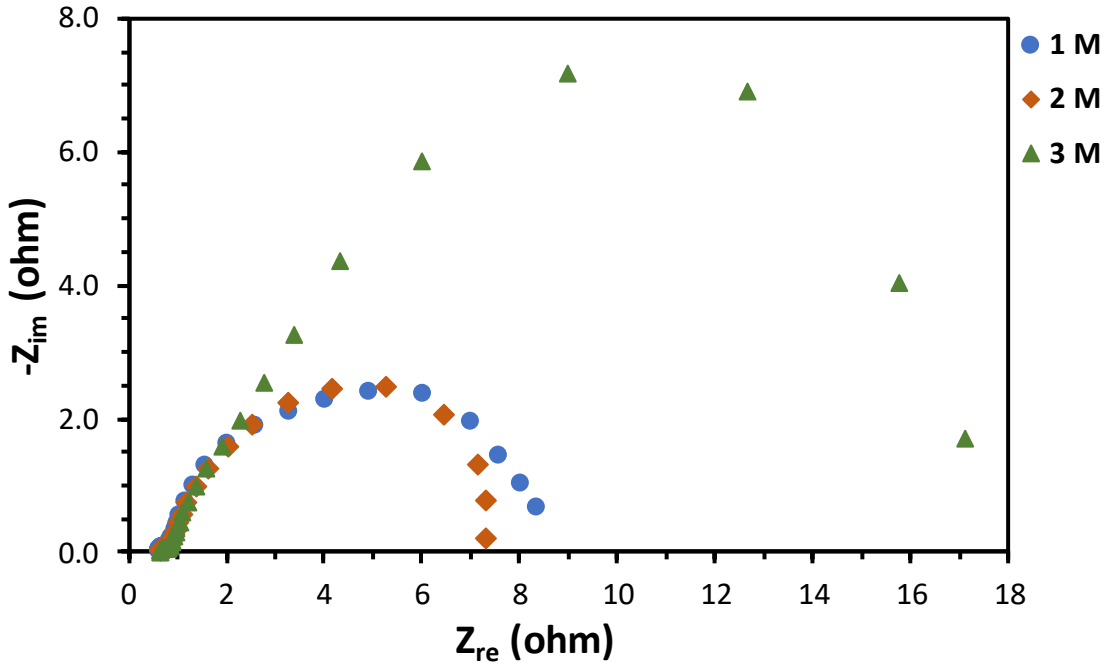

Figure A.83. Nyquist plot of a pDMFC for different methanol concentrations and 0.3 V using CC_4 as cathode CC.

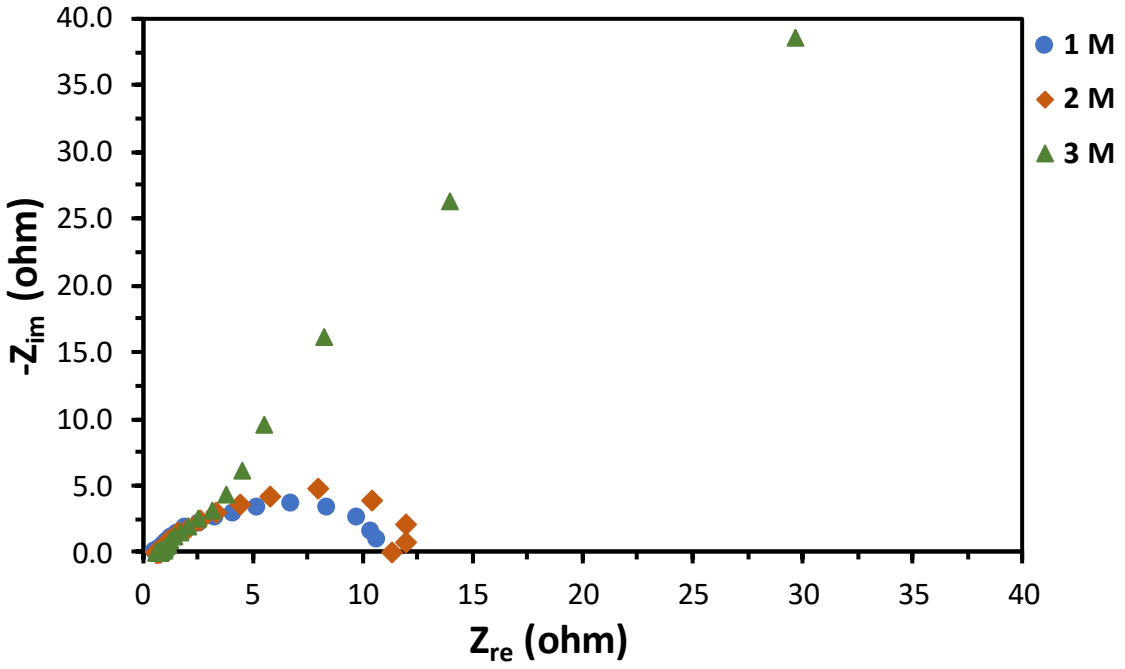

Figure A.84. Nyquist plot of a pDMFC for different methanol concentrations and 0.4 V using CC_4 as cathode CC.

A.5. Optimised current collectors design

All the results presented in this section were obtained with stainless steel current collectors at the anode and cathode sides and with CC_MPL as anode DL and CC as cathode DL.

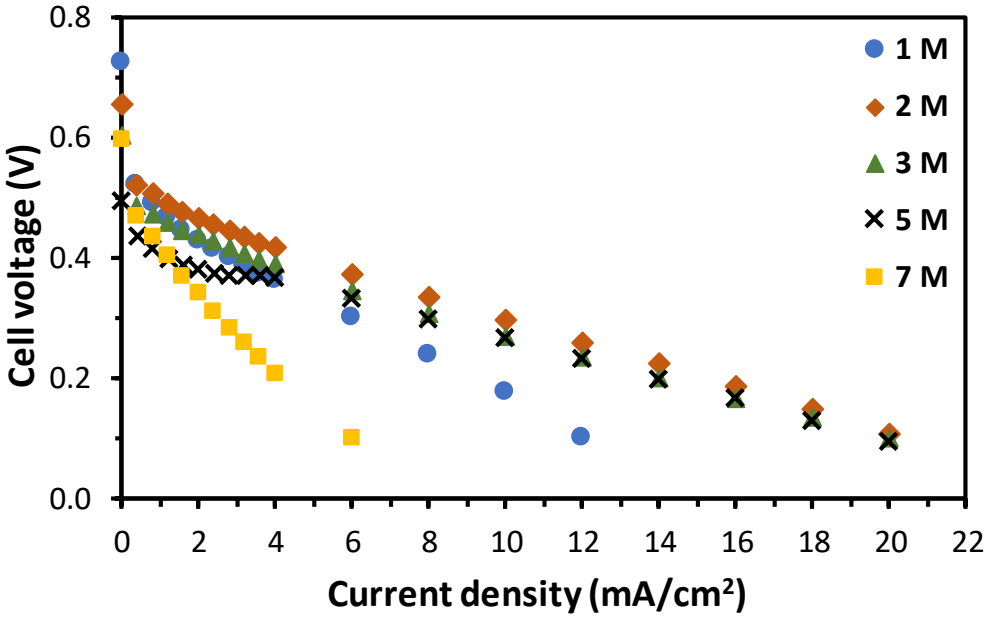

Figure A.85. Effect of methanol concentration on the cell performance using CC_1 as anode and cathode CC.

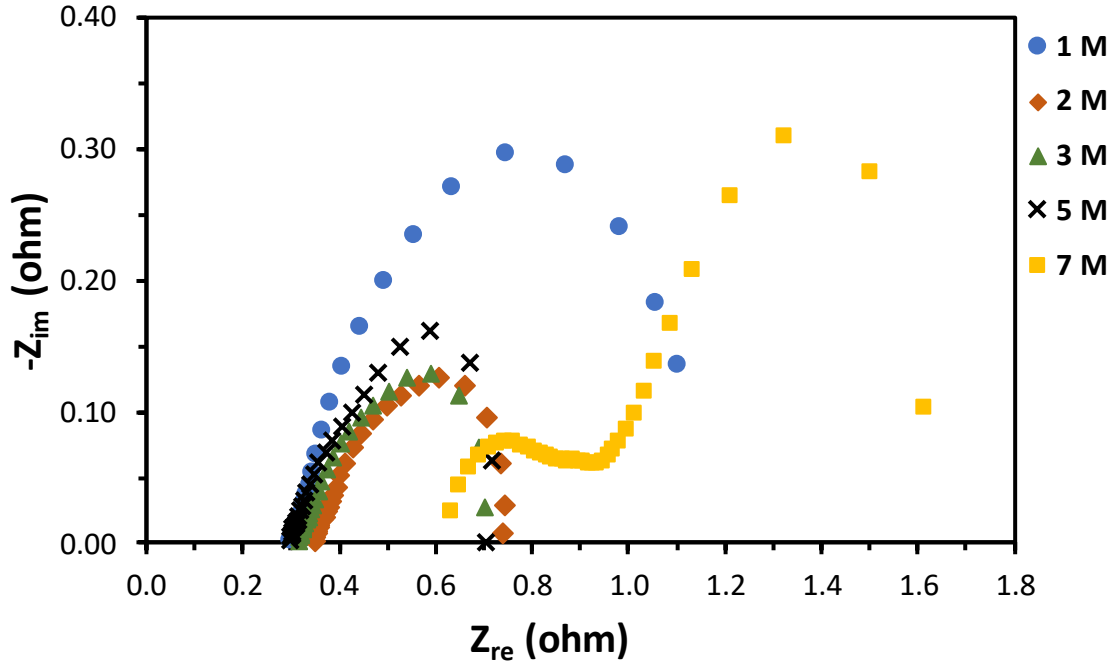

Figure A.86. Nyquist plot of a pDMFC for different methanol concentrations and 0.2 V using CC_1 as anode and cathode CC.

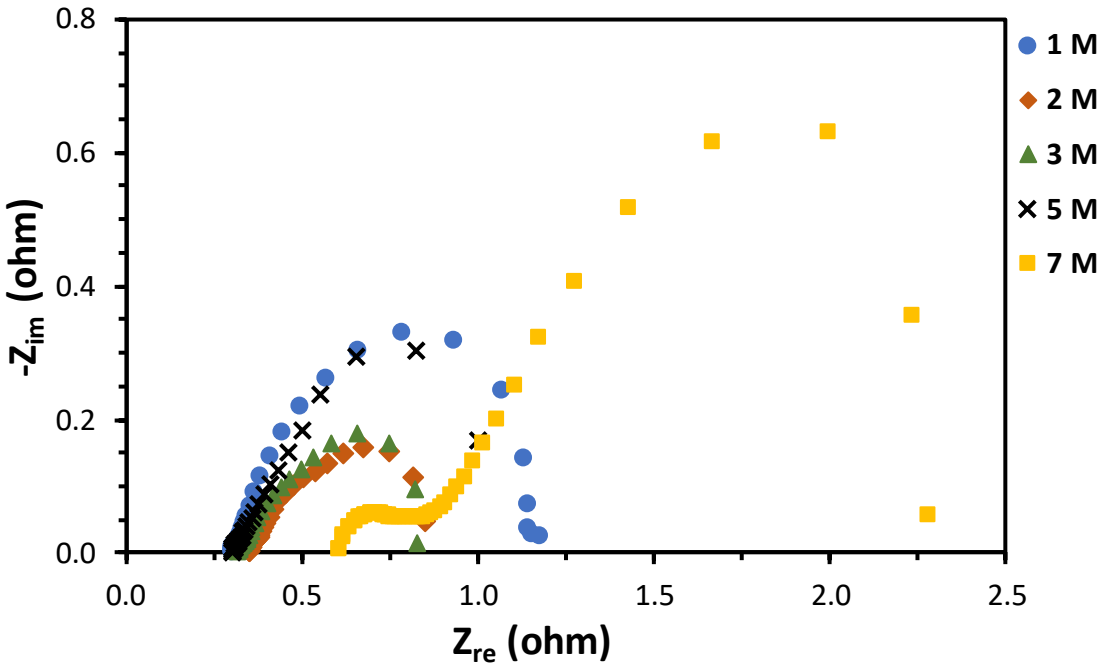

Figure A.87. Nyquist plot of a pDMFC for different methanol concentrations and 0.3 V using CC_1 as anode and cathode CC.

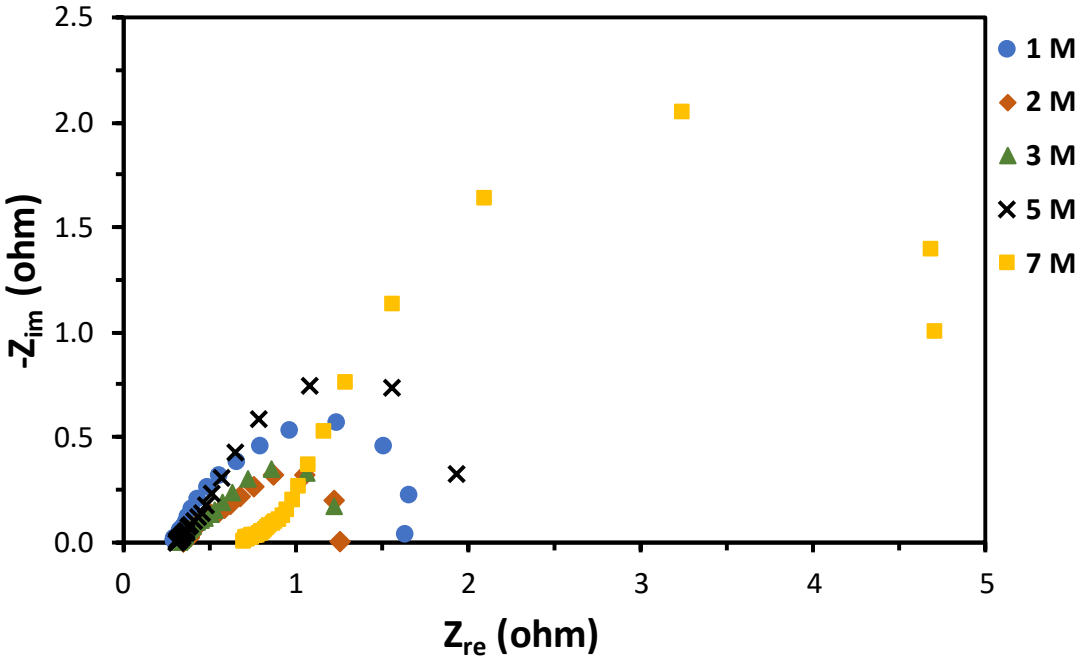

Figure A.88. Nyquist plot of a pDMFC for different methanol concentrations and 0.4 V using CC_1 as anode and cathode CC.

A.6. Effect of anode current collector material

All the results presented in this section were obtained with a stainless steel current collector, with an open ratio of 34 % (CC_1), at the cathode side and with CC_MPL as anode DL and CC as cathode DL.

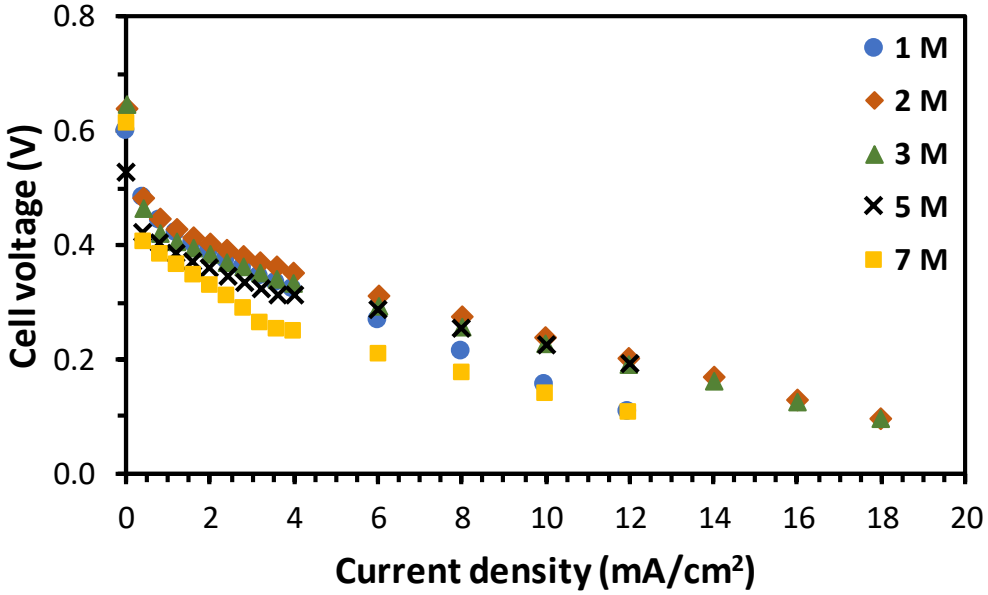

Figure A.89. Effect of methanol concentration on the cell performance using SS+Au as anode CC with an open ratio of 41 % (CC_2).

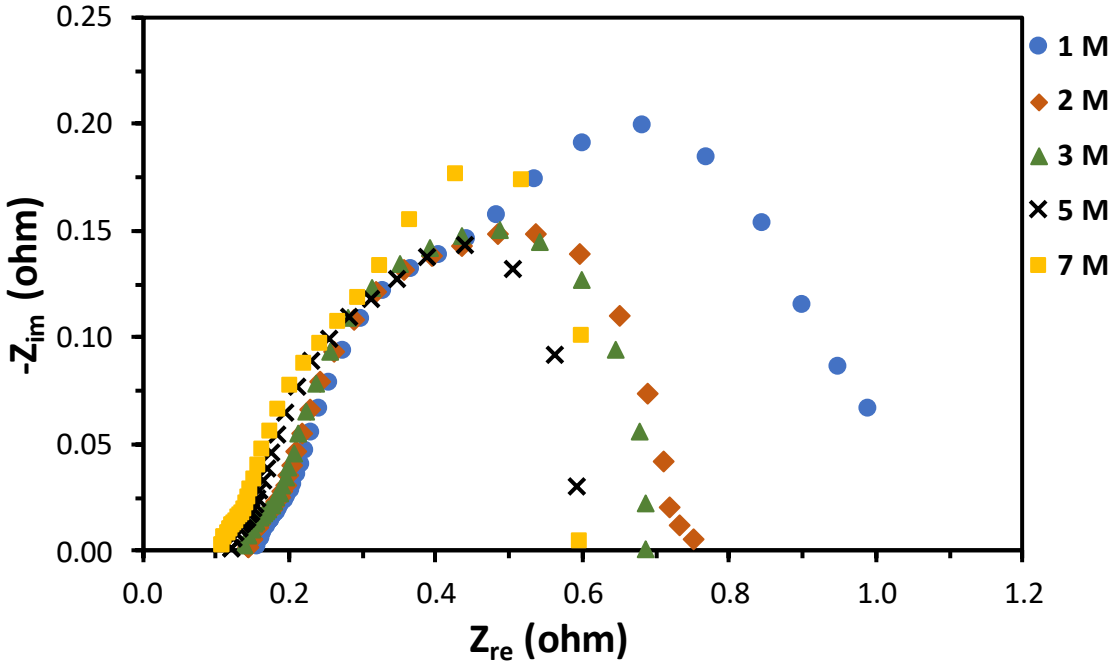

Figure A.90. Nyquist plot of a pDMFC for different methanol concentrations and 0.2 V using SS+Au as anode CC with an open ratio of 41 % (CC_2).

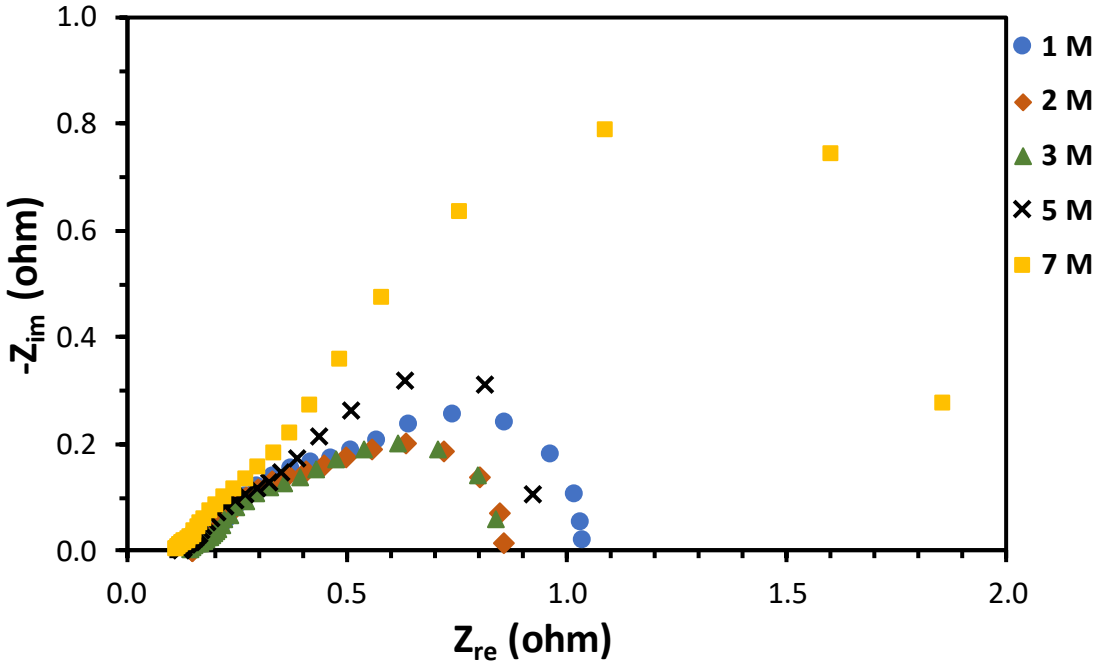

Figure A.91. Nyquist plot of a pDMFC for different methanol concentrations and 0.3 V using SS+Au as anode CC with an open ratio of 41 % (CC_2).

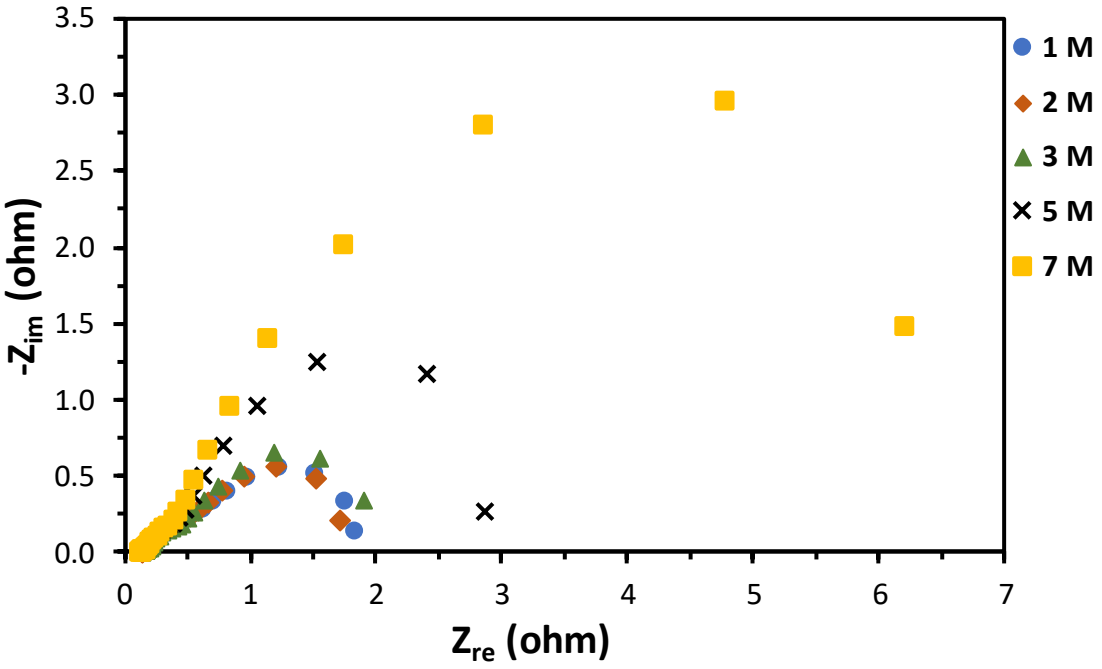

Figure A.92. Nyquist plot of a pDMFC for different methanol concentrations and 0.4 V using SS+Au as anode CC with an open ratio of 41 % (CC_2).

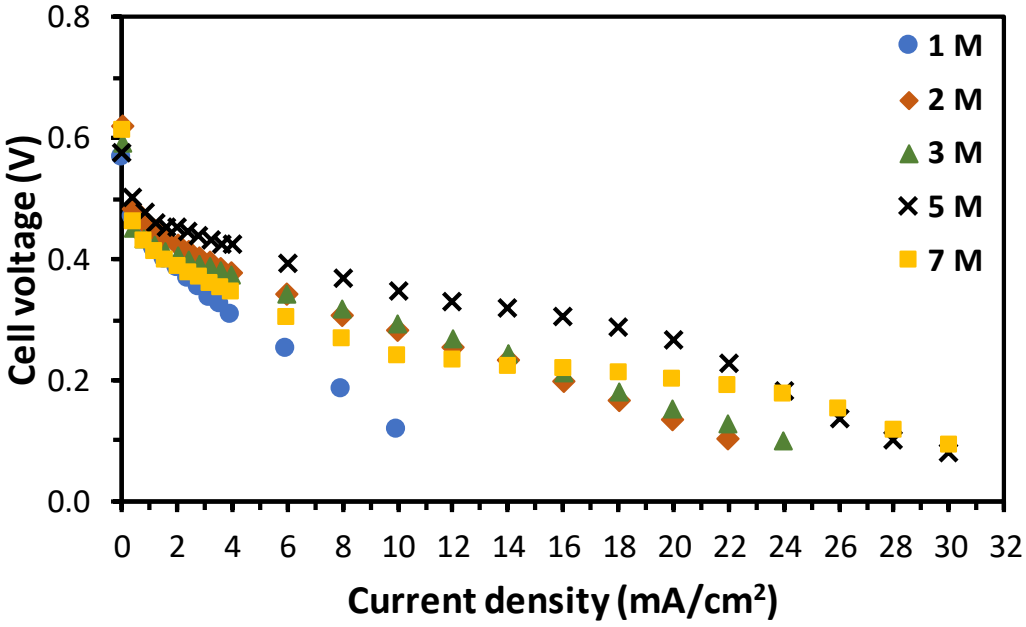

Figure A.93. Effect of methanol concentration on the cell performance using SS+Au as anode CC with an open ratio of 34 % (CC_1).

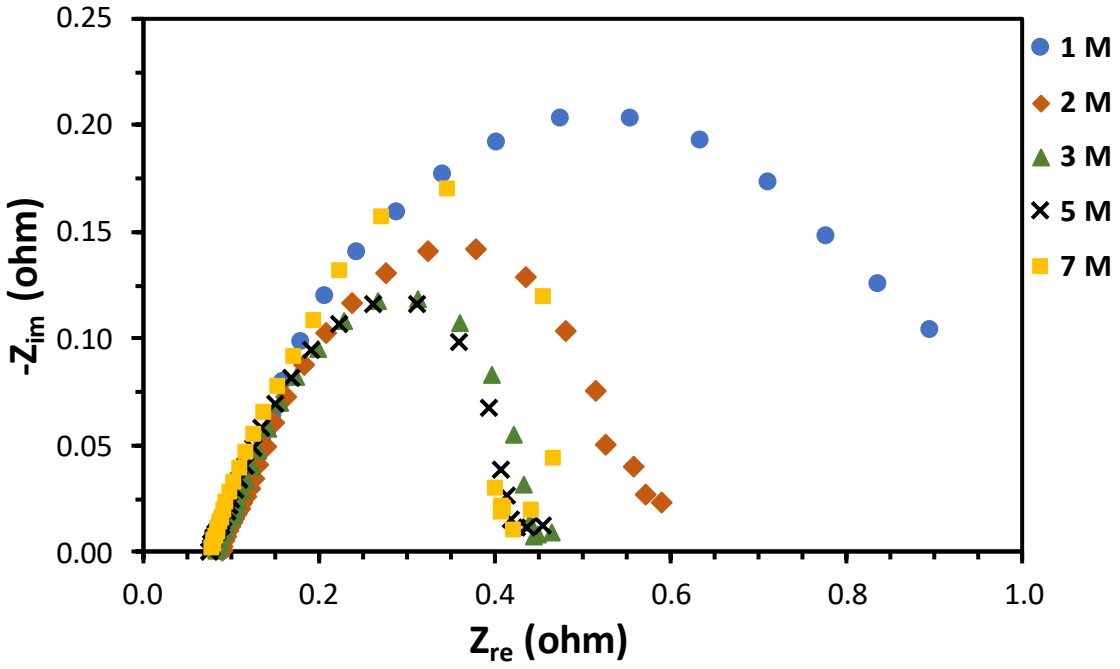

Figure A.94. Nyquist plot of a pDMFC for different methanol concentrations and 0.2 V using SS+Au as anode CC with an open ratio of 34 % (CC_1).

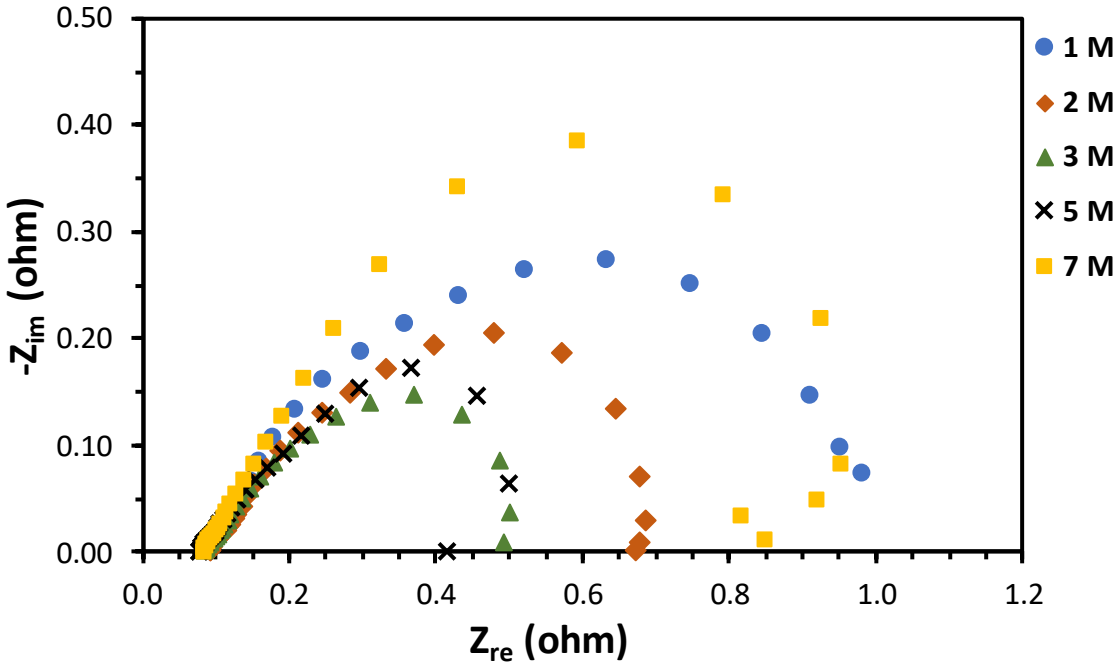

Figure A.95. Nyquist plot of a pDMFC for different methanol concentrations and 0.3 V using SS+Au as anode CC with an open ratio of 34 % (CC_1).

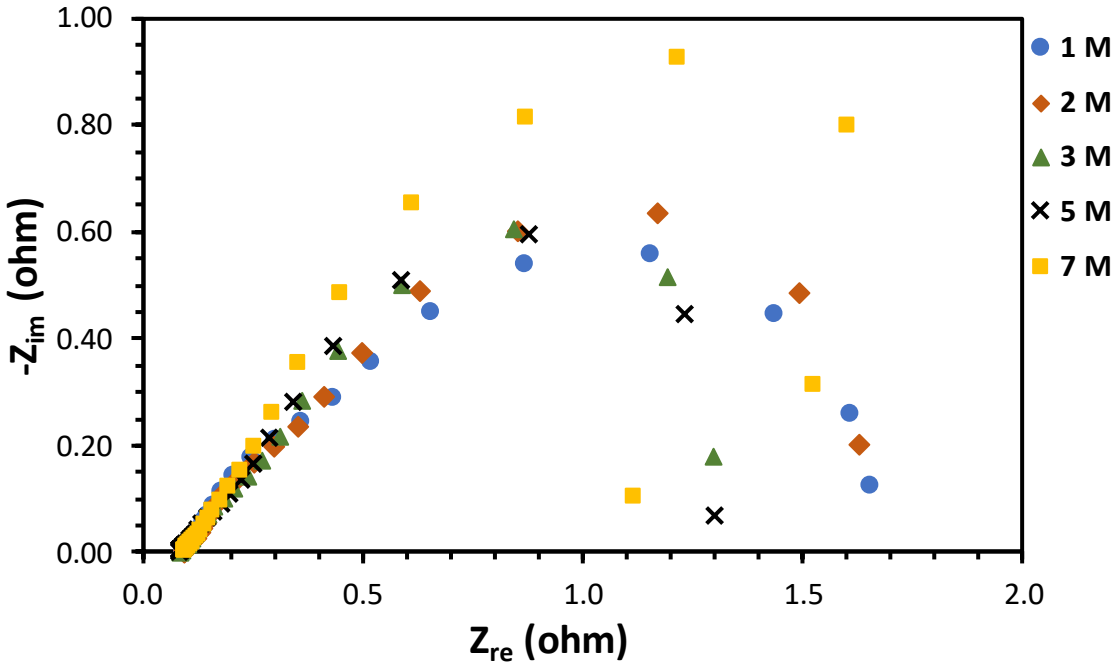

Figure A.96. Nyquist plot of a pDMFC for different methanol concentrations and 0.4 V using SS+Au as anode CC with an open ratio of 34 % (CC_1).

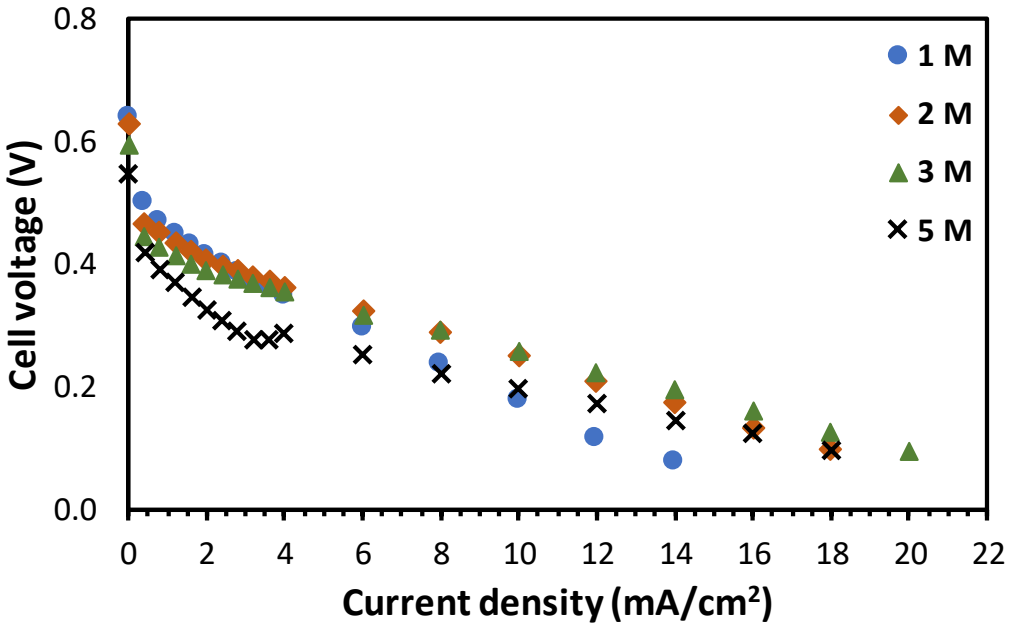

Figure A.97. Effect of methanol concentration on cell the performance using Ti as anode CC with an open ratio of 41 % (CC_2).

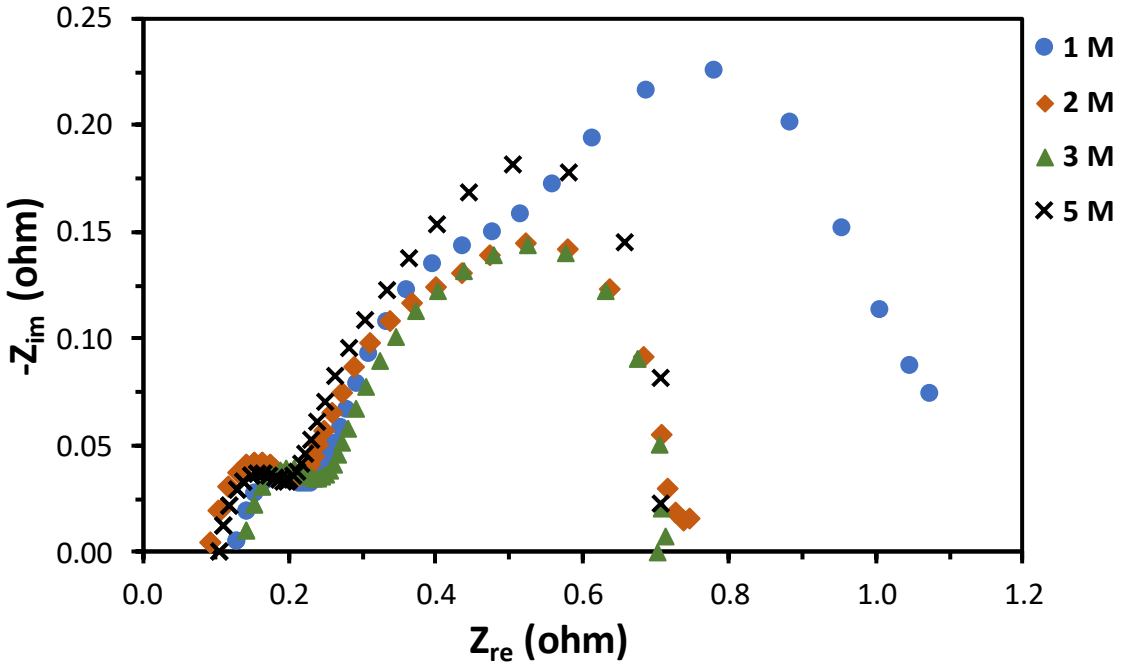

Figure A.98. Nyquist plot of a pDMFC for different methanol concentrations and 0.2 V using Ti as anode CC with an open ratio of 41 % (CC_2).

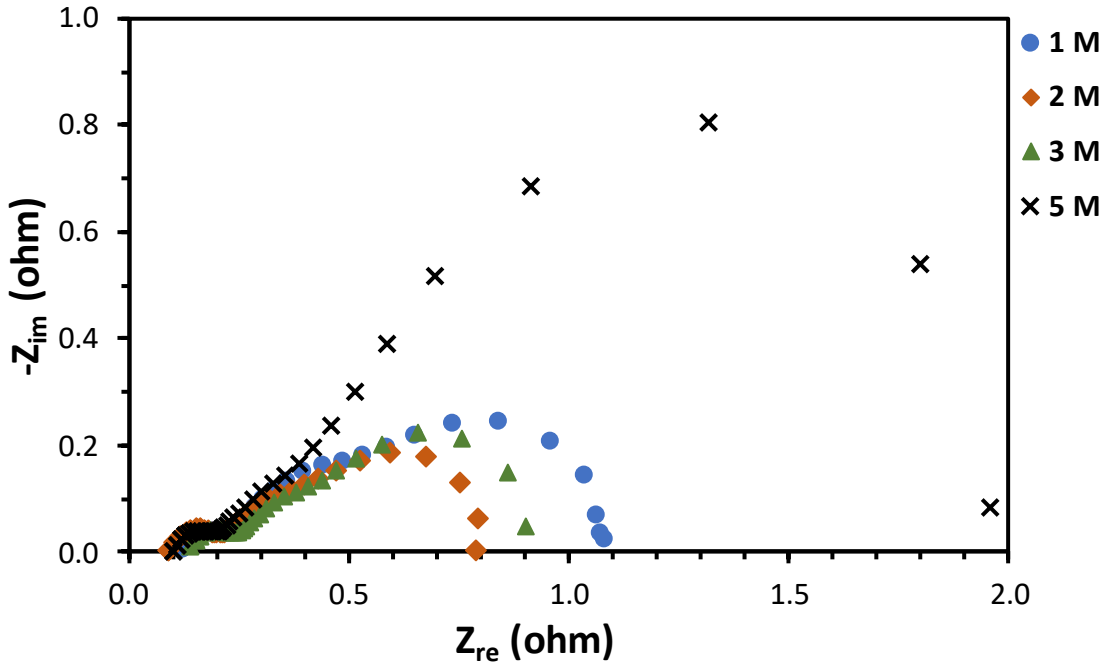

Figure A.99. Nyquist plot of a pDMFC for different methanol concentrations and 0.3 V using Ti as anode CC with an open ratio of 41 % (CC_2).

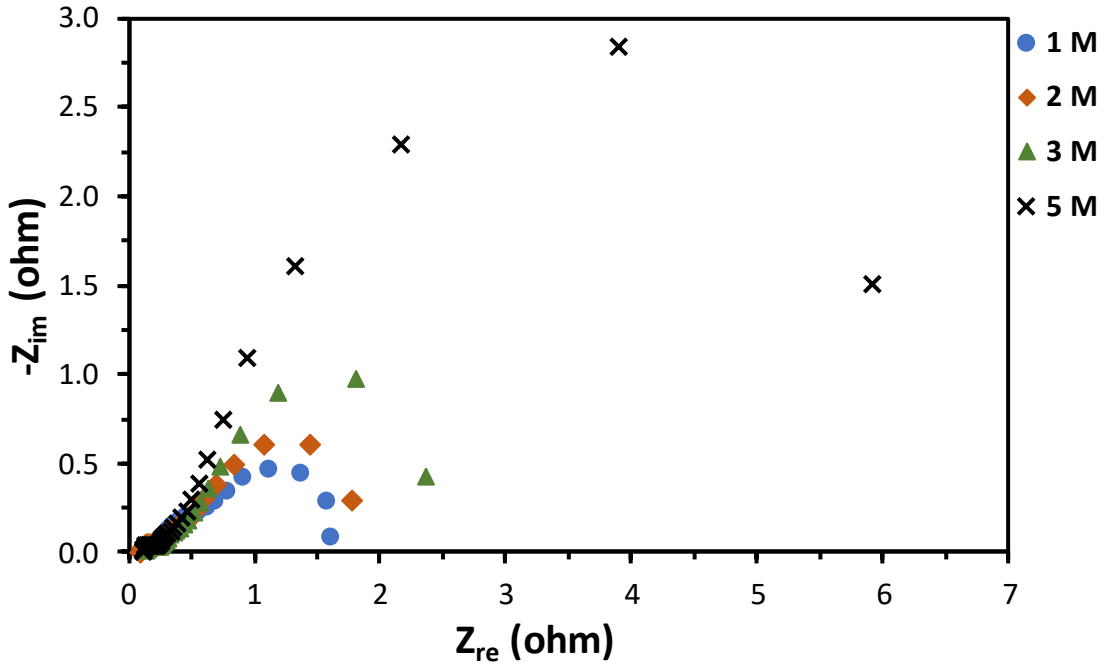

Figure A.100. Nyquist plot of a pDMFC for different methanol concentrations and 0.4 V using Ti as anode CC with an open ratio of 41 % (CC_2).

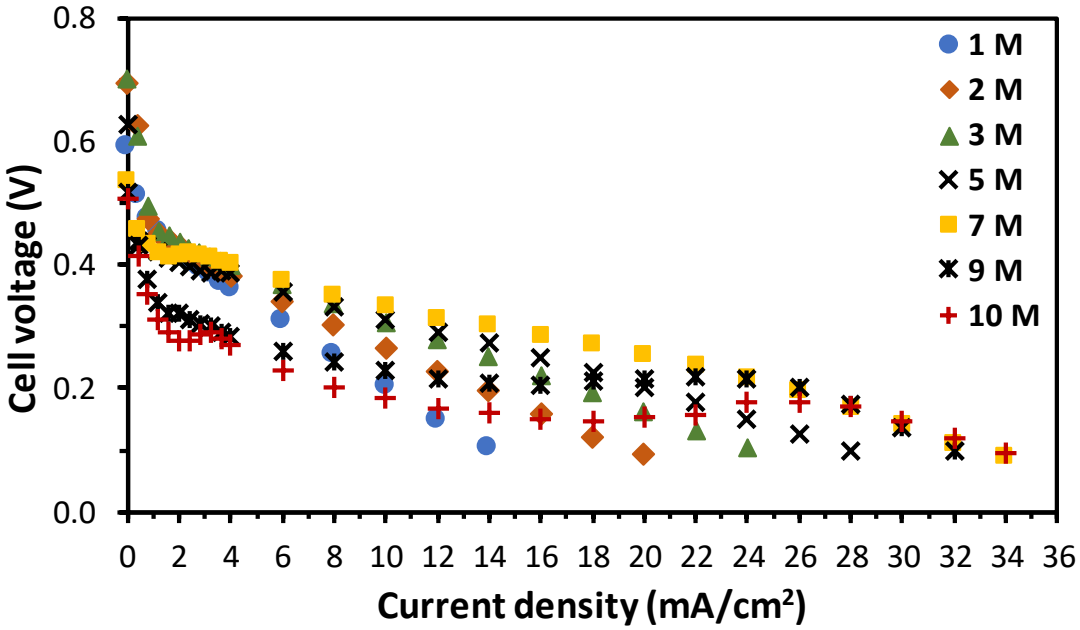

Figure A.101. Effect of methanol concentration on cell performance using Ti as anode CC with an open ratio of 34 % (CC_1).

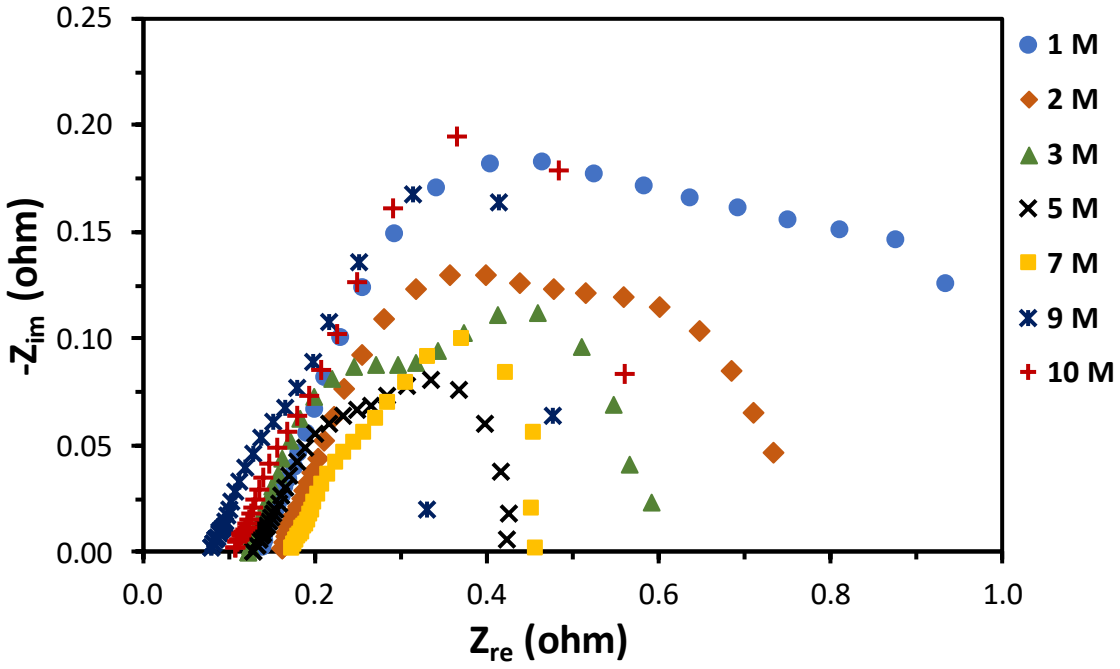

Figure A.102. Nyquist plot of a pDMFC for different methanol concentrations and 0.2 V using Ti as anode CC with an open ratio of 34 % (CC_1).

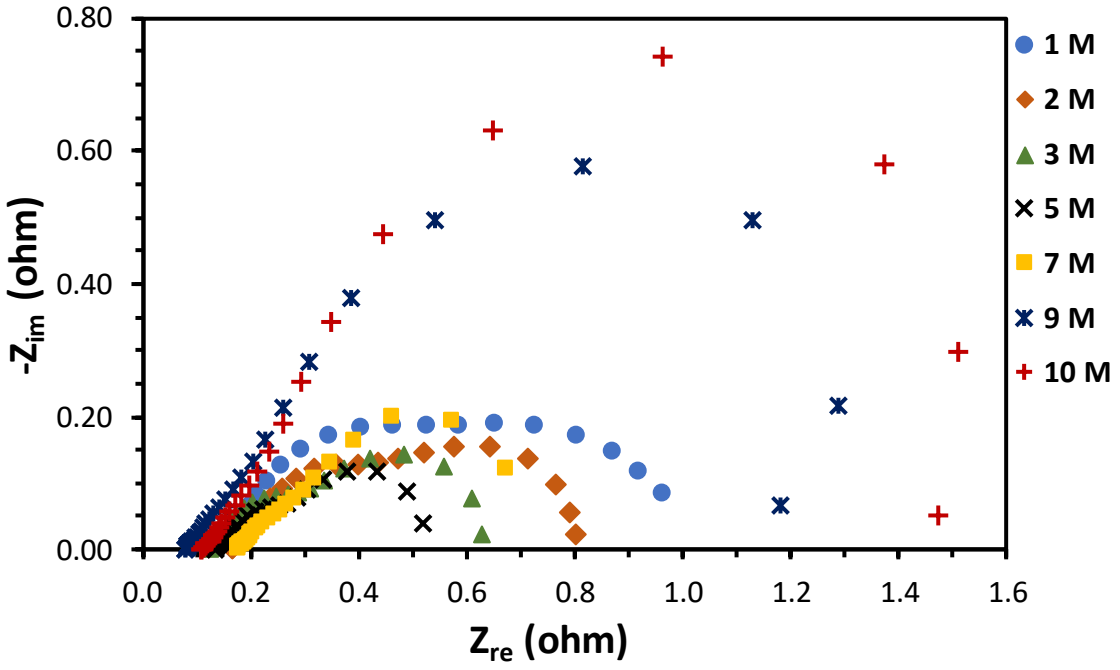

Figure A.103. Nyquist plot of a pDMFC for different methanol concentrations and 0.3 V using Ti as anode CC with an open ratio of 34 % (CC_1).

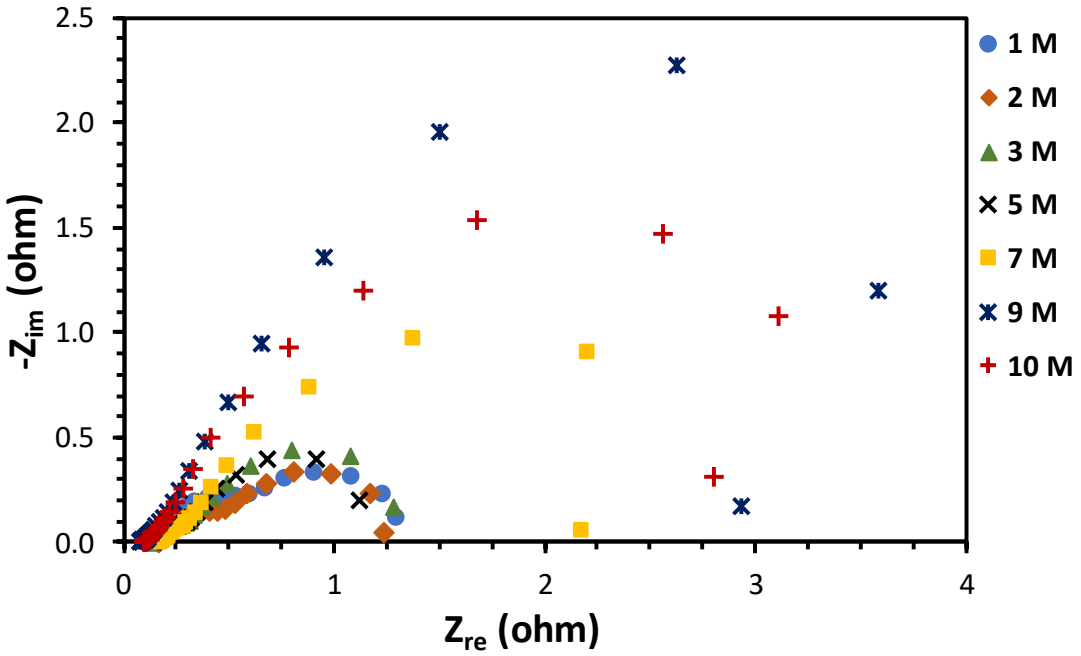

Figure A.104. Nyquist plot of a pDMFC for different methanol concentrations and 0.4 V using Ti as anode CC with an open ratio of 34 % (CC_1).

A.7. Effect of cathode current collector material

All the results presented in this section were obtained with a Titanium current collector, with an open ratio of 34 % (CC_1), at the anode side and with CC_MPL as anode DL and CC as cathode DL.

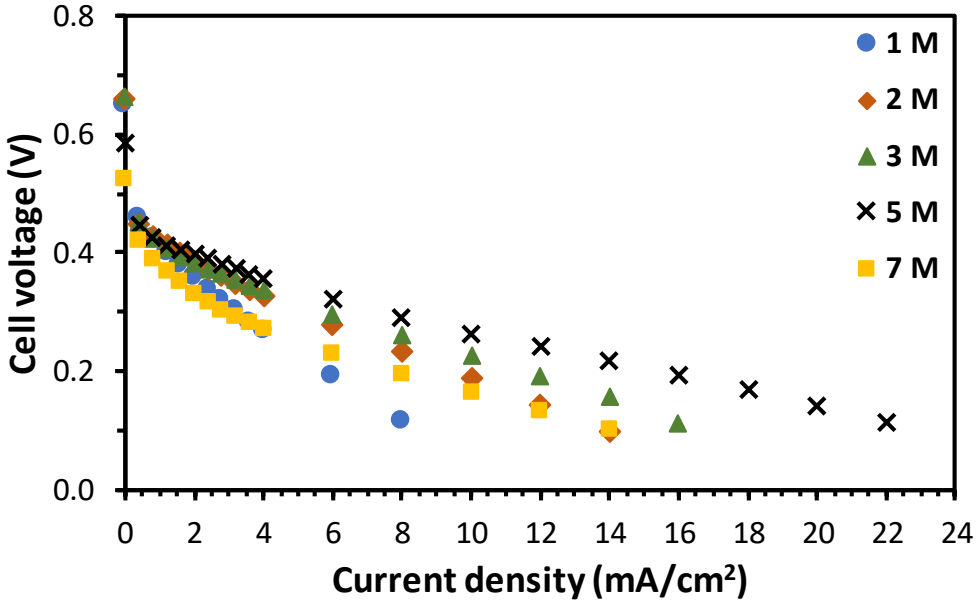

Figure A.105. Effect of methanol concentration on the cell performance using SS+Au as cathode CC with an open ratio of 34 % (CC_1).

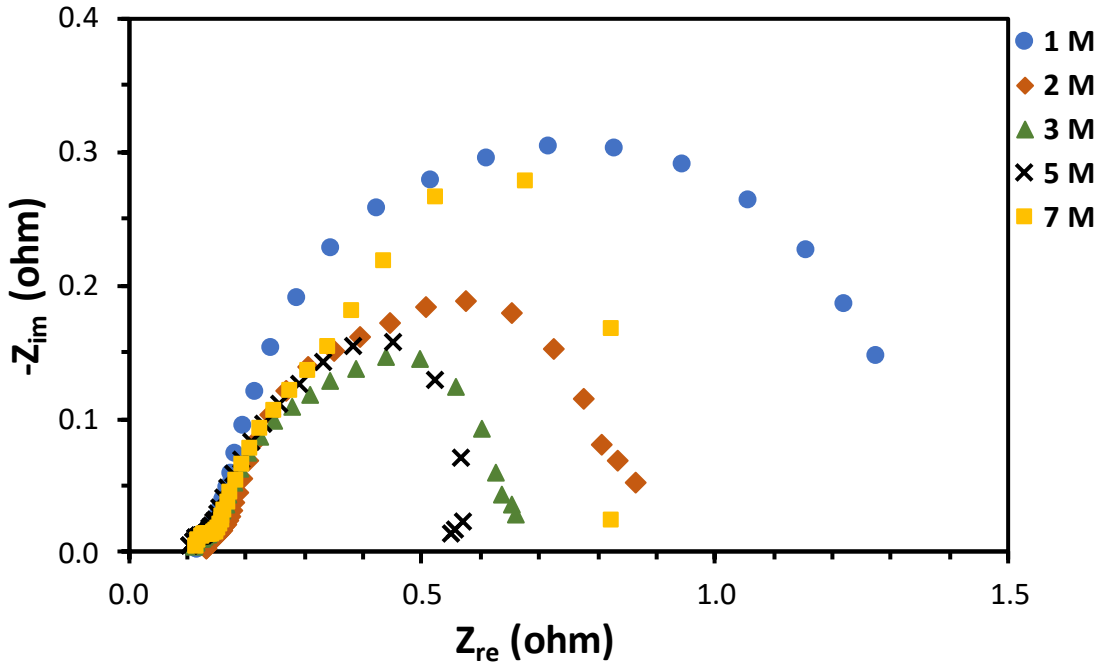

Figure A.106. Nyquist plot of a pDMFC for different methanol concentrations and 0.2 V using SS+Au as cathode CC with an open ratio of 34 % (CC_1).

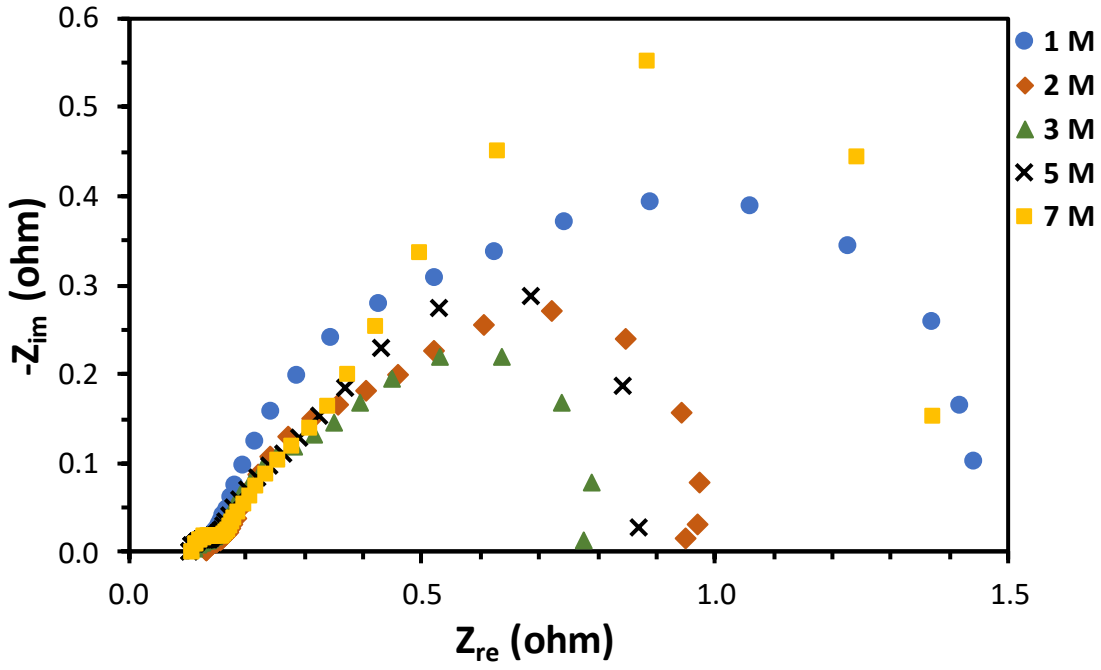

Figure A.107. Nyquist plot of a pDMFC for different methanol concentrations and 0.3 V using SS+Au as cathode CC with an open ratio of 34 % (CC_1).

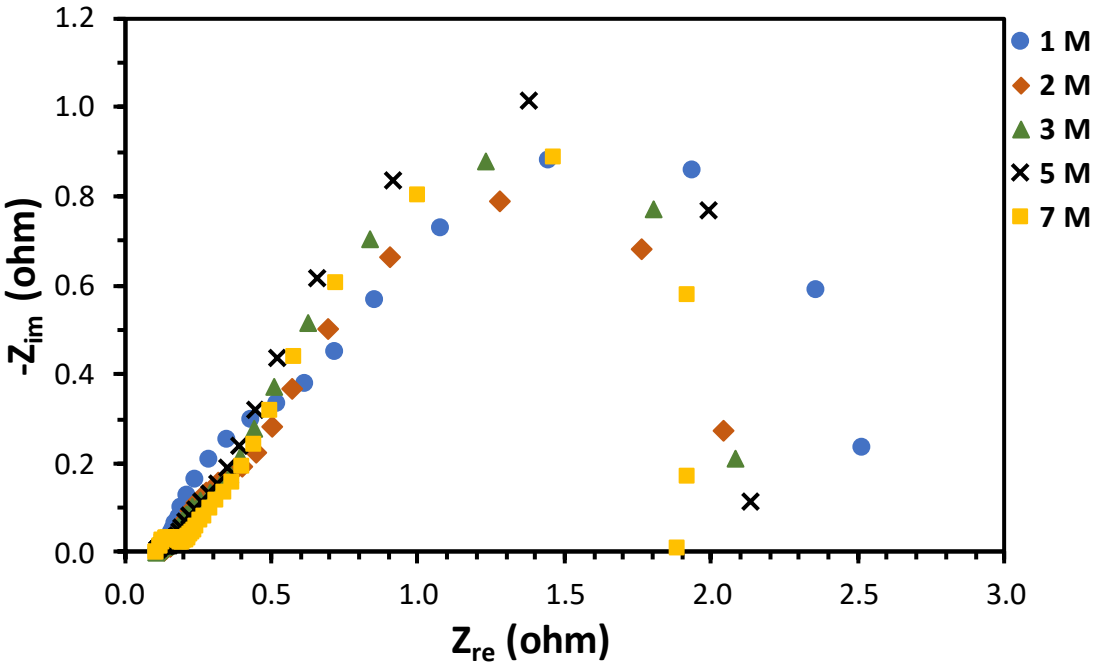

Figure A.108. Nyquist plot of a pDMFC for different methanol concentrations and 0.4 V using SS+Au as cathode CC with an open ratio of 34 % (CC_1).

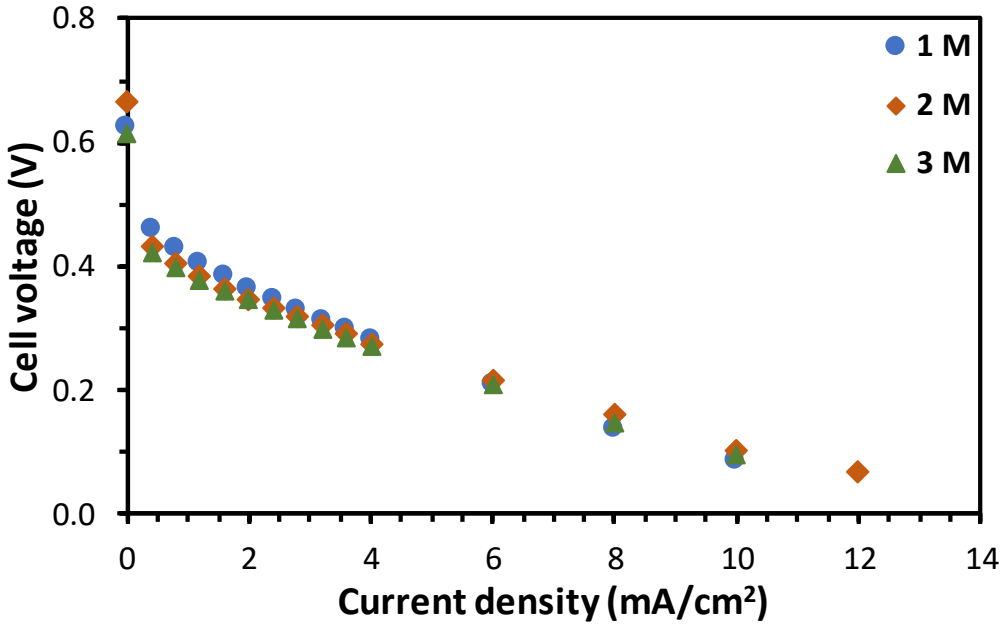

Figure A.109. Effect of methanol concentration on the cell performance using Ti as cathode CC with an open ratio of 34 % (CC_1).

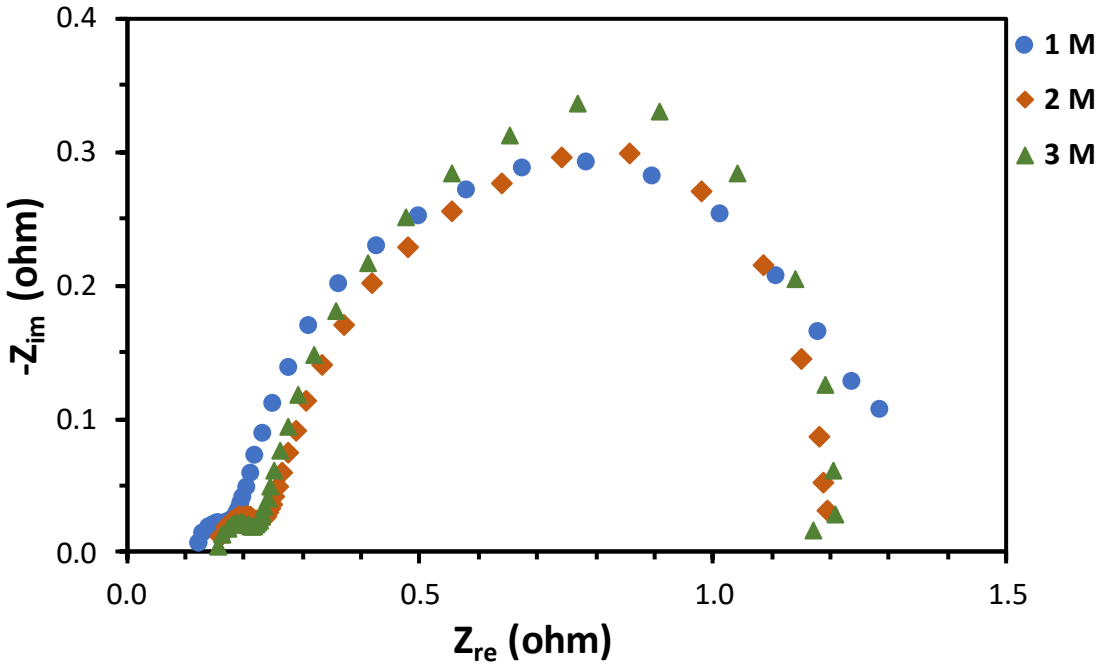

Figure A.110. Nyquist plot of a pDMFC for different methanol concentrations and 0.2 V using Ti as cathode CC with an open ratio of 34 % (CC_1).

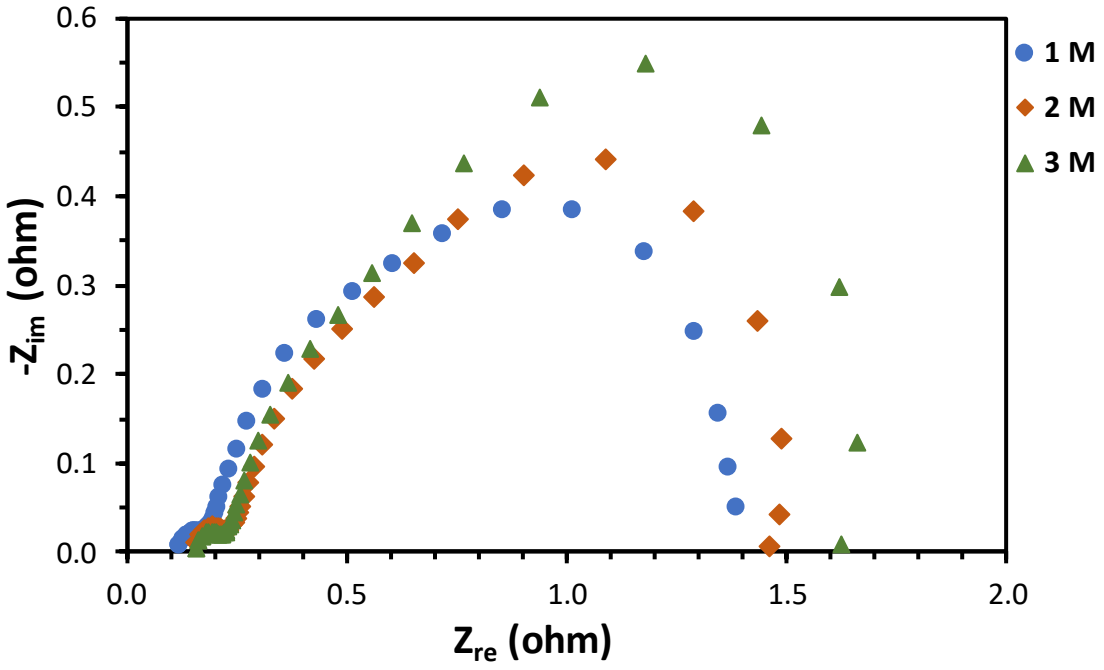

Figure A.111. Nyquist plot of a pDMFC for different methanol concentrations and 0.3 V using Ti as cathode CC with an open ratio of 34 % (CC_1).

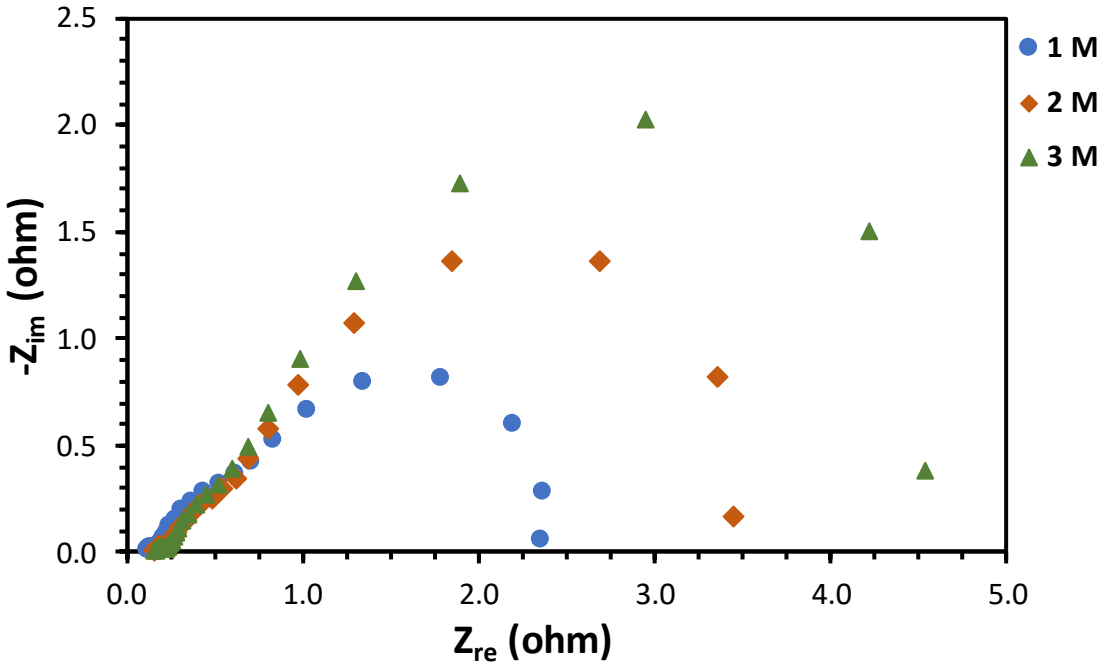

Figure A.112. Nyquist plot of a pDMFC for different methanol concentrations and 0.4 V using Ti as cathode CC with an open ratio of 34 % (CC_1).

A.8. Effect of methanol:ethanol ratio

All the results presented in this section were obtained with a stainless steel (SS) current collectors, with an open ratio of 41 % (CC_2), at the anode and cathode sides and with CC_MPL as anode DL and CC as cathode DL.

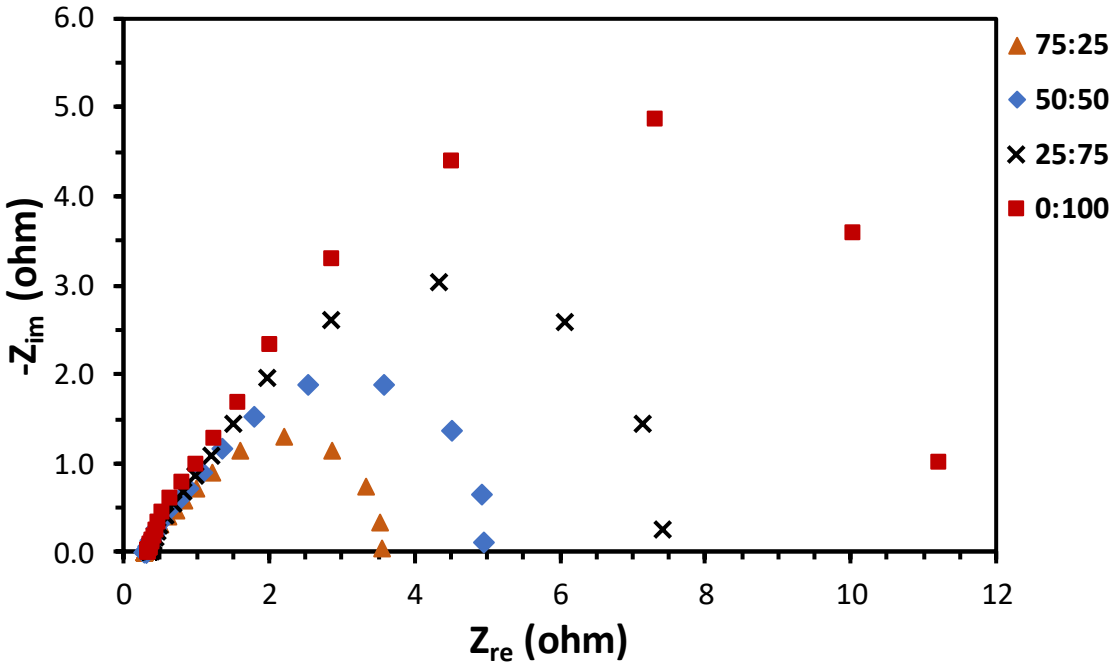

Figure A.113. Nyquist plot of a pDMFC for different methanol:ethanol ratios, a fuel concentration of 2 M and 0.2 V.

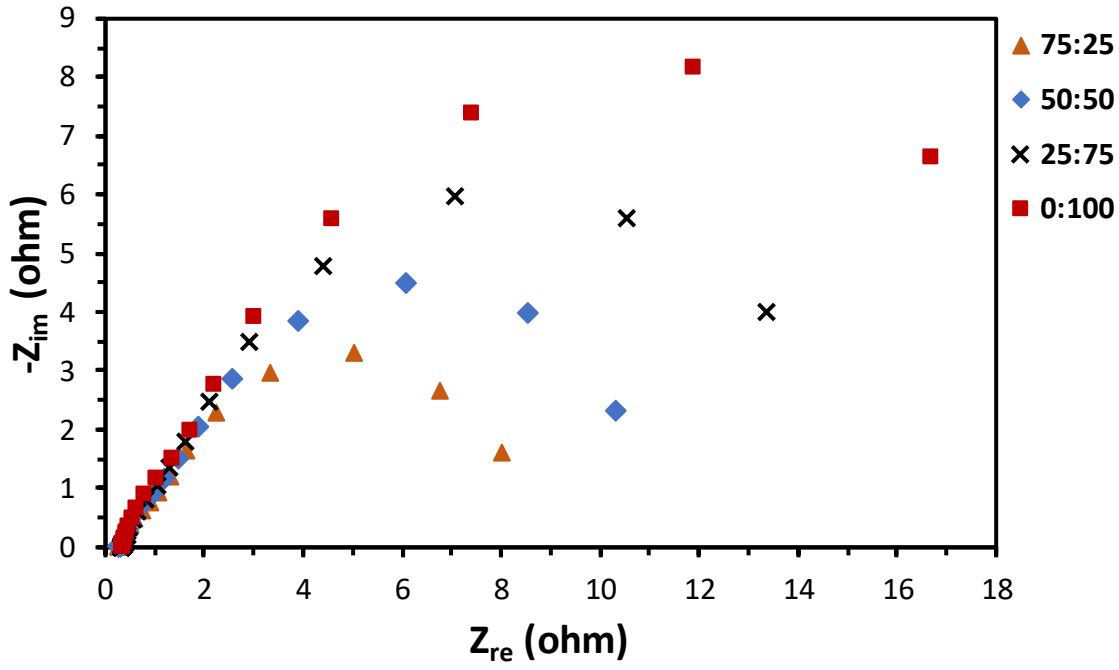

Figure A.114. Nyquist plot of a pDMFC for different methanol:ethanol ratios, a fuel concentration of 2 M and 0.3 V.

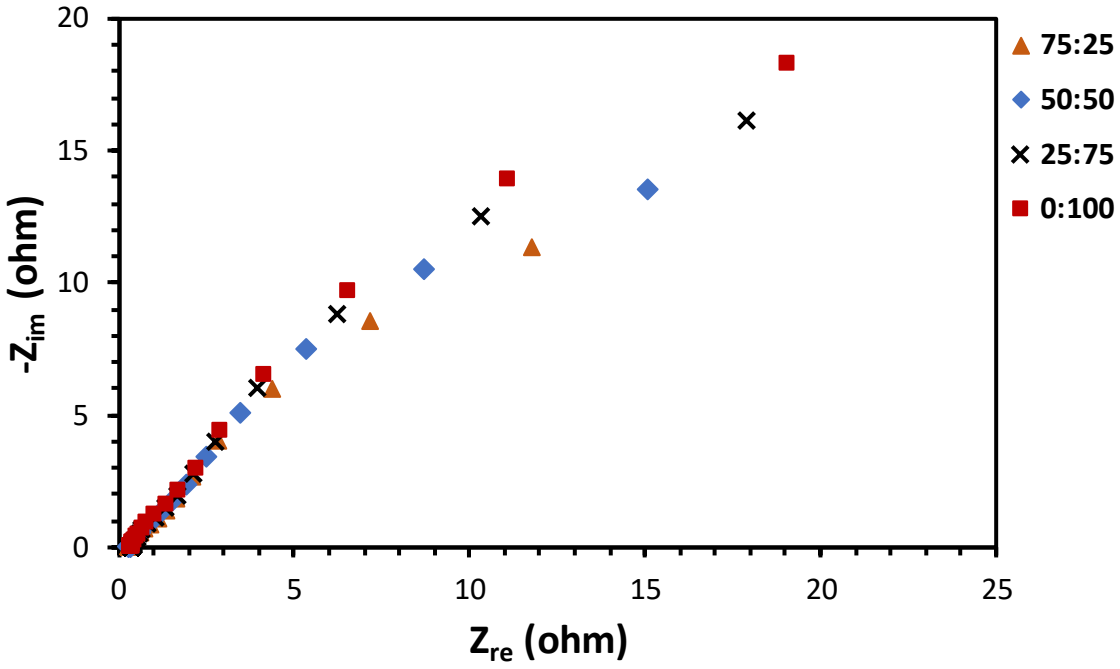

Figure A.115. Nyquist plot of a pDMFC for different methanol:ethanol ratios, a fuel concentration of 2 M and 0.4 V.

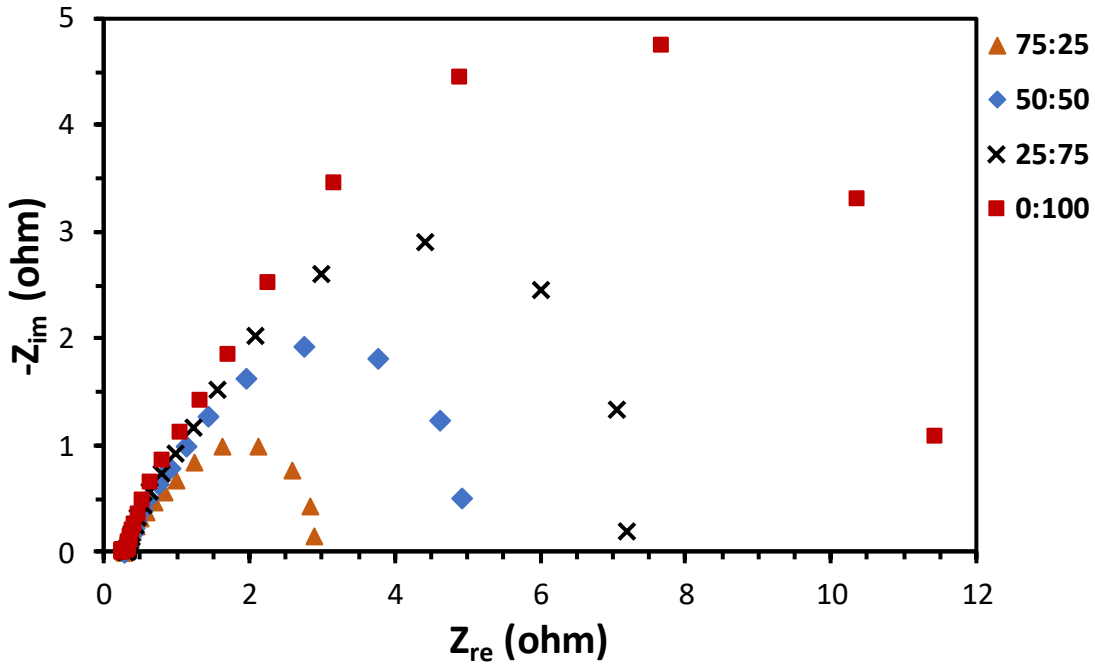

Figure A.116. Nyquist plot of a pDMFC for different methanol:ethanol ratios, a fuel concentration of 3 M and 0.2 V.

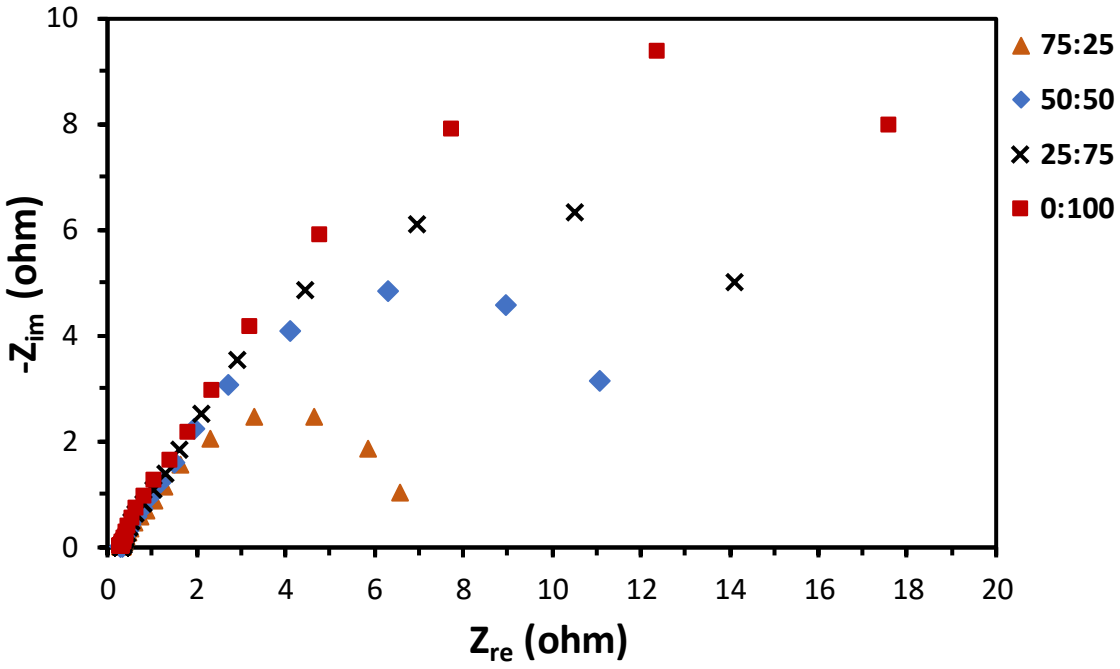

Figure A.117. Nyquist plot of a pDMFC for different methanol:ethanol ratios, a fuel concentration of 3 M and 0.3 V.

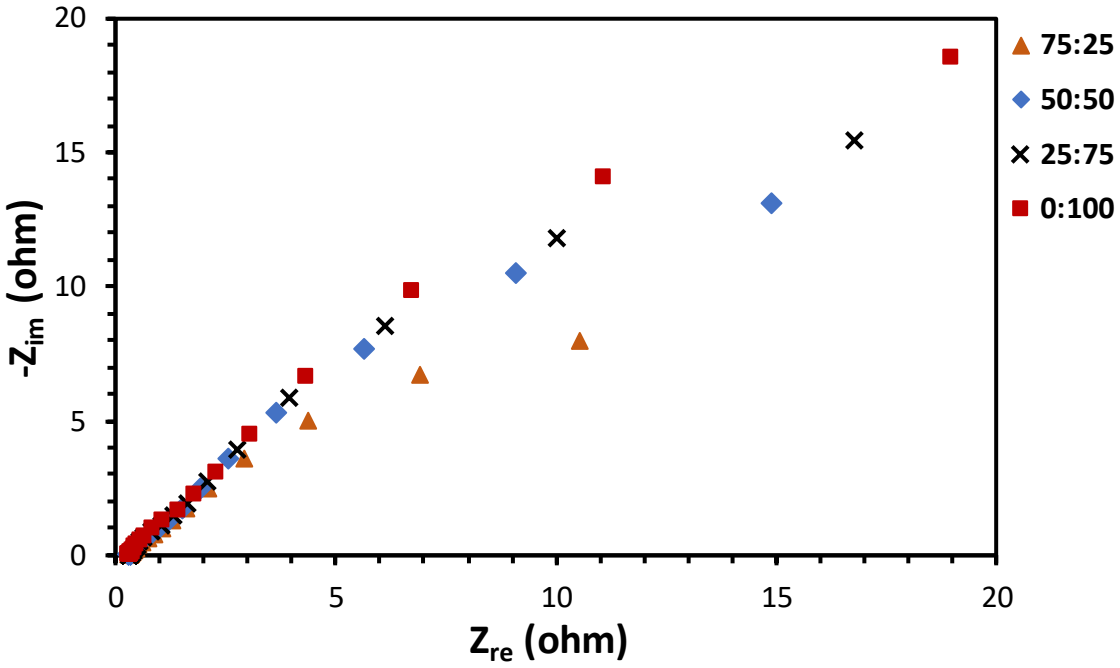

Figure A.118. Nyquist plot of a pDMFC for different methanol:ethanol ratios, a fuel concentration of 3 M and 0.4 V.

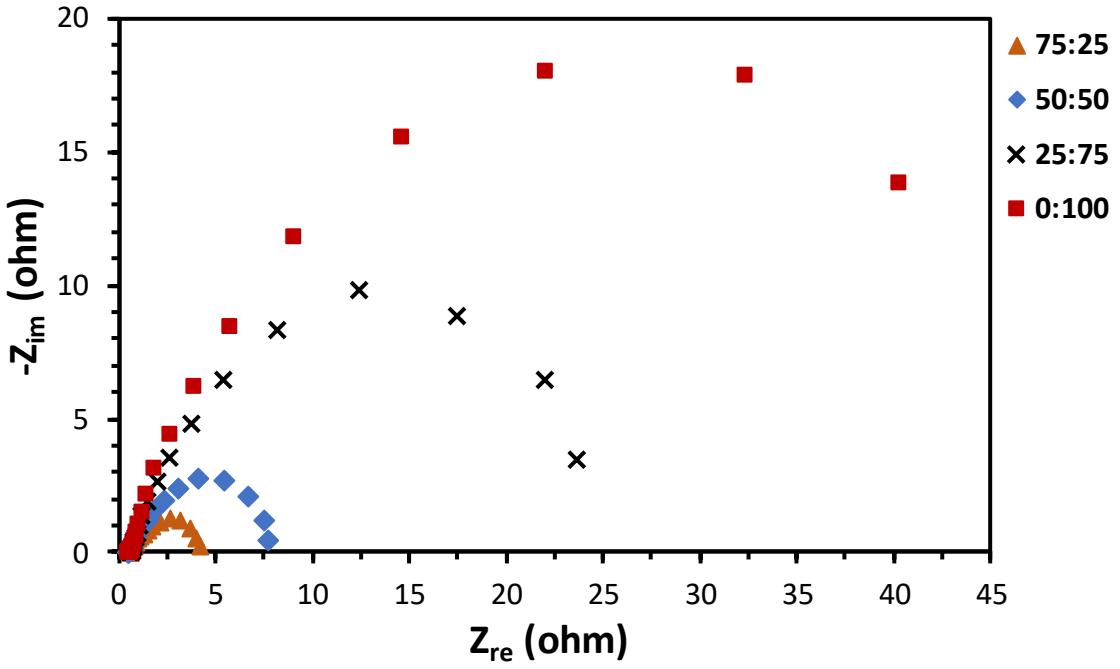

Figure A.119. Nyquist plot of a pDMFC for different methanol:ethanol ratios, a fuel concentration of 5 M and 0.2 V.

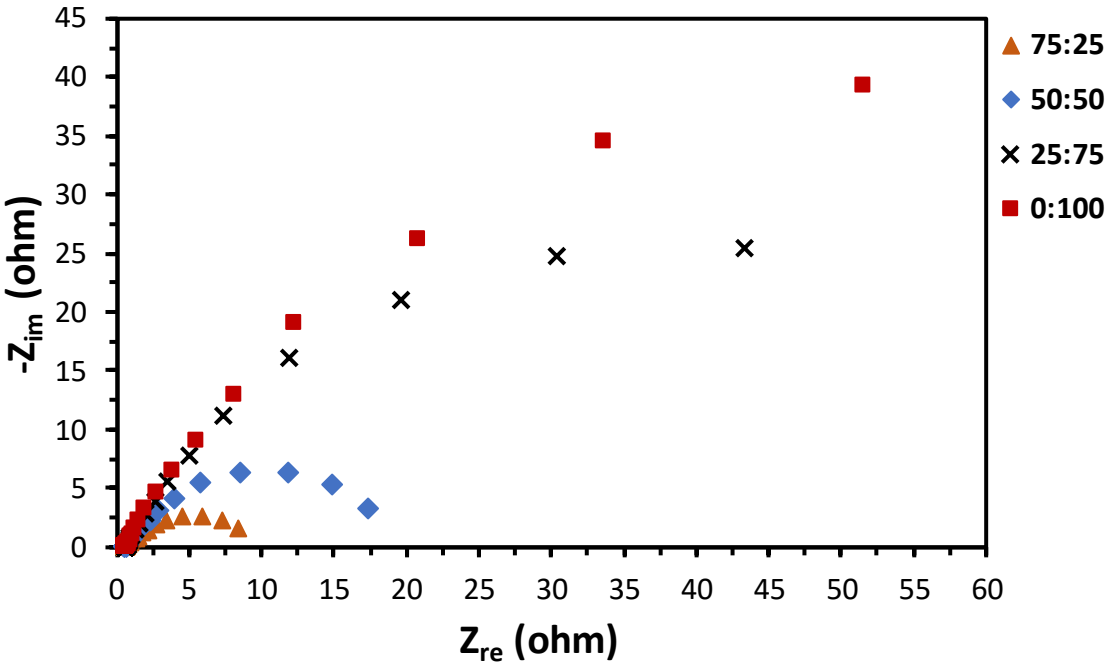

Figure A.120. Nyquist plot of a pDMFC for different methanol:ethanol ratios, a fuel concentration of 5 M and 0.3 V.

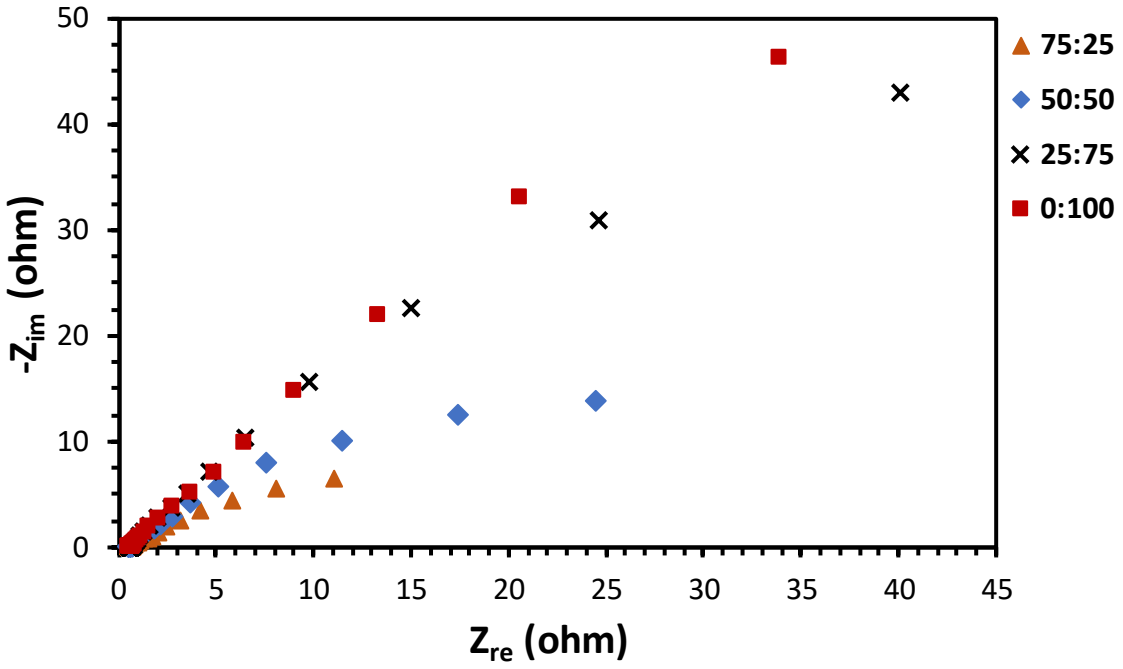

Figure A.121. Nyquist plot of a pDMFC for different methanol:ethanol ratios, a fuel concentration of 5 M and 0.4 V.

A.9. Durability

All the results presented in this section were obtained with a titanium current collector at the anode side and a stainless steel current collector ate the cathode side, both with an open ratio of 34 % (CC_1), and with CC_MPL as anode DL and CC as cathode DL.

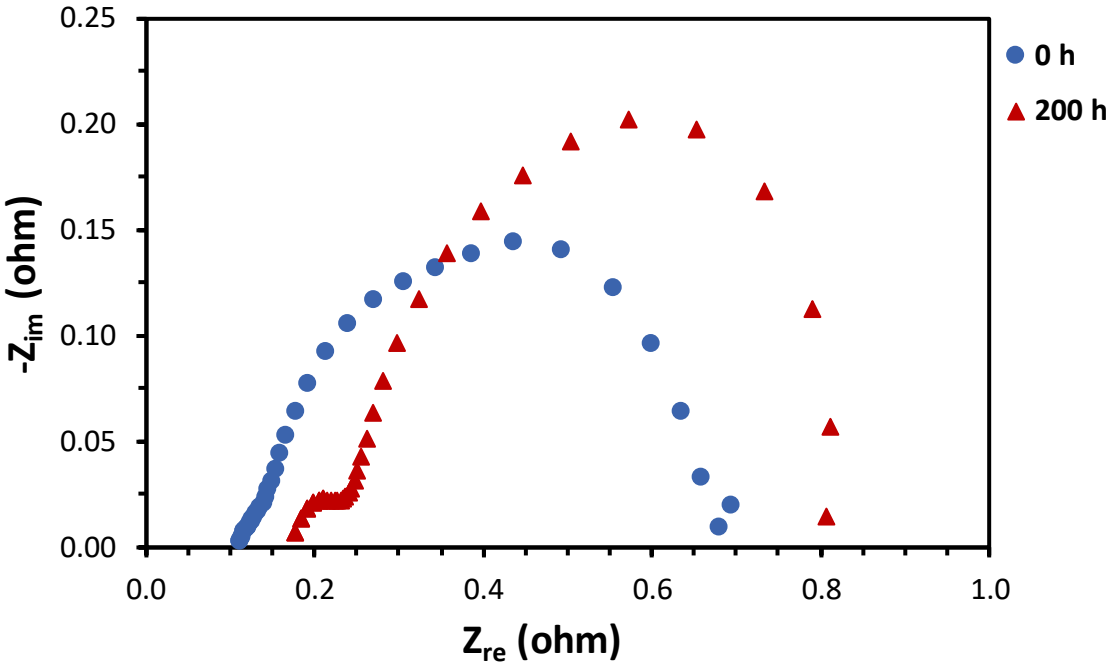

Figure A.122. Nyquist plot of a pDMFC at the beginning (0 h) and at the end (200 h) of the durability tests for 0.2 V.

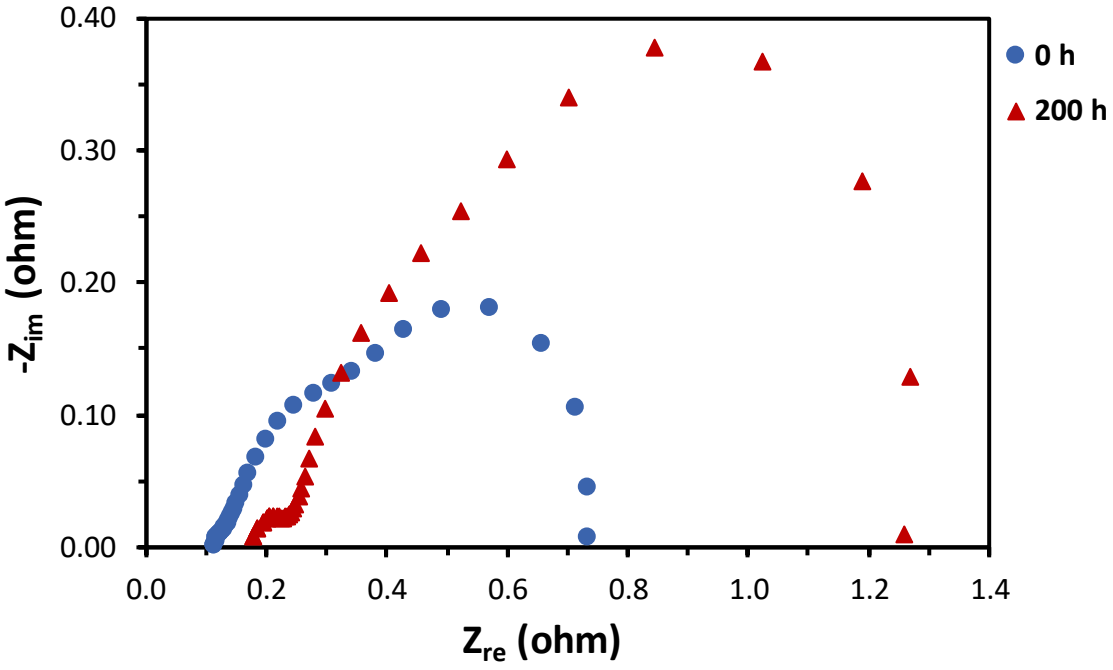

Figure A.123. Nyquist plot of a pDMFC at the beginning (0 h) and at the end (200 h) of the durability tests for 0.3 V.

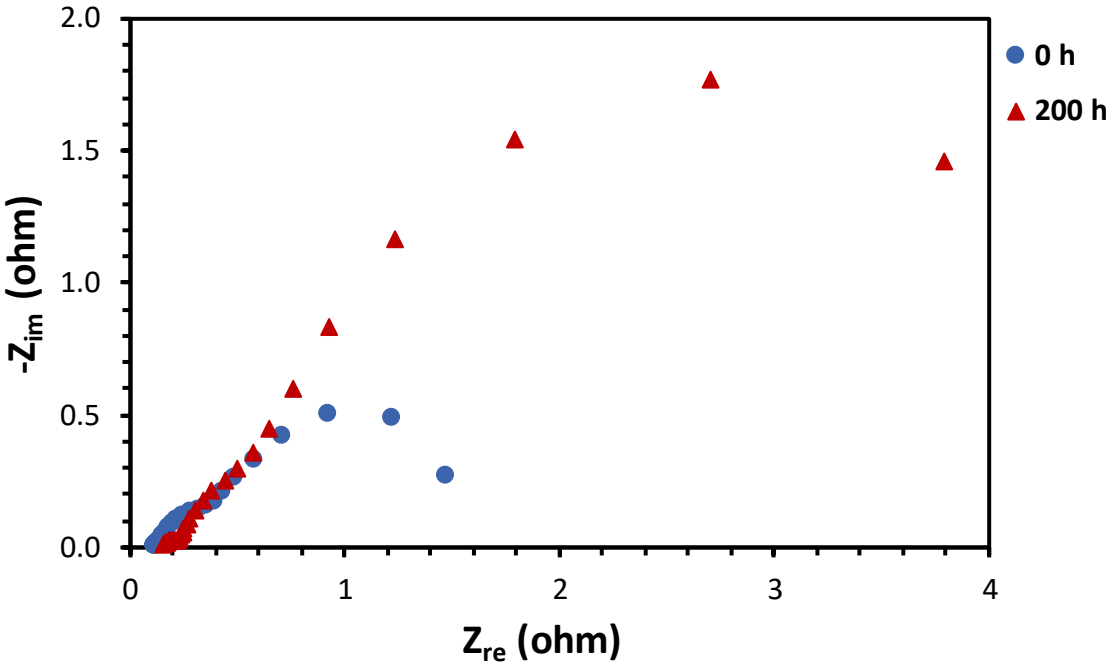

Figure A.124. Nyquist plot of a pDMFC at the beginning (0 h) and at the end (200 h) of the durability tests for 0.4 V.